

# **Formation of Precipitates in a Desalination Plant with Zero Liquid Discharge: Identification of the main Processes by Mineralogical-Geochemical Methods and Modelling**

Zur Erlangung des akademischen Grades einer  
DOKTORIN DER NATURWISSENSCHAFTEN  
von der Fakultät für  
Bauingenieur-, Geo- und Umweltwissenschaften

der Universität Fridericiana zu Karlsruhe (TH)

genehmigte

**DISSERTATION**

von

Dipl.-Min. Julia Scheiber  
aus Waibstadt

Tag der mündlichen  
Prüfung: 23.11.2011

Referent: Prof. Dr. H.-G. Stosch

Korreferent: Prof. Dr. M. Franzreb

Karlsruhe 2011



Julia Scheiber  
2a Route de Surbourg  
67250 Merckwiller Pechelbronn  
Frankreich

Hiermit erkläre ich, dass ich die vorliegende Dissertation selbständig und ohne unzulässiger Hilfe Dritter und ohne Benutzung anderer als die angegebenen und genau gekennzeichneten Hilfsmittel angefertigt habe. Die Grundsätze der Universität Karlsruhe (TH) zur Sicherung guter wissenschaftlicher Praxis habe ich in der aktuell gültigen Fassung beachtet.

Julia Scheiber

Merckwiller Pechelbronn, 2011



Das dieser Dissertation zugrunde liegende Vorhaben wurde mit Mitteln des Bundesministeriums für Bildung und Forschung unter dem Förderkennzeichen 02WT0775 gefördert.

Die Verantwortung für den Inhalt dieser Dissertation liegt bei der Autorin.



## ***Acknowledgements***

It was an honour for me to witness their  
inspiration and enthusiasm for discovery, scientific research and development

Prof. Dr. R. Nüesch

Prof. Dr. W. Höll

I am very grateful to Prof. Dr. Heinz-Günter Stosch and Prof. Dr. Matthias Franzreb who accepted to take over the part as supervisors for this thesis.

I owe my special thanks to Dr. Peter G. Weidler for hours of discussion, answering countless questions and his advice concerning the administrative part of the BMBF project. I am very grateful to Dr. Ute Schwotzer who was essentially involved in the project proposal.

I would like to thank the cooperation partners at the Zuckerberg Institute of the Ben Gurion University of the Negev, especially Prof. Dr. Yoram Oren and Dr. Jack Gilron, for many fruitful discussions.

I am grateful to the BMBF for funding this project. My special thanks are due to Dr. Hans Joachim Metzger from PTKA for his patience in answering all my questions concerning the administrative part of the BMBF project.

This thesis could not have been completed without the work of Marita Heinle (ICP-OES), Gudrun Hefner (IC, cations), Brigitte Kiehling (AAS) and Herrmann Köhler (WD-RFA). I am grateful to Stefan Heißler and Mike Füssler for their support concerning all the little and big questions regarding setup and optimising the experiments. I would like to thank Pia Donitzka for assisting during the flow-through experiments and Dr. Matthias Schwotzer and Dr. Frank Friedrich for the ESEM/EDX measurements.

I am indebted to many of my colleagues of the research group nanomineralogy, especially to PD. Dr. Katja Emmerich for the intense discussion of the TGA/DTA measurements.

I would like to thank Julia Süßmuth, Cherifa Bachir, Kerstin Petrick, Thomas Sollich, Anne Lebhardt, Natalia Herdt and Romain Heck for their social support.

I owe my deepest gratitude to my friends, to Peter Höllnigk and my family, especially to my parents Barbara and Günther Scheiber.



---

## Table of Content

<b>Abstract</b>	<b>I</b>
<b>Kurzfassung</b>	<b>III</b>
<b>1 Introduction</b>	<b>1</b>
1.1 General outline	1
1.2 Desalination of water	2
1.3 Brackish water desalination in remote areas	3
1.4 Concentrate disposal	3
1.5 Improvement of Zero Discharge Disposal: German - Israeli Cooperation Project	5
1.5.1 Key activities of the Israeli cooperation partners	5
1.5.2 Key activities of the German cooperation partners	7
1.6 Objective of Work	7
<b>2 Material and Methods</b>	<b>9</b>
2.1 Material	9
2.1.1 Original concentrates of the pilot plant and their formation	9
2.1.2 Synthetic laboratory concentrates	12
2.1.3 Stock solution of silicic acid	14
2.1.4 Synthetic seeding and adsorption material	15
2.2 Methods	16
2.2.1 Methods of solid samples analysis	16
2.2.1.1 X-Ray Diffraction (XRD)	16
2.2.1.2 Energy-Dispersive and Wavelength-Dispersive X-Ray Fluorescence (ED/WDXRF)	17
2.2.1.3 Optical Microscopy	18
2.2.1.4 Environmental Scanning Electron Microscopy (ESEM)	18
2.2.1.5 Thermogravimetric Analysis (TGA) and Simultaneous Differential Thermal Analysis (SDTA)	19
2.2.2 Methods of liquid sample analysis	20
2.2.2.1 Ionchromatography (IC)	20
2.2.2.2 Colorimetric measurements	22
2.2.2.3 Inductively-Coupled Plasma Optical Emission Spectrometry (ICP OES)	24
2.2.2.4 pH measurements	25
<b>3 Geochemical modelling of aqueous solutions</b>	<b>27</b>
3.1 Fundamentals of mineral solubility in aqueous solution	27
3.1.1 Interaction between water molecules and a solid phase	27
3.1.2 Interaction between electrolytes in aqueous solutions	28

---

3.2	Calculation of mineral solubility	29
3.2.1	Mineral saturation state in aqueous solutions	29
3.2.2	Calculation of activity coefficients in diluted aqueous solutions	30
3.2.2.1	Debye-Hückel equation	30
3.2.2.2	Davies equation	30
3.2.2.3	Extended Debye-Hückel equation	31
3.2.2.4	B-dot equation	31
3.2.3	Calculation of activity coefficients in concentrated aqueous solutions	32
3.3	Geochemical modelling of process concentrates of the pilot plant	34
3.3.1	Upgrading the database thermo_phrqptz with Pitzer parameters for silicic acid and nitrate	35
3.3.2	Testing the upgraded database	35
3.3.2.1	Solubility of SiO <sub>2</sub> , amorphous silica, in CaCl <sub>2</sub> and MgCl <sub>2</sub> solutions	36
3.3.2.2	Solubility of SiO <sub>2</sub> , amorphous silica, in Na <sub>2</sub> SO <sub>4</sub> and MgSO <sub>4</sub> solutions	37
3.3.2.3	Solubility of SiO <sub>2</sub> , amorphous silica, in NaCl and NaNO <sub>3</sub> solutions	38
3.3.2.4	Solubility of SiO <sub>2</sub> , amorphous silica, in KCl and KNO <sub>3</sub> solutions	39
3.3.2.5	Applicability of the theoretical solubility calculations for amorphous silica with the upgraded database	39
3.3.3	Calculation of the mineral saturation state in the process solutions of the membrane units of the pilot plant	40
3.3.3.1	Mineral saturation state in the feed water in dependence of the pH	40
3.3.3.2	Mineral saturation state in the RO concentrate in dependence of the pH	42
3.3.3.3	Mineral saturation state in the EDR concentrate in dependence of the pH	43
<b>4</b>	<b>Scaling in the Electrodialysis Unit</b>	<b>45</b>
4.1	Characterisation of the precipitates	45
4.1.1	Investigation of the precipitates by optical Microscopy	46
4.1.2	Investigations of the precipitates by Environmental Scanning Electron Microscope and Energy-Dispersive X-ray Fluorescence	48
4.1.3	Investigation of the precipitates by Wavelength-Dispersive X-ray Fluorescence (WD-XRF)	51
4.1.4	Investigation of the precipitates by X-ray Diffraction (XRD)	52
4.1.5	Summary and discussion of membrane deposit characteristics	53
4.2	Formation conditions of inorganic solids in the EDR unit: Laboratory experiments	57
4.2.1	Solubility of amorphous silica, SiO <sub>2</sub> , in the EDR concentrate	57
4.2.2	Seeding experiments	59
4.2.3	Titration experiments	65
4.2.3.1	Titration of silicic acid in DIW and MgCl <sub>2</sub> solution	65
4.2.3.2	Titration experiments with original EDR concentrate	67
4.2.3.3	Titration experiments with synthetic laboratory EDR concentrates	79
4.2.4	Discussion	80

---

4.3	Removal of silicic acid	100
4.3.1	Removal of silicic acid by adsorption on mineral surfaces	100
4.3.2	Adsorption of silicic acid on mineral surfaces of in situ precipitated brucite	102
4.3.3	Discussion	106
<b>5</b>	<b>Geochemical modelling of brine evaporation</b>	<b>111</b>
5.1	Parameterisation of a database: evaporation of EDR brine as a function of the relative humidity	111
5.2	Geochemical modeling: prediction of mineral precipitation	122
5.3	Discussion	124
<b>6</b>	<b>Final Conclusions and Outlook</b>	<b>129</b>
<b>7</b>	<b>References</b>	<b>135</b>
	<b>Appendix A</b>	<b>139</b>
	<b>Appendix B</b>	<b>142</b>

---

---

## List of Abbreviations

AEM:	Anion Exchanger Membrane
adj.:	adjusting
BSE:	Backscattered Electrons
CEM:	Cation Exchanger Membrane
CF:	Concentration Factor
comp.:	composition
conc.:	concentration
DIW:	Deionised Water
ED:	Electrodialysis
EDR:	Electrodialysis Reversal
ED-XRF:	Energy Dispersive X-ray Fluorescence
ESEM:	Environmental Scanning Electron Microscopy
FW:	Feed Water
GWB:	The Geochemist's Workbench 6.0
IC:	Ionchromatography
ICP OES:	Inductively-Coupled Plasma Optical Emission Spectrometry
LOI:	Loss on Ignition
PA:	Pro Analysis
PE:	polyethylene
ref.:	Reference
RO:	Reverse Osmosis
NF:	Nanofiltration
MF:	Microfiltration
SDTA:	Simultaneous Differential Thermal Analysis
SE:	Secondary Electrons
Si-stocksoln.:	Si-stock solution
synth.:	synthetic
TDS:	Total Dissolved Solids
TGA:	Thermogravimetric Analysis
UF:	Ultrafiltration
UV:	Ultraviolet
WAIV:	Wind Aided Intensified Evaporation
WD-XRF:	Wavelength-Dispersive X-Ray Fluorescence
XRD:	X-Ray Diffraction

---

## Abstract

Scaling in membrane units of desalination plants reduces membrane permeability significantly up to complete blockage of the respective membrane surfaces. Characterisation of these deposits and investigation of their formation conditions are essential to understand the involved reactions and their impact on the process flow. Especially formation conditions of inorganic solids during brackish water desalination depend mainly on composition of the feed water and on the applied method. Brackish water of a fossil water lense, located in the inland of Israel, is desalinated by a interrelated membrane systems, Reverse Osmosis (RO) and Electrodialysis Reversal (EDR) to produce potable water. This pilot plant is managed by the research group of Prof. Dr. Yoram Oren at the Zuckerberg Institute, Ben Gurion University of the Negev. The volume of the EDR concentrate is reduced to near zero liquid by Wind Aided Intensified Evaporation (WAIV). Water treatment to Near Zero Liquid Discharge (NZLD) produces brines with high ionic strength.

The focus of this thesis is the calculation of the mineral saturation state, chemical and mineralogical characterisation of deposits in the membrane units, investigation of formation conditions of these precipitates and identification of measures to avoid scaling in the membrane units.

Mineral saturation state in brines, produced by water desalination and evaporation, as a function of the salt concentration was calculated with the geochemical modelling program *The Geochemist's Workbench*. Therefore, Pitzer parameters for  $\text{H}_4\text{SiO}_4$ ,  $\text{H}_3\text{SiO}_4^-$ ,  $\text{H}_2\text{SiO}_4^{2-}$  and  $\text{NO}_3^-$  taken from the literature were included in the database. Prediction of mineral formation in the desalination process is possible up to high ionic strength with one limitation concerning the metastable state of aqueous species of silicic acid. Amorphous silica was calculated to be saturated in the EDR concentrate. The formation conditions of inorganic deposits in the EDR unit were examined by laboratory experiments. Results of solubility and seeding experiments proved that the polymerisation rate of silicic acid in the EDR brine is very slow. The formation of  $\text{SiO}_{2(\text{am})}$  takes weeks to month and oligomerisation of silicic acid is strongly related to the pH. Measurements of reactive silicic acid fractions with the molybdenum yellow method show that oligomerisation starts at pH values above 4. Thereafter, scaling in the EDR unit as a consequence of precipitation of amorphous silica or blockage of membrane pores by large oligomers of silicic acid can be excluded.

Brucite ( $\text{Mg}(\text{OH})_2$ ) and gypsum ( $\text{CaSO}_4 \times 2\text{H}_2\text{O}$ ) were identified to form the main components of deposits on exchanger membrane surfaces. Within these deposits, the amount of silicon increases with increasing amount of magnesium. Furthermore, metal ions of  $\text{Cu}^{2+}$ ,  $\text{Zn}^{2+}$ ,  $\text{Ni}^{2+}$  and  $\text{Mn}^{2+}$ , present in the EDR brine due to corrosion of equipment of the plant, are the preferred forms of metal-hydroxides if pH increases above 9.5. On these surfaces dissociated sil-

ilic acid is adsorbed and thus removed from solution. In situ precipitation of hydroxides can be used for complete removal of silicic acid by addition of caustic soda. Flow-through experiments indicated that the required amount of NaOH depends on the initial concentration of silicic acid, on the initial pH and on the  $Mg^{2+}$  concentration in solution. The minimum dosage of caustic soda for a complete removal of silicic acid from EDR brine was determined from experiments. Additionally, it was found that the position of brine and additive dosage in the reaction vessel influences the efficiency of the removal significantly.

Results of the geochemical calculations of the evaporation of EDR brine were evaluated based on the results of evaporation experiments. Original and synthetic EDR brine were evaporated under controlled climate conditions (constant relative humidity and temperature). Evaporation rate, density, pH, electrolyte concentration and mineral formation as a function of the loss of water during evaporation were determined. Mineral saturation state was calculated up to high ionic strength in accordance to the experimental results. Concerning the kinetics, the precipitation of salts in the experiments were retarded in comparison to the calculations.

Presence of  $CO_2(g)$  in solution influences the pH during evaporation above an initial pH of 4.1. If brines contain  $CO_2(g)$  the pH increases during evaporation, if EDR concentrates contain no  $CO_2(g)$  pH decreases slightly. Below an initial pH of 4.1 the pH decreases continuously during evaporation. This effect can be related to the ability of the brine to neutralise acid. The point of equivalence of  $HCO_3^- = H^+$  for the EDR brine is at a pH of 4.1.

## Kurzfassung

Die Belagbildung auf Membranen, die in der Wasserentsalzung eingesetzt werden, haben eine Einschränkung der Permeabilität bis zu einer vollständigen Verblockung zur Folge. Die genaue Charakterisierung dieser Ablagerungen und Untersuchung der jeweiligen Bildungsbedingungen sind notwendig um die ablaufenden Reaktionen im Einzelnen und ihre Auswirkungen auf den Entsalzungsprozess zu verstehen. Insbesondere bei der Wasserentsalzung von Brackwässern aus ariden Gebieten ist die Ausbildung von anorganischen Ablagerungen stark von den Inhaltsstoffen des Rohwassers und von der verwendeten Methode abhängig. Die Arbeitsgruppe von Prof. Dr. Yoram Oren (Zuckerberg Institut, Ben Gurion Universität in der Negev, Israel) plant und betreibt eine Pilotanlage zur Wasserentsalzung mittels kombinierter Verfahren auf dem Außencampus der Ben-Gurion Universität des Negev. In dieser Anlage wird Brackwasser einer fossilen Grundwasserlinse im Inland von Israel zur Gewinnung von Trink- und Brauchwasser mittels kombinierter Membranverfahren, Umkehrosmose (RO) und Umkehr-Elektrodialyse (UED) entsalzt. Das UED Konzentrat wird in einem windgestützten Evaporationsprozess (WAIV: Wind Aided Intensified Evaporation) bis fast zur vollkommenen Trocknung reduziert. Bei dieser Form der Wasseraufbereitung (NZLD: Near Zero Liquid Discharge) entstehen Salzlösungen mit hoher Ionenstärke.

Im Rahmen dieser Arbeit wurde der Sättigungszustand von Mineralen berechnet, die Ausfällungsprodukte chemisch und mineralogisch charakterisiert und die Bildungsbedingungen dieser Präzipitate untersucht sowie Methoden zur Vermeidung der Belagbildung getestet und weiterentwickelt.

Die Berechnung des Sättigungszustandes von Mineralen, die während der Wasserentsalzung und Evaporation entstehen, wurde mit dem Modellierungsprogramm *The Geochemist's Workbench* in Abhängigkeit vom Salzgehalt berechnet. Dafür wurden Pitzer Parameter für  $\text{H}_4\text{SiO}_4$ ,  $\text{H}_3\text{SiO}_4$ ,  $\text{H}_2\text{SiO}_4^{2-}$  und  $\text{NO}_3^-$  aus der Literatur entnommen und in die entsprechende Datenbank eingefügt. Die Bildung von Mineralen im Entsalzungsprozess konnte bis zu hohen Ionenstärken bis auf eine Einschränkung vorausgesagt werden. Diese Einschränkung betrifft den metastabilen Zustand von wässrigen Elektrolytspezies wie der Kieselsäure. In den zum EDR-Konzentrat durchgeführten Berechnungen wurde für amorphes Siliciumdioxid ( $\text{SiO}_{2(\text{am})}$ ) stets eine Übersättigung berechnet und dieses dem System als Mineralausfällung entzogen.

Die Bildungsbedingungen von anorganischen Ausfällungen in der EDR Einheit wurden mittels Laborexperimenten untersucht. Experimente zur Bestimmung der Löslichkeit und dem Einfluss von Wachstumskeimen auf die Feststoffbildung belegten, dass die Polymerisierung von Kieselsäure in dem EDR-Konzentrat langsam verläuft. Die Bildung von  $\text{SiO}_{2(\text{am})}$  braucht Wochen bis Monate und die Oligomerisation von Kieselsäure ist sehr stark vom pH-Wert abhängig.

Messungen des Anteils an reaktiver Kieselsäure mit der Molybdängelb Methode ergaben, dass die Oligomerisation von Kieselsäure erst oberhalb von pH 4 innerhalb von wenigen Stunden stattfindet. Daher können die Ausfällung von  $\text{SiO}_{2(\text{am})}$  auf der Membranoberfläche oder die Verstopfung von Membranporen durch die Anlagerung von großen Oligomeren der Kieselsäure als Ursache von Membranverblockung ausgeschlossen werden.

Brucit ( $\text{Mg}(\text{OH})_2$ ) and Gips ( $\text{CaSO}_4 \times 2\text{H}_2\text{O}$ ) bilden die Hauptkomponenten der Ablagerungen auf den Oberflächen der Austauschermembranen. In diesen Ausfällungen nimmt der Siliciumanteil mit steigendem Magnesiumanteil in den Proben zu. Durch Korrosionsprozesse in der Pilotanlage enthält das EDR-Konzentrat geringe Anteile von Metallionen, die bevorzugt als Metall-Hydroxide ausgefällt werden, sobald der pH über 9,5 steigt. Dissoziierte Kieselsäure wird an diesen Oberflächen adsorbiert und so der Lösung entzogen. Daher kann die in situ Ausfällung von Hydroxiden durch die Zugabe von Natronlauge für einen vollständigen Entzug von Kieselsäure genutzt werden. Durchflusseperimente zeigten, dass die benötigte Menge NaOH von der Kieselsäurekonzentration, vom pH-Wert und von der  $\text{Mg}^{2+}$ -Konzentration in Lösung abhängt. Die minimal benötigte Menge an Natronlauge für den vollständigen Entzug von Kieselsäure aus dem EDR-Konzentrat wurde in den Experimenten bestimmt. In diesem Zusammenhang kommt der Position von Additiv und Konzentratzugabe im Reaktionsgefäß große Bedeutung zu, da diese die Effizienz des Entzugs stark beeinflussen.

Die geochemische Modellierung des Evaporationsprozesses wurde auf der Grundlage der Evaporationsexperimente beurteilt. In diesen Experimenten verdunsteten originales und im Labor hergestelltes EDR-Konzentrat unter kontrollierten klimatischen Bedingungen (konstante relative Luftfeuchte und Temperatur). Evaporationsrate, Dichte, pH, Ionenkonzentration und die Bildung von Mineralen wurden in Abhängigkeit vom Verdunstungsfortschritt bestimmt. Die Berechnungen des Sättigungszustandes der Minerale stimmten mit den Mineralausfällungen der Experimente bis zu hohen Ionenstärken überein. Allerdings trat durch die Kristallkeimbildung die tatsächliche Bildung von Mineralen in den Experimenten leicht verzögert im Vergleich zu den berechneten Sättigungszuständen auf.

Die Anwesenheit von Kohlendioxid in den Lösungen beeinflusst den pH-Wert während der Verdunstung der Salzlösungen signifikant oberhalb eines initialen pH-Wertes von 4,1. Ist zu Beginn der Evaporation  $\text{CO}_2(\text{g})$  in dem EDR-Konzentrat vorhanden, steigt der pH-Wert während der Verdunstung an. Enthält die Lösung kein  $\text{CO}_2(\text{g})$ , nimmt der pH leicht ab. Im Gegensatz dazu nimmt der pH unterhalb eines initialen Wertes von 4,1 mit fortschreitender Verdunstung kontinuierlich ab, was mit dem Neutralisierungsvermögen von Säure in der Salzlösung zusammenhängt. Der Äquivalenzpunkt des EDR-Konzentrats, an dem die Konzentration von  $\text{HCO}_3^-$  gleich der Konzentration von  $\text{H}^+$  ist, liegt bei pH 4,1.

# 1 Introduction

## 1.1 General outline

Dryland systems cover about 41% of the continents and are home to about 34% of the global population (Figure 1.1). While hyperarid and arid areas are characterised by an annual evaporation rate much greater than the total annual precipitation, semi-arid and dry subhumid regions are marked by low annual rainfall which is normally not predictable and highly variable.

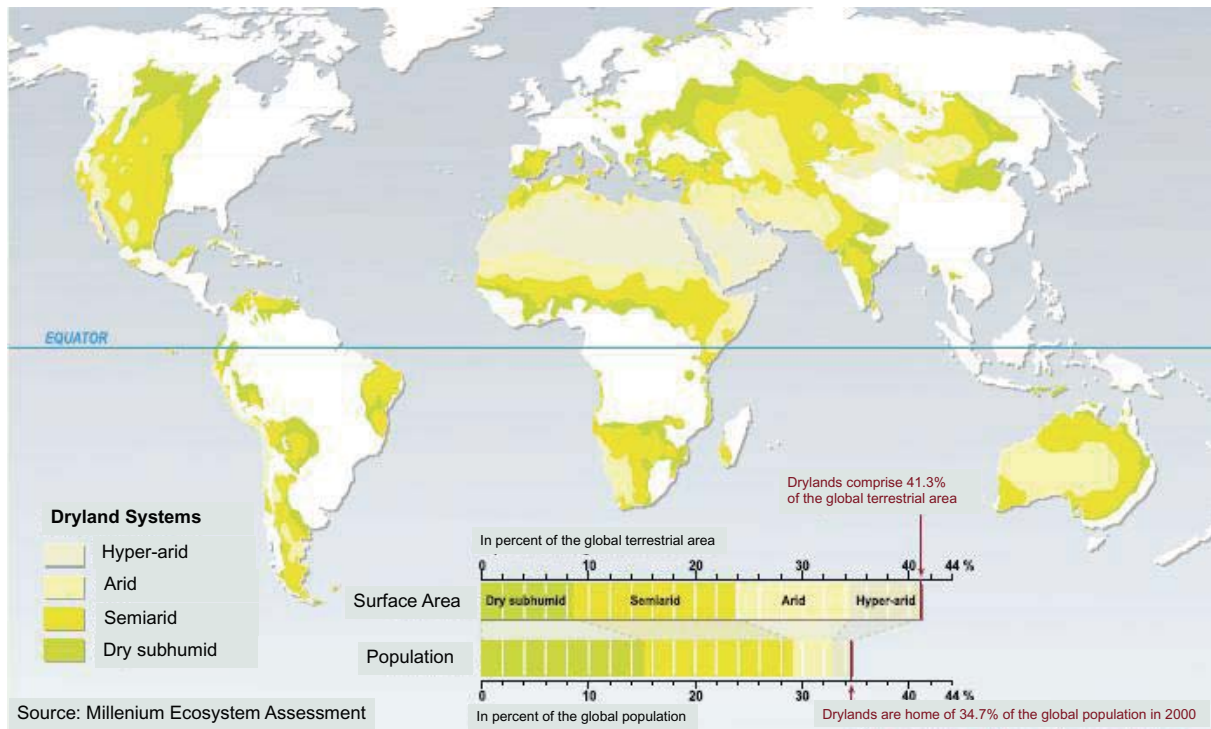


Figure 1.1: schematical illustration of terrestrial dryland systems **Notes:** The map is based on data from UNEP Geo Data Portal (<http://geodata.grid.unep.ch/>). Global area based on Digital Chart of the World data (147,573,196.6 square km); Data presented in the graph are from the MA core database for the year 2000.

Population growth and increasing settling in these low-moisture regions leads to the challenge to provide the inhabitants with potable water and water for domestic, agricultural and industrial use. Based upon local circumstances, several methods can be utilized for water recovery from additional resources. Deep wells or the use of cisterns can be a solution for a small group of people. Also reactivation of water treatment facilities of ancient cultures like the Nabataeans in Israel and Jordan can contribute to an ecological and sustainable use of rare natural water resources. However, such approaches cannot supply the water required for the infrastructure of a community. Seawater remains the biggest source of water for inshore regions but in remote areas it remains groundwater. For both sources the water must be purified to remove particulate matter and salt by filtration and desalination.

## 1.2 Desalination of water

In the last forty years desalination of water has become an important source for public water supply (Figure 1.2). Since 1970, the installed desalination capacity per year increased exponentially.

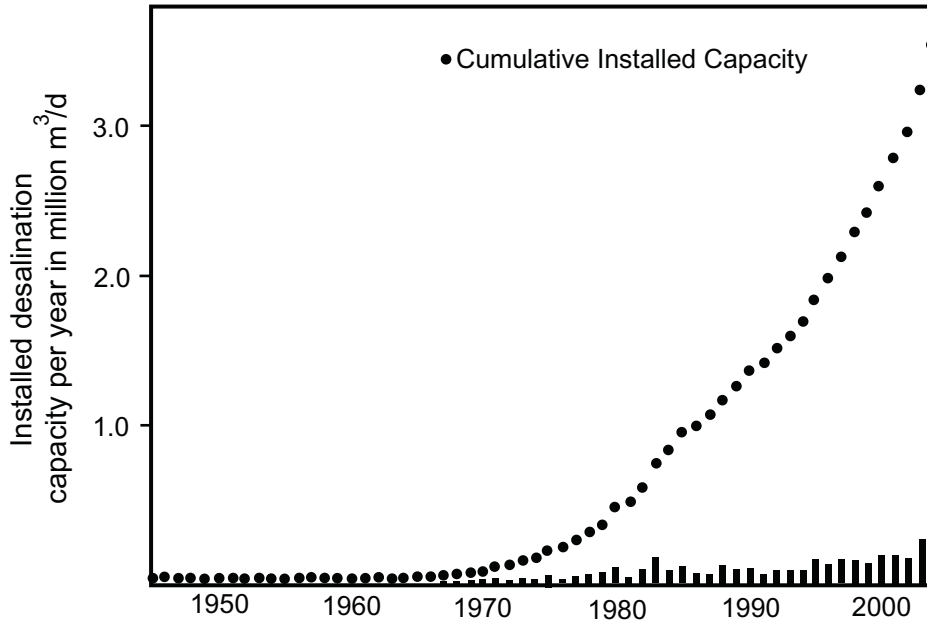


Figure 1.2: Worldwide newly installed desalination capacity from 1945 to 2004 (after Gleick, 2006)

Desalination of seawater and groundwater is based on different principles: On thermal techniques like multi-stage-flash evaporation, on pressure-driven membrane processes like reverse osmosis as well as on electrically driven separation processes like electrodialysis and on adsorption-driven processes like ion exchange. Application of these methods is dominated by treatment costs and depends on the raw water composition, local conditions and on the amount of water to be treated.

Seawater desalination plants like Ashkalon, Israel, produce approximately 11400 m<sup>3</sup>/h desalinated water (Einav and Lokiec, 2003). Further large seawater desalination plants are located in Fujairah in the United Arab Emirates (7100 m<sup>3</sup>/h), in Median/Yanbu in Saudi Arabia (5300 m<sup>3</sup>/h) and in Carboneras in Spain (5000 m<sup>3</sup>/h) (Kim et al., 2009). In Israel, the Ashkalon and Palmachim plants together produce 130 million m<sup>3</sup>/y demineralised water which covers 8% of the Israeli potable water demand. There are plans to enhance seawater desalination capacity to 500 million m<sup>3</sup>/a until 2015 (Dreizin et al., 2008). Seawater desalination produces a very large amount of desalinated water at comparatively low cost, however the transport especially to remote inland areas remains as an economic question.

### 1.3 Brackish water desalination in remote areas

Inland regions of arid areas need to use local water sources for water supply of the inhabitants. Gleick, 1996, pointed out that one percent of the world's water resources are brackish and slightly salty water in estuaries and groundwater in aquifers. These waters have a salinity between 1000 and 10000 mg/l TDS (Mickley, 2001 and Greenley et al., 2009).

In the last years great efforts were made to discover new groundwater sources in semi-arid and arid areas. Modern geophysical and drilling methods enable the detection and exploitation of these water bodies (Young, 2004). The biggest groundwater sources are water from deep aquifer, water lenses in depressions of rock formations which are episodically recharged by intense rainfall and enclosed fossil water bodies from the last glacial period (Allam et al., 2002 and Al-Jayyousi et al., 2001).

In most cases this groundwater must be demineralised before human consumption. For this purpose thermal distillation or membrane systems are the common measures (Van der Bruggen, 2003).

Since the 1980ies Reverse Osmosis (RO) is used in large scale for water desalination, particularly in combination with thermal plants (Van der Bruggen, 2003). Membrane technology is continuously developed to improve membrane quality; accordingly durability, flow rate, mechanical and chemical stability were advanced.

Today especially RO is an effective desalination method in comparison to thermal systems. Membranes which are used for water treatment in Electrodialysis (ED), Micro-, Nano- and Ultrafiltration (MF, NF and UF) are improved permanently (Van der Bruggen and Vandecasteele, 2002).

### 1.4 Concentrate disposal

During desalination of saline raw water, independent of the chosen method, pure water on one side (permeate), and salt concentrate on the other side are produced (Figure 1.3). Within the concentrate stream of desalination plants a huge amount of dissolved solids are persistent.

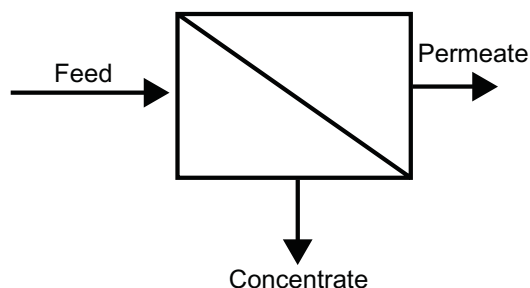


Figure 1.3: Reverse Osmosis: the feed water stream is divided by a pressure-driven membrane process into a permeate and a concentrate stream

Regarding the high salt content in these brines, the concentrate stream of desalination plants must be treated as waste and has to be disposed in an appropriate way. Costs of concentrate discharge of inland desalination plants at a distance larger than 80 km to the coast may constitute 15% of the total treatment costs (Gilron et al., 2003, Glueckstern and Priel, 1996).

For concentrate disposal several possibilities are manageable. Brines of seawater desalination are discharged to the sea. For plants, located at a large distance from the sea, other solutions have to be found. The most common methods for brine disposal are Surface Water Discharge and Sewer Disposal, Spray Irrigation Disposal, Deep Well Disposal, Evaporation Pond Disposal and Zero Discharge Disposal (Mickley, 2001). Only the last three of these methods might be applied in arid and semi-arid areas. Natural water bodies must be protected from contamination by the high salt content of the brines. The concentrates must not be disposed in deep wells or spray irrigation if there is danger to contaminate aquiferes or water lenses.

Evaporation Pond Disposal and Zero Discharge Disposal have both advantages and disadvantages. Evaporation Pond Disposal means disposal of concentrate in shallow but space consuming ponds where evaporation is driven by solar and wind energy (Figure 1.4). Evaporation rate decreases with increasing electrolyte concentration. As a result a complete evaporation of the brine cannot be reached. Hence, new evaporation ponds have to be built from time to time for maintaining a continuous operation of the desalination plant. Construction and restoration of these ponds are expensive. Additionally, the required space for these ponds is only available in sparsely populated areas.



Figure 1.4: Evaporation ponds of a Brackish Water Reverse Osmosis Plant (BWRO) in Israel near Ktziot, in close neighbourhood to greenhouses (Average area: 150 m x 800 m, depth ~1m), Photo: J. Scheiber (2008)

During Zero Discharge Disposal the concentrate is dewatered to an almost water free state by thermal methods. Advantages of this application are simple salt discharge by significant reduction of the concentrate volume which requires small areas. Concentrate discharge of a desalination plant can be carried out without liquid residues. Problems like salt water intrusion into the soil caused by pond leakage are minimized. The disadvantage of this method is the cost due to the high energy consumption.

Brine discharge in inland areas is the limiting factor of exploiting brackish water resources (Glueckstern and Priel, 1996). Improvements in Zero Discharge Disposal can be an important contribution to desalination. However, energy consumption has to be further minimized. An essential aim in improving this method is increasing the recovery rate of water for reducing the concentrate volume during the desalination process. Furthermore, the volume of the residual concentrate has to be decreased in an additional treatment to achieve nearly zero liquid drying of the brine.

## 1.5 Improvement of Zero Discharge Disposal: German - Israeli Cooperation Project

To achieve an improvement of Zero Discharge Disposal with respect to its energy consumption, a cooperation project, financed by the German BMBF (Bundesministerium für Bildung und Forschung (Ministry of Education and Research)) and the Israeli MOST (Ministry of Science and Technology) was carried out between 2006 and 2009.

### 1.5.1 Key activities of the Israeli cooperation partners

In Israel, the research group of Prof. Dr. Y. Oren designed and built a pilot plant at the Zuckerberg Institute of the University of Beer Sheva. Different membrane systems and a crystalliser were combined to increase water recovery rate. A “Wind Aided Intensified Evaporation” unit (WAIV) decreased the residual concentrate volume (Gilron et al., 2003). The main components of the pilot plant, operated by the Israeli group, are shown in Figure 1.5. It is described in detail by Oren et al., (2010).

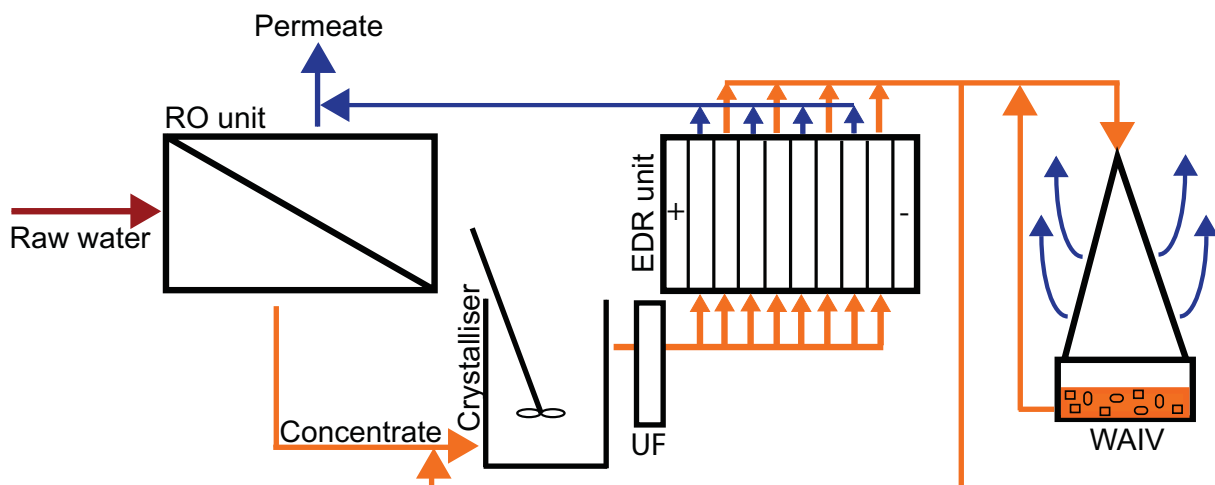


Figure 1.5: Simplified draft of pilot plant with the main units: Reverse Osmosis (RO), Crystalliser, Ultra-filtration (UF), Electrodialysis Reversal (EDR) and Wind Aided Intensified Evaporation (WAIV). Orange coloured lines mark the concentrate stream, blue lines mark the permeate stream.

Raw water is fed into a low pressure (10 bar) and thereafter into a higher pressure (20 bar) Reverse Osmosis Membrane Unit (RO). In this unit the feed is divided into a permeate and a concentrate stream. The RO concentrate is acidified to pH of 2 and treated in a crystalliser to remove gypsum. After passing the Ultrafiltration Membrane Unit (UF) where the precipitated gypsum crystals are held back, the concentrate enters the “Electrodialysis Reversal Membrane Unit” (EDR) for further desalination. Eventually the concentrate reaches the Wind Aided Intensified Evaporation Unit (WAIV) where it is dewatered to near zero liquid.

More detailed information about Reverse Osmosis (RO), Electrodialysis Reversal (EDR) and Wind Aided Intensified Evaporation (WAIV) is provided in **Appendixes A.1 to A.3**.

Desalination processes, using membrane systems, are limited in their water recovery by high concentration of electrolytes in the solutions. Here, the efficiency of the desalination processes is primarily limited by precipitation of sparingly soluble salts. Inorganic deposits lead to a decrease of the effective membrane surface and reduce the functionality of the membrane modules up to an inoperative state. Membrane scaling in desalination is the most important limiting factor for the recovery rate (Glueckstern und Priel, 1996). Several processes are responsible for membrane scaling: concentration of electrolytes in the brine, polarisation concentration, the excess of the solubility of sparingly soluble salts and precipitation of inorganic solids.

Dividing brackish water into permeate and brine leads to a concentration of the electrolytes in the brine. Additionally a concentration gradient on the membrane surface is generated by the separation process. In RO, MF, NF and UF pressure differences and in EDR the electric potential differences lead to concentration polarisation.

In the RO unit of the pilot plant the concentrate is pressed against the membrane. Diffusion of water molecules through the membrane results in a depletion of water in the feed solution. This evolves to a locally higher electrolyte concentration on the membrane surface compared to the total concentrate. During the desalination process the whole feed solution gets more & more concentrated.

Within the EDR unit the electrical potential is the driving force of the separation process. The electrolytes pass the membranes from the permeate to the concentrate channels traverse the respective exchanger membranes. Diffusion of electrolytes to the electrodes is stopped at the next contrary exchanger membrane. Within the concentrate channel the positive and negative ions are separated from each other caused by the electrical potential. To avoid this kind of concentration on the membrane surfaces the unit is operated with a continuous flow and the electrical poles are reversed at regular times.

Increasing concentration of electrolytes can exceed the solubility of sparingly soluble salts like Calcite ( $\text{CaCO}_3$ ), Gypsum ( $\text{CaSO}_4 \times 2\text{H}_2\text{O}$ ) and amorphous Silica ( $\text{SiO}_{2(\text{am})}$ ). As mentioned be-

fore, this affects the membrane permeability which is reduced by precipitation and accretion of salts on the membrane surface and in the membrane pores.

Mineral saturation of sparingly soluble salts limits of the maximum electrolyte concentration in the brine. Therefore, the maximum recovery rate in water desalination is governed by the electrolyte composition of the raw water and the electrolyte concentration factor of the applied method. In the case of the pilot plant brackish water from a fossil water lens is fed into the membrane units. Desalination of brackish groundwater means dealing with electrolyte compositions quite different from the well known seawater system.

### 1.5.2 Key activities of the German cooperation partners

In Germany, at the Karlsruhe Institute of Technology (KIT), Campus North, in the group of Dr. P.G. Weidler, theoretical investigations on the solubility of minerals generated during the desalination process were to be carried out. For this purpose, both saturated and undersaturated conditions needed to be calculated and precipitates characterised. Causes of these precipitations needed investigations. Furthermore, the best practical method for avoiding inorganic deposits within the membrane units had to be found and developed.

Regarding these investigations the geochemistry of the process brines has to be considered. Beside the procedural impact on the chemical equilibrium of the process solutions, the concentration of the feed stream of each membrane unit influences particularly mineral saturation of sparingly soluble salts. The mineral saturation state is mainly affected by salt concentration as well as by ionic charge and size of the ion species. Electrostatic interactions between the electrolytes changes the active concentration of every ion species which can deviate from the total concentration. For a controlled intervention in the chemical processes during desalination of raw water, equilibrium state of the solutions of high salinity at every process step must be known. Therefore, it is essential to understand the chemical reactions in each of the membrane units during the desalination.

## 1.6 Objective of Work

On the background of the key activities of the German part of the cooperation project the specific objectives of this work were as follows:

The first objective was to develop a tool for the reliable prediction of the mineral saturation state in the process concentrate. Prediction of mineral precipitation requires accurate information of the mineral saturation state of the process brines. For this project the modelling program *The Geochemist's Workbench 6.0* (GWB) should be used and its ability to calculate activity coefficients, chemical equilibrium and mineral saturation of the various process solutions should be

tested. Furthermore, the transfer of results from these theoretical calculations to the real process concentrates and their mineral saturation should be tested by comparing experimental with calculated data.

The second objective was the characterisation of the inorganic deposits on the membrane surface of the EDR unit of the pilot plant and investigations regarding their formation conditions. Based on detailed examinations of the scaling process measures of its prevention should be suggested.

The third objective was the compilation of a database for the evaporation of the EDR concentrate. Until the start of the cooperation project in 2006 experiments in the WAIV unit were done with synthetic single salt solutions only (Gilron et al., 2003). To overcome this limitation calculations of the mineral saturation in linear processes like the complete evaporation of EDR concentrate at different evaporation steps should be worked out. For validation of the GWB calculations the results from laboratory experiments had to be compared with the theoretical results. Therefore, evaporation rate in dependence of humidity had to be investigated under constant conditions in a climate chamber.

## 2 Material and Methods

### 2.1 Material

For the investigation of the formation conditions in the EDR unit, original inorganic deposits, precipitated on the membrane surfaces of the anion and cation exchanger membrane, as well as original brine of the pilot plant and synthetic laboratory concentrates were used. For evaporation experiments original brine and synthetic concentrates were utilized.

#### 2.1.1 Original concentrates of the pilot plant and their formation

Original EDR concentrate was used for precipitation, adsorption and evaporation experiments. For better understanding of the formation and consequentially of the composition of the EDR concentrate, a short overview of the desalination process and the resulting composition of the concentrates, produced by desalination and evaporation is given in Figure 2.1. The desalination process itself was described in Chapter 1.5.1. Brackish water from a fossil water lens in the SW of Israel is desalinated in the pilot plant and dried to near zero liquid by evaporation.  $\text{Na}^+$  and  $\text{Cl}^-$  are the main electrolytes of the feed water, followed by  $\text{SO}_4^{2-}$ ,  $\text{HCO}_3^-$ ,  $\text{Ca}^{2+}$  and  $\text{Mg}^{2+}$ . Remarkably high amounts of 35 mg/kg silicic acid ( $\text{H}_4\text{SiO}_4$ ), 24 mg/kg  $\text{K}^+$  and 6 mg/kg  $\text{Sr}^{2+}$  were detected (Table 2.1).

The **Feed Water** becomes desalinated in two steps. The first step takes place in the RO unit where raw water is concentrated from a salinity of nearly 3100 mg/l TDS to around 15200 mg/l. This **RO concentrate** is acidified with nitric acid to a pH of 2 and fed into the EDR unit (first circle).

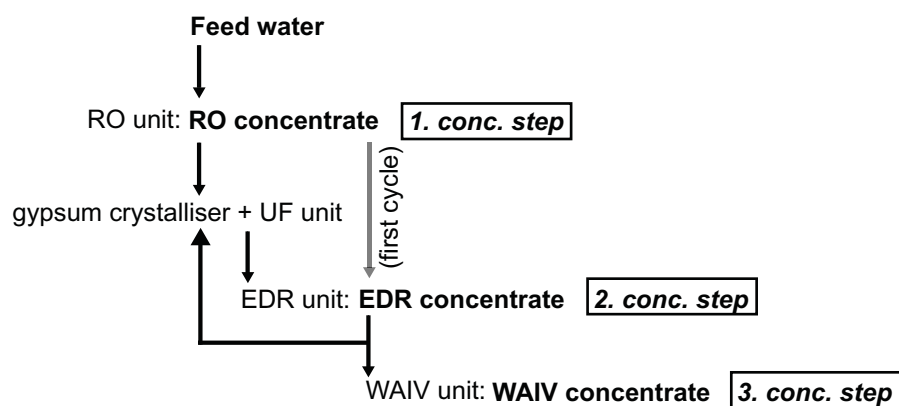


Figure 2.1: Outline of the process steps and the produced concentrates within the pilot plant

After passing this unit EDR concentrate stream is splitted into two streams. One part of the concentrate is mixed with RO concentrate, the other part is fed into the WAIV unit. The mixture of RO and EDR concentrate is treated in the gypsum crystalliser to keep  $\text{Ca}^{2+}$  and  $\text{SO}_4^{2-}$  concen-

tration on a constant level to avoid precipitation of gypsum within the EDR unit. During desalination of this RO/EDR concentrate mixture within the EDR unit, the TDS of the **EDR concentrate** rises to 82000 mg/l. One fraction of this concentrate is fed into the WAIV unit, where the volume of the EDR brine is reduced significantly to **WAIV concentrate** by evaporation. Composition and electrolyte concentration of the feed water and the process concentrates, produced during desalination and evaporation are given in Table 2.1.

Table 2.1: Composition of the main aqueous solutions of the pilot plant

	Feed Water		RO concentrate		EDR concentrate		WAIV concentrate <sup>a</sup>	
	mg/l	mg/kg	mg/l	mg/kg	mg/l	mg/kg	mg/l	mg/kg
<b>Cations</b>								
Na <sup>+</sup>	700	694	3419	3426	29888	31266	92702	106212
Ca <sup>2+</sup>	206	204	1047	1049	1773	1852	3089	3539
Mg <sup>2+</sup>	118	117	477	478	2734	2844	19234	22045
K <sup>+</sup>	24	24	86	87	569	594	3417	3909
Sr <sup>2+</sup>	6	6	26	26	130	134	164	188
<b>Anions</b>								
Cl <sup>-</sup>	1216	1251	6715	6730	52009	56370	195096	236824
SO <sub>4</sub> <sup>2-</sup>	533	527	2685	2690	5788	6042	2112	2421
H <sub>4</sub> SiO <sub>4</sub> <sup>b</sup>	35	35	164	164	177	185	n.d <sup>c</sup>	n.d.
NO <sub>3</sub> <sup>-</sup>	< 0.3	< 0.3	2	2	67	70	422	484
HCO <sub>3</sub> <sup>-</sup>	270	267	533	535	n.d	n.d	n.d	n.d
F <sup>-</sup>	1	1	5	5	19	19	72	72
<b>minor electrolytes</b>								
Fe <sup>2+</sup>	< 0.02	< 0.02	< 0.01	< 0.01	0.17	0.17	n.d.	n.d.
Mn <sup>2+</sup>	< 0.02	< 0.02	< 0.01	< 0.01	< 0.03	< 0.03	n.d.	n.d.
Ba <sup>2+</sup>	0.1	0.1	0.36	0.36	0.20	0.20	n.d.	n.d.
Al <sup>3+</sup>	< 0.08	< 0.08	0.24	0.24	0.38	0.38	n.d.	n.d.
pH	8		7.3		2		<1	
density in g/cm <sup>3</sup>	1.014		1.018		1.053		1.201	
TDS in mg/l	3111		15163		82257		316308	

a. after 48 h of evaporation

b. amount of silicic acid is calculated from Si concentration, measured by ICP-OES

c. n.d.: not determined

To ease the comparison of the various brine compositions, the increasing amount of every single electrolyte is expressed by the concentration factor (CF). The CF is calculated by the division of the amount of a single electrolyte within a higher concentrated brine by the amount of this electrolyte in a lower concentrated one. The CF of the main electrolytes for every concentration step are noted in Table 2.2.

Table 2.2: Concentration factor (CF) of the main electrolytes for the single desalination steps

	1. conc. step RO/FW	2. conc. step EDR/RO	3. conc. step WAIV/EDR	total concentration WAIV/FW
<b>Cations</b>				
Na <sup>+</sup>	4.9	9.2	3.4	153
Ca <sup>2+</sup>	5.1	1.8	1.9	17
Mg <sup>2+</sup>	4.1	6.0	7.8	192
K <sup>+</sup>	3.6	6.9	6.6	164
Sr <sup>2+</sup>	4.5	5.3	1.4	33
<b>Anions</b>				
Cl <sup>-</sup>	5.0	8.9	4.2	187
SO <sub>4</sub> <sup>2-</sup>	5.1	2.3	0.4	5
H <sub>4</sub> SiO <sub>4</sub>	4.8	1.1	n.m. <sup>a</sup>	-
NO <sub>3</sub> <sup>-</sup>	6.7	35.1	6.9	1620
HCO <sub>3</sub> <sup>-</sup>	2.0	n.m. <sup>a</sup>	n.m. <sup>a</sup>	-

a. n.m.: not measured

Within the first concentration step, where feed water is desalinated in the RO unit, the CF of most electrolytes in solution is around five. A fraction of the hydrogen carbonate ions diffuse through the membrane into the permeate which results in a CF of 2. For K<sup>+</sup> and Mg<sup>2+</sup> the CFs are lower than those of the other electrolytes which may be caused by diffusion of these ions into the permeate. The CF of the electrolytes in the EDR unit during the second desalination step varies more than in the RO unit. As mentioned before, several parameters are adjusted before feeding the RO concentrate into the EDR stack. The parameters and their influence on the concentration of the single electrolytes are explained in detail in the following paragraph.

First the RO concentrate is acidified with nitric acid to a pH of 2 which leads to the high CF of around 35 for NO<sub>3</sub><sup>-</sup>. After pH adjustment the RO concentrate passes the gypsum crystalliser where Ca<sup>2+</sup> and SO<sub>4</sub><sup>2-</sup> concentrations are kept constant by continuous precipitation of gypsum. CFs of Ca<sup>2+</sup> and SO<sub>4</sub><sup>2-</sup> are close to 2. Calcium ions are partially substituted by Sr<sup>2+</sup> in the gypsum crystals, therefore, the CF for Sr<sup>2+</sup> is 5.3. The average CF for Mg<sup>2+</sup> and K<sup>+</sup> in the EDR stack is around 6. These electrolytes are not affected by the crystalliser and pH adjusting. CF of silicic acid is nearly constant. The separation process of electrolytes within the EDR unit is driven by electric potential differences. Therefore, the uncharged monomer (H<sub>4</sub>SiO<sub>4</sub>) does not pass the exchanger membranes. As a consequence, every EDR membrane channel contains the same amount of silicic acid in the outflow as at the inflow. Hence, the EDR permeate contains nearly 165 mg/l H<sub>4</sub>SiO<sub>4</sub>.

To prevent silica scaling in the EDR unit, the EDR feed (RO concentrate) is adjusted to a constant concentration of silicic acid by adding raw water. This leads to a dilution of the whole concentrate. Furthermore, the brine is pumped in a cycle of **EDR unit - gypsum crystalliser / UF unit - EDR unit**, so it passes the EDR stack more than once before it is excluded from the de-

salination process. The CF of  $\text{Na}^+$  and  $\text{Cl}^-$  of nearly 9 is much higher than for the other main electrolytes in solution. This difference is caused by the preparation of the gypsum seeds in the crystalliser by adding calcium chloride ( $\text{CaCl}_2$ ) and sodium sulfate ( $\text{Na}_2\text{SO}_4$ ). While the main fraction of  $\text{Ca}^{2+}$  and  $\text{SO}_4^{2-}$  is removed by gypsum precipitation  $\text{Na}^+$  and  $\text{Cl}^-$  remain in the solution which leads to an increase of the total  $\text{Na}^+$  and  $\text{Cl}^-$  concentration.

Within the WAIV unit, the CF of the electrolytes depends on evaporation rate as well as on precipitation of various salts during the evaporation.

### 2.1.2 Synthetic laboratory concentrates

Synthetic laboratory concentrates were utilized in most of the experiments. Electrolyte composition and concentration are based on the EDR concentrate whereas only the main electrolytes were considered. Table 2.3 represents the reference values of the EDR concentrate in molal units, which were chosen to simplify the comparison between the experimental results and the theoretical calculations.

Table 2.3: Composition of synthetic concentrates based on the original EDR brine

	electrolyte concentration in mg/kg	electrolyte concentration in mmol/kg
<b>Cations</b>		
$\text{Na}^+$	31266	1360.0
$\text{Ca}^{2+}$	1852	46.2
$\text{Mg}^{2+}$	2844	117.0
$\text{K}^+$	594	15.2
$\text{Sr}^{2+}$	134	1.5
<b>Anions</b>		
$\text{Cl}^-$	56370	1590.0
$\text{SO}_4^{2-}$	5042	62.9
$\text{NO}_3^-$	70	1.1
$\text{H}_4\text{SiO}_4$	variable <sup>a</sup>	variable

a. c of silicic acid depends on the experimental setup

The composition of the synthetic salt concentrates depends on the problem and the respective experiment. Therefore, single salt systems as well as more complex salt solutions were utilized. Table 2.4 presents a compilation of the applied synthetic concentrates. Concentration of the electrolytes are related to the question of interest and are described in detail in the experimental part of Chapter 4.3.2.

Table 2.4: Composition of the applied synthetic concentrates. The combination and concentration of the single electrolytes depends on the experiment setup and the question of interest

	Composition of the applied synthetic concentrates								
	Na <sup>+</sup>	Ca <sup>2+</sup>	Mg <sup>2+</sup>	K <sup>+</sup>	Sr <sup>2+</sup>	Cl <sup>-</sup>	SO <sub>4</sub> <sup>2-</sup>	SiO <sub>2</sub>	NO <sub>3</sub> <sup>-</sup>
comp. 1	-	-	+	-	-	+	-	+	-
comp. 2	+	-	+	-	-	+	-	+	-
comp. 3	+	+	+	-	-	+	-	+	-
comp. 4	+	+	-	-	-	+	+	+	-
comp. 5	+	+	+	-	-	+	+	+	-
comp. ED/RO	+	+	+	+	+	+	+	+	+

## Chemicals

Various inorganic salts from Merck with PA (pro analysi) quality were used for the production of the synthetic concentrates: sodium chloride (NaCl), sodium sulfate (Na<sub>2</sub>SO<sub>4</sub>), strontium hydroxide octahydrate (Sr(OH)<sub>2</sub> × 8H<sub>2</sub>O), potassium chloride (KCl), magnesium chloride hexahydrate (MgCl<sub>2</sub> × 6H<sub>2</sub>O), calcium chloride dihydrate (CaCl<sub>2</sub> × 2H<sub>2</sub>O), nitric acid (HNO<sub>3</sub>, 65%), hydrochloric acid (HCl, 25%) and caustic soda (NaOH, 2M). Deionised water (DIW) was produced by a Millipore Milli-Q<sub>plus</sub> system with 18.2 MΩ.

## Laboratory equipment

To avoid changes in the concentration of the silicic acid in contact with glass dishes, solely plastic beakers and plastic bottles were used for production and storage of the synthetic concentrates.

## Procedure

Fabrication of the synthetic EDR brine, which is the most complex concentrate used for the experiments, is described in detail. During this procedure precipitation of sparingly soluble salts must be avoided. Concerning the influence of background electrolytes and the pH on the solubility of minerals, chemicals have to be added in a strict order (**Table 2.5 (1) to (13)**).

DIW and Si-stock solution were mixed in a plastic beaker (**(1) and (2)**). The solubility of amorphous silica decreases significantly by increasing salt concentration. To avoid the formation of SiO<sub>2(am)</sub> by adding the huge amount of sodium chloride, the pH is adjusted to a value ~12 with caustic soda (**3**) where silicic acid is soluble, independent of the NaCl concentration. Thereafter, sodium sulfate and nitric acid (**(4), (5) and (6)**) are added to the solution. The pH is adjusted with hydrochloric acid to pH < 9 (**7**). At higher pH the divalent ions Sr<sup>2+</sup> and Mg<sup>2+</sup> would form sparingly soluble hydroxides. Strontium hydroxide octahydrate and potassium chloride were added (**(8) and (9)**). Before adding the magnesium salt, the pH must be adjusted to a pH value slightly above the expected initial pH with 2M NaOH (**10**). Magnesium chloride hexahydrate and calcium chloride dihydrate are dissolved in the solution (**(11) and (12)**). The solubility of gypsum increases by increasing background electrolyte concentration. Therefore, the calcium salt must

be added during the final step to avoid precipitation of gypsum. In the presence of magnesium ions pH adjustment is allowed by the addition of hydrochloric acid only (**13**), caustic soda must not be added to avoid precipitation of brucite ( $\text{Mg}(\text{OH})_2$ ).

Table 2.5: mixing order of chemical products to produce an synthetic EDR concentrate with an initial  $\text{SiO}_2$  concentration of 100 mg/kg

sequence	chemical product	amount in g, respectively in ml	comments
1	$\text{H}_2\text{O}$ (DIW)	900	water + Si-stock solution = 1000g
2	Si-stock solution <sub>(l)</sub>	100	
3	$\text{NaOH}_{(s)}$	1.65	pH adjusting ~12
4	$\text{NaCl}_{(s)}$	69.42	
5	$\text{Na}_2\text{SO}_4_{(s)}$	8.93	
6	$\text{HNO}_3_{(l)}$ (65%)	0.11	
7	$\text{HCl}_{(l)}$ (25%)	6	pH adjusting < 9
8	$\text{Sr}(\text{OH})_2 \times 8\text{H}_2\text{O}_{(s)}$	0.41	
9	$\text{KCl}_{(s)}$	1.13	
10	$\text{NaOH}_{(l)}$ (2M)	v.v. <sup>a</sup>	final pH + 0.5 - 0.7
11	$\text{MgCl}_2 \times 6\text{H}_2\text{O}_{(s)}$	23.85	addition of the Mg salt at a pH < 9
12	$\text{CaCl}_2 \times 2\text{H}_2\text{O}_{(s)}$	6.79	
13	$\text{HCl}_{(l)}$	v.v.	final pH

a. v.v.: variable volume: depends on the final pH value of the experiment

### 2.1.3 Stock solution of silicic acid

The amount of silicic acid in the synthetic concentrates was varied to simulate undersaturated, saturated and oversaturated salt solutions with respect to amorphous silica. Therefore, a Si-stock solution of 1000 mg/l  $\text{SiO}_2$  was prepared. Likewise small and large amounts of silicic acid, which are required for undersaturated and saturated concentrates are easily to dose.

#### Chemicals

Sodium metasilicate nonahydrate ( $\text{Na}_2\text{SiO}_3 \times 9\text{H}_2\text{O}$ ) from Sigma Aldrich was used as Si source.

#### Laboratory equipment

Solely beakers, volumetric flasks and storage bottles made of plastic were used.

#### Procedure

A 1 l volumetric plastic flask is filled to three fourths with DIW. 4.73 g of sodium metasilicate nonahydrate ( $\text{Na}_2\text{SiO}_3 \times 9\text{H}_2\text{O}$ ) is weighed in a plastic beaker, material is flushed with DIW to the volumetric flask and stirred for 20 min. with a magnetic stirrer. After removing the magnetic stir bar the volumetric flask is filled up to one litre and manually shaken for mixing. Afterwards the solution is filtered through a 0.2  $\mu\text{m}$  Sartorius polyamide membrane filter by sub-pressure

filtration and stored in a plastic bottle. Each Si-stock solution was controlled by ICP-OES measurement.

#### 2.1.4 Synthetic seeding and adsorption material

Synthetic seeding materials were applied in solubility and adsorption experiments.

##### **Chemicals**

As seeding material solid silicic acid ( $\text{SiO}_2$ , precipitated, extra pure, light) purchased from Merck was utilized. For adsorption experiments brucite ( $\text{Mg}(\text{OH})_2$ ) and seasand ( $\text{SiO}_2$ , calcined and acid washed) from Merck, both pro analysi quality, were used as well as natural hydrotalcite ( $\text{Mg}_6\text{Al}_2(\text{CO}_3)(\text{OH})_{16} \times 4\text{H}_2\text{O}$ ) purchased from Südchemie. Furthermore, the technical product Circosil with a high amount of tobermorite ( $\text{Ca}_5[\text{Si}_3\text{O}_8(\text{OH})]_2 \times 3.5\text{H}_2\text{O}$ ) from Cirkel was utilized.

## 2.2 Methods

Sample analysis depends on the sample state, solid or liquid, as well as on the question of interest of the experiment. Elemental and mineral analysis by X-ray fluorescence, X-ray diffraction and thermogravimetric analysis as well as investigations of the aggregate state by light microscopy and electron microscopy were conducted at solid samples. For geochemical characterisation of the original brines and synthetic laboratory concentrates ion chromatography, photometric measurements, inductively coupled plasma - optical emission spectroscopy and pH measurements were applied.

### 2.2.1 Methods of solid samples analysis

#### 2.2.1.1 X-Ray Diffraction (XRD)

Solid, dry powdered samples were investigated by X-ray diffraction to identify crystalline components within the sample material.

##### **General principle**

Crystals are chemically homogeneous materials, which possess a strict order of ions and atoms in three dimensions. Electron shells of these ordered atoms and ions can interact with incident electromagnetic radiation of X-rays in a specific form of reflection. This diffraction of X-rays can be only observed under a specific geometric alignment of X-ray source and sample, when incident monochromatic X-rays are scattered at the electron shells and the reflected electromagnetic waves overlay each other in a constructive way. The diffraction is detected in dependence of the incidence angle, where every detected diffraction represents one lattice plane of the crystal. Due to Bragg's Law the distance between two identical lattice planes can be calculated:

$$n\lambda = 2d \sin\theta \quad (2-1)$$

n: integer, order of the diffraction

$\lambda$ : wavelength of the incident monochromatic X-ray beam (constant)

d: lattice spacing, distance of the lattice planes (unknown)

$\sin \theta$ : angle of diffraction (known)

Due to the specific structure of crystals very specific diffraction patterns can be detected, in dependence of structure and chemical composition of the respective crystals. By comparison of the detected diffraction patterns of unknown and/or multicomponent materials with a diffraction pattern database, the crystalline compounds can be identified.

### **Setup**

Powder samples were analysed by using a Siemens D5000 X-ray diffractometer, Bragg-Brentano-alignment, using a graphite secondary monochromator and  $\text{CuK}\alpha_1$  radiation of  $\lambda = 1.5406$  Å at 40kV and 40A. Diffraction patterns of original precipitates of the pilot plant were recorded in the range of  $2 - 80^\circ 2\theta$  (step size  $0.02^\circ 2\theta$ , step time 3s). Precipitates, produced by laboratory experiments were recorded in the range of  $5 - 65^\circ 2\theta$  (step size  $0.02^\circ 2\theta$ , step time 4s). Qualitative evaluation of the diffractograms was conducted by using the software *Diffra<sup>plus</sup>* 10.0 of Bruker AXS.

### **Sample preparation**

Precipitates were dried at room temperature, pulverized and homogenised manually in a mortar. The powder was filled in a plain sample holder and carefully compressed with a glass disk, to avoid preferred orientation. The sample was placed directly after preparation in the sample changer of the D5000.

#### **2.2.1.2 Energy-dispersive and wavelength-dispersive X-Ray Fluorescence (ED-XRF, WD-XRF)**

X-ray fluorescence analysis was applied for characterisation of the elemental composition of precipitates formed on membrane surfaces as well as during titration experiments.

### **General principle**

X-rays, interacting with electrons of the inner shells of atoms may transfer electrons to an excited state. By falling back to the ground state, the energy difference between these two states is emitted in form of a photon. The reachable excited state and, in the broader sense, the energy difference between excited and ground state is fixed on one hand by the stimulation energy, as well as the energy ground state of the electron itself. Every electron transfer to an excited state requires a specific energy input and results likewise in a specific energy emission by refilling the vacancy. This emitted energy varies significantly between the elements. By measuring the emitted energy (ED-XRF) or the wavelength (WD-XRF) of the emitted photons, the elemental composition of an unknown sample can be identified.

Within an X-ray tube electrons are shot at high velocity on a metal target. Interaction between impinged electrons and electron shells of the metal target atoms leads to the emission of X-rays. On one hand nearly monochromatic X-ray radiation of high intensity, and on the other hand a broad range of polychromatic X-ray radiation of lower intensity, bremsstrahlung, is emitted from the target material. Every emitted wavelength represents a specific energy. The emitted polychromatic X-ray radiation of high and low intensity of the target material is focused on the sample where photons interact with the solid matter and activate typical fluorescence radiation. In WD-XRF, the emitted fluorescence radiation of the sample is focused on detector crys-

tals, cut to a defined lattice plane. By stepwise variation of the geometric alignment of the crystal, the required wavelength (respectively energy) for diffraction are calculated from the Bragg-equation (2-1, p. 20), where  $\sin \theta$  is known,  $d$  remains constant and  $\lambda$  is detected.

### **Setup**

A MagiXPRO spectrometer from Philips was used for quantitative XRF analysis. The device was equipped with a 3.2 kW rhodium X-ray tube. Preparation of the melting pellets and conduction of the measurements were carried out in an external laboratory, specialised on quantitative elemental analysis.

Qualitative elemental analysis of precipitates was performed on a Bruker AXS S4 PIONEER as well as by EDX analysis on the Siemens electron microscope, see Chapter 2.2.1.4.

### **Sample preparation**

Samples for quantitative and qualitative analysis were dried at room temperature and manually ground to a fine powder in a mortar. Loss on ignition (LOI) was determined after heating the samples up to 1000°C, thereafter, samples were ground a second time.

For qualitative measurements of pure sample powder, ~ 5 mg was attached to a carbon sample holder for ESEM/EDX. For qualitative WD XRF measurement approximately 50 mg of the powder was clamped between two films.

For quantitative measurements samples were mixed with lithium tetraborate, Spectromelt 10 from Merck, and pellets were melted in platinum crucibles in a Vulcan 4MA, HD Electronic smelting apparatus.

#### 2.2.1.3 Optical Microscopy

##### **Setup Cations**

The optical microscope SteReo Discovery V.12 from Zeiss was used for visual inspection of the precipitates. Photographs of the deposits were made with the corresponding camera and software system.

##### **Sample preparation**

Precipitates were dried at room temperature. Particles were prepared on millimetre paper, precipitates, adhering on membrane surfaces were investigated directly on the exchanger membrane.

#### 2.2.1.4 Environmental Scanning Electron Microscopy (ESEM)

Deposits from exchanger membranes of the EDR unit were examined by Environmental Scanning Electron Microscopy (ESEM) to investigate surface topology, size and elemental composition of the different precipitates.

**General principle**

Environmental Scanning Electron Microscopy (ESEM) allows the examination of uncoated samples in a sample chamber at low water vapour pressure (1 Torr, this investigation). A focused electron beam is emitted from a metal needle and is focused by electromagnetic lenses on the sample surface. These electrons interact with the sample material causing the emission of electrons. Thereafter, a fraction of electrons is emitted as secondary electrons (SE), another fraction is backscattered (BSE). The atmosphere of water vapour in the sample chamber is used to amplify the scattered electrons on their way to the detector. A thin liquid film on the surface of the sample provides the material of charge overload by the electron beam. The incident beam of electrons stimulates the emission of X-ray fluorescence from the sample. The emitted X-rays consist of specific wavelengths, thereafter specific energies, which provides semi-quantitative information on the elemental composition of the sample. This radiation is detected by an energy-dispersive detector system (EDX).

**Setup Cations**

The device ESEM XL 30 FEG from Philips, equipped with an EDAX system was used for investigations by electron microscopy. The primary electron beam was emitted at 20 keV, water vapour pressure in the sample chamber was set to 1 Torr.

**Sample preparation**

Small amounts of powder samples were attached to a carbon foil sample holder. For examination of the samples with ESEM no further surface preparation of the samples like coating with metals or carbon was required due to the special water vapour pressure in the sample chamber.

**2.2.1.5 Thermogravimetric Analysis (TGA) and Simultaneous Differential Thermal Analysis (SDTA)**

Thermogravimetric analysis was conducted on one hand to determine the loss on ignition for XRF analysis, on the other hand it was used in combination with single differential thermal analysis to obtain information on the mineralogical composition of the precipitates, produced by titration experiments.

**General principle**

Weight loss of samples as a function of temperature and time is detected by thermogravimetric analysis. Decomposition of solid as well as liquid samples, caused by the loss of water, of hydroxyl groups, of carbon dioxide or sulphur dioxide can be detected and quantified by the decrease of sample weight within the respective temperature range of the decomposition reaction. Especially the decomposition of crystalline compounds manifests itself within a spe-

cific temperature range. In addition, simultaneous differential thermal analysis of endothermic and exothermic reactions of the samples caused by decomposition and/or rearrangement as well as oxidation of sample material can be determined by recording the difference between sample temperature and reference temperature of an inert material.

Main components of thermogravimetric devices are thermobalance, sample holder and furnace. The measurement procedure remains in most cases quite similar. A small amount of the sample is filled into an inert crucible. Most common crucibles are made of aluminium, aluminium oxide or platinum. This crucible is placed on the sample holder of the thermobalance and heated in a defined gas atmosphere to a maximum temperature. Linear increase of the temperature with a few degrees per minute is the most frequently applied method, but also statical stages can be included in heating sequences.

### **Setup**

The device Mettler Toledo TGA/SDTA851<sup>e</sup> combines thermogravimetric analysis (TGA) and simultaneous differential thermal analysis (SDTA). Samples are inserted at a temperature of 30°C and heated with a rate of 10°C/min to a maximum temperature of 1000°C. Crucibles and caps, used for all measurements, were made of aluminium oxide. The oven temperature acts as reference temperature, whereas sample temperature is measured at the platinum/rhodium sample holder. Before measuring the sample, an empty aluminium oxide crucible was measured as blank value which is subtracted from every sample measurement. The same crucible, used for measuring the blank was utilized for measurement of the sample. For evaluation of the detected thermograms, the Stare Software Stare Default DB V9.00 provided by Mettler Toledo was used.

TGA accuracy:  $\pm 0.25^\circ\text{C}$ , resolution: 1 $\mu\text{g}$ , noise:  $>_1\mu\text{g}$

SDTA accuracy:  $0.005^\circ\text{C}$ , noise:  $0.01^\circ\text{C}$  10values/sec.

### **Sample preparation**

Samples were dried at 30°C before inserting into the TGA/SDTA device. Synthetic materials from Merck (gypsum, brucite) consists of fine powder, no grinding was necessary for sample preparation. Precipitates, produced in laboratory experiments were dried at 30°C and carefully ground manually in an agate mortar for less than 1 min. Nearly 50mg of the powder was filled into the 70  $\mu\text{l}$  aluminium oxide crucibles.

## 2.2.2 Methods of liquid sample analysis

### 2.2.2.6 Ion Chromatography (IC)

Determination of cation ( $\text{Na}^+$ ,  $\text{K}^+$ ,  $\text{Mg}^{2+}$ ,  $\text{Ca}^{2+}$ ,  $\text{Sr}^{2+}$ ) and anion ( $\text{Cl}^-$ ,  $\text{NO}_3^-$ ,  $\text{SO}_4^{2-}$ ) concentration in original and synthetic brines was conducted by ion chromatography (IC).

#### **General principle**

This method relies on ion exchange processes on specific cation or anion exchangers in aqueous solution. Usually resins with functional surface groups are used for IC. On these surface groups coions are adsorbed and can be exchanged for counterions contained in the solvent. Ion charge is an important driving force during the exchange process. The higher the ionic charge, the more preferred is the adsorption process. Therefore, favoured ions require more time to pass through the exchange column than less preferred ions. This mechanism results in different retention times for different ions.

The exchanger column is flushed continuously with eluent, which transports a high concentration of coions. After sample injection coions and counterions are transferred simultaneously through the exchanger column where adsorption of counterions is at first the preferred adsorption process. Due to the high concentration of the coions the counterions are released from the functional resin after a certain time, depending on the adsorption affinity of the counterion. As a result different ion groups pass the resin within different time. Interfering ions are removed in the suppressor to advance the signal to noise ratio. Conductivity of solution is measured in a conductivity cell. Basic exchangers are used for anion exchange and acidic exchangers for cation exchange. For calibration four or five specific concentrations of the respectively electrolytes are analysed and the peak area within a given retention time range is calculated. For most ions a linear correlation between peak area and electrolyte concentration is obtained for small concentrations in the range of mg.

#### **Setup Anions**

Samples were determined with an DIONEX LC20 device, equipped with a DIONEX AS14A Column, an anion self-regenerating suppressor, ASRS 300(4-mm), and an electrochemical detector, ECD. Eluent was made of an 2.7 mmol/l  $\text{Na}_2\text{CO}_3$  / 0.3 mmol/l  $\text{NaHCO}_3$  solution. For calibration 1000 mg/l standard solutions for ion chromatography from Merck were utilized, a calibration range from 5 to 50 mg/l ( $\text{Cl}^-$ ,  $\text{SO}_4^{2-}$ ) and 1 - 20 mg/l ( $\text{NO}_3^-$ ) was set up. Chromatograms were evaluated by Dionex software Chromeleon 6.8.

#### **Setup Cations**

Samples were determined with an DIONEX DX-120 device, equipped with a DIONEX CS12A Column, an cation self-regenerating suppressor, CSRS 300(4-mm), and an electrochemical

cell detector, ECD. Eluent was made of a 20 mmol/l methane sulfonic acid. For calibration 1000 mg/l standard solutions for ion chromatography from Merck were utilized, a calibration range from 1 to 30 mg/l ( $\text{Na}^+$ ,  $\text{K}^+$ ,  $\text{Mg}^{2+}$ ,  $\text{Ca}^{2+}$ ) and 1 - 10 mg/l ( $\text{Sr}^{2+}$ ) was set up. Chromatograms were evaluated by Dionex software Chromeleon 6.8.

### **Sample preparation**

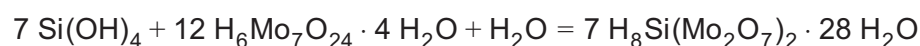
After sampling, liquids were directly passed through a Sartorius Minisart 0.45  $\mu\text{m}$  membrane syringe filter. The required sample volume was transferred from the filtrate by a pipette (Eppendorf) into a volumetric glass flask. For sample dilution exclusively DIW was utilized. The dilution factor, required for IC measurements depends on the electrolyte concentration in the sample. Cations are diluted to a concentration of 5 to 30mg/l, anions to a concentration of 5 to 50mg/l. In most cases two different dilutions of the liquids were necessary to determine all electrolyte compounds, caused by the high concentration of sodium and chloride within the original and synthetic brines.

#### 2.2.2.7 Colorimetric measurements

Dissolved silica species in aqueous solutions can be distinguished into low-molecular weight oligomers, dimers to octamers, on one hand and higher polymerised silicic acid species which form large molecules on the other hand. Reactive silica, monomers to octamers of silicic acid, are determined in aqueous solutions by colorimetric measurements.

### **General principle**

Molybdic acid reacts with the monomer of silicic acid,  $\text{H}_4\text{SiO}_4$ , in acidified solutions to the yellow silicomolybdic acid, Iler, 1979, p. 95.



With increasing silica concentration in solution the colour becomes more intense. The relation between colour intensity and  $\text{H}_4\text{SiO}_4$  concentration in solution is given by the Lambert-Beer law, (2 - 2).

$$E = \log \frac{I_0}{I} = \varepsilon \cdot c \cdot l \quad (2 - 2)$$

E = extinction

$I_0$  = initial intensity of light before passing through the sample

I = intensity of light after passing through the sample

$\varepsilon$  = molecular spectral adsorption coefficient

c = concentration of the analyte

l = thickness of the cuvette

After colour development of the yellow silicomolybdic acid, the sample is filled into a cuvette

and placed in a spectral photometer. The intensity of monochromatic light before and after passing through the sample is detected and extinction is calculated. The unknown analyte concentration is determined by measurement of various standards. For reliable measurements of the reactive silica concentration in solutions two facts must be taken into account. First, in acidified solutions, oligomers and polymers of silicic acid depolymerise to form the monomer species,  $\text{H}_4\text{SiO}_4$ . This reaction is time dependent (Iler, 1979, p. 198). Hence a measurement protocol must be strictly followed to ensure that only silicic acid of low molecular weight, like dimers to octamers, depolymerises to the monomer of silicic acid, which reacts with heptamolybdate. As a second fact, salt concentration reduces the intensity of the yellow silicomolybdic acid. Therefore, the calibration curve must be recorded using standard solutions of the same salt concentration as the sample.

### **Setup**

The concentration of reactive silica in liquid samples was analysed colorimetrically with a filter photometer photoLab S12 from WTW equipped with a tungsten halogen bulb. The extinction was detected at 410 nm, recommended by Iler (1979, p. 97) in 1 cm Polystyrol, PS, cuvettes. The applied measurement procedure was the Molybdosilicate Method C 4500-SiO<sub>2</sub> of Clesceri (1998).

### **Sample preparation**

To determine the reactive silica concentration in aqueous salt solutions, liquids were filtered directly after sampling with a sub-pressure filtration system of Sartorius, made of 250ml polycarbonate holders. Polyamide membrane filters of Sartorius, 47 mm in diameter and 0.2  $\mu\text{m}$  in pore size were used for filtration. For repeat determinations two samples from each filtrate were directly diluted 1:10 in volumetric plastic flasks. Solutions were directly measured within the time recommended by the method procedure.

For setting up the calibration curve, 7 standards including a silica-free standard with identical salt concentration, but defined silica concentration were prepared for each synthetic concentrate in dependence of the salt composition and concentration. The required stock solutions of hydrochloric acid, oxalic acid and ammonium molybdate as well as the caustic soda solution, used for pH adjusting of the ammonium molybdate solution, were exclusively prepared in plastic flasks and beakers. Only chemicals of pro analysi quality from Merck was utilized. Ammonium molybdate solution was passed through a 0.2  $\mu\text{m}$  membrane filter after preparation.

The relative error of this method was estimated by comparing the measured values of standard samples and ICP-OES measurements of the same samples. Results are listed in Table 2.6. The determined accuracy of the applied method is in accordance with the reported precision of Clesceri (1998).

Table 2.6: Results of the comparison between ICP-OES and colorimetric measurement of silicic acid standard samples in deionised water, 0.5 molar NaCl and 1 molar NaCl solution.

Standard samples	deionised water		
	ICP-OES SiO <sub>2</sub> in mg/l	colorimetric SiO <sub>2</sub> in mg/l	relative error of the colorimetric method in %
50	49	51	4.0
100	98	103	5.1
150	148	156	5.4
	<b>0.5 mol/l NaCl solution</b>		
50	49	52	6.1
100	100	103	3.0
150	151	157	3.9
	<b>1.0 mol/l NaCl solution</b>		
50	50	53	6.0
100	97	105	8.2
150	150	157	4.7

### 2.2.2.8 Inductively-Coupled Plasma Optical Emission Spectrometry (ICP OES)

Total Si concentration in liquid samples was analysed by inductively-coupled plasma optical emission spectrometry.

#### **General principle**

A liquid sample is injected into a nebuliser to create an aerosol which is transferred by carrier gas to the plasma torch of 5000 to 10000 K. Within shortest time the aerosol is dried, followed by melting and vaporisation of the solids. Molecules become atomised, respectively ionised. Due to the high energy input electrons are transfers to excited states. By falling back to a lower level, electromagnetic radiation of the energy difference between excited and lower state is emitted in the range of UV and visible light. By using the Czerny-Turner arrangement, the emitted divergent beam passes a collimator were it is transferred into convergent radiation and focused on an optical lattice which is moved stepwise. If the diffraction condition of equation 4-2 is reached, the reflected radiation of a single wavelength is focused on the detector. Elements are identified in dependence of the emitted wavelength.

$$n\lambda = 2d\sin\alpha$$

4 - 2

n: integer, order of the diffraction

$\lambda$ : wavelength of the emitted beam (unknown)

d: lattice plane of the optical lattice (known)

$\sin \alpha$ : angle of diffraction (known)

**Setup**

Silicon (Si) concentration in liquid samples were determined with a Horiba Jobin Yvon, Type JY38S, ICP OES device, equipped with a Burgener Teflon MiraMist nebuliser and a monochromator of Czerny-Turner arrangement. Si signal was detected at 251.611 nm, correction of the measurement was made by standard addition of lanthanum (detected at 333.749 nm) as internal standard. For data evaluation the software J-Yess 4.09 was used.

**Sample preparation**

After sampling, liquids were directly filtered through a Sartorius Polyamide filter, 47mm in diameter, by sub-pressure filtration with a 250 ml polycarbonate filtration station of Sartorius. For adsorption experiments of Chapter 4.3.2, Sartorius Minisart 0.45  $\mu\text{m}$  membrane syringe filters were utilized. The required sample volume was transferred from the filtrate by a pipette (Eppendorf) into a volumetric plastic flask and diluted 1:25 with DIW. Liquids were stored till measurement in plastic bottles.

**2.2.2.9 pH measurements**

Most experiments in this work were conducted as a function of the pH. Therefore pH was measured in solubility, titration, flow-through and evaporation experiments.

**General principle**

In ideal solutions the pH is described as the negative decimal logarithm of the  $\text{H}^+$  ion concentration. In real solutions the activity of  $\text{H}^+$  is used instead of concentration.

Usually, in brines of high salinity, the pH has to be corrected due to the influence of the high amount of charged electrolytes in solution which influences the mobility of ions and the measurement of the electrical potential of pH electrodes (Feldmann, 1956, Galster, 1991).

For this work it was decided to measure the pH without correction due to two reasons: First, the pH in the pilot plant was determined without corrections. To keep the lab experiments comparable to these measurement conditions the pH was not corrected. Second, experimental set-up of titration, flow-through and evaporation experiments made it extremely difficult to prepare equivalent artificial buffer solutions for pH correction. Any change of the amount or composition of electrolyte species in solution had to be considered. In all experiments, conducted during this work, chemical composition changed significantly within minutes to hours.

**Setup**

For pH measurement the pH meter WTW 401i from WTW combined with the pH electrode SENTIX 81 were used. Measurement of pH values were limited to the first decimal place.



## 3 Geochemical modelling of aqueous solutions

Calculation of the mineral saturation state of scarcely soluble salts in aqueous solutions requires the knowledge of the observed system. Parameters like electrolyte concentration and composition as well as the pH, temperature and pressure may influence the chemical equilibrium. Especially electrostatic interactions among ions and their influence on the active concentration of the electrolytes in highly concentrated salt solutions must be considered.

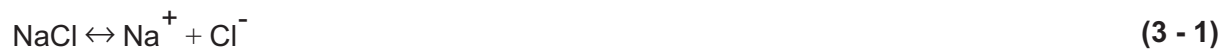
Basic principles of mineral saturation state and the calculation of activity coefficients in aqueous solutions have been described in textbooks and publications. (Krauskopf and Bird, 1995, Bethke, 1996, Merkel and Planer-Friedrich, 2005, Luckas and Krissmann, 2001, Mazo and Mou in Pitzer, 1991, Mortimer and Müller, 2007 and Riedel, 2002). Calculation of activity coefficients with the Pitzer-equation have been presented by Pitzer (1991), Mazo and Mou in Pitzer (1991), Harvie and Weare (1984) and Bethke (1996).

### 3.1 Fundamentals of mineral solubility in aqueous solution

#### 3.1.1 Interaction between water molecules and a solid phase

The solubility of minerals depends on their chemical composition as well as on bonding type and strength, ion charge, ion size and surface charge. While the ion charge inside the crystal is balanced by the charge of the surrounding electrolytes this compensation is not complete for ions near to or on the crystal surface. This charge imbalance allows water molecules to attach to surface ions and hydrate them. The size of the hydration shell depends on the charge and size of the dissolved ion.

Figure 3.1 depicts the solvation of a halite (NaCl) crystal in aqueous solution by hydration of the sodium and chloride ions.



The hydration energy required to dissolve single ions from a solid depends on the lattice energy. For scarcely soluble salts the hydration energy is much smaller than the lattice energy of the solid phase. For soluble salts the required hydration energy for dissolving the salt is equal to or higher than the lattice energy.

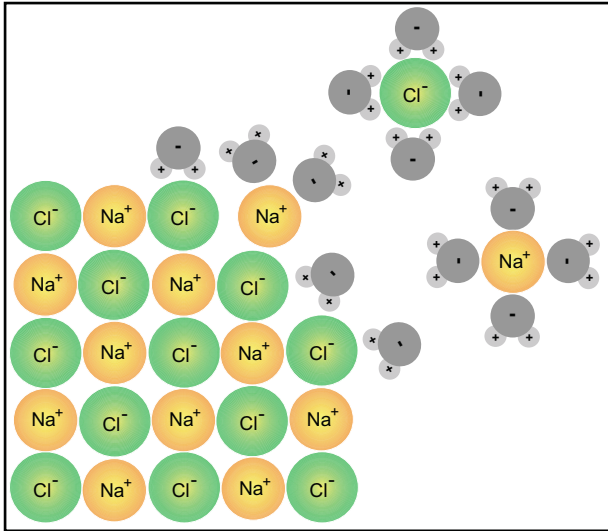


Figure 3.1: Scheme of the dissolution of halite (NaCl) in aqueous solution. Due to the dipole properties of water molecules  $\text{Na}^+$  and  $\text{Cl}^-$  ions are hydrated.

### 3.1.2 Interaction between electrolytes in aqueous solutions

Electrostatic interactions between the dissolved electrolytes influence the chemical equilibrium of aqueous salt solutions. In ideal dilute solutions the sphere of action of electrostatic forces of single electrolytes is separated from each other, hence no interaction occurs. In ideal solutions 100% of the total concentration  $c_i$  act as active concentration  $a_i$ . In real solutions only a fraction of the total concentration is active in real solutions due to interactions of electrostatic attraction or repulsion. For most electrolytes the active concentration in real solutions is smaller than the total concentration but for some species like silicic acid the activity may become higher than the total concentration.

To establish the relationship between the total concentration  $c_i$  of an electrolyte species  $i$  and the active concentration, the activity  $a_i$ , an activity coefficient  $\gamma_i$  must be introduced. Activity coefficients are not measurable directly. They can be estimated empirically from solubility experiments. For the prediction of mineral solubility they must be calculated. Various mathematical approaches for their calculation are mentioned in Chapter 3.2.2.

$$a_i = \gamma_i c_i \quad (3 - 2)$$

$a_i$ : activity of an electrolyte species  $i$

$\gamma_i$ : activity coefficient of the electrolyte species  $i$

$c_i$ : total concentration of an electrolyte species  $i$

For aqueous solutions of high salinity the concentration of electrolyte species is given in molal units. Contrary to molarity the molal units are independent of fluid density, temperature and volume contraction and expansion.

## 3.2 Calculation of mineral solubility

### 3.2.1 Mineral saturation state in aqueous solutions

The solubility product of a mineral is defined as the product of the activities of the electrolyte concentration in solution if the same amount of the salt is dissolved and precipitated at the same time. The solubility product for equation (3 - 2)  $K_{\text{SpNaCl}}$  is defined as:

$$K_{\text{SpNaCl}} = a_{\text{Na}^+} a_{\text{Cl}^-} \quad (3 - 3)$$

Ion concentration on aqueous solution is calculated as:

$$Q = a_{\text{Na}^+(\text{aq})} a_{\text{Cl}^-(\text{aq})} \quad (3 - 4)$$

The logarithm of the relation between the solubility product of the mineral and the ion concentration (Q) in solution is calculated to determine the mineral saturation state of a mineral in aqueous solution.

$$\log \frac{Q}{K_{\text{SP}}} \quad (3 - 5)$$

A mineral in an aqueous solution is saturated if the solubility product is equal to electrolyte activity.

$$0 = \log \frac{Q}{K_{\text{SP}}} \quad (3 - 6)$$

A solution is undersaturated if the solubility product exceeds the product of the electrolyte activities.

$$0 < \log \frac{Q}{K_{\text{SP}}} \quad (3 - 7)$$

If the product of the activities is bigger than the solubility product a solution is oversaturated with respect to the salt.

$$0 > \log \frac{Q}{K_{\text{SP}}} \quad (3 - 8)$$

### 3.2.2 Calculation of activity coefficients in dilute aqueous solutions

Electrolytes in ideal dilute solutions are isolated from each other. Therefore, no interactions must be considered. Activity coefficients of electrolyte species in these solutions are equal to 1. In the case of real dilute solutions electrostatic forces among the electrolytes influences the activity. Their interaction affects the real concentration and may lead to a decrease or increase in the active concentration.

#### 3.2.2.1 Debye-Hückel equation

Peter Debye and Erich Hückel developed a first approach, the Debye-Hückel equation (3 - 9), for calculating activity coefficients of electrolyte species in real dilute solutions in 1923.

$$\log \gamma_i = -Az_i^2 \sqrt{I} \quad (3 - 9)$$

A: depends on temperature, density and the dielectric constant of the solvent. In aqueous solutions at 25° A is 0.51.

$z_i$ : charge of an electrolyte species

$$I: \text{ ionic strength} \quad I = \frac{1}{2} \sum_i m_i z_i^2 \quad (3 - 10)$$

$m_i$ : total concentration of species  $i$  in molal units

Activity coefficients in the Debye-Hückel equation depend on ion charge and ionic strength of the solution. As a result the estimated activity coefficients for  $\text{Na}^+$  and  $\text{Cl}^-$  in a NaCl-solution are equal and activity coefficients decrease continuously with increasing concentration which is not consistent with the real behaviour. Furthermore, neutral electrolytes like silicic acid,  $\text{H}_4\text{SiO}_4$ , were not considered. The Debye-Hückel equation was improved in further studies by Davies (1962), Robinson and Stokes (1968) and Helgeson (1969).

#### 3.2.2.2 Davies equation

The Davies equation (3 - 11), Davies (1962), considers the trend of activity coefficients to increase at high concentrations. Instead of the factor 0.2 in some publications also 0.3 is used.

$$\log \gamma_i = -Az_i^2 \left( \frac{\sqrt{I}}{1 + \sqrt{I}} - 0.2I \right) \quad (3 - 11)$$

A: depends on temperature, density and the dielectric constant of the solvent. In aqueous solutions at 25° A is 0.51.

$z_i$ : charge of an electrolyte species

I: ionic strength

### 3.2.2.3 Extended Debye-Hückel equation

Robinson and Stokes (1968), developed the extended Debye-Hückel equation (3 - 12). They included the ion size and a second constant B which depends on temperature, density and the dielectric constant of the solution.

$$\log \gamma_i = -\frac{Az_i^2 \sqrt{I}}{1 + \dot{a}_i B \sqrt{I}} \quad (3 - 12)$$

A, B: depend on temperature, density and the dielectric constant of the solvent. In aqueous solutions at 25° the value of A is 0.51 and the value of B is 0.33.

$z_i$ : charge of an electrolyte species

I: ionic strength

$\dot{a}_i$  : hydrated ion size (diameter)

### 3.2.2.4 B-dot equation

The extension of the Debye-Hückel equation by Helgeson (1969) is called the B-dot equation (3 - 13). Factor  $\dot{B}$  is an empirical value which depends on the ion size. Within most geochemical modeling programs this equation is chosen to calculate the activity coefficients in dilute aqueous solutions to ionic strength up to a molality of 1.

$$\log \gamma_i = -\frac{Az_i^2 \sqrt{I}}{1 + \dot{a}_i B \sqrt{I}} + \dot{B}I \quad (3 - 13)$$

A, B,: depend on temperature, density and the dielectric constant of the solvent. In aqueous solutions at 25° the value of A is 0.51 and the value of B is 0.33.

$\dot{B}$  : depends on the ion size

$z_i$ : charge of an electrolyte species

I: Ionic strength

$\dot{a}_i$  : hydrated ion (diameter)

For neutral species the activity coefficients are calculated by the equation (3 - 14). The polynomial coefficients a, b and c depend on temperature.

$$\log \gamma_i = aI + bI^2 + cI^3 \quad (3 - 14)$$

### 3.2.3 Calculation of activity coefficients in concentrated aqueous solutions

For the calculation of activity coefficients the interaction of electrolytes on the molecular level must be taken into account. In dilute solutions long range forces or Van der Waals forces and their influence on macroscopic properties like the dielectricity of the solution were considered in form of the parameters A and B in equations (3 - 9) to (3 - 13).

In the case of aqueous solutions of high salinity short range forces among ion pairs and ion triplets, which are normally repulsive, also affect the activity of electrolyte species. In these solutions it is not longer possible to treat ions as separated particles.

Three different interactions take place. Firstly, the interaction between the dissolved species and water molecules, secondly, the interaction among all dissolved ions and thirdly, the interaction among all water molecules. The direct impact on neighbouring ions depends on the sphere of action of the single ions. Formation of hydration shells around the charged ions, repulsion and attraction between ions of the same and of different charge occur. The direct interactions of the electron clouds may induce dipole momenta in adjacent ions, also hydrated complexes of divalent cations may be formed. Furthermore, core repulsion caused by short-range forces occurs in concentrated solutions and becomes a significant impact on the interaction of electrolytes by increasing ionic strength.

Natural water bodies contain dissolved gases like hydrogen carbonate. The solubility of gas decreases with increasing salt concentration. Therefore, the gas fugacity is influenced by the salt content of a solution. This fact must be considered especially for solubility calculation of carbonate minerals like calcite and aragonite.

The active concentration of electrolytes, interaction between ions and changes in the fugacity influence the free energy of a solution significantly. To describe the theory of those chemical systems, more complex equations are required.

According to these conditions a system of equations, known as the Pitzer-equations, has been developed for homogenous salt solutions by K. Pitzer and co-authors and published in the years 1973 to 1975. In contrast to the calculation of activity coefficients in dilute solutions, short range forces between ion pairs and ion triplets are considered in this mathematical model. Therefore, the excess free energy of the salt solution is calculated by a series expansion in form of virial equations (3 - 15).

$$\frac{G^{\text{ex}}}{n_w RT_K} = f^{\text{dh}}(I) + \sum_i \sum_j \lambda_{ij}(I) m_i m_j + \sum_i \sum_j \sum_k \mu_{ijk} m_i m_j m_k \quad (3 - 15)$$

The parameter  $G^{\text{ex}}$  represents the excess free energy,  $R$  the gas constant,  $T$  the temperature in Kelvin and  $n_w$  the number of kilograms of water. Concentration  $m$  of ion species is in molal units.

The first virial coefficient  $f^{\text{dh}}$  includes the Debye-Hückel equation. The second virial coefficient  $\lambda_{ij}$  describes the interaction between two ionic species  $i$  and  $j$  and the third coefficient  $\mu_{ijk}$  represents the interaction of three ion species  $i$ ,  $j$  and  $k$  among each other. In contrast to the first two virial coefficients, the third coefficient is independent of the ionic strength.

Calculation of activity coefficients based on the Pitzer-equations are described in detail in **Appendix B.1**.

To visualize the differences of the Debye-Hückel, the extended Debye-Hückel, the Davies and the B-dot equation the activity coefficient of  $\text{Cl}^-$  is calculated depending on the ionic strength by the corresponding expression. For calculation of the activity coefficients for  $\text{Cl}^-$  with the Pitzer equations the modelling program *The Geochemist's Workbench (GWB) 6.0* was used. Activity of  $\text{Cl}^-$  was calculated in solutions of 0.001 mol/kg to 5 mol/kg NaCl. The results are presented in Figure 3.2.

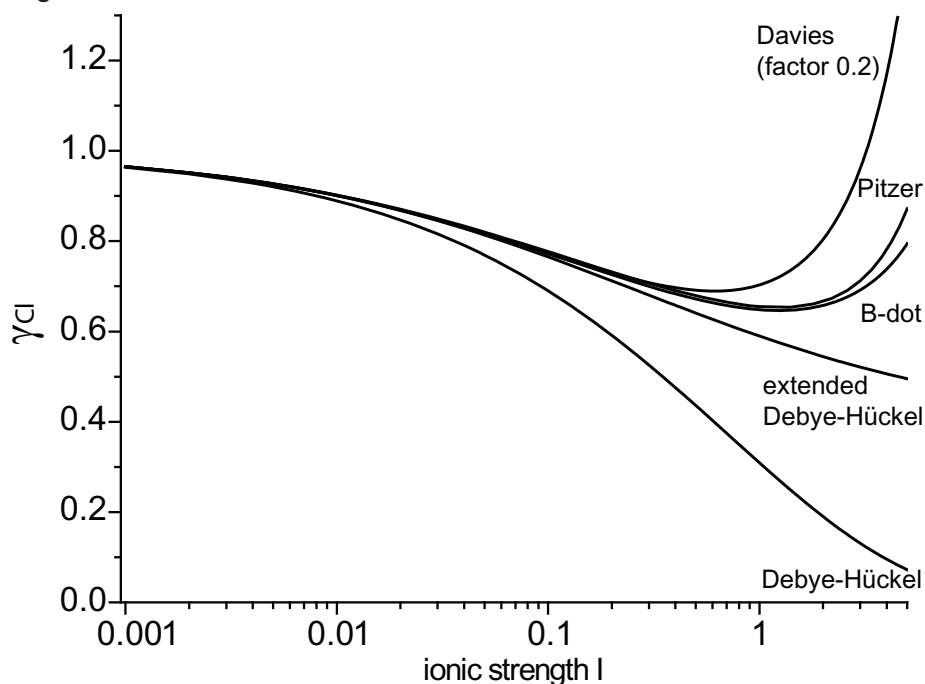


Figure 3.2: The activity coefficient of  $\text{Cl}^-$  is calculated, depending on the ionic strength, by the Debye-Hückel, the extended Debye-Hückel, the Davies equation and the B-dot equation. Activity coefficient of  $\text{Cl}^-$  based on the Pitzer-equations was calculated with the modelling program *GWB* in 0.001 to 5 mol/kg NaCl solutions.

Various methods for the calculation of activity coefficients result in different values of the coefficients. Solubility calculations like the solubility of gypsum in sodium chloride solutions with increasing salt concentration compared with experimental data visualize the impact of the different methods (Figure 3.3). The solubility of gypsum increases with increasing salt concen-

tration. This behaviour is called *salting in effect*. If the solubility of a mineral decreases with increasing salt concentration it is called *salting out effect* (Marshall, 1980). In NaCl solution with salt concentration above  $>3$  mol/kg solubility of gypsum decreases.

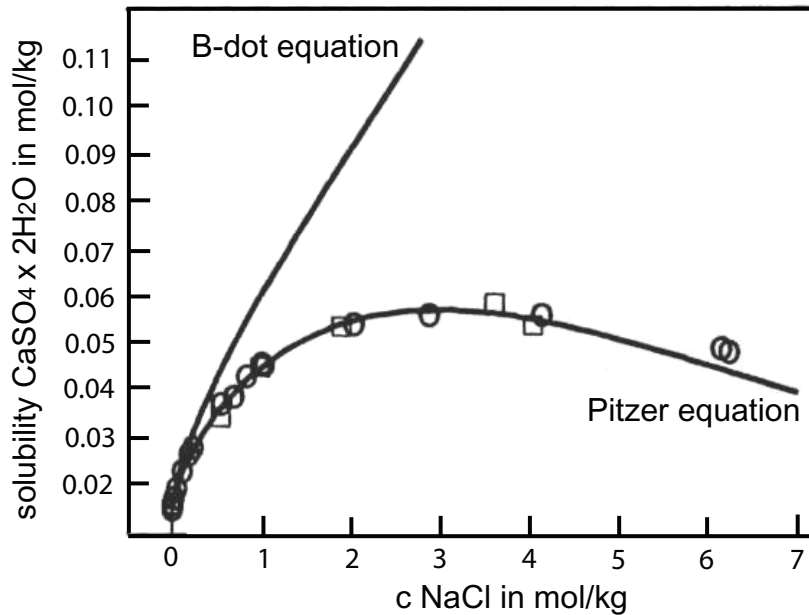


Figure 3.3: Solubility of gypsum in sodium chloride solutions of increasing concentration. Squares and Circles represents experimental values determined by Marshall and Slusher (1966) and Block and Waters (1968). Solid lines represent the calculated values of the B-dot equation and the Pitzer equation. [after Bethke, 1996]

### 3.3 Geochemical modelling of process concentrates of the pilot plant

For calculation of the mineral saturation state in the brines of the process, the modelling program *The Geochemist's Workbench 6.0 (GWB)* was used. The *GWB* contains several programs for application in different areas. Equilibrium calculation, mass balance of chemical reactions, calculation of activity coefficients with the B-dot equation as well as the Pitzer equations and calculation of Eh-pH diagrams are included. Moreover, species distribution of electrolytes in aqueous solution, the calculation of mineral saturation state, of stability diagrams and of reaction paths are also considered as well as a method for tracing isotope fractionation and modeling of the reactive transport in one and two dimensions. The data output is plotted directly through a graphical interface.

For the theoretical characterisation of the brines equilibrium calculations and calculations of the mineral saturation state were carried out. For this purpose the activity coefficients of the dissolved electrolytes in the highly concentrated solution were determined by the Pitzer equations. The dataset *thermo\_phrqitz* was selected for the calculations.

### 3.3.1 Upgrading the database *thermo\_phrqpit* with Pitzer parameters for silicic acid and nitrate

Before starting the calculations with GWB the database *thermo\_phrqpit* had to be extended for the interaction parameters of silicic acid and nitrate which are not included in the dataset but required for the brines. Pitzer parameters for both electrolytes are available from literature. For upgrading *thermo\_phrqpit* the neutral species,  $\text{H}_4\text{SiO}_4$ , is included as the basic species,  $\text{H}_3\text{SiO}_4^-$  and  $\text{H}_2\text{SiO}_4^{2-}$  as aquatic species. Reardon (1990) published Pitzer parameters  $\beta^{(0)}$ ,  $\beta^{(1)}$ ,  $\beta^{(2)}$ ,  $C^\phi$ ,  $\theta$ ,  $\lambda$  and  $\Psi$  for the interaction of  $\text{H}_4\text{SiO}_4$ ,  $\text{H}_3\text{SiO}_4^-$  and  $\text{H}_2\text{SiO}_4^{2-}$  with various electrolytes in cement/water systems. Pitzer parameters for  $\text{NO}_3^-$  are taken from Weber and Beahm (1996). Their values were calculated in the framework of chemical modelling of waste sludges.  $\text{NO}_3^-$  is included as basis species. The interaction parameters are listed in **Appendix B.2** in Tables B.1 to B.5.

Parameters  $\alpha_1$  and  $\alpha_2$  are fixed values due to the nomenclature mentioned in Appendix B.1. For 1-1 and 2-1 electrolytes, the values  $2.0 \text{ kg}^{1/2} \cdot \text{mol}^{1/2}$  and  $0.0 \text{ kg}^{1/2} \cdot \text{mol}^{1/2}$  for  $\alpha_1$  and  $\alpha_2$  are entered. In the case of 2-2 electrolytes  $\alpha_1$  and  $\alpha_2$  are  $1.4 \text{ kg}^{1/2} \cdot \text{mol}^{1/2}$  and  $12.0 \text{ kg}^{1/2} \cdot \text{mol}^{1/2}$ . Thermodynamic data for mineral species  $\text{SiO}_{2(\text{am})}$  were transferred from the GWB database *thermo.com.V8.R6+*. The upgraded database is called ***thermo\_zld\_3\_v2*** which was applied for all calculations presented in this work.

### 3.3.2 Testing the upgraded database

The solubility of amorphous silica in different salt solutions was calculated with GWB and compared with experimental data from Marshall and Warakomski (1980), for verification of the reliability of the upgraded dataset *thermo\_zld\_3\_v2*. Marshall and Warakomski determined the solubility of amorphous silica,  $\text{SiO}_2$ , in different salt solutions depending on the salt concentration at pH between 5 to 7. The main electrolytes of the feed water of the pilot plant were taken into account:  $\text{Na}^+$ ,  $\text{Ca}^{2+}$ ,  $\text{Mg}^{2+}$ ,  $\text{K}^+$ ,  $\text{Cl}^-$ ,  $\text{SO}_4^{2-}$  and  $\text{NO}_3^-$ . Solubility of amorphous silica in  $\text{CaCl}_2$ ,  $\text{MgCl}_2$ ,  $\text{NaCl}$ ,  $\text{NaNO}_3$ ,  $\text{NaSO}_4$ ,  $\text{MgSO}_4$ ,  $\text{KCl}$  and  $\text{KNO}_3$  solutions were compared.

Solubility of amorphous silica at 25°C may range from 70 mg/l to 130 mg/l (Iler, 1979). It depends on the degree of the local order of the solid, its degree of cross-linking as well as on the water content. In almost the same manner as the bulk properties, the surface properties like surface order, structure and size as well as the surface charge also influence the solubility.

In order to make the calculations comparable with the experimental data of Marshall and Warakomski (1980) log K of  $\text{SiO}_{2(\text{am})}$  in the database was altered to -2.6570.

Solubilities were calculated at 25°C, 1.013 bar and at a pH of 6.5. Results of the comparison

are presented in Figures 3.4 to 3.7. The concentration of dissolved  $\text{SiO}_2$  in the diagrams represents the equilibrium concentration with solid amorphous silica. Light grey lines in the diagrams mark the maximum concentration of the respective salt in the EDR brine of the pilot plant.

### 3.3.2.1 Solubility of $\text{SiO}_2$ , amorphous silica, in $\text{CaCl}_2$ and $\text{MgCl}_2$ solutions

Figure 3.4 presents the comparison between the experimentally determined and calculated solubilities of amorphous silica in  $\text{CaCl}_2$  and  $\text{MgCl}_2$  solutions as a function of the salt concentration.

In the presence of divalent cations the calculated values of amorphous silica are higher than the measured one up to a molality of 4.5 mol/kg. With increasing salt concentration the calculated values are lower than the values of Marshall and Warakomski (1980).

The difference between calculated and measured values of  $\text{SiO}_2$  in  $\text{CaCl}_2$  solutions varies from 2 mg/kg to a maximum of 11 mg/kg. In  $\text{MgCl}_2$  solutions the maximum difference reaches 15 mg/kg  $\text{SiO}_2$ . Within the concentration range in the EDR brine of 0.05 mol/kg  $\text{CaCl}_2$  and of 0.12 mol/kg  $\text{MgCl}_2$  the calculated values fit the experimental ones well.

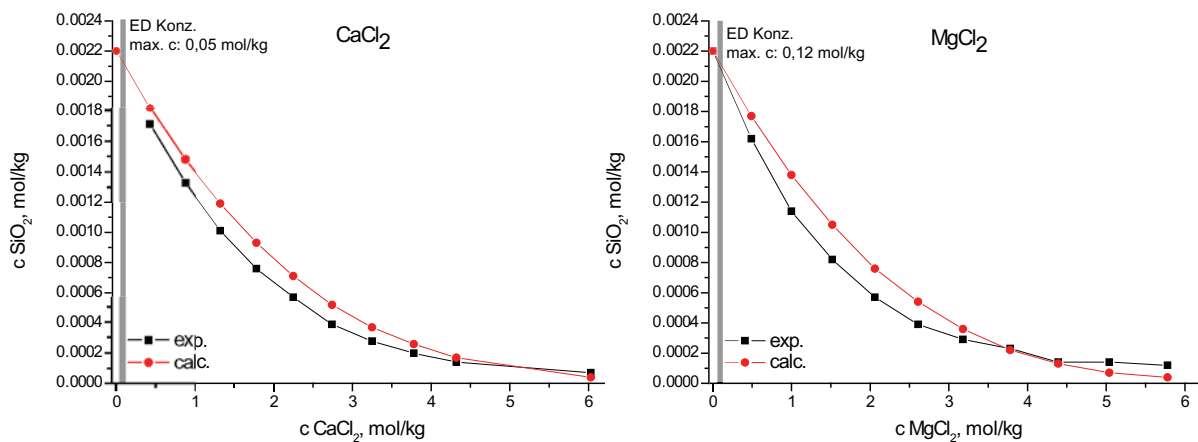


Figure 3.4: Comparison of the calculated and experimentally determined solubilities of amorphous silica in  $\text{CaCl}_2$  solution and in  $\text{MgCl}_2$  solution as a function of the salt concentration. Grey vertical lines in the diagrams mark the respective salt concentration in the original EDR brine.

### 3.3.2.2 Solubility of $\text{SiO}_2$ , amorphous silica, in $\text{Na}_2\text{SO}_4$ and $\text{MgSO}_4$ solutions

Figure 3.5 presents the results of the experimentally determined and calculated solubilities of amorphous silica in  $\text{Na}_2\text{SO}_4$  and  $\text{MgSO}_4$  solutions as a function of the salt content.

Except at very low concentrations the calculated solubilities in sodium sulphate solutions of different concentrations are significantly lower than the measured ones. With increasing salt concentration the difference between calculated and experimentally determined values becomes bigger. In the presence of magnesium sulphate the calculated solubilities are always higher than the measured ones. With increasing salt concentration the difference increases.

Sulphate ions in EDR brine reach a maximum concentration of 0.06 mol/kg. Up to this molality the calculated and measured values of the solubility of amorphous silica are comparable. The interaction parameter  $\lambda$  of  $\text{SO}_4^{2-}$  and silicic acid performs very poorly in the presence of high salt concentration.

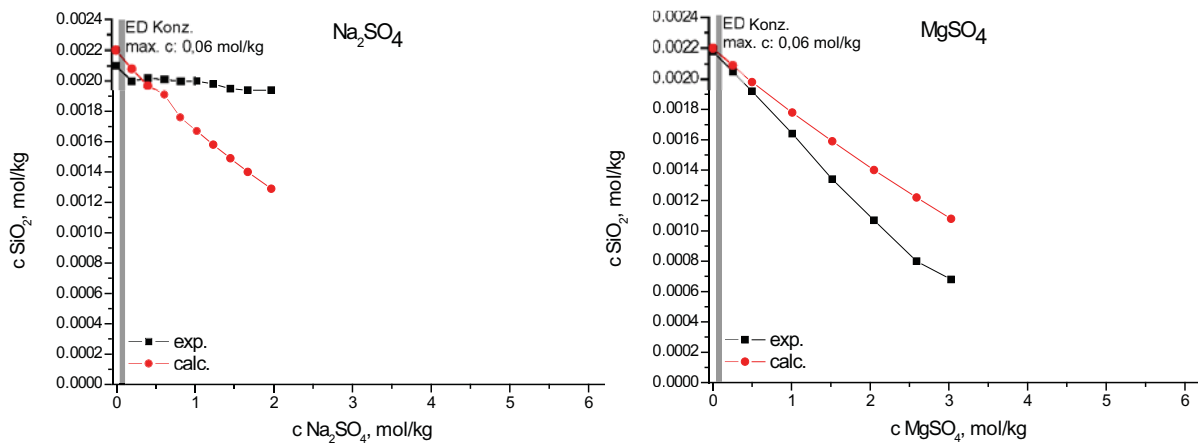


Figure 3.5: Comparison of the calculated and experimentally determined solubilities of amorphous silica in  $\text{Na}_2\text{SO}_4$  solution and in  $\text{MgSO}_4$  solution as a function of the salt concentration. Grey vertical lines in the diagrams mark the respective salt concentration in the original EDR brine.

### 3.3.2.3 Solubility of $\text{SiO}_2$ , amorphous silica, in $\text{NaCl}$ and $\text{NaNO}_3$ solutions

Figure 3.6 presents the comparison of the experimentally determined and calculated solubilities of amorphous silica in  $\text{NaCl}$  and  $\text{NaNO}_3$  solutions as a function of the salt content.

In the case of sodium chloride the calculated solubilities match the experimentally determined ones up to a molality of 1 mol/kg  $\text{NaCl}$  concentration. With increasing salt concentration the calculated values are smaller than the values of Marshall and Warakomski (1980). Within the EDR unit the maximum  $\text{NaCl}$  concentration may reach 1.3 mol/kg. The difference between measured and calculated solubilities of amorphous silica at this molality constitute 5% which equates 6 mg  $\text{SiO}_2$  per kg water.

In the presence of  $\text{NaNO}_3$  the calculated values of the solubility of amorphous silica are comparable with the measured values up to a molality of 1.03 mol/kg. Above this concentration the calculated values are smaller than the values of Marshall and Warakomski. With increasing salt concentration the difference increases. Within the EDR brine the maximum concentration of  $\text{NaNO}_3$  may reach 0.001 mol/kg. Within this range the calculated values fit the experimentally determined values well.

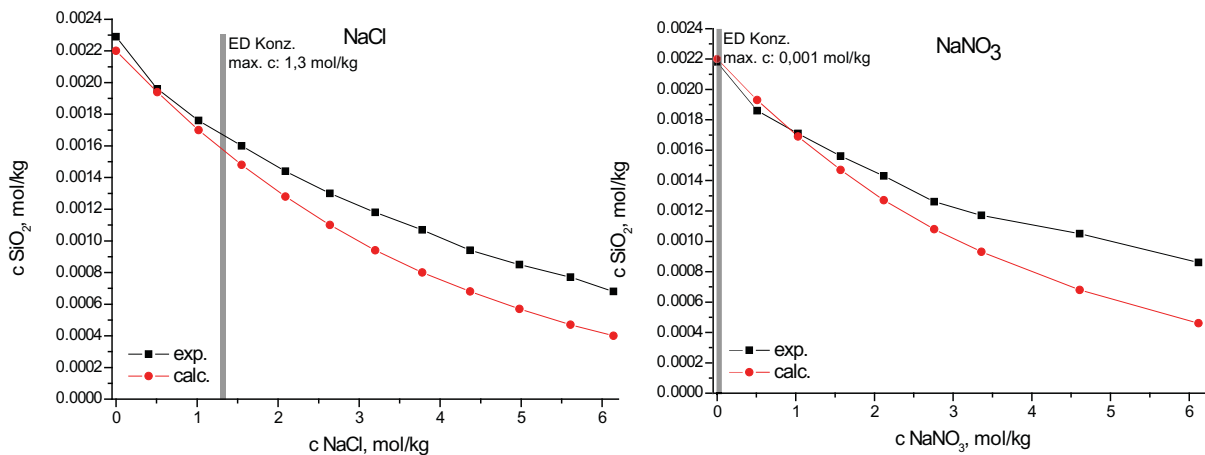


Figure 3.6: Comparison of the calculated and experimentally determined solubilities of amorphous silica in  $\text{NaCl}$  solution and in  $\text{NaNO}_3$  solution as a function of the salt concentration. Grey vertical lines in the diagrams mark the respective salt concentration in the original EDR brine.

### 3.3.2.4 Solubility of $\text{SiO}_2$ , amorphous silica, in KCl and $\text{KNO}_3$ solutions

Figure 3.7 presents the comparison of the experimentally determined and calculated solubilities of amorphous silica in KCl and  $\text{KNO}_3$  solutions as a function of the salt content.

By increasing concentration of potassium chloride the calculated solubility decreases significantly and much stronger than the measured solubility. Data are comparable up to a molality of 1 mol/kg.

In the presence of potassium nitrate the solubility is also below the measured one but the decrease of the solubility by increasing salt concentration is not as strong as for potassium chloride. Calculated and measured values of the solubility of amorphous silica are comparable up to 1 mol/kg.

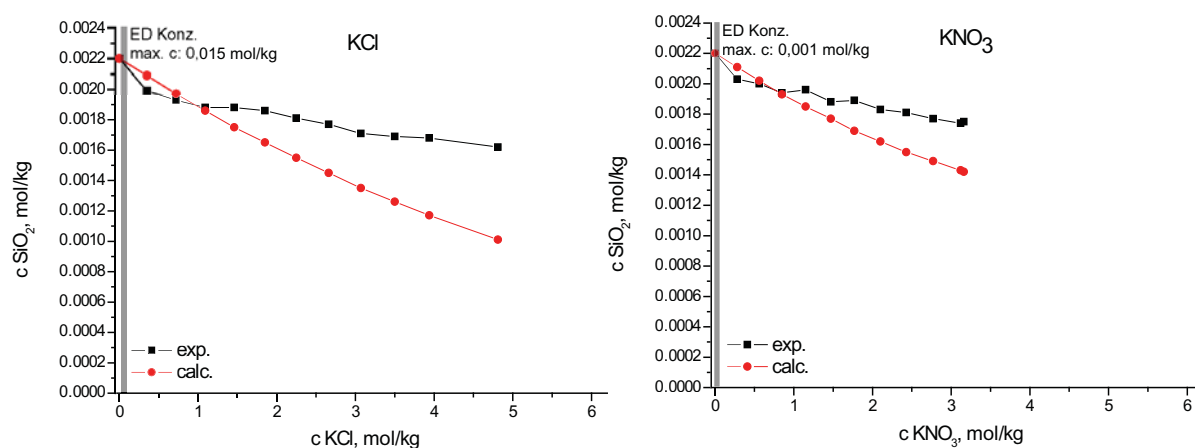


Figure 3.7: Comparison of the calculated and experimentally determined solubilities of amorphous silica in KCl solution and in  $\text{KNO}_3$  solution as a function of the salt concentration. Grey vertical lines in the diagrams mark the respective salt concentration in the original EDR brine.

### 3.3.2.5 Applicability of the theoretical solubility calculations for amorphous silica with the upgraded database

Upgrading the dataset *thermo\_phrqpit* to *thermo\_zld\_3\_v2* was successful for the concentration range of the electrolytes in the process concentrates of the pilot plant.  $\text{Na}^+$  and  $\text{Cl}^-$  are the main electrolytes of the feed- and the process water of the pilot plant. The comparison of calculated and measured solubilities of amorphous silica in sodium chloride solutions of different concentrations shows that the GWB calculates reliable values with the dataset *thermo\_zld\_3\_v2* in the concentration range of the electrolytes in the process brines. In the presence of divalent ions the calculated solubility values remain continuously 2 to 15 mg/kg  $\text{SiO}_2$  higher than expected. In the presence of  $\text{K}^+$  and  $\text{NO}_3^-$  the calculated and measured solubilities are comparable at concentrations up to 1 mol/kg.

### 3.3.3 Calculation of the mineral saturation state in the process solutions of the membrane units of the pilot plant

The influence of the pH as well as the influence of electrolyte concentration and composition of the pilot plant brines on the mineral saturation state were calculated. For all calculations the values for temperature and pressure were set to 25°C and 1.013 bar. Due to the results of the solubility experiments of solid silicic acid (Merck) in doubly deionised water, described in Chapter 4.2.1, log K of -2.7136 of the dataset *thermo.com.V8.R6.+* was used in the dataset *thermo\_zld\_3\_v2* for the calculation of the mineral saturation state of amorphous silica in the process concentrates.

Mineral saturation states of the various process solutions were calculated for the operation condition of each membrane unit as a function of the pH in the pH range from 2 to 13. Each calculation was conducted in form of a titration path. Therefore, the pH was increased stepwise from 2 to 13 and chemical equilibrium and mineral saturation state were calculated for every step.

First diagram in the chapters 3.3.3.1 to 3.3.3.3 show the undersaturated ( $\log Q/K < 0$ ), the saturated ( $\log Q/K = 0$ ) and the oversaturated state ( $\log Q/K > 0$ ) of minerals in solutions. For simulation of the oversaturated state, no precipitation of minerals was allowed.

The second diagram shows the amount of minerals formed in solutions if precipitation is allowed at every single step. Precipitates were not allowed to be removed from the system, they stay in contact with solution.

#### 3.3.3.1 Mineral saturation state in the feed water in dependence of the pH

Composition of the Raw Water is noted in Table 3.1.

Table 3.1: Composition of the Raw Water

cations in mg/kg					anions in mg/kg					
Na <sup>+</sup>	Ca <sup>2+</sup>	Mg <sup>2+</sup>	K <sup>+</sup>	Sr <sup>2+</sup>	Cl <sup>-</sup>	SO <sub>4</sub> <sup>2-</sup>	H <sub>4</sub> SiO <sub>4</sub>	NO <sub>3</sub> <sup>-</sup>	HCO <sub>3</sub> <sup>-</sup>	F <sup>-</sup>
694	204	117	24	6	1251	527	35	< 0.3	267	1

Mineral saturation state of the raw water was calculated as a function of the pH (Figure 3.8). Gypsum (CaSO<sub>4</sub> × 2H<sub>2</sub>O) and amorphous silica (SiO<sub>2</sub>) are undersaturated between pH 2 to 13. If the pH is raised above a pH of 7 calcite (CaCO<sub>3</sub>) exceeds saturation and becomes oversaturated in solution. Above a pH of 9.9 brucite (Mg(OH)<sub>2</sub>) becomes oversaturated in solution.

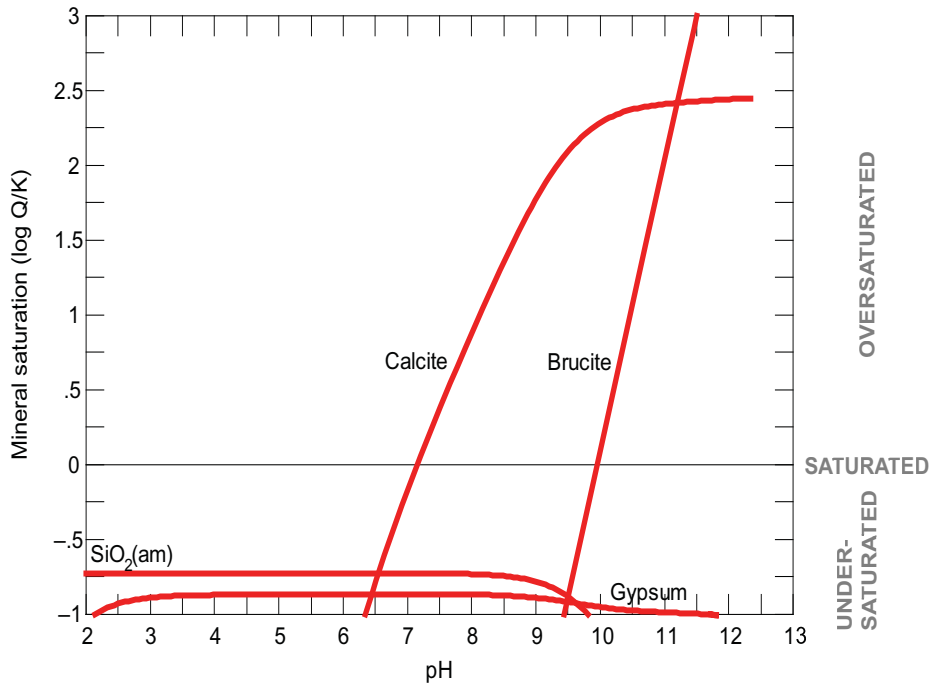


Figure 3.8: Calculated mineral saturation states in the RO concentrate as a function of the pH. At  $\log Q/K > 0$  minerals are oversaturated in solution, at  $\log Q/K = 0$  minerals are saturated in solution and at  $\log Q/K < 0$  minerals are undersaturated in solution.

The raw water of the fossil lense enters the RO unit with an initial pH of 8 (Figure 3.9, grey line). At this condition the water is slightly oversaturated with respect to calcite (~300 mg calcite per kg solution). Due to the utilisation of antiscalants precipitation of calcite is inhibited in the RO unit. At pH values  $> 9.9$  brucite is formed.

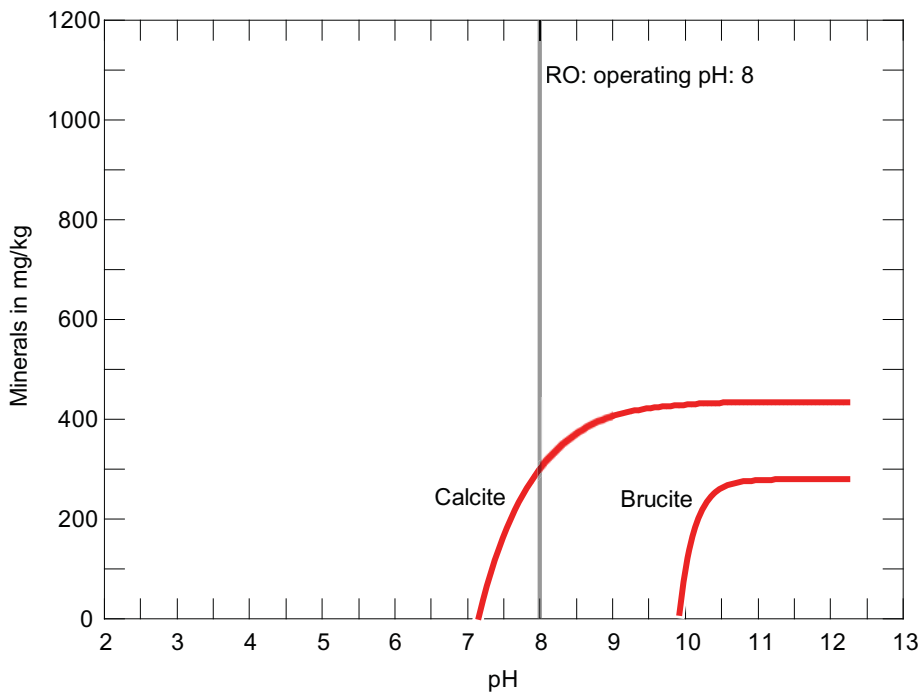


Figure 3.9: Calculation of the amount of minerals in mg per kg solution in the raw water as a function of the pH. The RO unit is operated at a pH of 8 (grey line).

## 3.3.3.2 Mineral saturation state in the RO concentrate in dependence of the pH

Composition of the RO concentrate is noted in Table 3.2.

Table 3.2: Composition of the RO concentrate

cations in mg/kg					anions in mg/kg					
Na <sup>+</sup>	Ca <sup>2+</sup>	Mg <sup>2+</sup>	K <sup>+</sup>	Sr <sup>2+</sup>	Cl <sup>-</sup>	SO <sub>4</sub> <sup>2-</sup>	H <sub>4</sub> SiO <sub>4</sub>	NO <sub>3</sub> <sup>-</sup>	HCO <sub>3</sub> <sup>-</sup>	F <sup>-</sup>
3426	1049	478	87	26	6730	2690	164	2	535	5

Mineral saturation state was calculated for the RO concentrate as a function of the pH (Figure 3.10). Gypsum and amorphous silica are slightly undersaturated in the RO concentrate up to a pH of 8.5. At higher pH values they become more undersaturated. Calcite is oversaturated at pH values > 6.5. Above a pH of 9.8 solution is oversaturated in respect to brucite and above a pH of 12.7 solution is oversaturated in respect to portlandite (Ca(OH)<sub>2</sub>).

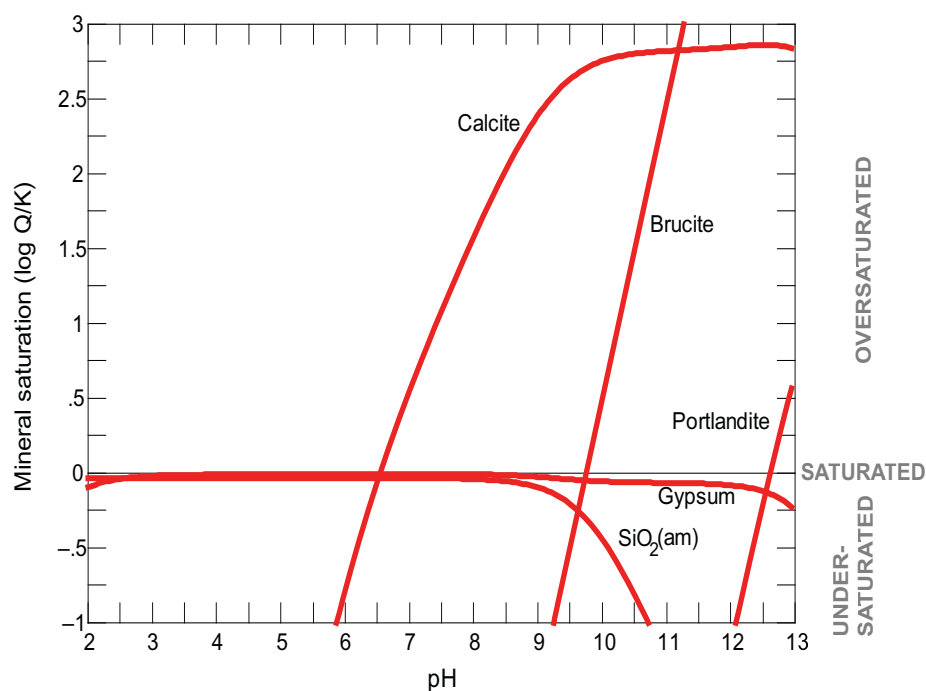


Figure 3.10: Calculated mineral saturation states in the RO concentrate as a function of the pH. At  $\log Q/K > 0$  minerals are oversaturated in solution, at  $\log Q/K = 0$  minerals are saturated in solution and at  $\log Q/K < 0$  minerals are underaturated in solution.

Amount of minerals in the RO concentrate are calculated as a function of the pH (Figure 3.11). After desalination in the RO unit the pH of the concentrate is 7.3. At this pH calcite was calculated to be present in solution. As mentioned before, antiscalants inhibit precipitation of calcite. Before feeding the RO concentrate into the EDR unit it is acidified with nitric acid to pH 2. At this condition no minerals exist in solution. At pH values > 9.7 brucite is calculated to exist in solution and portlandite is calculated to precipitate at pH values > 12.7.

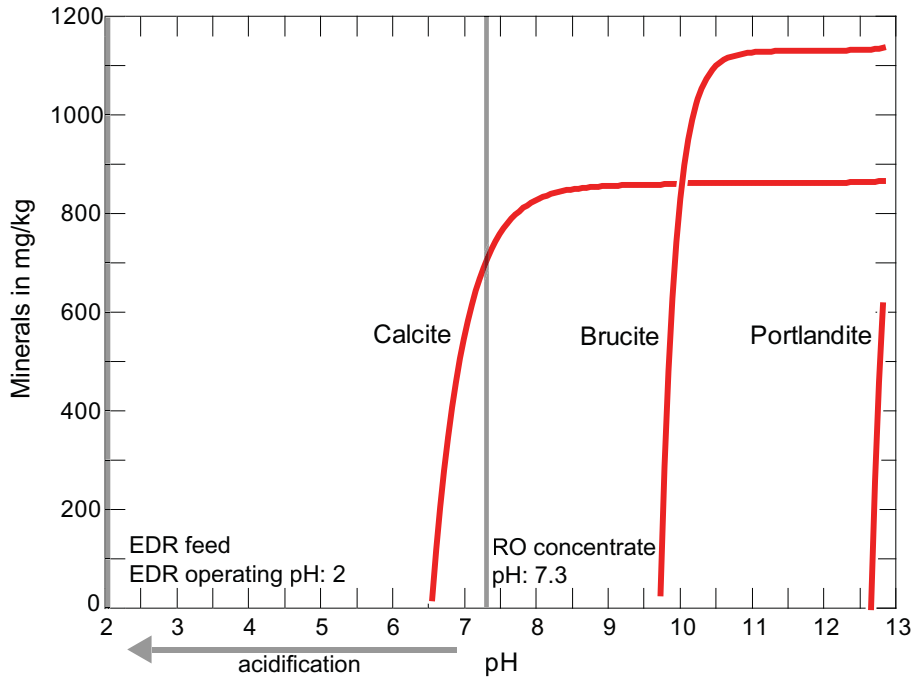


Figure 3.11: Calculation of the amount of minerals in mg per kg solution in the RO concentrate as a function of pH. Grey lines show the pH at the respective operation condition of the membrane unit.

### 3.3.3.3 Mineral saturation state in the EDR concentrate in dependence of the pH

Composition of the EDR concentrate is noted in Table 3.3

Table 3.3: Composition of the electrolytes of the EDR concentrate

cations in mg/kg					anions in mg/kg					
Na <sup>+</sup>	Ca <sup>2+</sup>	Mg <sup>2+</sup>	K <sup>+</sup>	Sr <sup>2+</sup>	Cl <sup>-</sup>	SO <sub>4</sub> <sup>2-</sup>	H <sub>4</sub> SiO <sub>4</sub>	NO <sub>3</sub> <sup>-</sup>	HCO <sub>3</sub> <sup>-</sup>	F <sup>-</sup>
31266	1852	2844	594	134	56370	6042	185	70	-	19

The mineral saturation state of the EDR concentrate was calculated as a function of the pH (Figure 3.12). Gypsum is slightly undersaturated in the pH range from 2 to 9.5. Up to a pH of 12.5 it is oversaturated in the EDR concentrate. Above pH 12.5, portlandite, instead of gypsum is saturated in the brine. Brucite exceeds saturation similar to gypsum at a pH of 9.5. In contrast, amorphous silica is oversaturated at pH values below 9.5 and becomes undersaturated at higher pH values.

Amounts of minerals in the RO concentrate are calculated as a function of the pH (Figure 3.13). The EDR unit is operated at a pH of 2. Here, amorphous silica is the only solid to be formed in solution. If the pH of the operating conditions is shifted from 2 to pH 13, the solubility product of several minerals is exceeded. At pH >9.5 brucite and gypsum are formed. Brucite remains stable up to high pH values, the solubility of gypsum decreases at pH levels above 12.5.

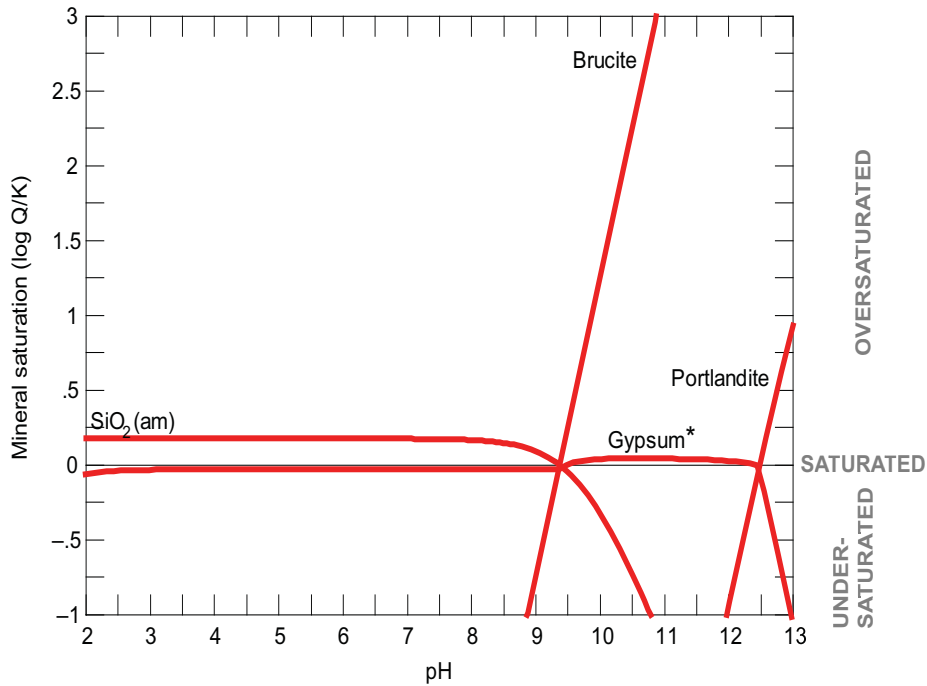


Figure 3.12: Calculated mineral saturation states in the EDR concentrate as a function of the pH. At  $\log Q/K > 0$  minerals are oversaturated in solution, at  $\log Q/K = 0$  minerals are saturated in solution and at  $\log Q/K < 0$  minerals are underaturated in solution. \*: mineral saturation state of gypsum was calculated by allowing for of brucite precipitation.

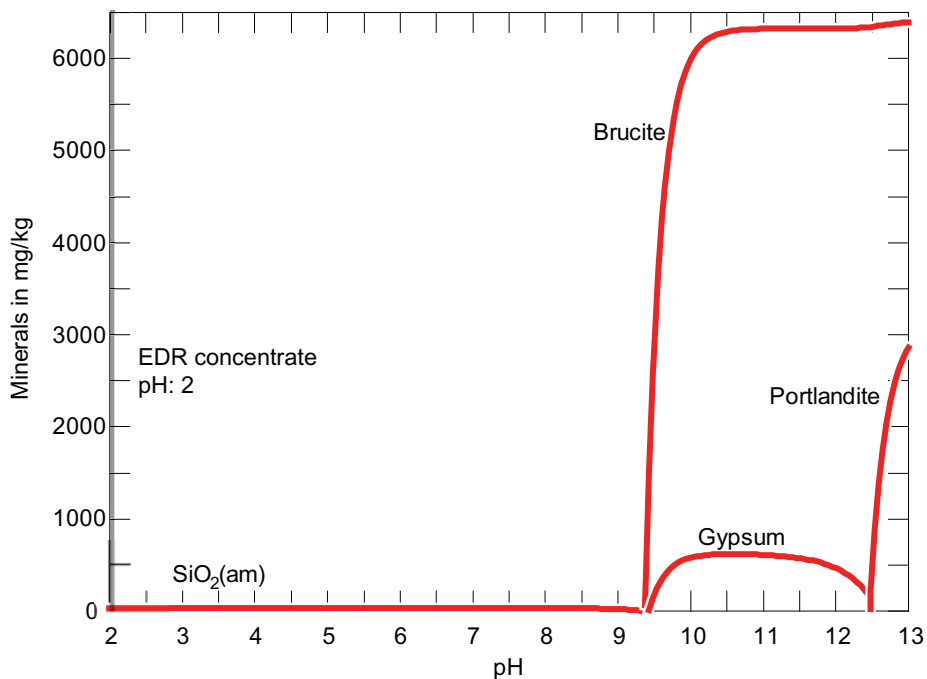


Figure 3.13: Calculation of the amount of minerals in mg per kg solution in the EDR concentrate as a function of pH

## 4 Scaling in the Electrodialysis Unit

Scaling of inorganic solids occurred within the EDR unit of the pilot plant on the membrane surfaces of the anion and cation exchanger membrane as well as on the spacer. In April 2007 one membrane channel was completely blocked by deposits. In April 2008 precipitates build up a thin film on the membrane surfaces. In both cases permeability of the membranes were constrained to a minimum and had to be replaced by new membranes. To avoid precipitation of inorganic solids in the EDR unit, a better understanding of the formation mechanism of these solids is necessary. Therefore, precipitates were characterised chemically and mineralogically. Formation conditions of inorganic solids in the EDR unit were investigated by laboratory experiments and, based on this results, methods to avoid scaling in the EDR unit were worked out.

### 4.1 Characterisation of the precipitates

The precipitates of the scaling events of April 2007 and April 2008 were analysed by optical Microscopy (LM), Environmental Scanning Electron Microscopy in combination with Energy-Dispersive X-ray Fluorescence (ESEM-EDX), Wavelength-Dispersive X-ray Fluorescence (XRF) and X-ray Diffraction (XRD). Sample description is listed in Table 4.1.

Table 4.1: 4.1: Sample description of original precipitates of two scaling events in April 2007 and April 2008

scaling event	sample indication	description
April 2007	CEM 1	precipitates, detached from the cation exchanger membrane by the israeli partners
	AEM 1	precipitates, detached from the anion exchanger membrane by the israeli partners
	spacer 1	precipitates, detached from the spacer by the israeli partners
April 2008	CEM 2	precipitates, adhering to the cation exchanger membrane surface
	AEM 2	precipitates, adhering to the anion exchanger membrane surface

Original samples from the EDR unit and analytical methods are listed in Table 4.2. Due to the small amount of the precipitates in April 2008 only optical and EDX analyses were conducted.

Table 4.2: 4.2: List of original samples and applied analytical methods

	LM	ESEM/EDX	WD-XRF	XRD	sample amount in g
<b>April 2007</b>					
CEM 1	x	x			< 0.1
AEM 1	x	x	x	x	0.5
spacer 1	x	x	x	x	1.0
<b>April 2008</b>					
CEM 2	x	x			< 0.1
AEM 2	x	x			< 0.1

### 4.1.1 Investigation of the precipitates by optical Microscopy

The deposits on the cation exchanger membrane in April 2007 consist of white and compact grain aggregates with a maximum size of 1.5 mm (Figure 4.1a). Precipitates of the anion exchanger membrane were made up also by white and transparent grain aggregates and additionally by massive light blue fragments 2 mm size at maximum (Figure 4.1b).

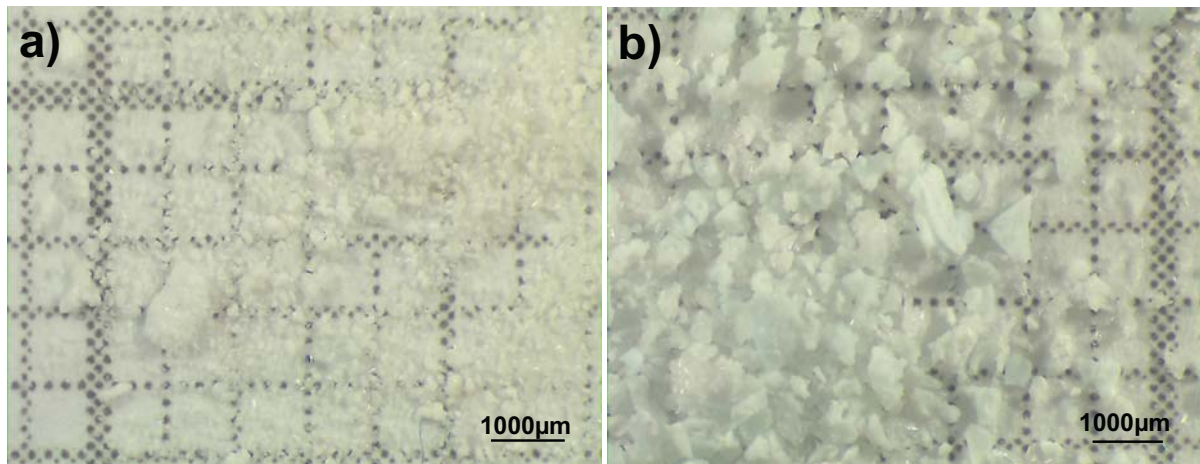


Figure 4.1: Optical Microscope exposure of the **CEM 1** fragments (a) and of the **AEM 1** fragments (b)

On the spacer of the EDR unit a deposit of massive and turquoise to white coloured solids were formed. This compact film break into small pieces by detaching the deposits from the spacer (Figure 4.2). Similarly to the precipitates on the membrane surfaces no idiomorphic crystals were visible by optical microscope up to a magnification of factor 50.

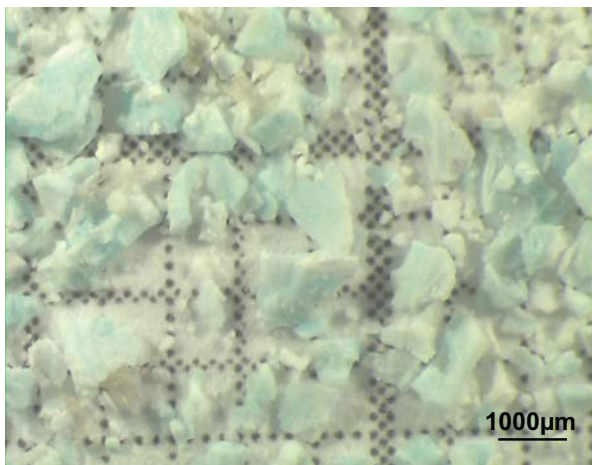


Figure 4.2: Optical microscope exposure of the **spacer 1** fragments

In April 2008 another scaling event occurred in the EDR unit. A small amount of precipitates formed a thin film of white and turquoise coloured deposits on the surfaces of the exchanger membranes (Figure 4.3 a and b). On the cation exchanger membrane surface the precipitates mimic the contact area of the spacer (Figure 4.3 a).

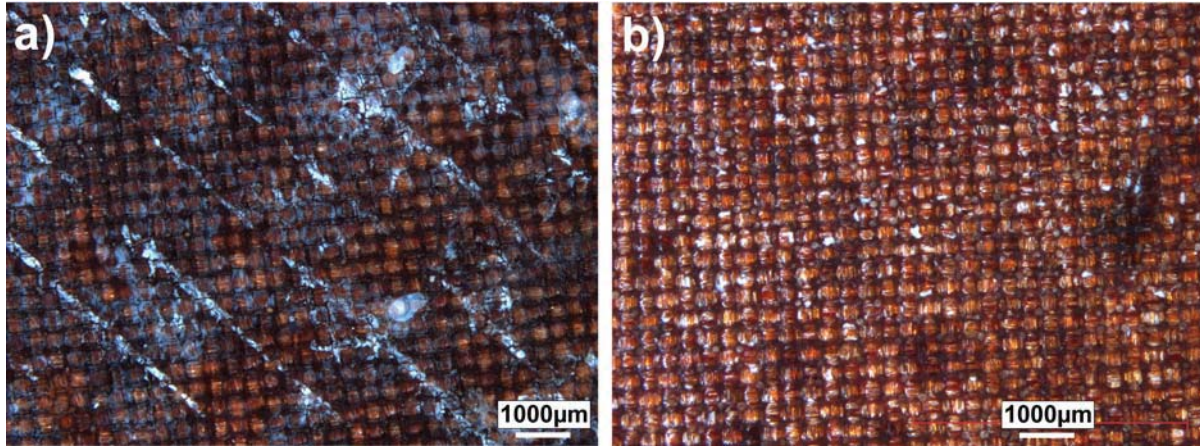


Figure 4.3: Optical Microscope exposure of the **CEM 2 (a)** and the **AEM 2 (b)** samples

### 4.1.2 Investigations of the precipitates by Environmental Scanning Electron Microscope and Energy-Dispersive X-ray Fluorescence

Fragments of the deposits as well as precipitates adhering to the membrane surfaces were investigated by Environmental Scanning Electron Microscopy (ESEM) and Energy-Dispersive X-ray Fluorescence (EDX). Images of fragments of the deposits, removed from the cation exchanger membrane, are presented in Figure 4.4. The grain aggregates are composed of a multitude of tangly, non idiomorphic crystals with a maximum size of 100 to 120  $\mu\text{m}$ . Calcium, sulphur, oxygen and carbon were determined by semi-quantitative EDX analysis of this aggregates.

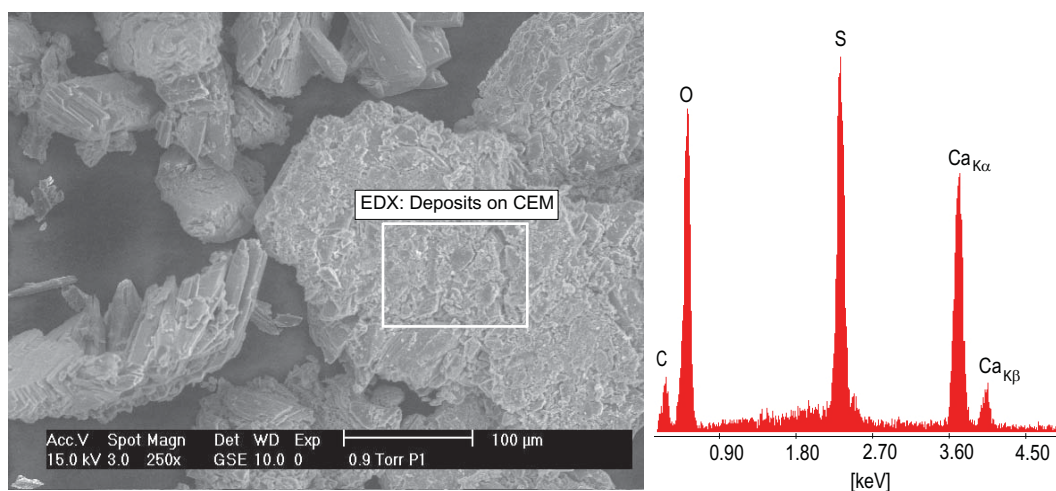


Figure 4.4: Electron-microscope image and EDX analysis of the **CEM 1** fragments

Deposits on the anion exchanger membrane exhibit compact and massive shapes (Figure 4.5). Embedded in these fragments are idiomorphic gypsum crystals with sizes up to 150  $\mu\text{m}$  and prismatic elongated to the (010) surface. Magnesium, calcium, silicon, oxygen, sulphur, carbon and small amounts of sodium, chlorine and phosphorus were determined by EDX Analysis.

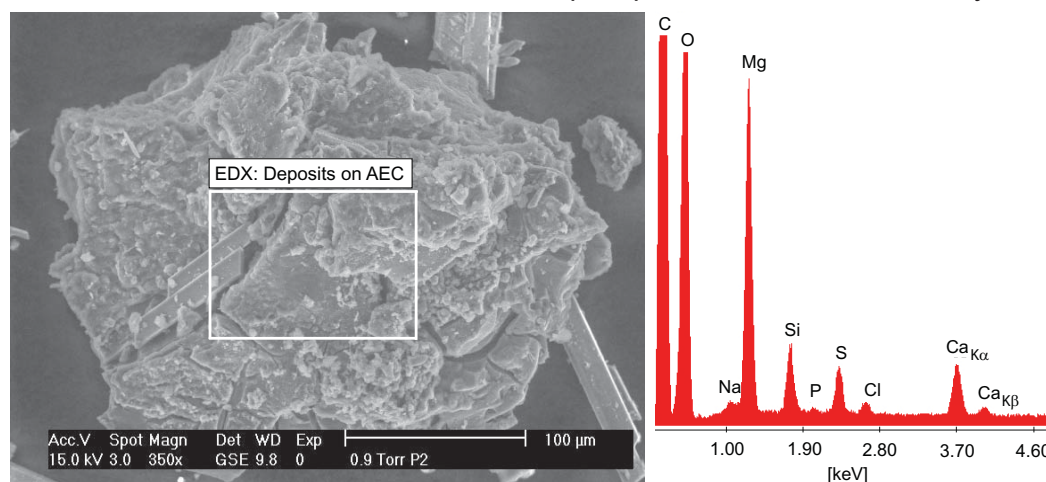


Figure 4.5: Electron-microscope exposure and EDX analysis of the **AEM 1** fragments

Figure 4.6 presents a cross section of one of the fragments, removed from the anion exchanger membrane. The bulk is made of a massive deposit, whereas the surface is coated by small spherical particles. These spheres consist of very thin ( $<0.2 \mu\text{m}$ ) lamellar arranged solids (Figure 4.6 b).

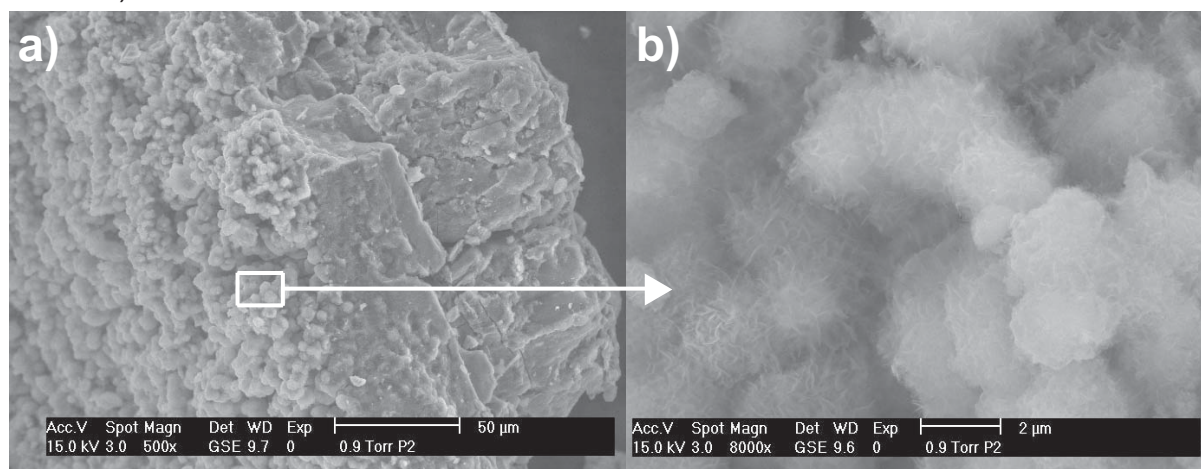


Figure 4.6: Electron-microscope exposure of a cross section of the **CEM 1** fragments (a) and the magnification of the white marked sector (b)

Fragments of the spacer are compact and massive non idiomorphic deposits with groups of disconnected cracks at the surfaces (Figure 4.7). Determination of the elemental composition by EDX resulted in high amounts of magnesium and oxygen and small amounts of calcium, silicon, phosphorus, sulphur and carbon.

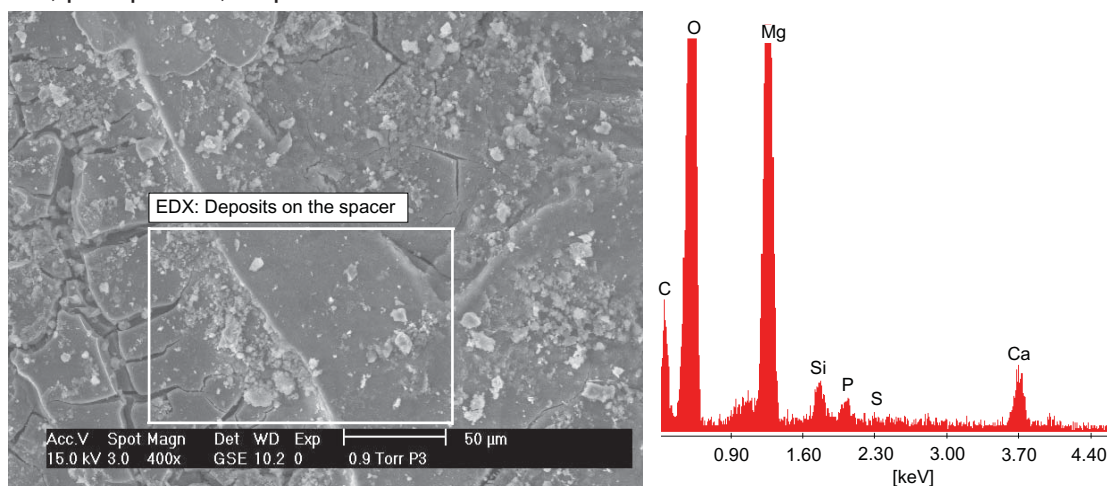


Figure 4.7: Electron-microscope exposure and EDX analysis of the **spacer 1** fragments

In April 2008 precipitates formed local thin deposits on the exchanger membrane surfaces. In contrast to the precipitates of the scaling event of April 2007 the deposits were investigated by electron microscopy directly on the membrane surface. In Figure 4.8 the cross-linked polymer fibres of the cation exchanger membrane are visible. Irregular ordered precipitates formed a thin film and grain aggregates on the membrane surface. Calcium, oxygen, magnesium, silicon, chlorine and sulphur were measured by semi-quantitative EDX analysis.

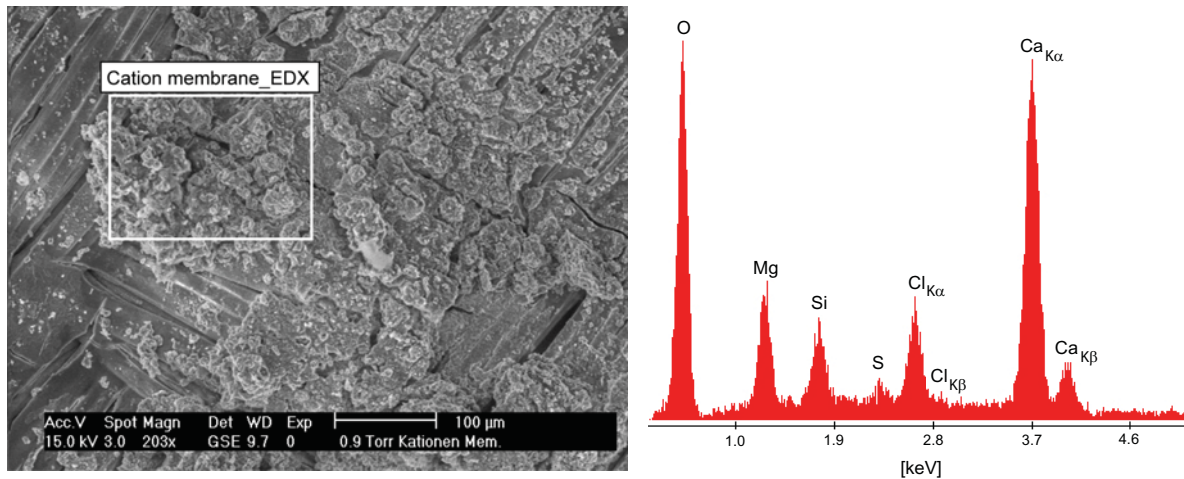


Figure 4.8: Electron-microscope exposure and EDX analysis of the **CEM 2** samples

Precipitates on the anion exchanger membrane form local aggregates up to a size of 500  $\mu\text{m}$  in diameter (Figure 4.9). Elemental composition of these deposits, determined by EDX, exists mainly of silicon, oxygen, calcium, chlorine, magnesium and sodium.

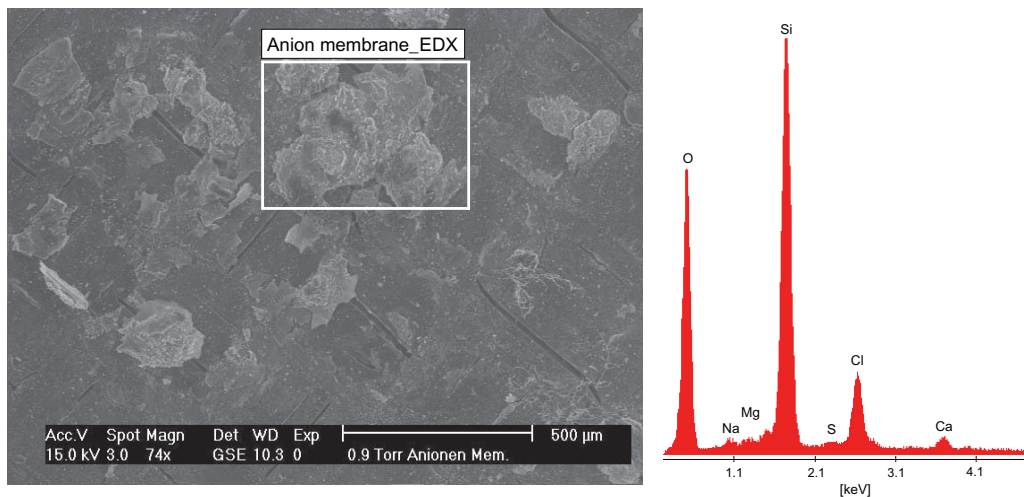


Figure 4.9: Electron-microscope exposure and EDX analysis of the **AEM 2** samples

### 4.1.3 Investigation of the precipitates by Wavelength-Dispersive X-ray Fluorescence (WD-XRF)

Precipitates of the cation exchanger membrane as well as the deposits of the spacer of the scaling event April 2007 were quantitatively analysed by Wavelength-Dispersive X-ray Fluorescence (WD-XRF). Due to the marginal amount of incrustation on the anion exchanger membrane in April 2007 and on the exchanger membranes in April 2008, no quantitative analysis could be conducted.

Loss on ignition (LOI) was 31.3% for the **AEM 1** fragments, and 44.5% for the **spacer 1** fragments. Figure 4.10 presents the mass percentage of the main components, SiO<sub>2</sub>, MgO, CaO and SO<sub>3</sub>, of the WD-XRF analysis. The deposits, detached from the anion exchanger membrane consist on SO<sub>3</sub>, of CaO and MgO, whereas the amount of SO<sub>3</sub> is slightly higher. In contrast to this composition MgO dominates the **spacer 1** fragments and CaO and SO<sub>3</sub> are accessory components. Small amounts of SiO<sub>2</sub> were detected in both samples. The concentration in the spacer 1 sample is twice as much as in the **AEM 1** sample.

Both samples contain Na<sub>2</sub>O, K<sub>2</sub>O, Fe<sub>2</sub>O<sub>3</sub>(t), ZnO, CuO, NiO, Cr<sub>2</sub>O<sub>3</sub>, Al<sub>2</sub>O<sub>3</sub>, TiO and MnO. According to DIN 32 645 the amount of these components is lower than the lower limit of the method.

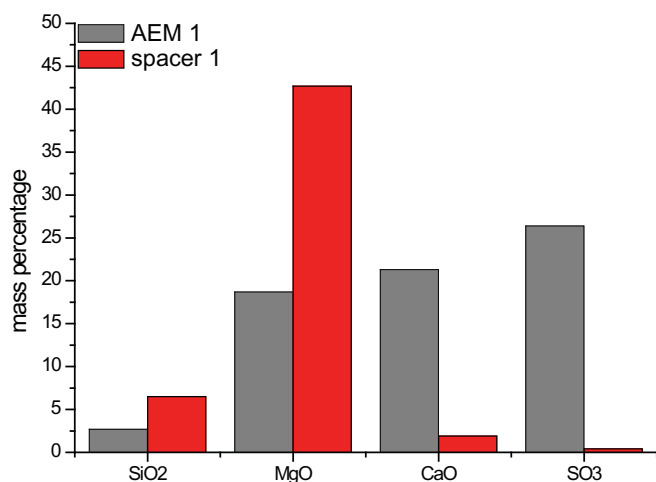


Figure 4.10: Analytical investigation by wavelength-dispersive X-ray fluorescence of the **AEM 1** and the **spacer 1** fragments

#### 4.1.4 Investigation of the precipitates by X-ray Diffraction (XRD)

The precipitates of the anion exchanger membrane as well as the precipitates of the spacer from April 2007 were analysed by X-ray diffraction (XRD). Both deposits contain gypsum ( $\text{CaSO}_4 \times 2 \text{H}_2\text{O}$ ) and brucite ( $\text{Mg}(\text{OH})_2$ ) (Figure 4.11 and 4.12).

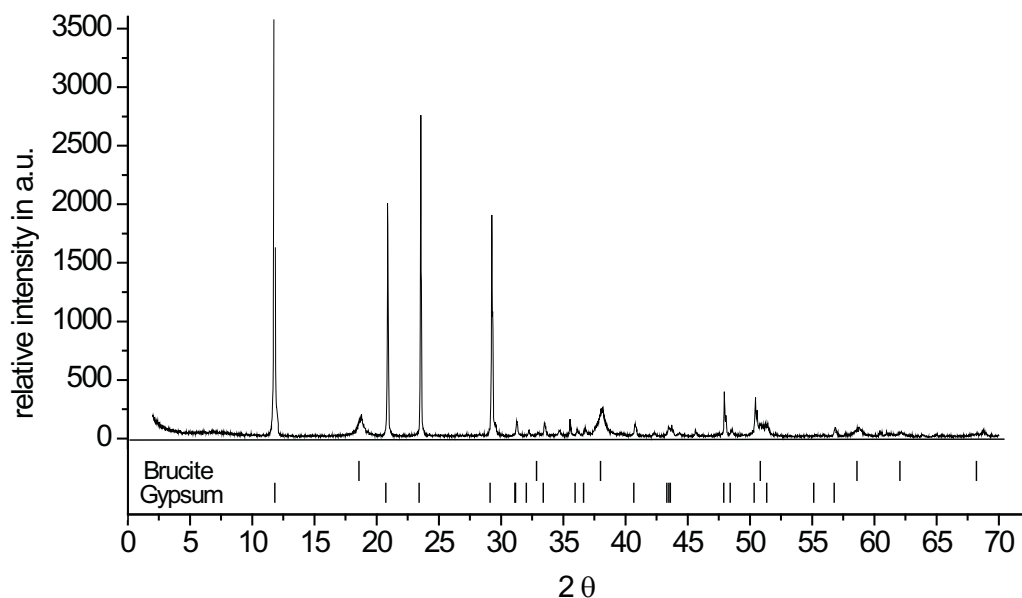


Figure 4.11: X-ray diffraction pattern of precipitates adhering to the anion exchanger membrane from April 2007

Whereas gypsum remains the dominant mineral in the precipitates detached from the anion exchanger membrane, brucite makes up the main phase of the precipitates detached from the spacer. The width of the brucite peaks in Figure 4.12 indicate poorly ordered and/or very small crystals.

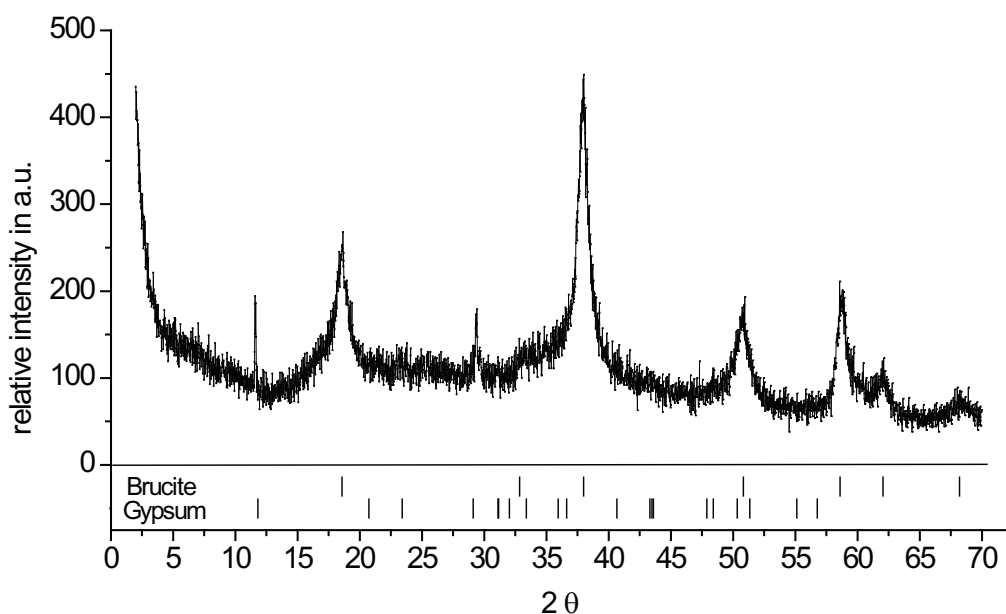


Figure 4.12: X-ray diffraction pattern of precipitates adhering to the spacer from April 2007

#### 4.1.5 Summary and discussion of membrane deposit characteristics

Original deposits, formed at two independent scaling events, were characterised chemically and mineralogically. Results are discussed separately for every event before similarities and differences of these precipitates are reviewed.

##### *Scaling in the EDR unit in April 2007*

**Sample CEM 1:** Deposits on the cation exchanger membrane, **CEM 1**, are made of fine-grained, very compact white aggregates. Inferred from semi-quantitative analysis they are mainly constituted of oxygen, sulphur and calcium. Due to the semi-quantitative elemental analysis it is very probable that gypsum,  $\text{CaSO}_4 \times 2\text{H}_2\text{O}$ , precipitated on the membrane.

**Sample AEM 1:** High intensity of XRD peaks and quantitative elemental analysis by WD XRF revealed gypsum as the main constituent in deposits on the anion exchanger membrane. This result stands in excellent agreement with investigation by electron microscopy. Here, idiomorphic gypsum crystals were identified within the white precipitates. Semi-quantitative elemental analysis of the mostly bluish dyed, massive fragments show a high amount of magnesium and silicon. Due to investigations by XRD it is probable that they are mainly made of brucite,  $\text{Mg}(\text{OH})_2$ . The blue dye of the samples arises from of a small fraction of metals like copper, nickel, iron and chromium. Tiny amounts of these metals are required for dyeing the precipitates.

**Sample spacer 1:** Due to the relatively high amount of magnesium in combination with the XRD measurements, brucite was identified as the main component in the deposits of the spacer. Low intensities of the main peaks of gypsum at 11.588 and 20.722  $2\theta$  as well as low concentration of CaO and  $\text{SO}_3$  indicate only a small amount of gypsum in the fragments. As mentioned before, colouration of the precipitates is caused by the presence of additional constituents like copper, nickel, iron and chromium. Increasing colour intensity in contrast to AEM 1 fragments indicates a higher amount of metal ions in fragments of the spacer. A summary of the results is given in Table 4.3.

Table 4.3: Results of the characterisation of deposits formed in April 2007 on membrane surfaces and on the spacer in the EDR unit of the pilot plant

method <sup>a</sup>	CEM 1	AEM 1	spacer 1
LM	white grainy, compact aggregates	white and light blue, compact aggregates	turquoise to white coloured, compact aggregates
ESEM	tangly, non idiomorphic crystals in grainy aggregates	idiomorphic gypsum crystals, embedded in a compact and massive matrix	compact grainy aggregates without idiomorphic crystals
EDX	O, S, Ca	O, Ca, S, Mg, Si, Na, P, Cl	O, Mg, Si, S, Ca, P
WD XRF	not determined	CaO, $\text{SO}_3$ , MgO, $\text{SiO}_2$	MgO, $\text{SiO}_2$ , CaO, $\text{SO}_3$
XRD	not determined	gypsum, brucite	gypsum, brucite

a. abbreviation of methods see Chapter 4.1.

### *Scaling in the EDR unit in April 2008*

Investigation of the deposits were conducted directly on the membrane surface as a consequence of the very small amount of precipitates. Therefore, no analysis by XRD and WD XRF was carried out.

**Sample CEM 2:** Precipitates formed a thin film on the cation exchanger membrane surfaces with locally massive aggregates. Due to the semi-quantitative EDX analysis and in support by the analysis of the deposits of April 2007 it is assumed that the deposits are mainly made of brucite and small amounts of gypsum.

#### **Sample AEM 2:**

EDX analysis revealed remarkably high amounts of magnesium, silicon and oxygen and minor amounts of calcium and sulphur. Likewise as for fragments of CEM 2 it can be assumed that deposits are made of brucite and very small amounts of gypsum. A summary of the results are noted in Table 4.3.

Table 4.4: results of the characterisation of deposits formed in April 2008 on membrane surfaces and on the spacer in the EDR unit of the pilot plant

method <sup>a</sup>	CEM 2	AEM 2
LM	white and turquoise coloured, plane film of aggregates	white, isolated aggregates
ESEM	thin, plane film of precipitates with local grainy deposits	separated, grainy, non idiomorphic aggregates
EDX	O, Mg, Si, S, Cl, Ca	O, Mg, Si, Ca, S, Na, Cl

a. abbreviation of methods see Chapter 4.1.

### *Comparison of the two scaling events*

Variable amounts of gypsum and brucite constitute the main minerals in all deposits. Silicon was detected always in combination with magnesium. Due to small sample amounts the applied analytical methods were not able to reveal whether silicon forms single precipitates like amorphous silica or is attached to mineral surfaces.

Chlorine and sodium were detected by EDX in all samples except in the sample spacer 1. As a result of the high solubility of halite the presence of sodium and chlorine may be caused by residual moisture of small amounts of EDR brine after sampling. Membranes were taken out of the EDR stack without washing off the brine. Hence, small amounts of sodium and chlorine remain on the precipitates. Carbon was measured solely by EDX in the fragments of CEM 1, AEM 1 and spacer 1, it was not detected in the precipitates AEM 2 and CEM 2, which were directly measured on the membrane surfaces. The presence of calcite in the samples was excluded by XRD measurements. From these results it is inferred that the detected carbon fraction belongs to the sample holder where the fragments were directly glued on.

### *Reasons for the formation of gypsum and brucite in the EDR unit*

Analysis of the scaling deposits on the membrane surfaces and the spacer in the EDR unit are composed of various amounts of the minerals gypsum and brucite. Based on the results of the geochemical modelling with the GWB, both minerals are saturated in the EDR brine at  $\text{pH} > 9.5$ , see Chapter 3.3.3.3 (Figure 18). Below this  $\text{pH}$ , both minerals remain undersaturated in the EDR brine. Due to the operation condition of the EDR unit, the EDR feed is adjusted to  $\text{pH} = 2$  and remains at this value during the treatment of the concentrate in the EDR unit, where gypsum and brucite are undersaturated. The occurrence of these minerals in the EDR membrane stack leads to the conclusion that the  $\text{pH}$  of the solutions changed to values above 9.5.

This is an alarming conclusion concerning the continuous operation of the pilot plant. As mentioned before, every scaling event reduces the permeability of the respective exchanger membrane to a minimum. In this case the membrane has to be replaced, which means the whole membrane stack has to be shut down. Chemical cleaning of the membrane surfaces of exchanger membranes for EDR units remains a difficult process. A damage of functional surface groups must be avoided. It is absolutely necessary to find out which processes may cause  $\text{pH}$  values  $>9.5$  in the EDR unit.

Therefore, different scenarios were considered. Concentration polarisation of electrolytes on the membrane surfaces can result in locally extreme  $\text{pH}$  values. Cations and also  $\text{H}_3\text{O}^+$  migrate towards the cathode. In the presence of high amounts of electrolytes an accumulation of cations may be formed before passing the cation exchanger membrane. In contrast, anions and also  $\text{OH}^-$  migrate in the direction of the anode and can also accumulate at the anion exchanger membrane. Concentration polarisation leads to locally low  $\text{pH}$ s directly on the cation exchanger surface and, in the opposite, to locally high  $\text{pH}$  values at the anion exchanger membrane. In case of the EDR unit of the pilot plant, increasing  $\text{pH}$  will result in exceeding the solubility product of gypsum and brucite. As a consequence the minerals precipitate and the membrane surface will be blocked.

Especially exchanger membranes of electrodialysis units are prone to concentration polarisation. Three mechanisms were used to avoid this problem during operation of an ED unit. First, the electric potential of the EDR unit is reversed in regular intervals and thus migration direction of charged ion species is reversed. Secondly, the flux of the feed water is kept relatively high in comparison to the migration velocity of the electrolytes to flush accumulated ions. Thirdly, concentrate flow is disturbed on the spacer which leads to vortexing and remixing of the feed solution. Flow decrease or constant electrical potential instead of reversed potential may cause concentration polarisation.

On the other hand, formation of sparingly soluble salts on membrane surfaces may also reduce permeability of the exchanger membranes, as a consequence electrolytes may accumulate on membrane surfaces. If so, inorganic scaling must occur at pH 2 in the EDR unit due to the acidified RO concentrate, continuously mixed with EDR concentrate, which acts as feed water.

At this pH, formation of gypsum and brucite can be excluded, so one reason of membrane pore blockage could be the formation of large, polymerised molecules of silicic acid in the EDR brine. Another scaling reason at pH 2 can be the formation of amorphous silica. Results of the geochemical modelling show that solely amorphous silica is oversaturated in the EDR process solution at this low pH. Quantitative and semi-quantitative elemental analysis indicates silicon in several scaling deposits but XRD measurement gave no indication for the formation of Si-containing crystalline phases. The applied analytical methods give no information whether the silicon is a compound of amorphous silica ( $\text{SiO}_2$ ) or silicic acid is adsorbed at the mineral surfaces of brucite or gypsum. Formation of amorphous silica may occur at pH below 9.3. If scaling deposits are formed at pH values higher than 9.5, an adsorption-driven process is most likely due to the high solubility of silicic acid at this high pH.

If silica scaling blocks membrane surfaces and membrane channels, flow velocity decreases and thereby pH locally increases. As a consequence gypsum and brucite precipitate. Polymerisation of silicic acid and also the formation of amorphous silica in concentrates of the EDR unit have to be investigated by laboratory experiments to reveal more information about the process which triggers precipitation and how to avoid the formation of inorganic solids in the EDR unit. These experiments are presented in the next Chapter.

## 4.2 Formation conditions of inorganic solids in the EDR unit: Laboratory experiments

To investigate whether polymerisation of silicic acid or precipitation of amorphous silica is responsible for scaling in the EDR unit, solubility and seeding experiments were conducted. First, solubility of amorphous silica in different solutions was determined and compared with the calculated values and values from literature. Secondly, the formation of amorphous silica and the influence of seeding material in synthetic laboratory experiments were investigated in short-duration experiments as a function of the pH. Additionally, polymerisation of silicic acid and the formation of large dissolved molecules in these experiments were detected. Titration experiments were conducted to investigate the influence of pH shifts to basic pH values on silicic acid and formation conditions of precipitates.

### 4.2.1 Solubility of amorphous silica, $\text{SiO}_2$ , in the EDR concentrate

Solubility experiments were conducted to investigate the influence of the electrolyte combination and concentration on the solubility of amorphous silica in EDR brine and in deionised water (DIW).

#### Experimental setup

Solubility of amorphous silica (Merck) was investigated using three different solutions: doubly deionised water (DIW) at pH 6.5, and in two different synthetic laboratory EDR concentrates at pH 2, one being  $\text{SiO}_2$ -free and another one with an initial concentration of 135 mg/l  $\text{SiO}_2$ . 18 flasks per test series were filled with 40 ml liquid and 0.5 g of amorphous silica (solid silicic acid, Merck). Experiments were carried out at 25°C in a water bath on a shaking table under air (Figure 4.13). At sampling two flasks per test series were removed from the water bath and liquid was filtered through a 0.2 µm membrane filter. The initial Si concentration in solution was measured before adding solid silicic acid. During the experiment Si concentration was determined after 1, 3, 5, 7, 14, 22, 28 and 36 days by ICP-OES with repeat determination. For ICP-OES measurements samples were directly diluted 1:10.

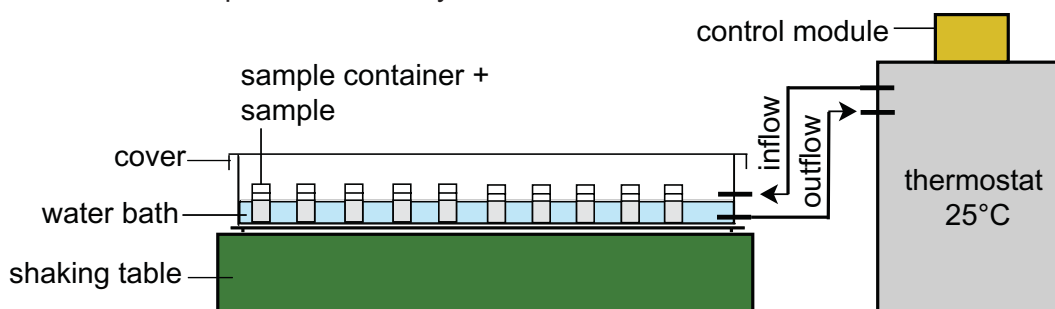


Figure 4.13: Sketch of the experimental setup of the solubility experiments

## Results

Results of the solubility experiments are presented in Figure 4.14. In DIW the  $\text{SiO}_2$  concentration sharply increases up to 118 mg/l during the first 7 days of the experiment. The equilibrium concentration of 123 mg/l  $\text{SiO}_2$  was not reached before day 28.

Significant differences between  $\text{SiO}_2$ -free and  $\text{SiO}_2$ -containing were observed for the synthetic EDR concentrates. Dissolution of solid silicic acid in a  $\text{SiO}_2$ -free synthetic EDR concentrate, initial pH = 2, remains as a slow but continuous process were the equilibrium concentration, 58 mg/l  $\text{SiO}_2$ , between solid and solution is reached after 28 days. In contrast to this behaviour the influence of seeding material on a synthetic EDR concentrate, oversaturated with respect to silicic acid, is much slower and does not reach equilibrium between seeding material and solution within the duration of the experiment. The concentration of  $\text{SiO}_2$  in solution decreases from 135 to 115 mg/l  $\text{SiO}_2$ .

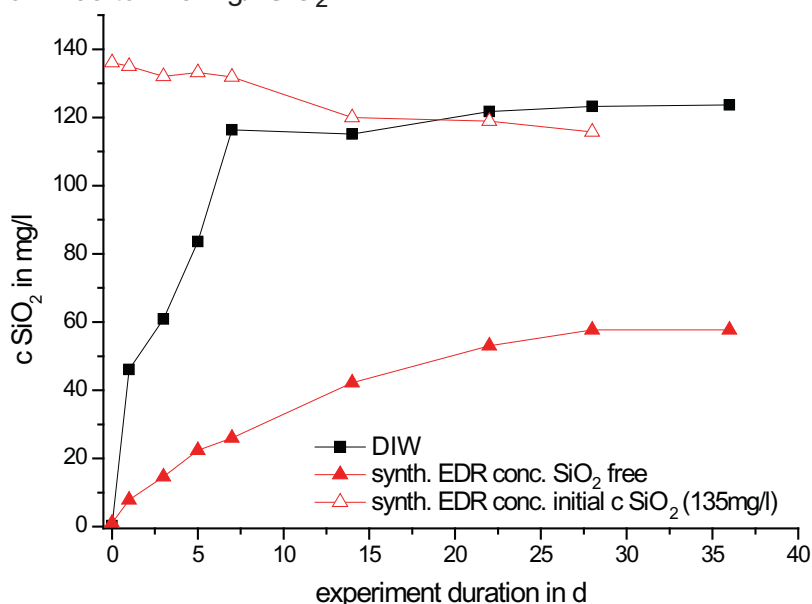


Figure 4.14: Solubility of amorphous silica ( $\text{SiO}_2$ ) in doubly deionised water (DIW), in synthetic  $\text{SiO}_2$ -free EDR concentrate and in synthetic EDR concentrate with an initial concentration of 135mg/l  $\text{SiO}_2$  and an initial pH of 2

A comparison between experimental data and calculated solubilities is given in Table 4.5.

Table 4.5: Solubility of amorphous silica ( $\text{SiO}_2$ ) in doubly deionised water (DIW) and in synthetic  $\text{SiO}_2$ -free EDR concentrate

	solubility of $\text{SiO}_2$ in mg/l $\text{SiO}_2$	
	experimental	calculated (this work)
DIW	123	117
synth. EDR concentrate, $\text{SiO}_2$ -free	58	34

## 4.2.2 Seeding experiments

In contrast to the equilibrium experiments of Chapter 4.2.1, the short-time effect on the solubility of amorphous silica, polymerisation of silicic acid and influence of seeding material on the  $\text{SiO}_2$ -oversaturated solution were investigated as a function of pH and time. Polymerisation in the experiments was determined by the ratio between the amount of total and reactive silica in the concentrates. Terms of total and reactive silica were already described in Chapter 2.2.2.2. Retention time of the EDR process solution in the EDR membrane stack lies in the range of minutes. Therefore, short-time experiments with sampling periods between 2h and 8h were chosen.

### Experimental setup

Three different experimental systems were defined:

**System A:** synthetic laboratory EDR concentrate with an initial  $\text{SiO}_2$  concentration of 155mg/l

**System B:** system A + seeding material

**System C:**  $\text{SiO}_2$ -free synthetic laboratory EDR concentrate + seeding material

$\text{SiO}_2$  concentration and degree of polymerisation in systems **A** to **C** were measured at various pH values between 2 and 6. Eight flasks per test series were filled with 40 ml liquid and 0.5 g of amorphous silica (solid silicic acid, Merck) were added to the test series of systems B and C. Experiments were conducted at 25°C in a water bath on a shaking table (Figure 4.13). After 2, 4, 6 and 8h two flasks per test series were removed from the water bath and suspension was filtered through a 0.2  $\mu\text{m}$  membrane filter by sub-pressure filtration. Dilution for colorimetric and ICP-OES measurements was made directly after sampling. The concentration of the monosilicic acid, the reactive silica, in the filtrate was measured colorimetrically with repeat determination in a 1:10 dilution. The total Si-concentration was measured by ICP-OES with repeat determinations, in a 1:25 dilution.

## Results of the seeding experiments at pH 2

Figure 4.15 shows the results of the seeding experiments at pH 2.

**System A:** Without the influence of seeding material the total  $\text{SiO}_2$  concentration deviates slightly in comparison to the initial amount. Approximately 5% of the silicic acid form oligomere species. The concentration of the reactive silica as well as of the total silica remain constant during the experiment.

**System B:** Total and reactive silica concentration remain constant, polymerisation of silicic acid reaches approximately 5 to 6%.

**System C:** Only a little amorphous silica was dissolved with a maximum amount of 4% in comparison to the supersaturated brine of system A.

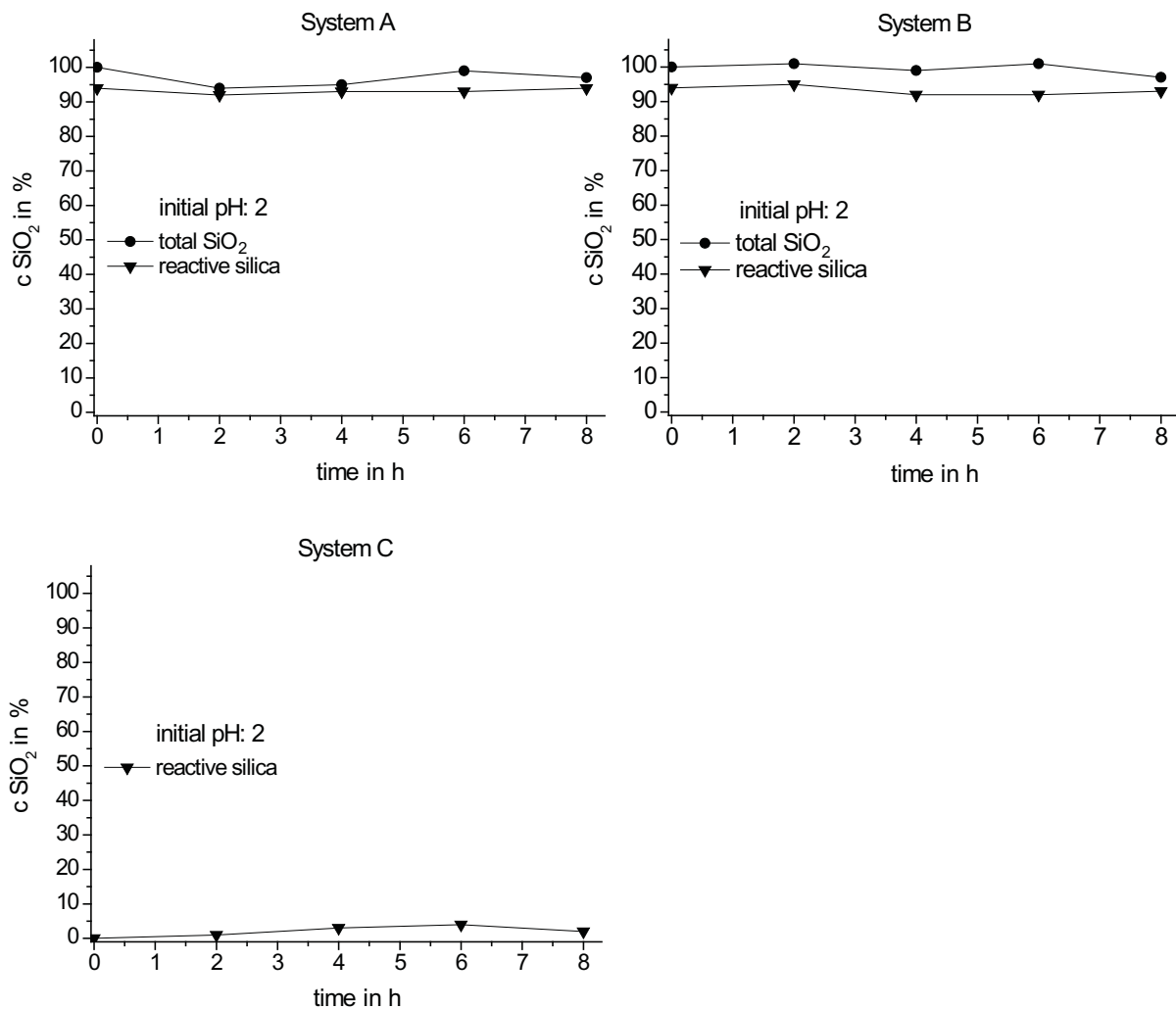


Figure 4.15: Total and reactive  $\text{SiO}_2$  concentration of the seeding experiments at pH 2 in the systems **A** to **C**. In system **C** the maximum concentration of 100%  $\text{SiO}_2$  is based on the initial concentration of systems **A** and **B**.

### Results of the seeding experiments at pH 3

Figure 4.16 shows the results of the seeding experiments at pH 3.

**System A:** Similarly to the experiments at pH 2 a polymerisation of silicic acid of about 5% was detected. The total and the reactive silica concentration did not change significantly during the 8h of the experiment.

**System B:** The total silica decreases to 95% in comparison to the initial  $\text{SiO}_2$  concentration after 6h of the experiment. The amount of the reactive silica remains constant.

**System C:** The  $\text{SiO}_2$  concentration in solution increases continuously from 0 to 6% in comparison to the initial silica concentration of system A and B during 8h of the experiment.

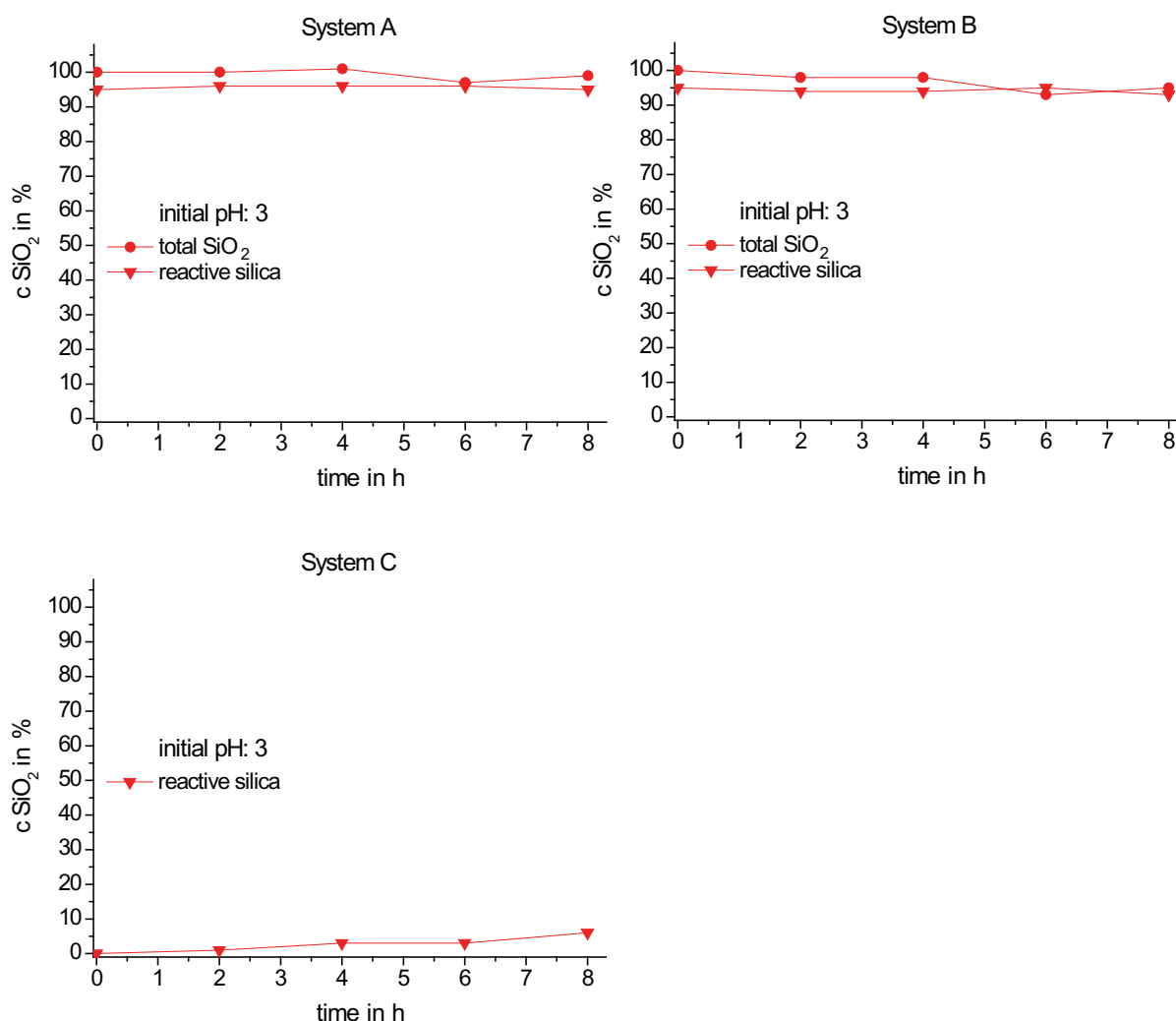


Figure 4.16: Total and reactive  $\text{SiO}_2$  concentration of the seeding experiments at pH 3 in the systems **A** to **C**. In system **C** the maximum concentration of 100%  $\text{SiO}_2$  is based on the initial concentration of systems **A** and **B**.

### Results of the seeding experiments at pH 4

Figure 4.17 shows the results of the seeding experiments at pH 4.

**System A:** The total and the reactive silica concentration remains constant during the experiment. The amount of monosilicic acid in solution constitutes 96%, the amount of the oligomerised fraction is 4%.

**System B:** By adding amorphous silica to the brines with an initial pH of 4, a slight deviation was detected in the total silica concentration. The amount of reactive silica at 8h remains at 97%, thus 3% of the total silica polymerises at pH 4.

**System C:** Total and reactive silica increases up to 13% in comparison to the initial concentration of the systems A and B. A maximum polymerisation of 2 to 3% was reached after an experimental duration of 4 and 6h.

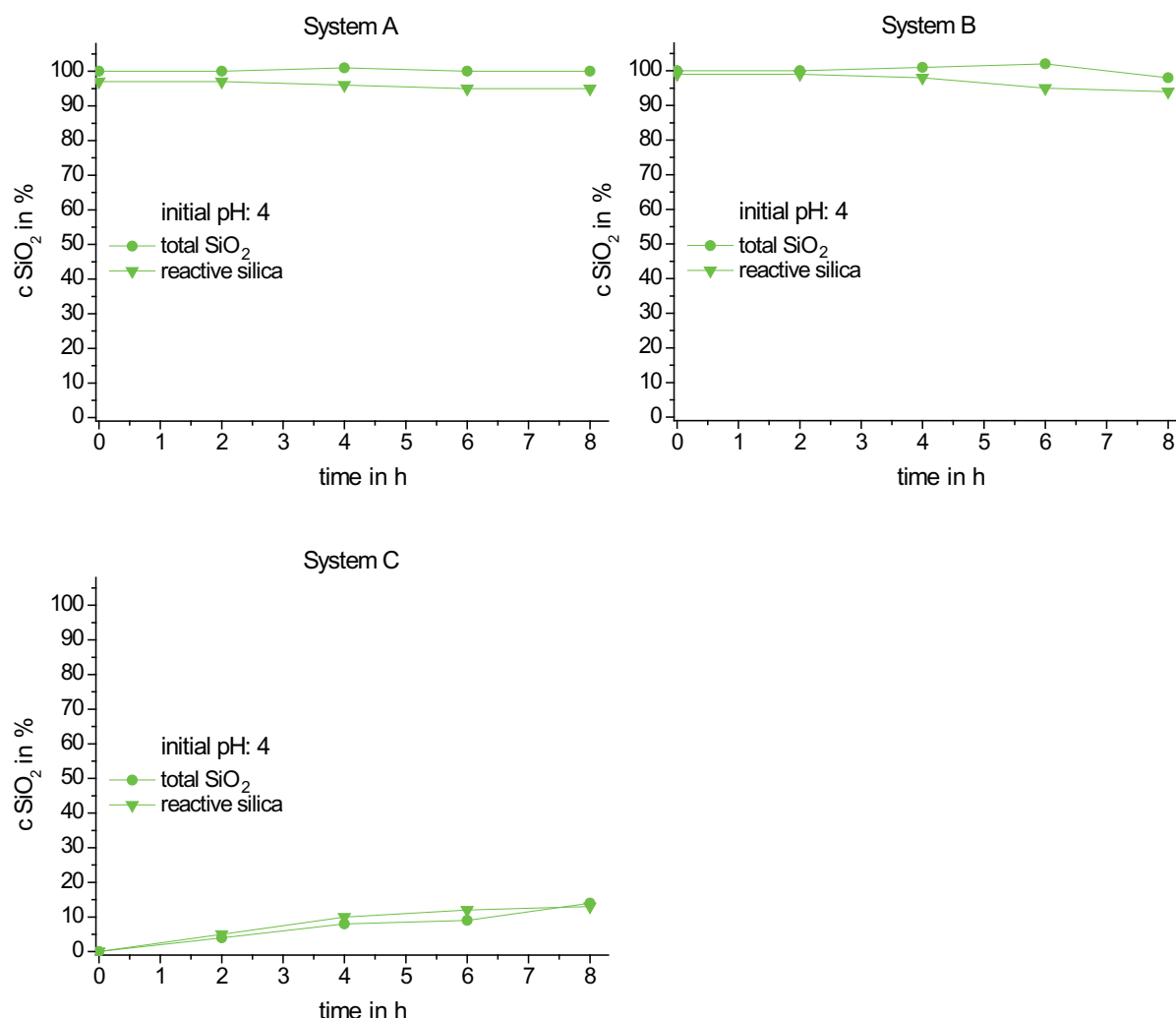


Figure 4.17: Total and reactive SiO<sub>2</sub> concentration of the seeding experiments at pH 4 in the systems A to C. In system C the maximum concentration of 100% SiO<sub>2</sub> is based on the initial concentration of systems A and B.

### Results of the seeding experiments at pH 5

Figure 4.18 shows the results of the seeding experiments at pH 5.

**System A:** The concentration of the total and the reactive silica remains constant during the experiment. The amount of monosilicic acid constitutes 87% while 13% of the total silica form oligomers of the silicic acid.

**System B:** After the addition of the seeding material to the brines the total silica concentration decreases to 90% and remains constant at this value. The amount of reactive silica in solution decreases from 87% at time 0 (before adding the seeding material) to 75%. The difference between the total and the reactive silica deviates between 12 and 13% during the experiment.

**System C:** The concentration of total and reactive silica increases continuously. During the first 2h of the experiment the total silica concentration constitutes 18% and reactive silica 15%. After 8h 29% of total silica and 25% of the reactive silica was detected. 5% of the total silica are present as polymerised species of the silicic acid.

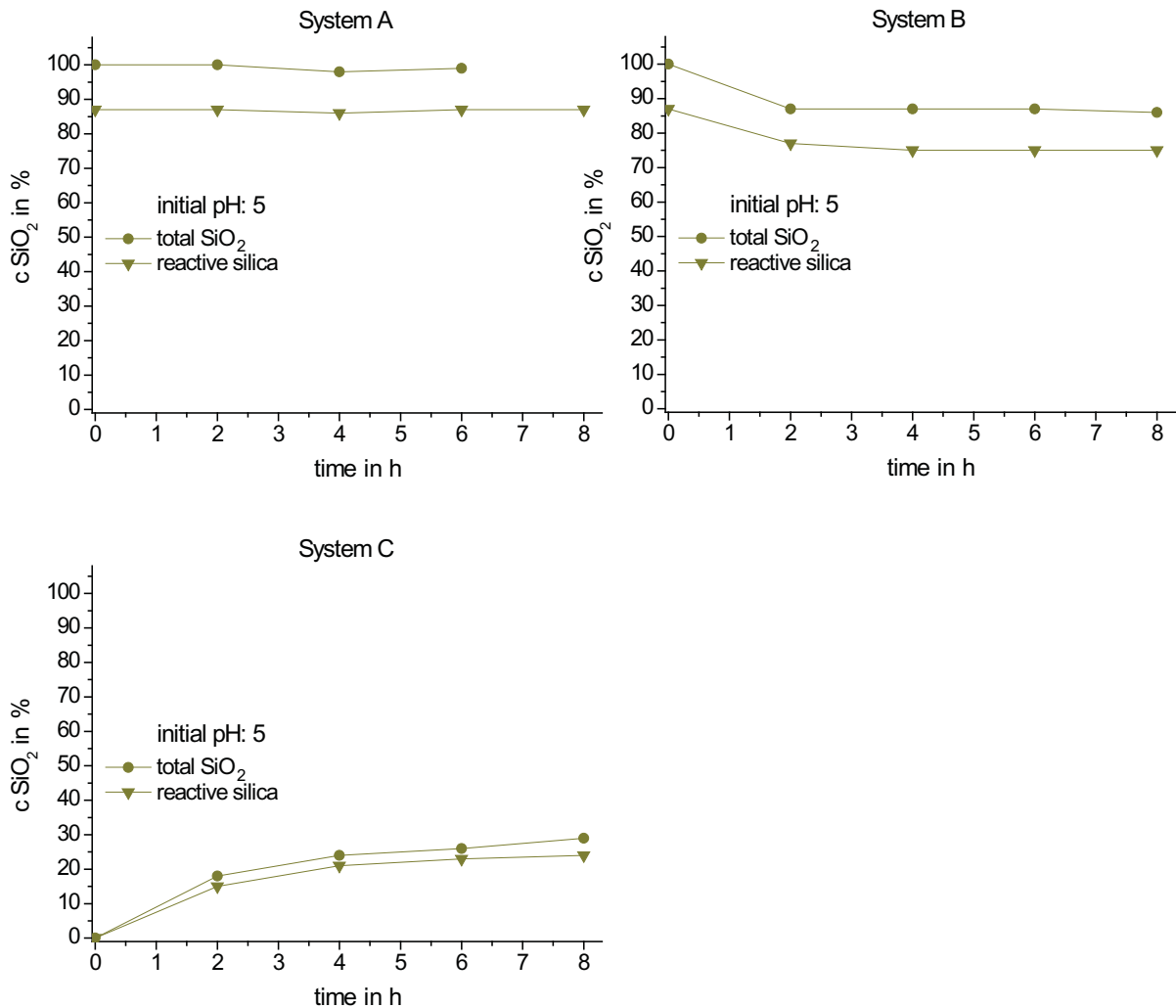


Figure 4.18: Total and reactive SiO<sub>2</sub> concentration of the seeding experiments at pH 5 in the systems **A** to **C**. In system **C** the maximum concentration of 100% SiO<sub>2</sub> is based on the initial concentration of systems **A** and **B**.

## Results of the seeding experiments at pH 6

Figure 4.19 shows the results of the seeding experiments at pH 6.

**System A:** The amount of total and reactive silica remains constant during the experiment. Monosilicic acid forms 87% and oligomers form 13% of the total silica concentration.

**System B:** After addition of amorphous silica the total silica concentration decreases to 87% of the initial concentration and remains constant at this value. Similarly to system A, oligomers are formed and constitute 13% of the initial total silica concentration. With decreasing amount of total silica, the reactive silica concentration decreases during the first two hours and remains constant to the end of the experiment.

**System C:** the total silica concentration increases to 52% of the initial silica concentration, whereas the main amount was dissolved within the first two hours. Reactive silica concentration reaches 43% after 8h of the experiment, approximately 9% of the silicic acid form oligomers.

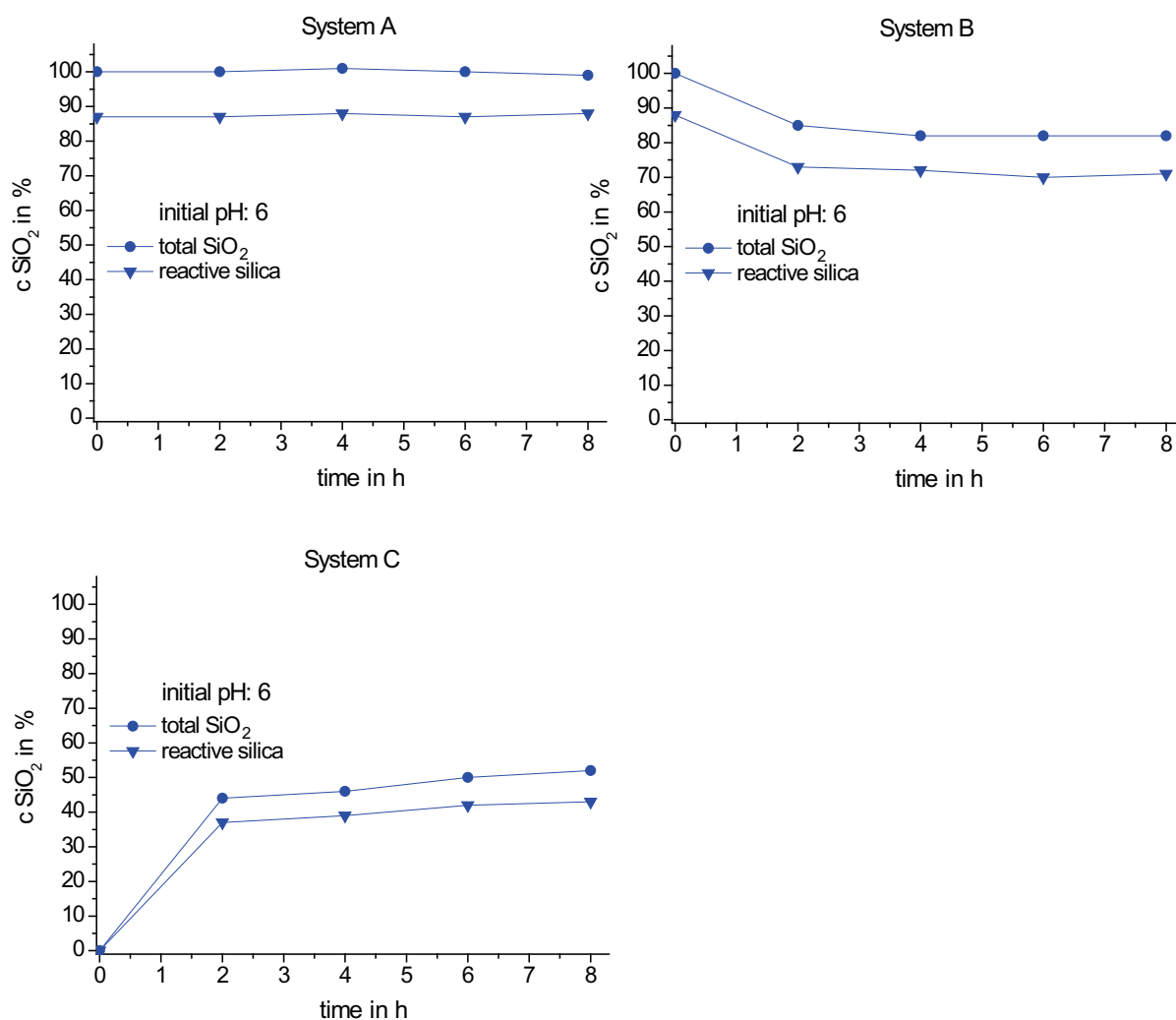


Figure 4.19: Total and reactive SiO<sub>2</sub> concentration of the seeding experiments at pH 6 in the systems **A** to **C**. In system **C** the maximum concentration of 100% SiO<sub>2</sub> is based on the initial concentration of systems **A** and **B**.

## 4.2.3 Titration experiments

Increasing pH in the EDR unit was simulated in titration experiments in dilute as well as in single salt solutions and in original EDR concentrate.

### 4.2.3.1 Titration of silicic acid in DIW and $\text{MgCl}_2$ solution

Titration experiments were conducted in DIW and in 0.12 mol/kg  $\text{MgCl}_2$  solution whereas NaOH consumption was investigated as a function of the silicic acid concentration.

#### **Experimental setup**

Nearly salt-free aqueous solutions, containing 50, 100 and 200 mg/l  $\text{SiO}_2$  were prepared by the addition of different amount of Si-stock solution to DIW. Additionally 0.12 mol/kg  $\text{MgCl}_2$  solutions, containing 50, 70, 100, 150 and 200 mg/kg  $\text{SiO}_2$  were prepared. The pH of all solutions was adjusted to 2.2 with hydrochloric acid. Increasing pH in solutions was obtained by the dropwise addition of 0.1 molar caustic soda. Changes in the pH of the different solutions were investigated as a function of the NaOH consumption. For every solution 3 titration curves were measured and averaged. For this purpose, 100 ml of solution was stirred in a plastic beaker. 0.1 mol/l NaOH was added dropwise using a burette and pH was measured with a pH meter (electrode by WTW: SenTix81). In DIW solutions a stable pH value was observed in less than one minute after addition of caustic soda. In  $\text{MgCl}_2$  solutions above pH 8, no stable value was reached within this short time. It was decided to record the value observed at 5 min. after addition of caustic soda.

#### **Results**

In Figure 4.20 titration curves of  $\text{SiO}_2$ -free solutions of DIW and 0.12 molal  $\text{MgCl}_2$  are shown. In pure DIW the pH increases slowly to 3.7 by addition of 6.5 mmol NaOH. Between pH 3.7 and 9.9 the transition range of the titration curve is passed, which requires 0.5 mmol NaOH. With further addition of caustic soda pH increases slowly. Titration was stopped after an addition of 15.8 mmol NaOH at a pH of 11.7. The transition range of the titration in pure 0.12 molal  $\text{MgCl}_2$  solution lies between pH 3.8 and 9.2 which requires 6.1, respectively 6.6 mmol NaOH to be added. The titration in DIW water shows an ideal shape of a titration curve, whereas the curve of the titration in  $\text{MgCl}_2$  solutions is non-ideal. In contrast to the titration in DIW, where the pH strives continuously to a maximum value, the maximum pH of 9.8 in  $\text{MgCl}_2$  solution was reached after a addition of 7.6 mmol NaOH. With further addition of NaOH, the pH decreases slightly to 9.6.

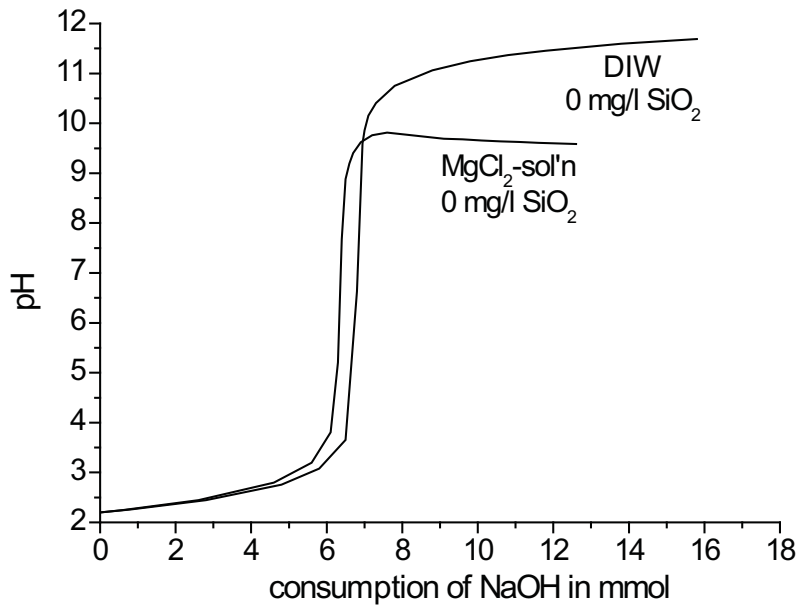


Figure 4.20: Titration curves of pure solutions of DIW and 0.12 molal  $\text{MgCl}_2$  titrated with 0.1 molar NaOH

The presence of silicic acid in DIW influences the titration significantly (Figure 4.21). With increasing amount of silicic acid in DIW, the end of the transition range is reached at lower pH and a higher consumption of NaOH was measured to reach the same pH value above pH 9. In Figure 4.21 grey lines mark the respective pH in the different solutions which is reached by addition of 8 mmol NaOH. The more silicic acid in solution, the less is the respective pH value. In DIW, containing 0, 50, 100 and 200 mg/l  $\text{SiO}_2$ , respectively pH values of 10.8, 10.5, 9.8 and 9.3 were detected (Figure 4.21, grey lines). All titration curves strive to a maximum pH around 11.8. Therefore, nearly the same amount of NaOH is required.

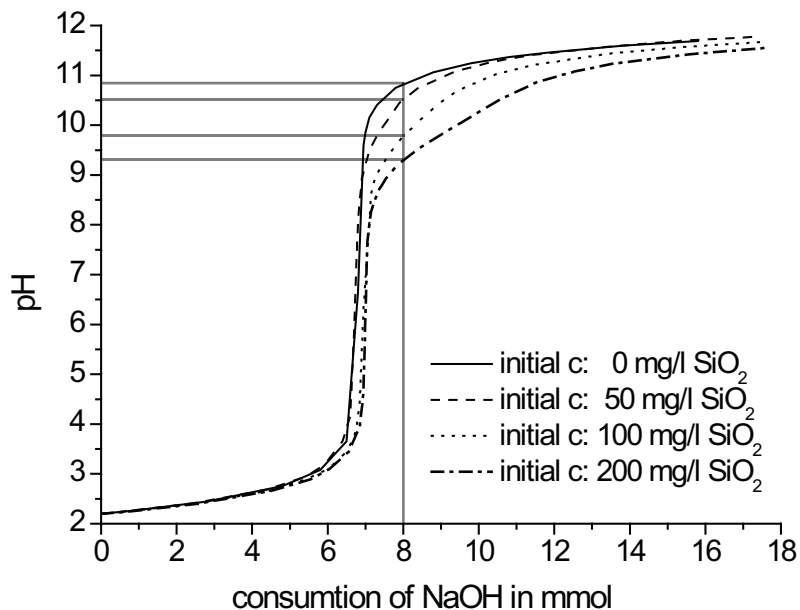


Figure 4.21: Titration curves for various concentrations of silicic acid in DIW

Titration of 0.12 molal  $\text{MgCl}_2$  solutions, containing 0, 50, 70, 100, 150 and 200 mg/l  $\text{SiO}_2$ , show a similar shape of the curves to the titration curves in DIW, up to a pH of 8.3 (Figure 4.22). Here the transition range ends for all solutions, independently of the initial  $\text{SiO}_2$  concentration. From this pH upward, with increasing amounts of silicic acid in solution an increasing amount of caustic soda was required to reach the same pH. The respective pHs, measured after addition of 8 mmol NaOH are marked in Figure 4.22 by grey lines. A persistent, whitish turbidity of the solutions was observed at pH values <8.5.

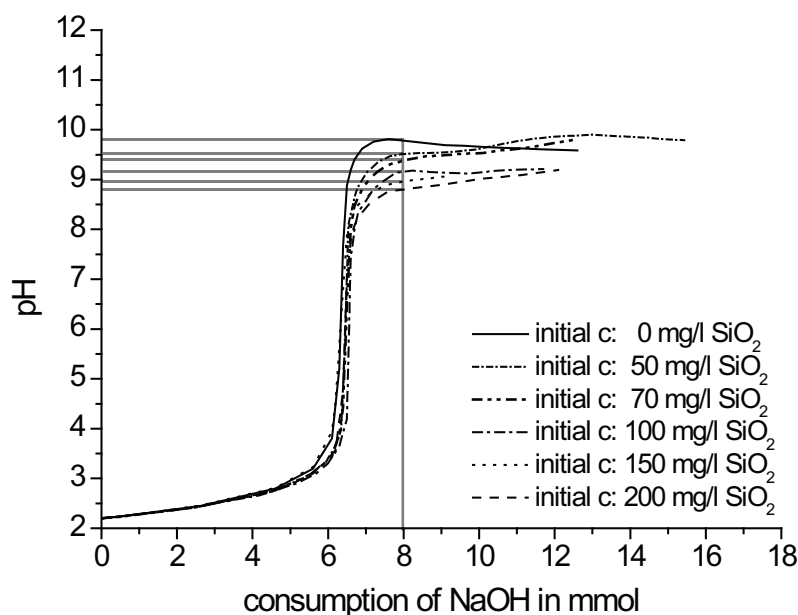


Figure 4.22: Titration of various initial amounts of  $\text{SiO}_2$  in 0.12 molal  $\text{MgCl}_2$  solutions

#### 4.2.3.2 Titration experiments with original EDR concentrate

To investigate the formation of inorganic solids with increasing pH in the EDR brine precipitation experiments were conducted. Increasing pH was obtained by addition of caustic soda.

##### Experimental setup

Solely original EDR concentrates were used for the precipitation experiments. Original EDR brine with an initial pH of 2.1 was filled into twelve plastic beakers and vigorously stirred with a magnetic stirrer. For fast and homogenous mixing of the additive, the NaOH (2M) was added dropwise in various amounts to this solutions. After preliminary tests of the experiment it was decided to use bigger volumina of the EDR brine for precipitation A to F in order to produce enough precipitates for the following analysis of the solids (Table 4.6). After 2h of aging the pH was measured and solution filtered through a 2  $\mu\text{m}$  membrane filter. For liquid analyses parts of the filtrate was diluted directly after sampling and filtration 1:25 (ICP-OES), 1:100 and 1:1000 (IC). The filtration residue was dried at 30°C and carefully grounded for further analysis. XRD, TGA, optical microscopy and qualitative XRF measurements were conducted to characterise the precipitates.

Table 4.6: Volume of utilized EDR brine and added concentration of NaOH

sample	V EDR brine in ml	NaOH in mmol/100ml	NaOH in mmol/V <sub>sample</sub>	NaOH in mmol/l
A1	100	0.50	0.50	5.0
A	500	1.00	5.00	10.0
B	500	1.20	6.00	12.0
C	500	1.40	7.00	14.0
D	500	1.60	8.00	16.0
E	500	1.80	9.00	18.0
F	500	2.00	10.00	20.0
G	250	2.50	6.25	25.0
H	250	3.00	7.50	30.0
I	250	4.00	10.00	40.0
J	250	5.00	12.50	50.0
K	250	6.00	15.00	60.0

### Results of the analysis of the filtrate: IC, ICP-OES, pH

The concentration of  $\text{SiO}_2$  decreases slightly up to an addition of 10 mmol/l NaOH. With further addition of 10 mmol/l NaOH, the concentration of  $\text{SiO}_2$  decreases sharply to 6 mg/l (Figure 4.23). After treatment of the original EDR concentrates with 30 mmol/l NaOH, no silicic acid was detected, it was completely removed from solution. With increasing addition of caustic soda the pH increases. The pH rises from 2.1 to 8.4 after addition of 12 mmol/l NaOH; with further NaOH addition up to 20 mmol/l, the pH increases slowly and reaches a constant value of 9.6 after the addition of 30 mmol/l NaOH.

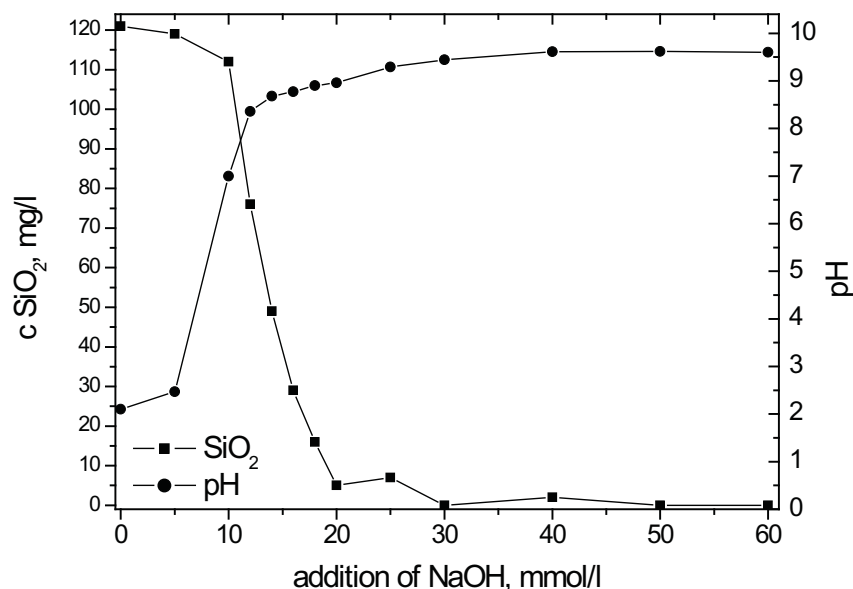


Figure 4.23: Changes of the pH and the  $\text{SiO}_2$  concentration as a function of the added amount of NaOH

The concentration of  $\text{Mg}^{2+}$  in solution decreases after the first addition of 5 mmol/l NaOH and remains nearly constant up to an addition of 20 mmol/l, further treatment of the solution with caustic soda leads to a steady decrease of  $\text{Mg}^{2+}$  (Figure 4.24). In contrast, the  $\text{Ca}^{2+}$  concen-

tration decreases after the first addition of caustic soda and remains nearly constant by further addition.

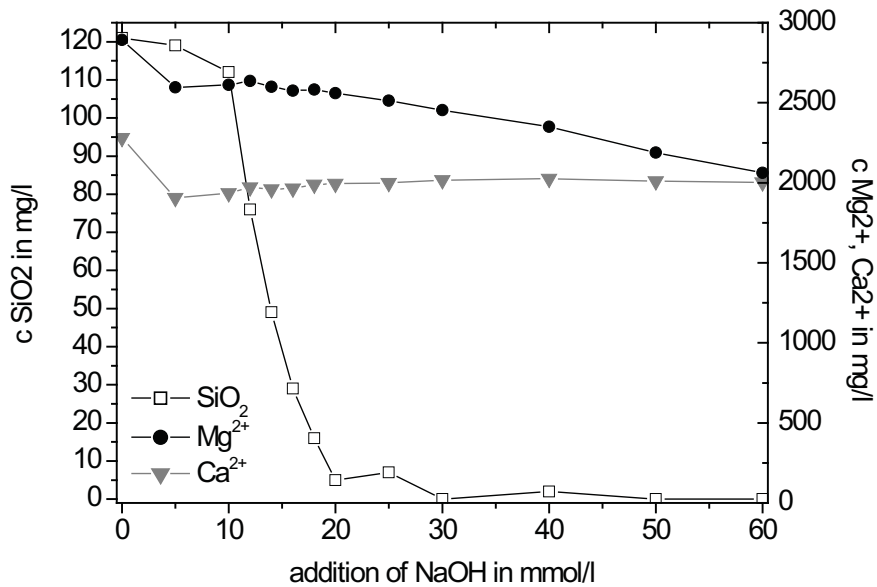


Figure 4.24: Changes of the SiO<sub>2</sub>, Mg<sup>2+</sup> and the Ca<sup>2+</sup> concentration as a function of the added amount of caustic soda

### Results of the analysis of the filter residues

After filtration, a gel-like film remains on the membrane filter which breaks into various massive fragments by drying at 30°C. Filter residues of the precipitation experiments are coloured from dark green to light blue. With increasing addition of caustic soda the amount of precipitates increases (Figure 4.25). Colouration of the samples changed during heating. Colour of sample A changed from dark green to dark brown, the green samples B to E changed to light brown whereas the light blue samples F to K changed to nearly white.

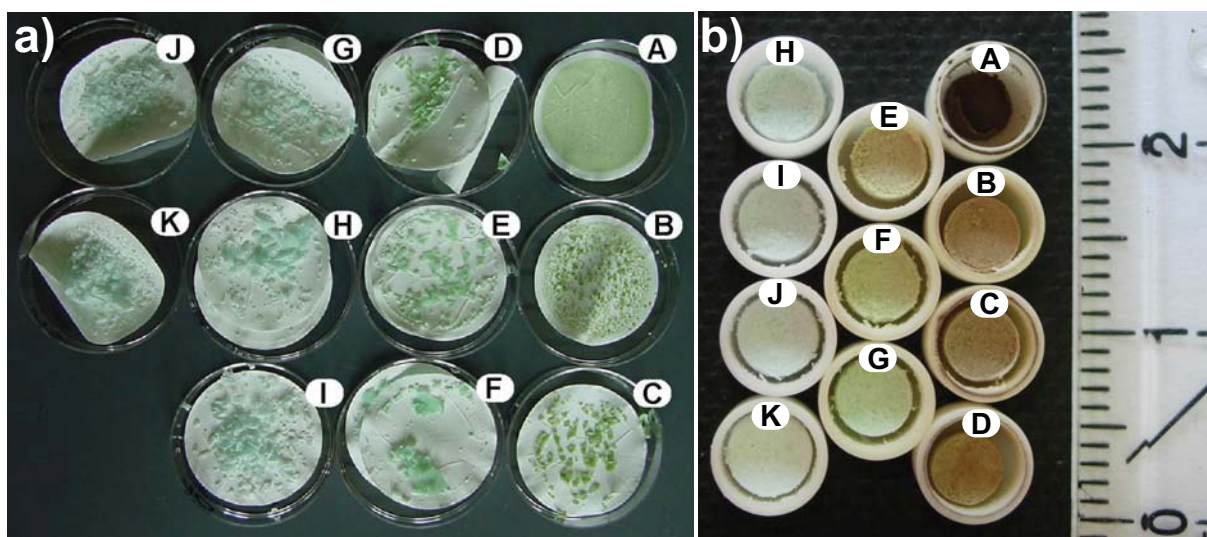


Figure 4.25: Filter residues of the precipitation experiments on membrane filter after drying at 30°C, 43a, and exposure of the precipitates A to K after heating up to 1000°C, 43 b. For explanation of sample names see Table 4.6.

### Results of the analysis of the filter residues: XRD

Samples C to I consist of gypsum and halite, samples J and K contain increasing amount of brucite (Figure 4.26). Whereas all halite peaks are distinctive, solely the strongest lines of gypsum are detected throughout the samples and only with weak intensity. Intensity of brucite peaks increases from sample I to K and all peaks show a line broadening which indicates small and /or less ordered crystals.

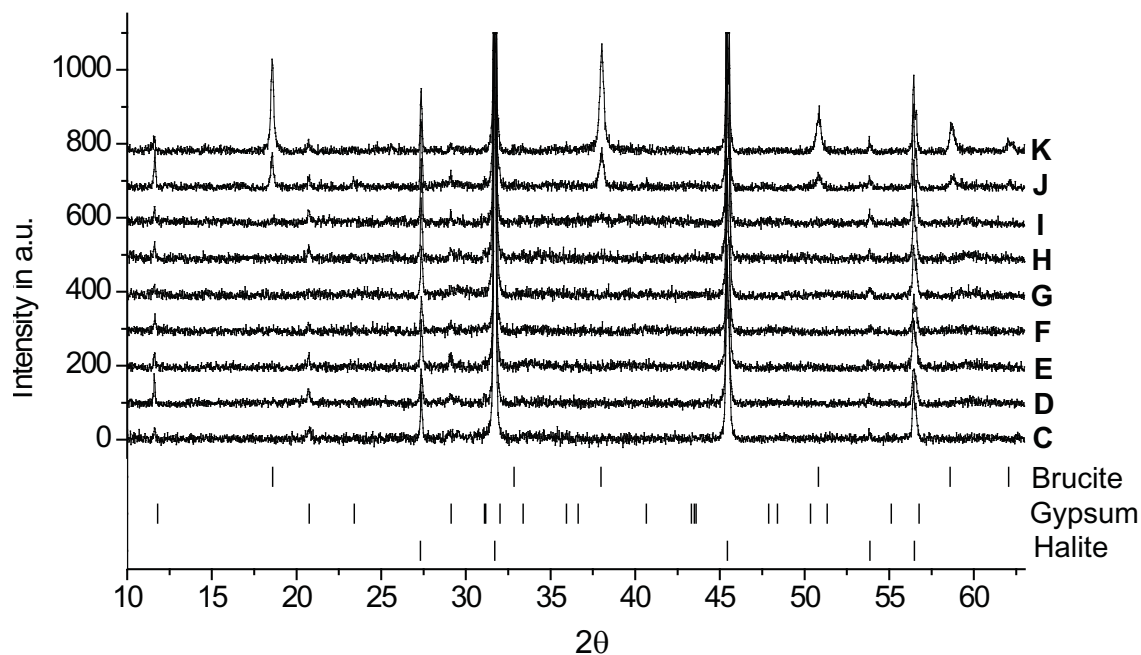


Figure 4.26: X-ray diffractogram of the precipitates C to K after filtration, drying at 30°C and grinding. For explanation of sample names see Table 4.6.

### Results of the analysis of the filter residues: TGA/DTA

Thermogravimetric analyses of the precipitates are presented in Figure 4.27. Weight loss in samples A to K starts slowly between 60 and 80°C followed by a more distinctive reaction between 100 and 250 °C. Sample weight of precipitates A to C decreases slightly but continuously with increasing temperature. A second step of weight loss was measured in the temperature range between approximately 400 and 550°C in samples D to F and between 300 and 550°C for samples G to K. At higher temperature sample weight remains nearly constant.

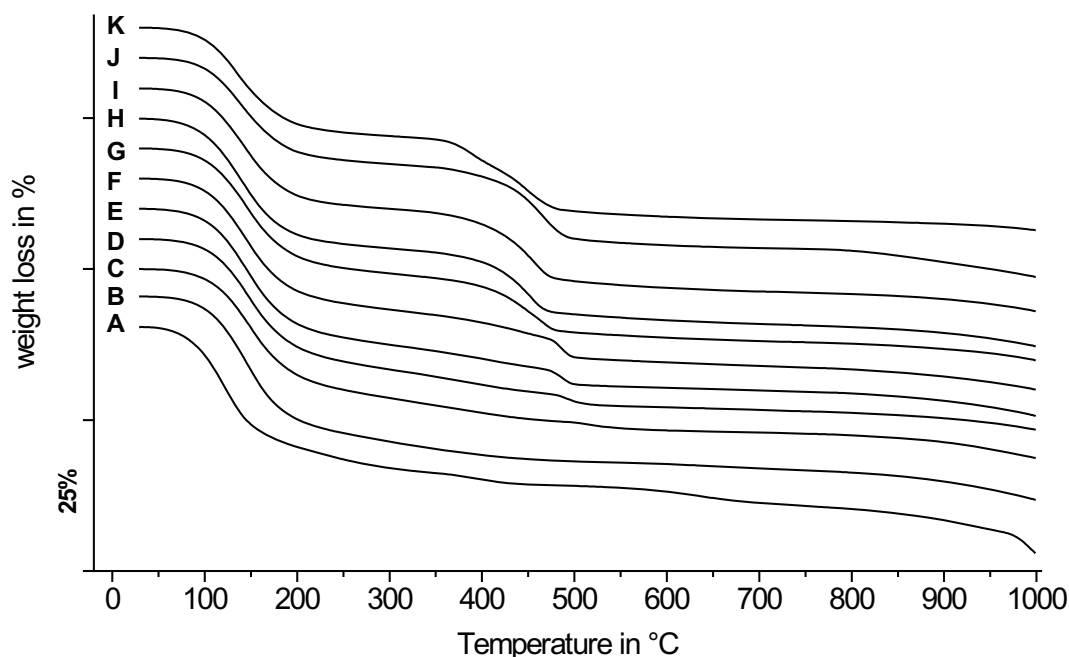


Figure 4.27: Results of the TG measurements of the precipitates of the titration experiments with original EDR brine. For explanation of sample names see Table 4.6.

Weight and percentage weight loss of samples A to K are reported in Table 4.7. For every measurement 49 to 53 mg of the precipitates were analysed thermogravimetrically, except for sample A, for which only 17 mg material was obtained in the precipitation experiment. For calculation of the specific weight loss, the temperature ranges were defined regarding to the beginning and the end of the respective reactions in the SDTA signal (Figure 4.29). In sample B to K the weight loss up to 100°C is attributed to the evaporation of adsorbed water on the mineral surfaces. As a consequence, weight loss below 100°C is not berücksichtigt. Due to the small amount of sample A the dehydration of the precipitates starts at lower T, therefore the beginning of the first T range was set to 80°C.

Percentual weight loss of samples A to K decreases within the first temperature range from around 24.4% of sample B to 16% of sample K. Within the second temperature range the opposite behaviour was measured. Whereas in sample A a small weight loss of 2.5% was detected the loss of weight increases with higher order of the samples to nearly 13% in samples I to K.

Table 4.7: Sample weight of the precipitates and weight loss in percent as a function of temperature

	sample mass in mg	range T1 in °C	weight loss T1 in %	range T2 in °C	weight loss T2 in %	weight loss T1 and T2 in %	weight loss total in %
<b>A</b>	17.1	80 - 320	21.96	320 - 490	2.54	24.50	37.34
<b>B</b>	49.0	100 - 400	24.42	-	-	24.42	33.63
<b>C</b>	52.0	100 - 320	20.22	320 - 600	4.84	25.06	31.25
<b>D</b>	52.2	100 - 320	20.49	320 - 600	5.82	26.31	31.54
<b>E</b>	50.6	100 - 320	20.88	320 - 600	6.76	27.84	34.26
<b>F</b>	52.2	100 - 320	20.10	320 - 600	8.38	28.48	34.92
<b>G</b>	51.6	100 - 320	19.30	320 - 600	10.34	29.64	35.05
<b>H</b>	52.7	100 - 320	18.97	320 - 600	11.78	30.75	37.66
<b>I</b>	51.6	100 - 300	17.77	320 - 600	12.89	30.66	36.87
<b>J</b>	51.8	100 - 300	15.90	320 - 600	13.26	29.16	36.23
<b>K</b>	52.6	100 - 300	15.97	320 - 550	12.81	28.78	33.53

Though in the thermogravimetric analysis of samples A and C no significant weight loss was measured during heating above 300°C, the first derivation of the TG curves shows a minimum between 340 and 470°C for sample A and a small but very sharp contoured minimum between 480 and 600°C for sample C (Figure 4.28). The minima of samples A to I of the first weight loss around 150°C are broadened to 10 - 20°C which indicates more than one reaction within this temperature range. The shape of the left shoulder of this minimum is more diffuse than the right one. Derivation of TG curves of samples I to K shows a second minimum at around 170°C. Within the second endothermic reaction range of precipitates C to K, the reaction minima of samples C to F were calculated for higher T than for samples G to K. Moreover, the form of the calculated curves show significant differences between the curves for samples C to F and samples G to K. For samples C to F the endotherm is enclosed by sharp shoulders whereas curves of samples G to K show a widely broadened shoulder at lower temperature and a sharp shoulder at higher temperature. Between 300 and 550°C, sample K shows three distinctive minima at 380, 450 and 460°C. In samples G to J one significant minimum around 450°C was calculated, whereas another more diffuse minimum at 350°C affects a widened shoulder at lower temperature.

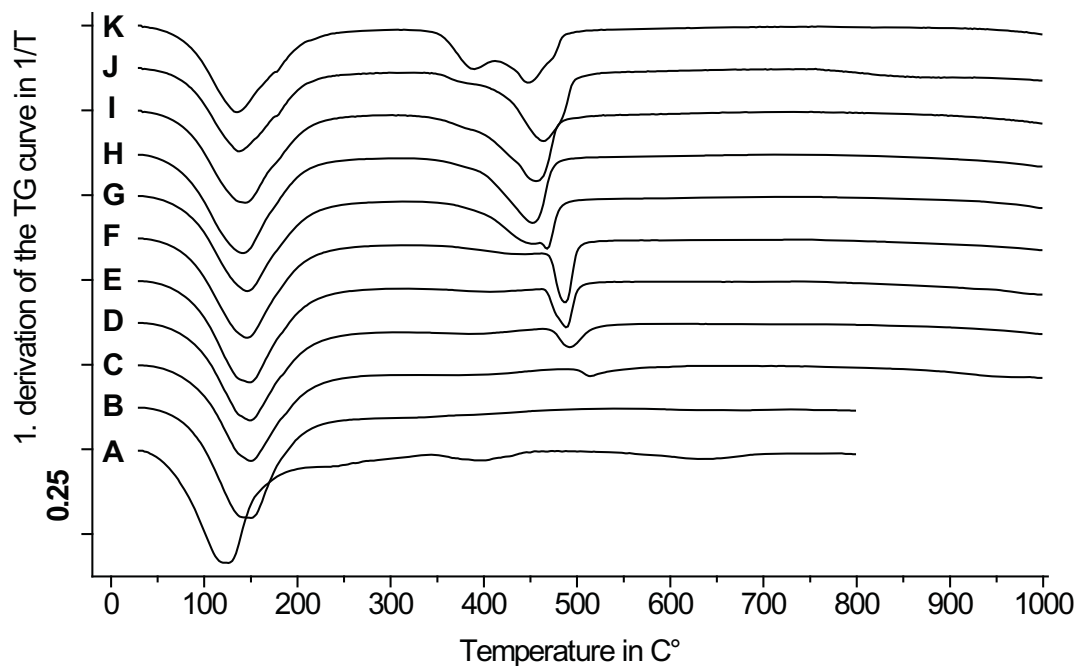


Figure 4.28: First derivation of the TG curves of samples A to K. For explanation of sample names see Table 4.6.

SDTA signals of the precipitates A to K are presented in Figure 4.29. All curves show a first endotherm between 40 and 300°C with one minimum at 60°C and a second minimum around 145°C. Sample A is an exception: here the first minimum lies at 40° and the second minimum at 125°C, which can be explained by less material. In samples J and K a third minimum was detected at 175°C. A second endothermic reaction range was observed for samples D to F between 320 and 515°C with a the peak minimum at 480°C. In samples G to K the second endothermic reaction range lies between 320 and 515 °C with a peak minimum at 450°C. Additionally in samples I and K a second minimum within this range was detected at 440°C (sample I) and at 380°C (sample K). Peak shoulders at lower temperatures of all measurements are more diffuse in contrast to the well defined left shoulders at higher temperatures. A third endothermic reaction was found for all samples, A to K, between 750 and 800°C.

Up to 80°C in sample A and up to 100°C in samples B to K weight loss and first minimum of the endothermic reaction is attributed to the dehydration of adsorbed water. The shoulder width of the endothermic reaction indicates more than one dehydration reaction between 100 and 300°C. Usually the dehydration of gypsum is very distinctive, however in samples A to K it is overlapped by one or more unknown endothermic reactions. Apart from gypsum and halite also brucite ( $\text{Mg}(\text{OH})_2$ ) was detected in samples I to K. The dehydration of brucite is an endotherm reaction with one minimum between 350 and 450°C (see Figure 4.29) (Webb, 1970, p. 264). Within the temperature range 350 and 550°C the endotherm reaction shows two minima for samples I to K, which indicates the dehydration of further water-containing minerals in the sam-

ple. The shift of the minimum of the endothermic reaction between 350 and 550°C in samples A to K from higher to lower temperatures in combination with the loss of weight within this range indicates dehydration of other hydroxides. A shift of minima in endothermic reactions from lower to higher temperatures can be caused by increasing concentration of the respective mineral in the sample. During this process the area of the SDTA curve increases but the shape does not change significantly. For samples A to K the minimum shifts to lower temperatures and the shapes of the curves change significantly. This indicates the presence of other hydroxides than brucite in samples A to H and additional minerals in samples I to K. The minimum of the endothermic reaction between 750 and 800°C shifts from lower to higher temperature in samples A to K. No weight loss was detected in this temperature range. This reaction is related to the melting point of halite (NaCl) the shift of the minimum depends on the increase of the halite concentration. During the measurements of samples A and B a technical problem with the TG device occurred and led to erroneous measurements for the reference crucibles between 800 and 1000°C. The respective values were cut off in Figure 4.29.

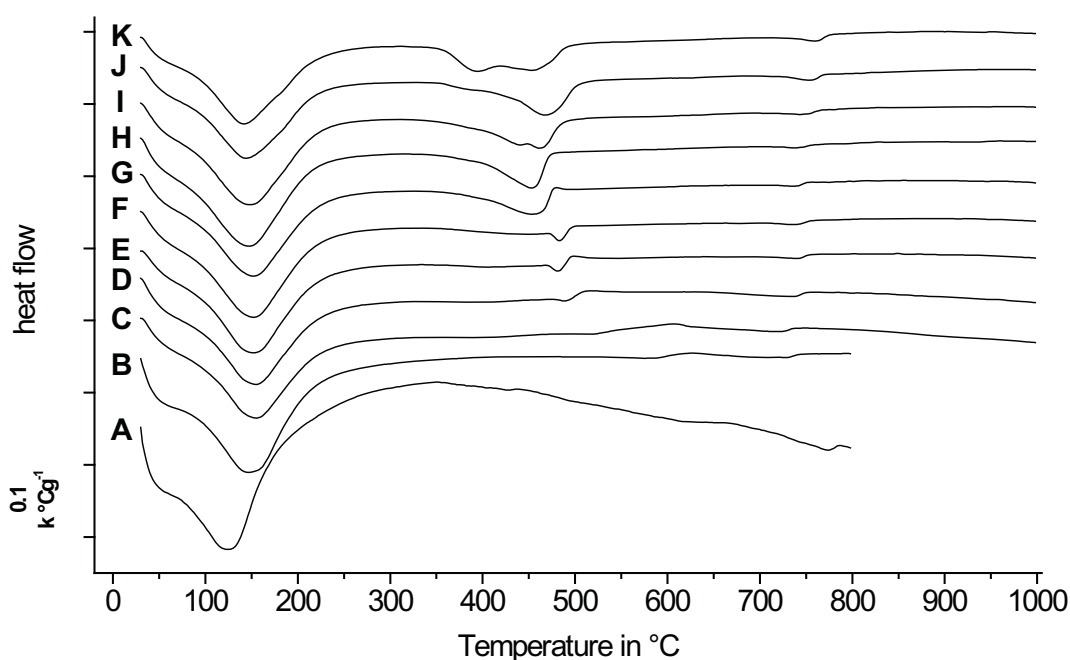


Figure 4.29: SDTA curves of the precipitates A to K of the EDR brine titration experiments. For explanation of sample names see Table 4.6.

To identify the respective mineral reactions of the first endotherm (100 to 250°C) and of the second endotherm (320 to 550°C), pure minerals and mixtures in various ratios as well as their thermodynamic reactions were investigated in dependence of the sample amount. SDTA curves and additionally PA curves of pure materials were compiled for gypsum, brucite and spertiniite ( $\text{Cu}(\text{OH})_2$ ). PA curves (German: **P**robenmengen-**A**bhangigkeit) describe the temperature dependence of endothermic (respectively exothermic) reactions as a function of the sample amount (Smykatz Kloss, 1967).

Figure 4.30 presents the SDTA and PA curves of technical gypsum (Merck). They show the typical shape of the dehydration of gypsum between 120 and 250°C. The loss of water from the dihydrate to the water-free calcium sulphate, requires two steps. First, the dehydration of gypsum,  $\text{CaSO}_4 \times 2\text{H}_2\text{O}$ , to bassanite,  $\text{CaSO}_4 \times 0.5\text{H}_2\text{O}$ , at temperature 1 (T1) and second the dehydration from bassanite to anhydrite ( $\text{CaSO}_4$ ) at temperature 2 (T2), (Smykatz Kloss, 1974). The respective dehydration temperatures T1 and T2 depend mainly on the concentration of gypsum in the sample. With increasing sample amount the minima of the endotherm T1 and T2 shift significantly to higher temperatures.

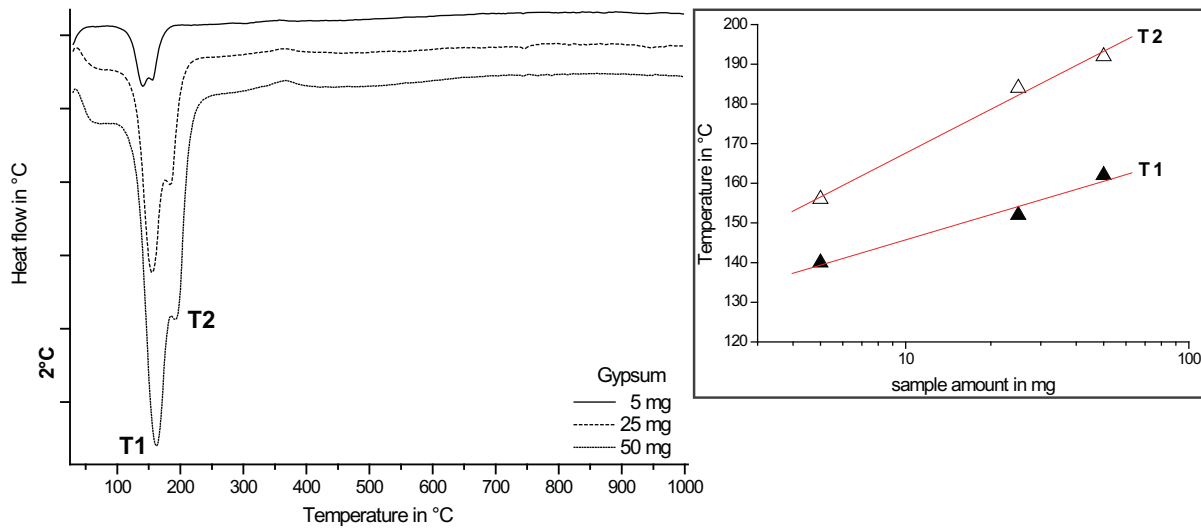


Figure 4.30: SDTA curves of defined amounts of gypsum and PA curve of gypsum

Figure 4.31 presents the SDTA and PA curves of technical brucite (Merck). Dehydroxylation of brucite results in an endotherm between 300 and 500°C. With increasing sample amount the minimum of the reaction shifts slightly to higher temperatures.

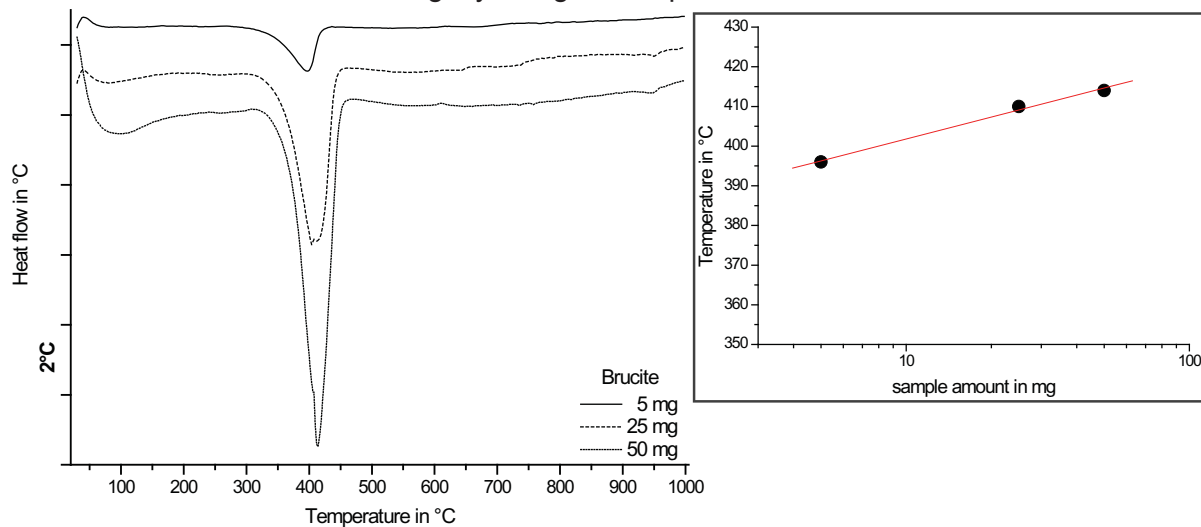


Figure 4.31: SDTA curves of defined amounts of brucite and PA curve of brucite

The change of colouration of the samples during the heating process of the thermogravimetric analysis indicates the presence of copper in the sample material. During the precipitation experiments copper may be precipitated in form of blue copper hydroxide which reacts to black copper oxide. To investigate the dehydroxilation of spertiniite ( $\text{Cu}(\text{OH})_2$ ) SDTA and PA curves of spertiniite were measured additionally to the curves of gypsum and brucite. Spertiniite shows a sharp endotherm between 160 and 220°C (Figure 4.32).

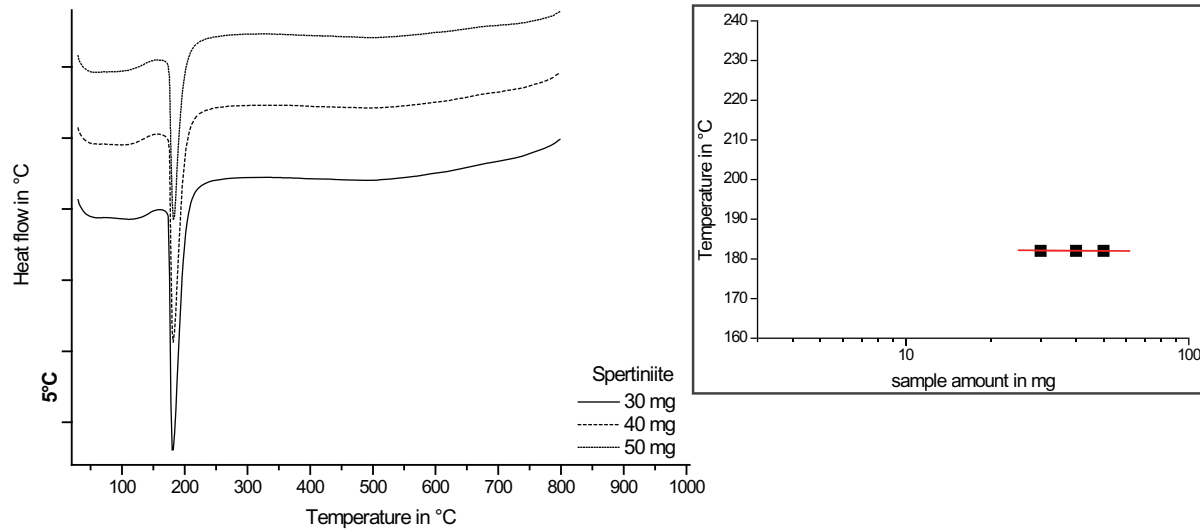


Figure 4.32: SDTA curves of defined amounts of spertiniite and PA curve of spertiniite

Natural brucite may show differences in the dehydroxilation temperature and shape of the endotherm in comparison to synthetic brucite due to impurities of other cations in the structure. In Figure 4.33 SDTA curve of natural brucite (*Wakerfield, Canada*) is plotted. Smykatz-Kloss, 1974, p. 38 presented a similar measurement of natural brucite.

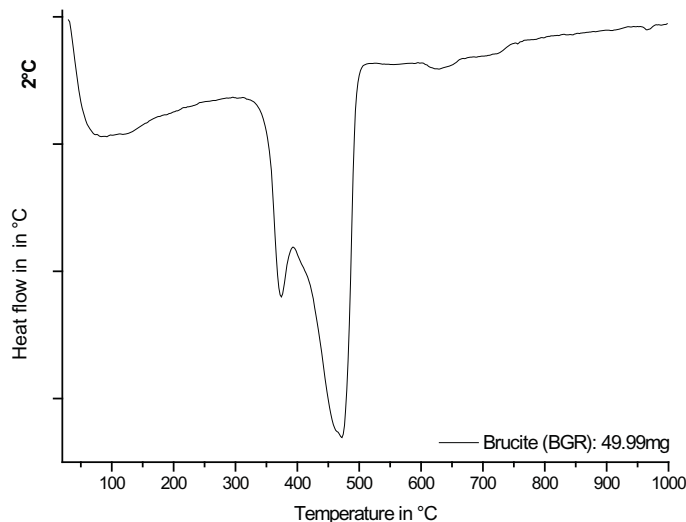


Figure 4.33: SDTA curve of natural brucite (BGR)

The dehydration of gypsum, spertiniite and brucite was investigated in dependence of the mineral concentration of the mixtures. Due to technical problems with the TG device during measurements of the reference crucibles between 800 and 1000°C, all values above 800°C had to be cut off in Figure 4.34. Dehydration reaction of bassanite to anhydrite is overlapped with the endotherm of the dehydroxylation of spertiniite. As a consequence the second minimum at T2 is not as sharp as the dehydration of bassanite to anhydrite and additionally the minimum is shifted to higher values.

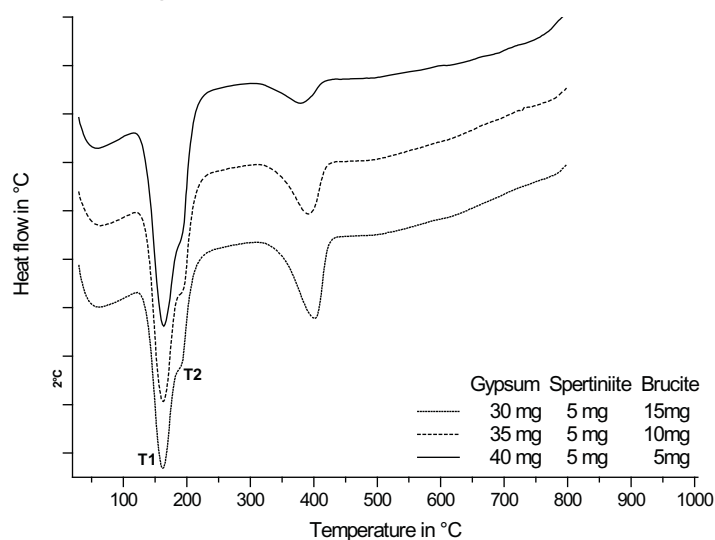


Figure 4.34: SDTA curves of mixtures of gypsum, spertiniite and brucite

### Results of the analysis of the filter residues after thermal treatment at 1000°C: XRF

Qualitative elemental analyses of the filter residues after thermal treatment up to 1000°C were conducted by ESEM/EDX (Figure 4.35 a). All samples are made of the same elemental composition, whereas element concentrations show significant variation. For a more detailed view of the elemental analyses of the main components, the x-ray energy-range between 1 and 4.25 keV was expended (Figure 4.35 b). A decrease of the silicon concentration was observed with increasing addition of caustic soda, samples B to K. In contrast, the Mg content of the samples shows is lowest in samples B, C, D and highest in samples H, I, K.

Semi-quantitative analyses of major and minor compounds in the samples A to K were made using a XRF/WDX unit (Bruker D4). Major elements of the samples are O, Mg, Na and Cl. Smaller amounts, < 5%, of Ca, S and Si were detected in the samples and additionally Cu, Zn, Ni, Mn, P and Al as accessory constituents < 1%. Among these Cu and Zn were the most abundant elements.

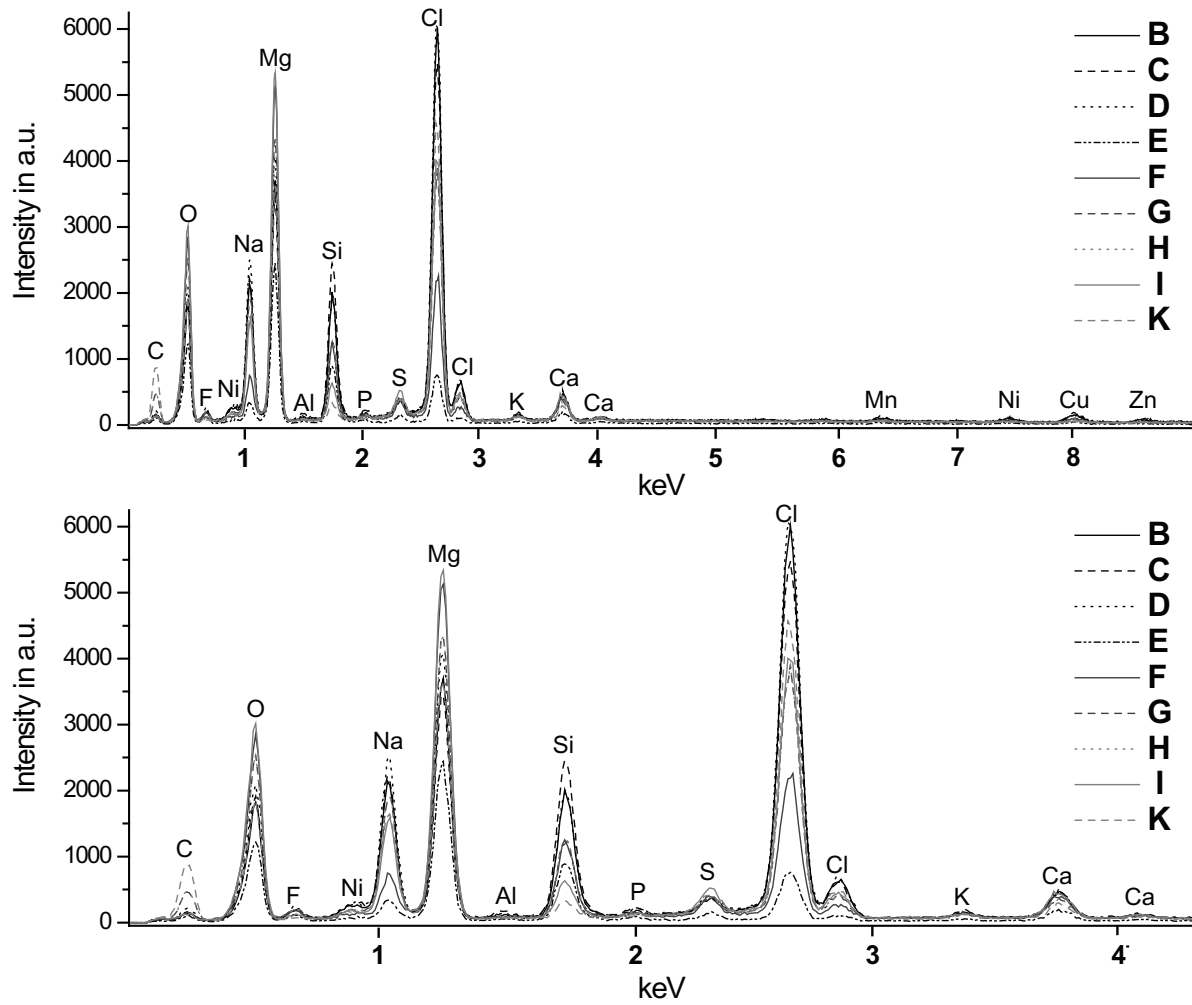


Figure 4.35: EDX analysis of precipitates B to K and an expanded view of the energy range between 1 and 4.25 keV.

#### 4.2.3.3 Titration experiments with synthetic laboratory EDR concentrates

Titration experiments with synthetic laboratory concentrates were conducted in order to investigate the influence of the initial concentration of silicic acid on the removal of silicic acid by addition of caustic soda to salt concentrates .

##### Experimental setup

A similar experimental setup like the one, described for the EDR brine titration experiments in Chapter 4.2.3.2 was chosen to investigate the removal of silicic acid from synthetic laboratory EDR concentrates with an initial pH of 6 as a function of the initial silica concentrations and as a function of the pH. For this purpose, three synthetic laboratory concentrates with initial  $\text{SiO}_2$  concentration of 45, 91 and 140 mg/l were prepared. For every concentrate eight plastic beakers were filled with 100 ml and mixed with various amounts of caustic soda. NaOH (2M) was added dropwise to the solutions and stirred rapidly with a magnetic stirrer. After 2h of aging, the pH was measured and the solution was filtered through a 2  $\mu\text{m}$  membrane filter. For repeat determinations of  $\text{SiO}_2$  in solution twice times respectively 1ml of every filtrate was diluted directly by a factor of 1:25 for ICP-OES measurements.

##### Results

In Figure 4.36 every data point represents one experiment. The concentration of silicic acid decreases directly after addition of caustic soda, independent of the initial silica concentration. Silica removal decreases with decreasing content of silicic acid in solution. The higher the amount of silicic acid in the concentrates, the more caustic soda has to be used to achieve 100% removal. With complete removal of  $\text{SiO}_2$  the pH reaches a value of 9.5.

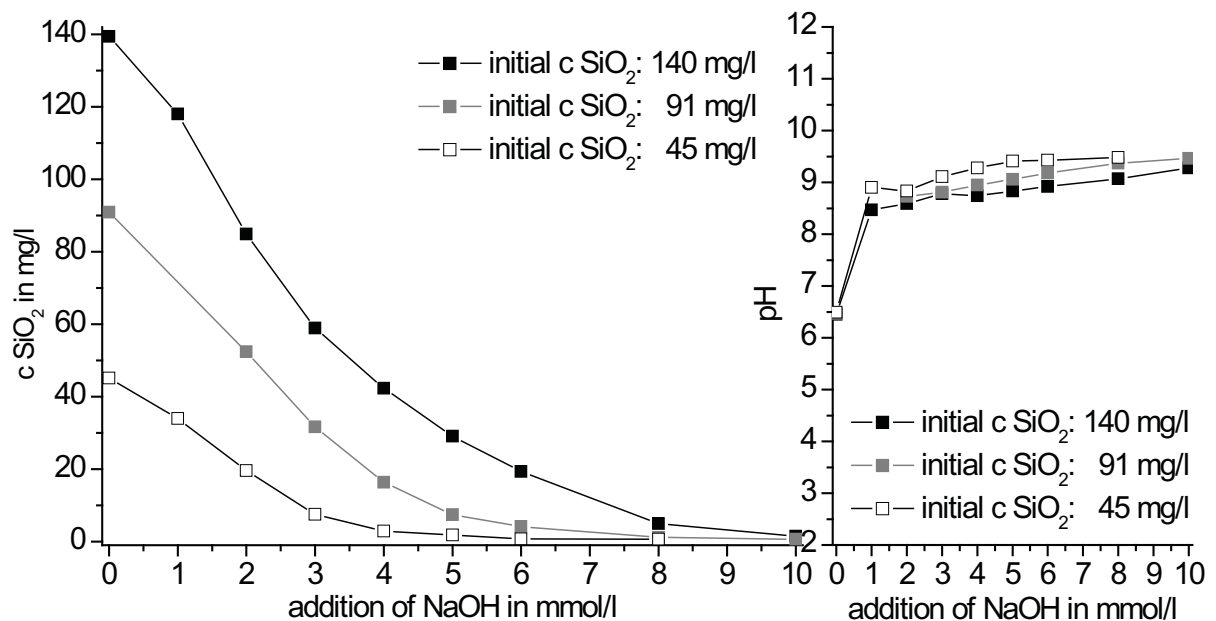


Figure 4.36:  $\text{SiO}_2$  removal from synth. concentrates with initial pH of 6 and various concentrations of initial silicic acid, as a function of the amount of admixed NaOH as well as a function of the pH

#### 4.2.4 Discussion

Experiments which are described in Chapter 4.2 were conducted to elucidate the formation conditions of precipitates in the EDR unit of the pilot plant, which are mainly made up of brucite and gypsum, as well as adsorbed or precipitated amorphous silica (see Chapter 4.1). The huge discrepancy between the initial pH of 2 of the process concentrate and pH values above 9.3, required for the formation of brucite and gypsum, leads to the question which kind of process triggers changes in the pH during the desalination procedure within the EDR unit. Two formation scenarios are described in Chapter 4.1, first, a procedural reason and second, the precipitation of amorphous silica at a pH of 2. As a consequence of both scenarios concentration polarisation on the membrane surfaces would cause locally high pH values on the anion exchanger membranes due to the electrical potential of the EDR unit.

Solubility, titration and precipitation experiments explain whether silicon occurs in the precipitates either as amorphous silica, formed during the desalination of salt concentrates in the EDR unit, or as a result of coprecipitation or adsorption on the surface of other minerals. The experiments reveal whether precipitated minerals are responsible for the scaling events on the membrane surfaces. Therefore various questions have to be discussed in the following paragraphs.

##### ***Solubility of amorphous silica in the EDR brine***

As mentioned in Chapter 3.3.2, the solubility of amorphous silica depends on one hand on properties of the solid and on the other hand on electrolyte concentration in the aqueous system. While Marshall (1980) and Marshall and Warakomski (1980) describe solely the *salting out effect* (decreasing solubility of amorphous silica with increasing salt concentration) on amorphous silica in single salt systems, information about combined multi electrolyte systems and their influence on the solubility of amorphous silica is quite rare. Therefore, a general characterisation of the solubility of amorphous silica from Merck, utilised as seeding component in the experiments, was determined in DIW as well as in synthetic EDR concentrate in equilibrium experiments (Chapter 4.2.1).

The solubility of amorphous silica was determined as 123 mg/l SiO<sub>2</sub> in DIW. In EDR concentrate the solubility was measured as 58 mg/l (Figure 4.14), but calculated as 34 mg/l SiO<sub>2</sub> (Table 4.5). This discrepancy will be discussed later. A solubility of 34 mg/l SiO<sub>2</sub> was obtained in the experiments of Marshall (1980), for a NaCl concentration of 2.6 mol/kg in a single salt system, whereas the NaCl concentration in the concentrate was 1.35 mol/kg.

##### **Impact of the electrolyte concentration on the solubility of amorphous silica**

The difference of the solubility in a pure system (single salt like NaCl), and in a multi component

system (like synth. EDR concentrate) indicates a summation of the influences of all electrolytes in the aqueous system on the *salting out effect* of amorphous silica. Marshall and Warakomski (1980) pointed out that bivalent ions affect the solubility of amorphous silica much more than monovalent ions. Even comparatively low concentrations of 0.12 mol/kg  $Mg^{2+}$  and 0.048 mol/kg in the EDR brine, effect a significant decrease of the solubility of amorphous silica in the EDR concentrate.

### **Time dependency of the stability of the saturation state as a function of initial silicic acid concentration and pH**

As reported above, a correlation was observed between initial silica concentration and saturation state in the equilibrium experiments. The equilibrium between seeds and liquid was determined after 28 d for the  $SiO_2$ -free synth. EDR concentrate. In contrast, the adjustment of the equilibrium in synth. EDR concentrate, which was initially oversaturated with respect to silicic acid, takes several months. This observation is coherent with experimental results of Krauskopf (1956) who describes the long-term stability of aqueous solutions, supersaturated with silicic acid at low pH values.

Iler (1979, p. 62) and Sjöberg (1996) described the dissolution of amorphous silica in water as a hydrolysis of the Si-O-Si bonds, whereas the formation of amorphous silica is ascribed to polymerisation. At the time when polymerisation of silicic acid and depolymerisation of amorphous silica reach equilibrium, the solubility equilibrium has been reached. Results of the experiments lead to the conclusion that depolymerisation of amorphous silica in synth. EDR concentrates at pH 2 is faster than the polymerisation of silicic acid, even in the presence of seeds. Additionally, the rate of polymerisation and depolymerisation of silicic acid at a pH of 2 is much slower than at higher pH values.

The influence of the different initial pH values on the dissolution rate of amorphous silica from Merck was revealed as a function of the time required for equilibrium adjustment in the synth. EDR concentrate at a pH of 2 and in DIW with an initial pH of 6.5. In general, the dissolution of solid silicic acid accelerates with increasing pH (Iler, 1979, p. 63). This fact leads to the significant increase of the  $SiO_2$  concentration to the equilibrium level in DIW at pH 6.7 during the first 7 days of the experiment. In contrast to this observation, dissolution of solid silicic acid in synthetic EDR concentrate at a pH of 2 remains as a slow and continuous process were equilibrium between solid and solution is reached at least after 28 d (Figure 4.14).

### **Will amorphous silica be formed spontaneously in the EDR brine at pH 2?**

As a result of the discussion of the solubility of amorphous silica in the EDR unit at a pH of 2, the formation of amorphous silica, as a consequence of supersaturation of the brine with re-

spect to silica, has to be excluded.

### ***Formation of large silicic acid polymers in the EDR brine***

Nevertheless, silica scaling may be triggered not only by precipitation of amorphous silica but also by formation of large molecules, due to polymerisation of silicic acid. These oligomers of high molecular weight may block membrane pores of the ion exchange membranes.

Some important facts about polymerisation of silicic acid in aqueous solutions, which are required for a better understanding of the experimental results, are pointed out in the following paragraph. In dilute aqueous solutions, undersaturated with silicic acid with respect to amorphous silica and  $\text{pH} < 8$ , the monomer exists as the main species (Sjöberg, 1996). Only small amounts of dimer or other low-weight oligomers can be formed. Their amount increases with increasing pH. Polymerisation of silicic acid depends on the pH (Iler, 1979, p.213, 214 and Felmy et al., 2001) and on  $\text{SiO}_2$ -concentration in solution (Iler, 1979, p.175). Surface charge and the formation of silicic acid oligomers are at a minimum around pH 2 (Iler 1979, p. 185-186, 195). The monomer of silicic acid exists over long time periods in water at concentrations below solubility of amorphous silica, whereas concentration greater than the solubility of amorphous silica abet polymerisation of silicic acid (Iler, 1979, p.174, 177).

To investigate whether polymerisation of silicic acid occurs in the EDR concentrate as a function of pH and time, seeding experiments were conducted (see Chapter 4.2.2). These experiments were focused on three topics:

- polymerisation of silicic acid as a function of the pH in synth. EDR concentrates, **System A**
- impact of seeds on the metastable state of synth. EDR concentrates, oversaturated with respect to amorphous silica, as a function of the pH, **System B**
- dissolution rate of amorphous silica as a function of the pH, **System C**

### **Polymerisation of silicic acid as a function of the pH and the initial concentration of $\text{SiO}_2$**

The solubility of amorphous silica in aqueous solutions like the EDR concentrates was calculated as 34 mg/l  $\text{SiO}_2$ . Therefore, in synth. EDR concentrates, the initial  $\text{SiO}_2$ -concentration of 155 mg/l was 3.6 times higher than the solubility of amorphous silica; polymerisation is triggered by the high amount of  $\text{SiO}_2$  in solution. Additionally, experiments revealed, that up to a pH of 4 a constant ratio between reactive and total silica exists, no matter if concentrates contain seeds or not (**System A**, Figure 4.37).

A significant increase of the fraction of polymerised species (12-13% of the total silica) was detected above pH values of 4. This result was obtained even in the presence of seeds, when the total  $\text{SiO}_2$  concentration decreased by formation of amorphous silica. This result is in accord-

ance with Iler (1979, p.175). Iler described the relation between increasing pH (increasing concentration of  $\text{OH}^-$ ) and polymerisation of silicic acid in a general theory of polymerisation. He pointed out that self-condensation of the neutral silicic acid monomer,  $\text{H}_4\text{SiO}_4$  is catalysed by hydroxide ions above a pH of 2 (Iler, 1979, p. 209):

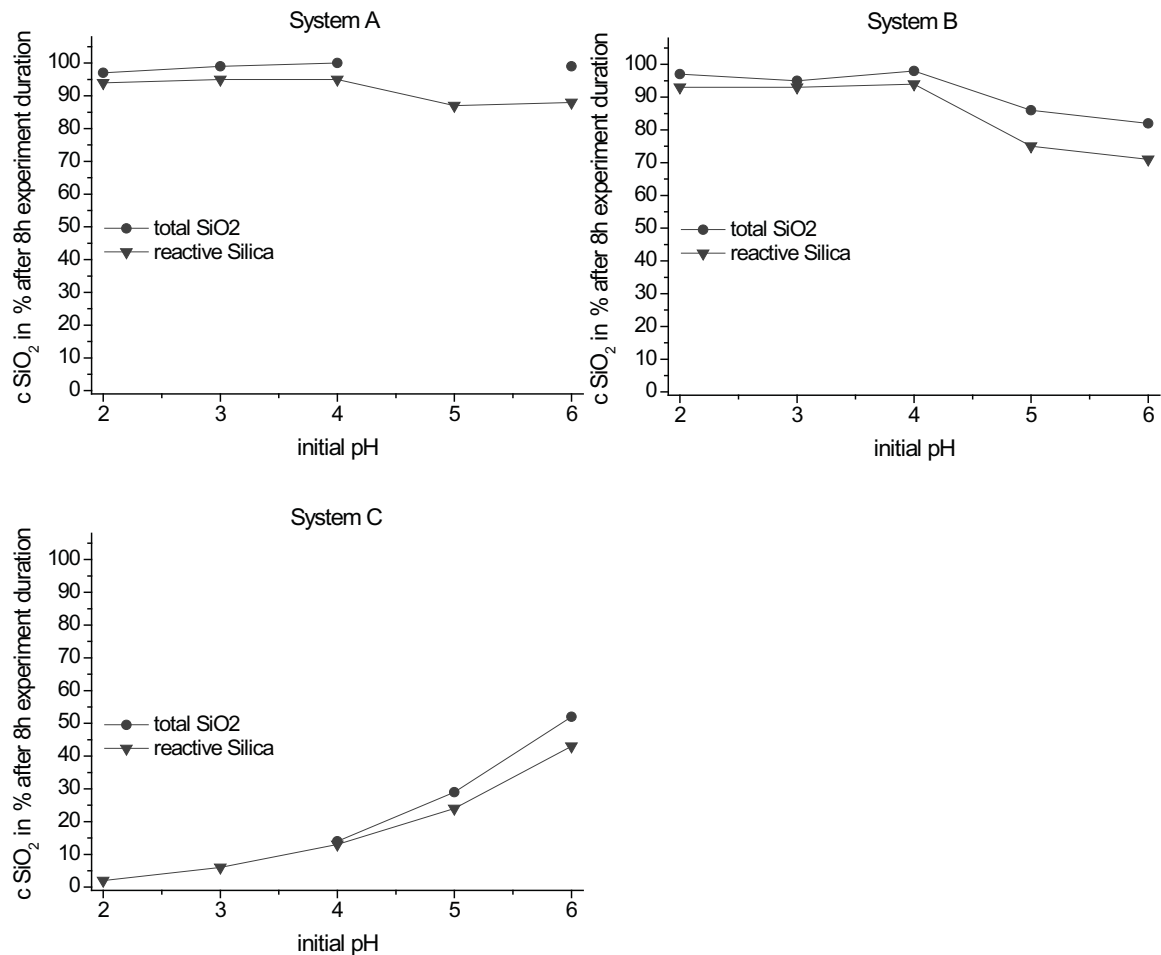
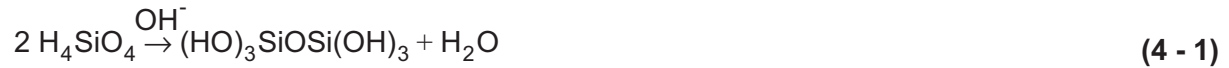


Figure 4.37: Amount of total and reactive silica after 8h experimental duration as a function of the pH in systems **A**, **B** and **C**. In system **C** the maximum concentration of 100%  $\text{SiO}_2$  is based on the initial concentration of systems **A** and **B**.

Nevertheless, 12 to 13% of polymerised silica at pH 5 and 6 can not be explained just by parameters like pH and  $\text{SiO}_2$ -concentration. Furthermore, polymerisation of silicic acid seems to be triggered by high amounts of electrolytes in the EDR brine. The influence of sodium on the gelling time of silica gels was discussed by Iler (1979, p. 176). He observed a significant decrease of the gelling time in the presence of 0.2 - 0.3 mol sodium at pH values between 4 and 6.

### Impact of seeds on the metastable state of EDR brine as a function of the pH

At pH 5 and 6 Iler (1979) observed a rapid conversion of the monomer to polymer species, which is accompanied by condensation of particles. This observation is in excellent agreement

with experimental result of this work, where increasing amounts of polymeric species in the synth. EDR concentrates come along with increasing influence of seeds on the total silica content at pH 5 and pH 6 (**System B**, Figure 4.37). Iler (1979) describes the influence of salt on the polymerisation of silica gels. There is evidence that in weak acid solutions of high salinity, polymerisation of silica species of high molecular weight occurs also in slightly supersaturated brines (Figure 4.37, **Systems A, B and C**). The supersaturated state of the synth. EDR concentrates is affected by seeds of solid amorphous silica in the presence of polymerised silicic acid, which is present in the concentrates at pH values above 4. Without seeding material the metastable state of supersaturation is not disturbed by polymerisation.

### Polymerisation rate of silicic acid and dissolution rate of amorphous silica as a function of the pH

A discrepancy regarding the influence of seeds, polymerisation of silicic acid and dissolution of amorphous silica at pH values equal to or above 5, in contrast to lower values, was observed. Therefore, exemplarily experimental results of **Systems A, B and C** at pH 4 and pH 6 are shown in Figure 4.38 to focus the discussion on the most important details.

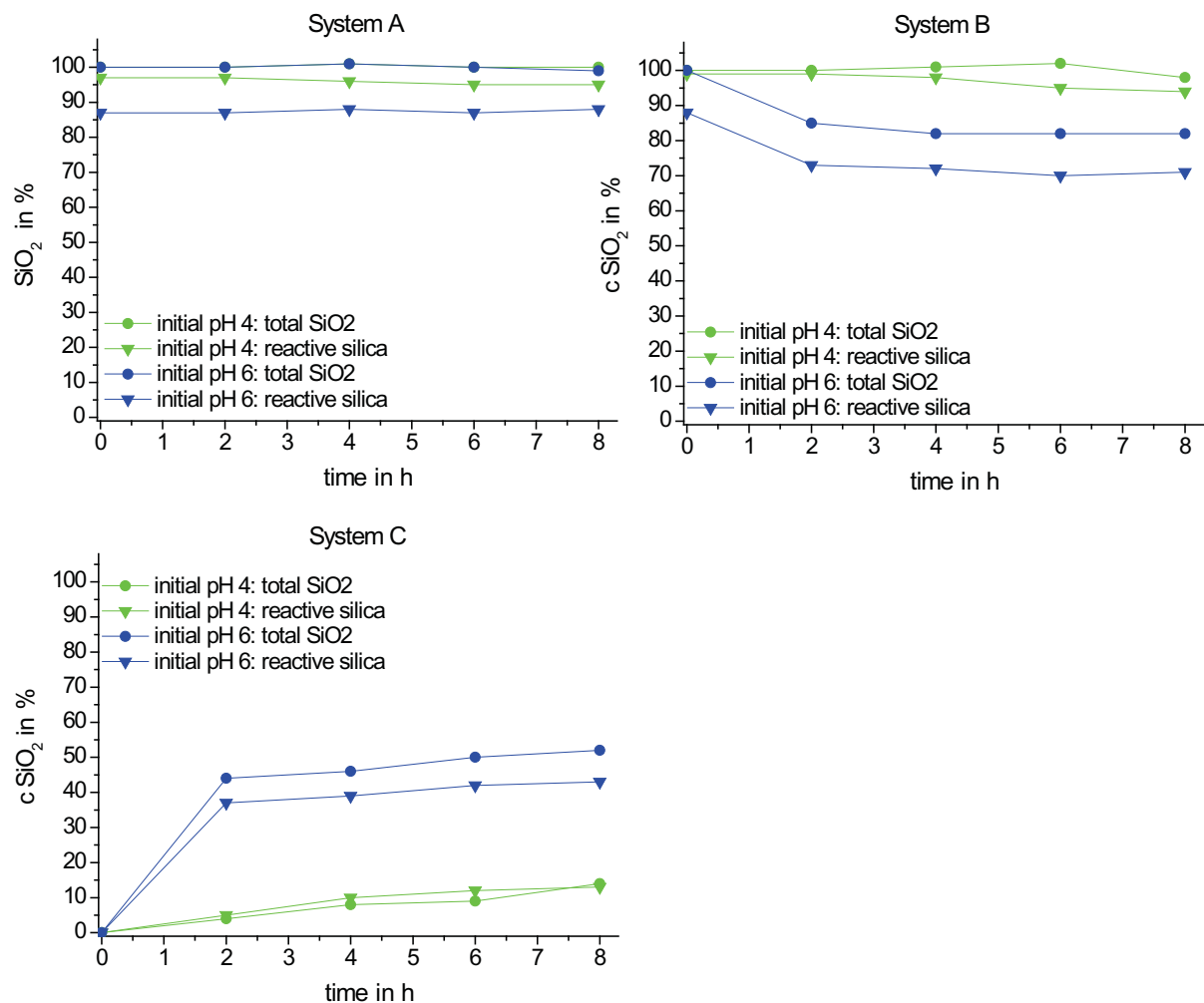


Figure 4.38: Comparison of the results of the seeding experiments in systems **A**, **B** and **C** with initial pH values of 4 and 6. In system C the maximum concentration of 100% SiO<sub>2</sub> are based on the initial concentration of system **A** and **B**.

In **System A** a “steady state”, with regard to the 8h of experimental duration, was reached immediately at  $t = 0h$  (Figure 4.38). This is equivalent to completion of the synth. EDR concentrate production, independent of the initial pH. According to Icopini et al. (2005) the degree of supersaturation with respect to amorphous silica affects oligomerisation and polymerisation of silicic acid. In addition, an induction period was observed before oligomers or polymers were detected in slightly supersaturated solutions. Results of the seeding experiments have shown that **System A** remains in a slightly supersaturated but metastable state during the experiment, which could be a part of the induction period, as noted by Icopini et al. (2005). Oligomers of silicic acid were detected only at pH values of 5 and 6. Their formation is mainly ascribable to the increasing OH<sup>-</sup> concentration in solution, which catalyses the polymerisation of silicic acid. At  $t = 0h$  **Systems A** and **B** are quite similar, no seeds are in the solutions. The addition of seeding material to **System B** at  $t = 0h + 1 min$  has no impact on the total silica concentration in solutions of an initial pH of 2, 3 and 4, but it does have on solutions with an initial pH of 5 and 6. Notably, after 2h a decrease of the SiO<sub>2</sub> concentration was observed which is equal to the amount of oligomerised silicic acid at  $t = 0h$  (**System B**, Figure 4.38).

#### Isolation of the main reactions in the EDR brine - seed system

In a first approach it will be assumed, that the nearly equal amounts of oligomerised and removed silica is not a coincidence (Figure 4.38, **System B**), the interaction between solid and oligomerised silicic acid constitute the main parameter of the removal process. As a consequence, a removal of SiO<sub>2</sub> from solutions with an initial pH of 4 and lower would likely not be due to the lack of oligomerised silicic acid. Even after decrease of silicic acid in **System B** at pH 5 and 6 a significant amount of 12% oligomerised silicic acid was detected. Anyhow, no further decrease of SiO<sub>2</sub> concentration in solution was observed which seems to be inconsistent with the previously claimed approach. On closer examination of the chemical reactions, taking place by striving a steady state in the aqueous system, at least three different reactions have to be taken into account:

- hydrolysis of seeding material results in dissolution of the solid amorphous silica
- oligomerisation of silicic acid monomers
- condensation of oligomers and/or accretion on seeding surfaces

Due to the experimental results of **System A** condensation of oligomers up to a critical nuclei size can be excluded. More likely seems to be a removal of SiO<sub>2</sub> by accretion of silicic acid oligomers on seeding surfaces. Initially existing oligomers can be removed from solution before

a significant hydration shell is formed. This process requires a very high accretion rate. As soon as a hydration shell is formed, hydrolysis of seeding material may become the main chemical reaction in the system. As a consequence monomer of silicic acid and also new oligomers are formed. In contrast to the initially existing oligomers with no seeds in solution, an accretion of the new oligomers on the seeding surfaces is inhibited by the hydration shell.

Based on a second approach, that the amount of oligomerised and removed silica are not associated, accretion of oligomers on seeds and dissolution of solid amorphous silica may occur side by side. In this case no information about reaction kinetics is available because a steady state was reached within the first 2h and reactions are mainly driven by  $\text{OH}^-$  concentration in solution.

### **Dissolution rate vs. adjustment of a solid liquid equilibrium**

The impact of  $\text{OH}^-$  catalysis on dissolution of amorphous silica and on decomposition of silicic acid oligomers to the monomer species  $\text{H}_4\text{SiO}_4$  was most obviously observed in **System C**. Here, amorphous silica was added to a  $\text{SiO}_2$ -free synth. EDR concentrate (**System C**, Figure 4.38). Within the experimental duration a nearly linear increase of the  $\text{SiO}_2$  concentration was detected for solutions with an initial pH value of 2 to 5. In contrast, in solutions with an initial pH of 6 a significant acceleration of the dissolution process was observed within the first 2 h of the experiment, where the main part of the dissolution occurred. The amount of dissolved  $\text{SiO}_2$  (80 mg/l after 8 h) exceeded the equilibrium concentration with respect to the solubility of amorphous silica in the synth. EDR brine (58 mg/l experimental value, respectively 34 mg/l calculated value, Table 4.5).

At this point of the discussion two facts should be considered:

- a)** The solubility of amorphous silica in pure water remains constant at pH values between 2 and 8 (Iler, 1979, p. 43, Marshall and Warakomski, 1980, and Stumm and Morgan, 1996, p. 368). Therefrom, it can be assumed that also for aqueous solutions of constant salt concentration the solubility of amorphous silica remains constant at pH values between 2 and 8.
- b)** The solubility of amorphous silica in synth. EDR brine was determined at a pH of 2 (Chapter 4.2.1, Figure 4.14). The respective seeding experiment, mentioned above, was conducted at an initial pH of 6. Despite of the different initial pH values in both experiments, the same solubility of amorphous silica should have been reached. In addition, at saturation dissolution and condensation processes are at equilibrium. The observed significant increase of the  $\text{SiO}_2$  concentration during the seeding experiments at pH 6 indicates a strong discrepancy between dissolution of amorphous silica and condensation of silicic acid within the solutions.

Formation of the silicic acid monomer is solely related to hydrolysis and subsequently dissolu-

tion of solid amorphous silica. Oligomerisation of these monomers occurs as a successive process. In contrast to dissolution, the condensation depends on the formation of oligomers of a specific size. When reaching this critical nuclei size, self condensation and spontaneous growth of the particles occur (Icopini et al., 2005). Due to the acceleration of the dissolution of amorphous silica (Figure 4.38, **System C**), catalysed by  $\text{OH}^-$  ions at a pH of 6, the released monomer outnumbers the monomers which condensate. This leads to a very high value of 80 mg/l  $\text{SiO}_2$  in solution. Polymerisation of silicic acid is also catalysed by  $\text{OH}^-$  ions. Seeding experiments at a pH of 6 revealed low concentration of oligomers around 9% in contrast to approximately 91% of monomeric silicic acid in solution. Hydration shells around solid amorphous silica particles inhibit accretion of oligomers. This approach was discussed in detail for **System B**, p. 86. In consequence of the fast dissolution rate, a supersaturated metastable state with respect to amorphous silica was established in the salt solutions. A supersaturated state may occur also in solutions of initial pH values lower than 6. Due to the slower dissolution rate at lower pH values this phenomenon was not observed during the 8 h of experimental duration but it was observed in solubility experiments of Chapter 4.2.1: During the solubility experiment in synth. EDR brine (initial pH of 2) the amount of  $\text{SiO}_2$  in solution increases and seems to reach a constant value of 58 mg/l after 28 d. Concerning the theoretical calculations of the solubility which gave a value of 34 mg/l for the solubility of amorphous silica in the EDR brine, the experimental value exceeded the calculated one by 24 mg/l.

### **Membrane pore blockage by the formation of large silicic acid polymers?**

At pH 2 membrane pore blockage by the formation of large oligomers of silicic acid can be excluded. It becomes more probable at pH values of 5 and higher.

### ***Simulation of increasing pH and the impact on silicic acid in solution***

Discussion of solubility and seeding experiments indicates that precipitation of amorphous silica or accretion of polymerised silicic acid at seeding surfaces will not occur at relatively low pH values as present in the EDR unit. On the other hand, analysis of the exchanger membrane deposits implies an increase of the pH in this desalination unit. Influence of increasing pH on silicic acid in ideal and non ideal systems were simulated in titration experiments (see Chapter 4.2.3). In summary, the results of the seeding experiments at pH values of 5 and 6 indicate that the reaction dynamics of silicic acid polymerisation and dissolution amorphous silica increase significantly.

### **Impact of the initial concentration of silicic acid on its dissociation**

The transition range of the titration curves of DIW, containing silicic acid in various amounts, already starts at pH 4, whereas pH 5 and 6 lies fully within this transition range (Figure 4.39).

A correlation between increasing reaction rate of silicic acid and  $\text{OH}^-$  concentration was observed in titration experiments. Within the pH range of 4 - 8,  $\text{OH}^-$  ions catalyse the self condensation of silicic acid (Iler, 1979, p. 62). At pH values above 8, consumption of  $\text{OH}^-$  ions with increasing amounts of silicic acid in solution can be related to the dissociation of the silicic acid (4 - 2) at a pK of  $10^{-9.8}$  (Iler, 1979, p. 11).



In Figure 4.39 the distribution of silicic acid monomer species are opposed to the titration curves as a function of the pH.

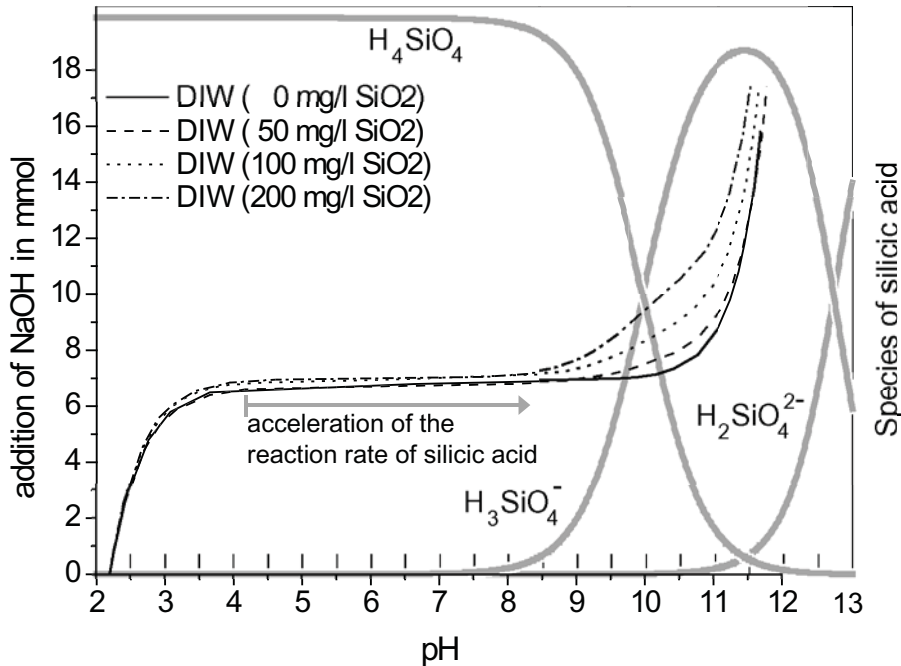


Figure 4.39: Distribution of silicic acid monomer species and titration curves of various amounts of silicic acid in DIW as a function of the pH

Within this sketch it becomes visible as higher the concentration of silicic acid in solution as earlier the transition range of the titration is ceased. For 100 and 200 mg/l  $\text{SiO}_2$  the end point of transition range overlaps with the beginning of formation of  $\text{H}_3\text{SiO}_4^-$  at pH 8. Each of this solutions contains silicic acid close to or beyond the saturation state of amorphous silica, in contrast to the undersaturated solution, containing 50 mg/l  $\text{SiO}_2$ . This observation indicates that concentration of silicic acid in nearly saturated and oversaturated solutions is big enough so as to observe the beginning of silicic acid dissociation directly by titration.

### Impact of $\text{MgCl}_2$ in solution on silicic acid dissociation

The presence of magnesium chloride in solution affects the significantly shift and shape of titration curves in dependence of the silicic acid concentration (Figure 4.40).

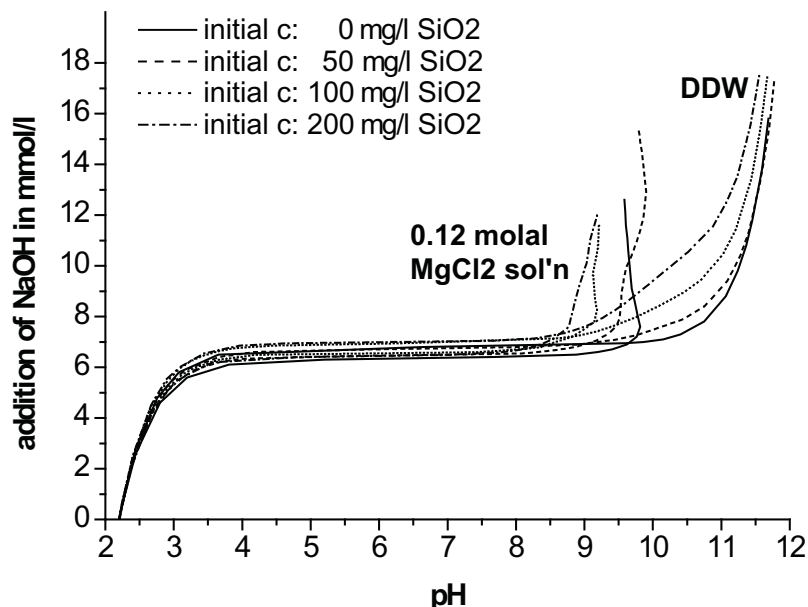


Figure 4.40: Comparison of the titration curves of various amounts of silicic acid in DIW and in 0.12 molal  $\text{MgCl}_2$ -solution

### Titration of silicic acid vs. titration in $\text{MgCl}_2$ solution

The most important discrepancies between the titration of silicic acid in  $\text{MgCl}_2$  solution in and the pure and undisturbed solutions of silicic acid in DIW are shortly summarized for further discussion:

- By titration of various amounts of silicic acid in DIW, the end of the transition range depends on the amount of silicic acid in solution. In contrast, the titration of various amounts of silicic acid in 0.12 molal  $\text{MgCl}_2$ , the transition range ceased at a pH of 8.3, independent of the initial concentration of  $\text{SiO}_2$  in solution.
- Equilibrium after addition of caustic soda was adjusted within short time in DIW, whereas in 0.12 molal  $\text{MgCl}_2$  solutions the steady state of the system was not adjusted within minutes or hours, thus it was decided to read out the pH continuously after 5 min at pH values  $>8$ .
- The occurrence of white, fluffy precipitates was observed at pH values  $>8.5$ .
- A pH of 9.8 was not exceeded by titration of various amounts of silicic acid in magnesium chloride solutions

Notably, all titrations keep one fact in common: with increasing initial  $\text{SiO}_2$  concentrations a high-

her amount of caustic soda was required to reach the same pH after leaving the transition range. This observation correlates with the beginning dissociation of the uncharged monomer  $\text{H}_4\text{SiO}_4$  to the single-charged monomer  $\text{H}_3\text{SiO}_4^-$  for silicic acid in DIW. Regarding the titrations in  $\text{MgCl}_2$  solutions, the dissociation of silicic acid must be one cause for the higher consumption of caustic soda with increasing concentration of silicic acid in the salt solutions after leaving the transition range.

### **Interaction between brucite and silicic acid**

Apparently with the first formation of single-charged monomers of silicic acid in solutions the end of the transition range was determined. Nevertheless, a distinctive buffer reaction similar to the dissociation of silicic acid in DIW was not detected and also the maximum pH of 9.8 was never exceeded. This observation leads to the question in which way the observed precipitates interacts with silicic acid. Due to the participating reactants, formation of magnesium hydroxide (brucite,  $\text{Mg}(\text{OH})_2$ ) occurs, triggered by addition of hydroxide ions to the  $\text{MgCl}_2$  solution (4 - 3):



The solubility of brucite depends on the pH and the salt concentration in solution. However, below pH values of 9.5 no brucite was expected to exist in solution. The presence of this mineral at lower pH values can be explained by the experimental setup. Here caustic soda was added dropwise to the solutions. Even fast stirring does not avoid the formation of locally high pH values and, as a result, precipitation of brucite. Precipitates remains in solution due to the slow dissolution rate in contrast to the fast precipitation rate of this mineral. Due to the precipitation conditions of brucite, the pH will not rise above 9.8 in solutions as a result of the very fast consumption of added hydroxide ions by formation of the Mg-hydroxide.

Both reactions, dissociation of silicic acid and formation of brucite proceed simultaneously. The formation of brucite is responsible that a maximum pH of 9.8 is not exceeded during the titrations. Increasing hydroxide consumption by increasing concentration of silicic acid is related to the dissociation of silicic acid. Subsequently with increasing amount of silicic acid in solution lower pH values were adjusted after adding the same amount of caustic soda. In addition to these two processes (dissociation of silicic acid and precipitation of brucite) also the interaction between silicic acid and freshly precipitated brucite has to be considered.

### **How does the composition of the EDR concentrate change during titration with caustic soda and which precipitates can be obtained?**

In contrast to the already discussed titration experiments for DIW and 0.12 molal  $\text{MgCl}_2$  solution, the titration experiments performed with original EDR brine were focused on changes in the composition of solution. Furthermore, it was investigated what kind of precipitates were

formed within this multi-electrolyte system during a controlled increase of the pH. Resultant on this fact titration conditions were changed from short time experiments (minutes) to long time experiments (hours). Therefore, titration was divided into single steps and precipitates of every step were characterised. Titration experiments with original EDR brine were focused on four specific questions:

### **Does the $\text{SiO}_2$ and $\text{Mg}^{2+}$ concentration depend on the pH?**

Results of these titration experiments show clearly that silicic acid is not removed from solution until the pH reaches a value above 8 (Figure 4.23). At this pH also dissociation of silicic acid from the uncharged monomer to the single-charged monomer starts. As observed in earlier titration experiments, only a slow increase of the pH was measured within the pH range between 8 and 9.5 in the presence of silicic acid. It becomes obvious that the complete removal of  $\text{SiO}_2$  occurred within this pH range. Based on the observed turbidity in titration experiments in single salt solutions, made of 0.12 molal  $\text{MgCl}_2$ , a significant decrease of the  $\text{Mg}^{2+}$  concentration was expected to be measured at pH values  $>8.5$ . However, a constant concentration of 300 mg/l  $\text{Mg}^{2+}$  was removed until the pH exceeds a value of 9 (Figure 4.24). Notably, a significant decrease of the  $\text{Mg}^{2+}$  concentration was detected onto complete removal of  $\text{SiO}_2$  from solution. Thereafter, the pH remains at a constant value of 9.6, whereas amount of  $\text{Mg}^{2+}$  decreases continuously. In this context XRD measurements of the precipitates revealed that solids, formed at pH 9.6, contain significant amounts of brucite (Figure 4.26). The most interesting reactions in solutions occur within the pH range between 8 and 9.5. Here, only a small removal of  $\text{Mg}^{2+}$  occurred and no brucite was detected within the respective precipitates. Therefrom, at this point of discussion,  $\text{OH}^-$  consumption must be related on one hand to the formation of unknown solids on one hand and on the other hand to the dissociation of silicic acid.

### **Species distribution of silicic acid in the EDR concentrates**

Removal of  $\text{SiO}_2$  started at pH values of 8 and was completed below pH values of 9.6. This fact leads to the question whether the required amount of the single-charged silicic acid ( $\text{H}_3\text{SiO}_4^-$ ) can be formed at this pH. Regarding this question, species distribution of silicic acid monomers as a function of the salt concentration in aqueous solutions was taken into account.

Sjöberg (1996) investigated the influence of the ionic strength on the  $\text{pK}_1$  and  $\text{pK}_2$  values of silicic acid. He pointed out that pK values of silicic acid decrease with increasing ionic strength. Especially for very complex multi-electrolyte systems like the EDR brine, it was interesting to calculate the respective distribution of silicic acid species as a function of pH and salt concentration. In Figure 4.41 the calculated distributions of the monomeric species of silicic acid in DIW, in 0.12 molal  $\text{MgCl}_2$  solution and in EDR brine are presented. In accordance with Sjöberg

(1996) pK values of silicic acid shift to lower pH values. This effect is more distinctive for the  $pK_2$  than for the  $pK_1$  value. Furthermore, an increase of the respective species is much more pronounced in the presence of salt than in DIW. Concerning the titration experiments in 0.12 molal  $MgCl_2$  solution and in original EDR brine, the formation of the single-charged monomer,  $H_3SiO_4^-$  has to be estimated for lower pH values in original EDR brine. In addition, the increasing gradient of species distribution indicates a higher concentration of  $H_3SiO_4^-$  at lower pH values in comparison to DIW. Both facts result in the already observed acceleration of the dissociation reaction as a function of the initial  $SiO_2$  concentration and as a function of the amount of salt in the respective solution. These facts were visible in the shift of the end of the transition range to lower pH values. When titrating the EDR brine it was observed indirectly by a significant removal of silicic acid at pH values below the saturation pH of brucite. It has to be pointed out that dissociation of silicic acid is not only promoted by increasing concentrations of  $OH^-$  ions in solution but also by increasing amounts of salts.

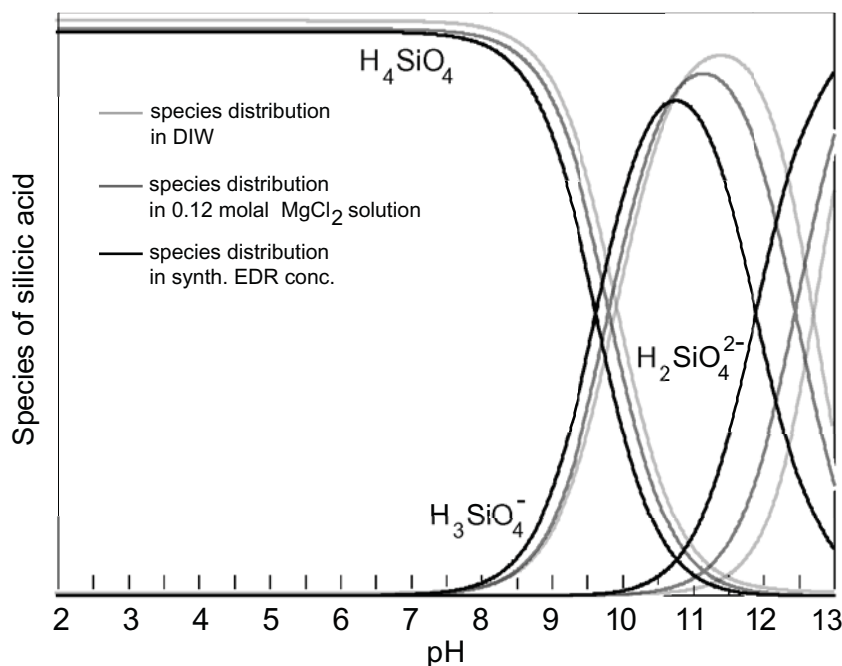


Figure 4.41: Geochemical modelling of the species distribution of silicic acid monomers ( $H_4SiO_4$ ,  $H_3SiO_4^-$  and  $H_2SiO_4^{2-}$ ) as a function of the pH in DIW, 0.12 molal  $MgCl_2$  solution and EDR brine

### Does the $Mg^{2+}$ concentration depend on the pH and on the amount of $SiO_2$ in solution?

Removal of  $SiO_2$  starts at pH values  $>8$ , which is related to the formation of single-charged monomers of silicic acid. These monomers polymerise to polysilicic acid which acts as a stronger acid than the monomeric species (Sjöberg, 1996, Lagerström, 1959, Ingri, 1959). At the same time a slow decrease of  $Mg^{2+}$  was observed which was so far considered to be associated with the formation of brucite. Within the pH region of  $SiO_2$  removal (pH 8 to 9.5) neg-

atively charged silicic acid monomers and especially polysilicic acid may show a high affinity to the positively charged surface of the hydroxide due to electrostatic interactions. The point of zero charge for this mineral was determined for a pH of 11 (Pokrovsky and Schott, 2004). However, brucite was not detected by XRD and TGA/DTA measurements until pH values of 9.6 were reached. Due to the increasing solubility of amorphous silica at pH >8 the formation of amorphous silica as a reason for the decreasing SiO<sub>2</sub> concentration can be excluded. This leads to the question of the composition of the precipitates, formed at each titration step. Therefore, extensive studies were carried out to characterise the precipitates, formed during the EDR brine titration experiments.

### **What is the composition of the precipitates at each titration step?**

Small amounts of gypsum were detected by XRD in all precipitates A to K, independent of the added amount of caustic soda. IC measurements of divalent cations pointed out a constant removal of nearly 300 mg/l Ca<sup>2+</sup>, independent of the added amount of caustic soda. The presence of gypsum in all precipitates of the EDR brine titration experiments seems to be surprising of first sight. Calculation of the saturation state of gypsum in EDR brine as a function of the pH (Chapter 3.3.3.3, Figure 3.10) demonstrate that the saturation of this mineral is reached at pH values ≥ 9.5. However, the Ca<sup>2+</sup> concentration decreases immediately after the first addition of small amounts of caustic soda although pH values of the solutions were definitely below 9.5. As mentioned before, caustic soda was added dropwise to the fast-stirred EDR brine. During this procedure locally high pH >9.5 develop and as a consequence the saturation state of gypsum was exceeded. In contrast to the fast formation of gypsum, dissolution remains a slow process even at comparatively low pH values in the EDR brine. As a result gypsum was detected in all precipitates (Figure 4.26). XRD measurements revealed all precipitates to contain halite (NaCl) which can be related to the sampling procedure. To avoid dissolution of the unknown solids, filter residues were not washed with DIW. Residual brine, containing sodium and chloride, leads to the formation of halite when drying the filter cake. Other crystalline materials, barring gypsum, halite and brucite, were not detected by XRD, which may be due to a smaller amount of crystalline material (below 1 - 2 wt.-%) or by the presence of amorphous material.

### **Presence of metal ions in the precipitates?**

Change of the colouration before and after heating up to 1000°C gave first information regarding the presence of heavy metals in the precipitates (Figure 4.25). Copper and nickel hydroxides may be bluish to greenish. Though only hydroxides containing copper change their colour to black or dark brown as a consequence of the decomposition of copper(II)-hydroxide to copper(II)-oxide (Holleman and Wiberg, 1995, p.1335). Intensely green nickel(II)-hydroxide was

converted to greyish to green nickel(II)-oxide upon dehydroxilation. Therefrom, the brownish colour of the precipitates after heating suggests the presence of copper and nickel, especially in the dark green sample A (minimum addition of NaOH), and greenish, samples B to E (increasing addition of NaOH). With increasing removal of  $Mg^{2+}$ , observed in titration steps of samples G to K (maximum addition of caustic soda), the colour shifts from light green to light blue.

### **Were single-metal hydroxides formed during the titration experiments?**

Based on the considerations of the last paragraph, TGA/DTA results of precipitates A to K and the results of defined mixtures of single- and multi-component powders are of special interest. An evaluation of the thermal gravimetric measurements (Figure 4.27) indicates the presence of perfectly to poorly crystalline and additionally amorphous constituents in the samples. Slight but continuous loss of weight during the whole gravimetric measurements as a function of temperature may be an indication of amorphous material. Notably, the decrease of sample weight beyond the two temperature ranges, where a significant decrease of weight was determined, (see table 4.7), was higher for the dark-green precipitates A and B (lowest addition of NaOH) in comparison to samples with decreasing intensity of colouration. Combined with the IC and ICP measurements this indicates that an increasing removal of silicon and magnesium, especially for samples H to K (highest addition of NaOH), results in a decrease of the colour intensity. Additionally the fraction of amorphous material remains constant between 5 and 7% for samples C to K (addition of 14 - 60 mmol/l NaOH).

Gypsum, identified by XRD measurements in all titration samples A to K, is mainly responsible for the weight loss between 80 and 250°C. Furthermore, the first derivative of the TG signal as well as the endotherm of the SDTA show broad minima, 10 to 20 °C, of the endotherm, which are not characteristic of gypsum dehydration (Figure 4.28 and 4.29). Within this temperature range the dehydration of gypsum is overlapped by one or more endothermic reactions. On one hand, adsorbed water is released up to 100°C, on the other hand the sustained minima and the diffuse shoulders at higher temperature indicate the presence of dehydroxilation of poorly crystalline material. The relative weight loss within this temperature range decreases from samples A to K. This fact results from the increasing weight loss within a second temperature range between 300 and 550°C. In the respective SDTA signal of this region, a direct correlation becomes visible between the increasing addition of caustic soda and, as a consequence, the significant removal of  $SiO_2$  from the EDR brine. With increasing amounts of  $SiO_2$  in the precipitates, an endotherm appears in the DTA signal and becomes more distinctive with each titration step. Notably, with increasing removal of  $Mg^{2+}$  and the adjustment of a nearly constant pH of 9.6 of titration steps G to K (highest addition of NaOH) the endotherm of the second temper-

ature range shifts to lower temperature. As mentioned before, halite (NaCl) was detected by XRD measurements in every sample. The melting of halite was observed by a small endotherm in the SDTA curves at temperatures of 720 to 760°C. A loss of weight was not associated with this reaction, as a consequence this reaction was not visible in the first derivative of the TG curve. Shift of the minima with ascending order of the titration steps indicates an increasing amount of halite in the samples.

Until now, the discussion of the thermal analysis of the precipitates, formed during EDR titration experiments has revealed important information about the correlation between SiO<sub>2</sub> and Mg<sup>2+</sup> removal from the EDR brine and shapes of the TG, respectively SDTA curves. Investigations of various amounts of pure material and defined mixtures were conducted to obtain more information on the composition of the precipitates. The minimum of the endotherm of samples B to K was detected around 145°C within the first temperature range. By assuming that this minimum corresponds to the dehydration step of gypsum to bassanite, the amount of gypsum within these samples was estimated at 10 mg, or 20 wt.%, based on the PA curve of gypsum (Figure 4.30). This result is in excellent agreement to IC and XRD measurements: At every titration step a constant amount of nearly 300 mg/l Ca<sup>2+</sup> was removed.

If the change of the colouration before and after heating the samples is mainly caused by copper and nickel, this raises the question whether the metals are present as single hydroxides. Presence of nickel(II)-hydroxide in the precipitates can be excluded. Dehydroxylation of this hydroxide exhibits a sharp endotherm with a minimum near 300°C (Liang et al., 2004). Around this temperature no endotherm was determined for all titration samples A to K. In contrast to nickel(II)-hydroxide, the formation of pure copper(II)-hydroxide, spertiniite, can not be excluded. Within the temperature range of the dehydroxylation minimum of spertiniite near 180°C, an overlay of several endothermic reactions was obtained. The PA curves of copper(II)-hydroxide reveal no shift of the minimum of the endotherm as a function of sample mass (Figure 4.32). The minimum remains constant at 182°C. Furthermore, reaction of dehydroxylation is expressed by a sharp endothermic profile of the SDTA curves. Additionally, mixtures of various amounts of gypsum and spertiniite indicates that increasing amounts of copper(II)-hydroxide in relative to gypsum lead to a more diffuse left shoulder of the endotherm (Figure 4.34). However, the presence of copper(II)-hydroxide within the precipitates is not sufficient to explain the elongated endotherm between 80 and 250°C in the SDTA signal. Also dehydroxylation of brucite is not influenced by the presence of spertiniite.

It has to be taken into account that in general metal ions can be precipitated, by addition of caustic soda, as sparingly soluble metal hydroxides (Nalco, 2009, p. 25.17). As a consequence of the unexpected colouration of the precipitates, solids were investigated by XRF. Copper,

zinc, nickel and iron were identified by qualitative XRF measurements in all titration samples A to K. Usually metal hydroxides show typical, sharp endotherms by dehydroxylation. For example, the minimum of copper(II)-hydroxide lies at 182°C (this work) and the minimum of zinc hydroxide at 130°C (Srivastava and Secco, 1967). Furthermore, endothermic reactions of the dehydroxylation of copper and zinc are much stronger than the endotherm of gypsum dehydration. Therefore, small amounts of these metal hydroxides may overlay the endotherm of gypsum. In addition, the broad endothermic reaction within the first temperature range indicates coprecipitation of copper and zinc. Also the formation of hydroxides, containing copper as well as zinc in various stoichiometric relations by coprecipitation can not be excluded.

These considerations of the coprecipitation of hydroxides with variable stoichiometric compositions must also be taken into account when discussing the SDTA signal of the precipitates within the second temperature range between 300 and 550°C. Within this context, pure magnesium hydroxide was detected in samples I, J and K (maximum amount of NaOH added), which is in accordance to the XRD measurements. In addition, the elongation of the right shoulder of the SDTA signal of sample H indicates the presence of small amounts of brucite which is in accordance with the EDX analysis. Here, the highest amount of magnesium was detected in samples H to K (addition of 30 - 60 mmol/l NaOH).

The SDTA curve of natural brucite deviates significantly from the SDTA curves of technical brucite. The differences between both samples arise from small impurities of calcium in the natural brucite which may effect a second endotherm at higher temperature. SDTA signals of sample K, EDR titration experiments, of technical and natural brucite are shown in Figure 4.42.

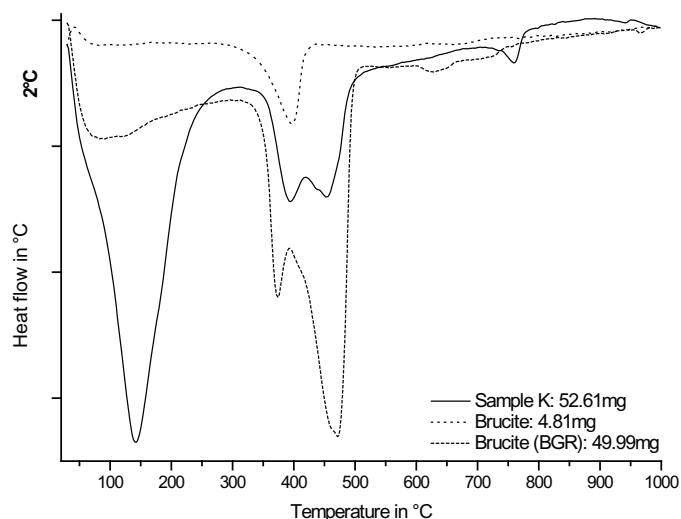


Figure 4.42: SDTA curve of sample K (52.61mg) is opposed to the DTA curve of technical brucite from Merck (4.81mg) and natural brucite from BGR (52.61)

It should be noted that metal hydroxides of copper, zinc and nickel are less soluble than brucite

(Nalco, 2009, p. 25.5). Nevertheless, by IC, EDX and XRF analyses all samples A to K are formed to contain magnesium. Solely in samples H to K (addition of 30 - 60 mmol/l NaOH) the concentration of magnesium was high enough to form pure brucite. Due to the similar crystal structure of magnesium and nickel hydroxides, the formation of a mixed hydroxide is likely. During the formation of mixed hydroxides it may be possible that due to the relatively high concentration of magnesium, in relation to nickel, solids are precipitated in a brucite-like structure and heavy-metal ions are incorporated by substitution.

### **Origin of the heavy metals in original EDR brine?**

So far one important fact was not discussed: the origin of the heavy-metal ions, detected in precipitates of the EDR brine titration experiments. Their occurrence within these precipitates was surprising due to the fact, that they were not detected by careful analysis of the feed water of the pilot plant. As sources of the metal ions all stirrers, vessels and pipes made of metal must be considered. The solubility of metal hydroxides increases significantly with decreasing pH and increasing ionic strength (Nalco, 2009, p. 25.6 and p. 25.17). Regarding the pilot plant, low pH of the EDR feed concentrate which is made of acidified RO concentrate, pH 2, and the high salt content of the solution may lead to corrosion although solely metal equipment made of stainless steel was utilized.

### **Adsorption of silicic acid on mineral surfaces of metal-hydroxides?**

The simultaneously observed removal of silicic acid is related to the high affinity of negatively charged monomeric and polysilicic acid to positively charged hydroxide surfaces. Sjöberg (1996) described the affinity of various metal ions to hydroxyl groups on surfaces of silica, here he noted a higher affinity of hydroxyl groups with  $\text{Cu}^{2+}$  than to  $\text{Mg}^{2+}$ . Inverse, a high affinity of silicic acid to positive surface groups on metal hydroxides can be considered.

EDR titration experiments have revealed that dissociation of silicic acid, precipitation of hydroxides and adsorption of silicic acid on hydroxide surfaces depend on the amount of caustic soda, added to the EDR brine. One of the most interesting facts concern the nearly constant removal of metal ions ( $\text{Mg}^{2+}$  and  $\text{Ca}^{2+}$ ) up to an addition of 20 mmol/l NaOH. It is possible that the dynamics of various reactions in the aqueous system has to be considered here. After addition of NaOH, due to locally high pH values, the formation of hydroxides and gypsum occurs. At the same time silicic acid begins to dissociate. Immediately after dissociation, charged monomers and oligomers of silicic acid adsorb on hydroxide surfaces and may block or inhibit further growth of the hydroxide particles. With every titration step increasing amounts of  $\text{OH}^-$  ions are mainly consumed by the dissociation reaction. With  $\text{OH}^-$  additions higher than the required amount for the complete dissociation of silicic acid, the formation of further hydroxides starts,

as observed in the EDR brine titration experiments. As soon as the added amount of caustic soda is high enough for complete removal of  $\text{SiO}_2$ , the  $\text{Mg}^{2+}$  concentration in solution decreases significantly. At the same time, the magnesium concentration in the precipitates increases. In addition, brucite was detected in these precipitates. With beginning formation of brucite, the pH is adjusted to a constant value of 9.6, which results of brucite saturation as a function of the pH in the EDR brine. As long as the EDR brine contains magnesium, the pH remains stable at a constant value of 9.6 despite of increasing addition of caustic soda.

### **Applicability of the discussed results for the development of controlled removal of $\text{SiO}_2$ from EDR brine**

Assuming that the theory, developed in the last paragraph, can be applied to the multi-electrolyte system of the EDR brine, it can be used for the presumption concerning the required amount of caustic soda for removal of various amounts of silicic acid in those solutions. Due to the observation that  $\text{OH}^-$  consumption depends mainly on the dissociation reaction of silicic acid, a lower consumption of caustic soda is expected for lower concentrations of silicic acid in solution. Contrariwise, a higher amount of silicic acid requires a higher amount of caustic soda, whereat the removal of silicic acid requires only very small amounts of freshly precipitated hydroxides. This theory stands in excellent agreement to the results of the titration experiments of various amounts of silicic acid in 0.12 molal  $\text{MgCl}_2$ -solution (Figure 4.22).

Experiments of Chapter 4.2.3.3 were focused on  $\text{SiO}_2$  removal as a function of the addition of caustic soda and of pH. The required amount of caustic soda for a complete removal of  $\text{SiO}_2$  from brine was investigated. Therefore, it was necessary to control three parameters: a) the precipitated hydroxide has to be known (brucite), b) the initial salt concentration of the solution must be equal and c) the initial  $\text{SiO}_2$  concentration must be variable.

In consequence, it was decided to conduct titration experiments in synth. EDR concentrates without any heavy metals in solution, solely brucite should be allowed to be formed. As expected, a complete removal of  $\text{SiO}_2$  was achieved with lesser amounts of caustic soda the lower the initial concentration of silicic acid in solution. Notably, the removal rate of  $\text{SiO}_2$  seems to be higher, the higher the amount of silicic acid in solution. As expected, the pH was adjusted to 9.6 after complete removal of silicic acid (Figure 4.36) which is the pH where brucite reaches the saturation state in those solutions. Every addition of caustic soda will result in the consumption of  $\text{OH}^-$  ions required for the formation of brucite.

Within this context it is conspicuous that brucite remains stable in these solutions at pH values < 9.6. As discussed in detail, precipitation of brucite at pH values < 9.6 is related to locally high pH values due to the experimental setup. It is possible that the velocity of brucite dissolution is much slower than precipitation, and in consequence brucite particles remain in solution for a

long period of time. Additionally it has to be kept in mind that the rate of brucite dissolution depends mainly on hydroxylation of the surface groups  $>\text{MgOH}_2^+$  and  $>\text{MgOH}^0$  (Prokovsky et al., 2004). In case of adsorption of negatively charged silicic acid instead of  $\text{OH}^-$ , hydroxylation of  $>\text{MgOH}_2^+$  and  $>\text{MgOH}^0$  may be blocked and, in consequence, dissolution of brucite may be inhibited.

***Are inorganic deposits the reason for the membrane blockage in the EDR unit?***

As far as it is known from the experiments of this work, the formation of amorphous silica, gypsum and brucite and the formation of large oligomers of silicic acid in the EDR brine at pH values below 5 can be excluded. These substances can be formed if locally high pH values occur in the EDR unit, but it needs another trigger to form them. Here further investigation of the direct interaction between functional groups of the membrane surface and electrolytes of the brine needs to be conducted.

Nevertheless, the of metal-hydroxides provide ideal surfaces for silicic acid adsorption. This means in consequence that an inhomogeneous mixture of hydroxide and adsorbed silicic acid forms deposits on membrane surfaces which are very difficult to remove. Therefore it can be an advantage to remove silicic acid from the feed water of the EDR unit.

### 4.3 Removal of silicic acid

Two different methods were investigated regarding their applicability to remove silicic acid from EDR brines. First, adsorption on inorganic mineral surfaces by using technical materials. Second, adsorption of silicic acid on in situ precipitated brucite by controlled addition of caustic soda.

#### 4.3.1 Removal of silicic acid by adsorption on mineral surfaces

Different inorganic materials were tested with regard to their adsorptivity for silicic acid.

Therefore, two Si-containing minerals, seasand ( $\text{SiO}_2$ ) and tobermorite,  $(\text{Ca}_5[\text{Si}_3\text{O}_8(\text{OH})]_2 \times 3.5\text{H}_2\text{O})$  as well as two hydroxides, brucite ( $\text{Mg}(\text{OH})_2$ ) and hydrotalcite ( $\text{Mg}_6\text{Al}_2(\text{CO}_3)(\text{OH})_{16} \times 4\text{H}_2\text{O}$ ) were chosen.

##### Experimental setup

Adsorption of silicic acid by using technical inorganic compounds was investigated in batch experiments. 100 ml original EDR brine with an initial pH of 2.1, containing 112 mg/l  $\text{SiO}_2$ , was mixed with different amounts of inorganic materials in PE bottles and shaken for 3 h at 175 rpm. In addition, brucite and hydrotalcite were mixed with synth. EDR brines, containing different amounts of silicic acid. For sampling, solutions were filtered through a 0.2  $\mu\text{m}$  membrane filter by sub-pressure filtration.  $\text{SiO}_2$  concentrations were determined by colorimetry, repeat determinations were carried out for every sample. Also, the pH was measured after sampling.

##### Results

With increasing amount of seasand in contact with 100 ml EDR brine an increasing concentration of  $\text{SiO}_2$  was measured (Figure 4.43), pH remains constant at 2.1 (Table 4.8). Likewise, the amount of  $\text{SiO}_2$  increases significantly in the presence of tobermorite, here, the pH value reaches 6.8. For brucite and hydrotalcite a significant decrease of the  $\text{SiO}_2$  concentration was observed as a function of increasing amounts of solids in solution. Here, the removal of silicic acid was more effective by using hydrotalcite. Also, increasing addition of hydroxides leads to a significant increase of the pH. With increasing amounts of brucite, the pH was adjusted to higher values up to a pH of 9.

Table 4.8: pH values of the filtrates of the batch experiments as a function of the added amount of solid material

	Seasand	Tobermorite	Brucite
1 g	2.1	6.8	8.4
5 g	2.1	no experiment	8.8
10 g	2.1	no experiment	9.0
50 g	2.1	no experiment	no experiment
100 g	2.2	no experiment	no experiment

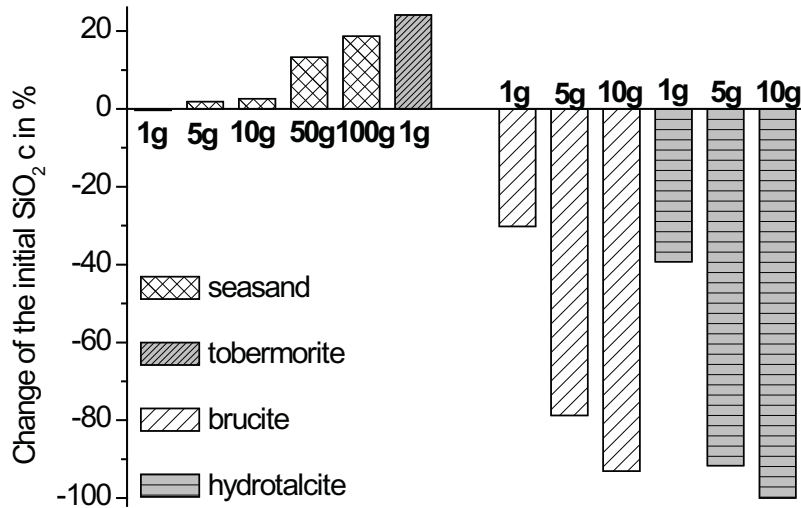


Figure 4.43: Changes of the  $\text{SiO}_2$  concentration of original EDR brine as a function of utilised material and amount of this material

The adsorptivity of hydrotalcite as a function of the initial amount of  $\text{SiO}_2$  in solutions of synthetic EDR concentrate is greater than the one of brucite. With increasing amount of utilised material, also the amount of  $\text{SiO}_2$  removed from solution increases (Figure 4.44).

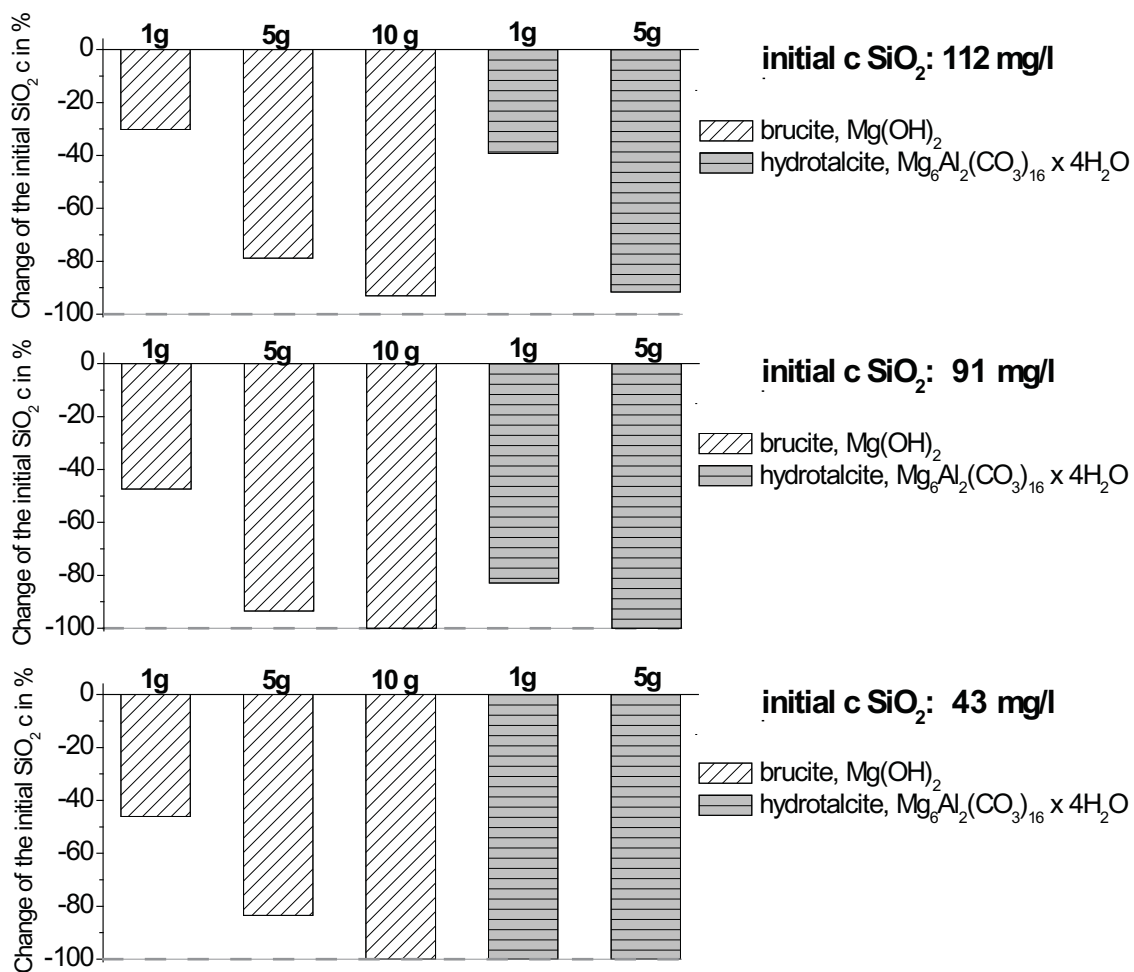


Figure 4.44: Change of  $\text{SiO}_2$  concentration of synth. EDR brine as a function of the initial amount of  $\text{SiO}_2$  in solutions as well as a function of utilized material and amount of this material

### 4.3.2 Adsorption of silicic acid on mineral surfaces of in situ precipitated brucite

The controlled and continuous removal of  $\text{SiO}_2$  by in situ precipitation of brucite from multi-electrolyte solutions, similar to the EDR brine of the pilot plant, by the addition of caustic soda was investigated in flow-through cell experiments. For this purpose, several parameters were taken into consideration: influence of the background electrolytes, salt concentration, influence of the initial concentration of  $\text{SiO}_2$ , retention time as a function of the cell volume, influence of the flow as well as of the amount of utilised caustic soda.

#### Experiments

Flow-through cell experiments were conducted at room temperature at normal atmosphere, to keep conditions close to environmental parameters of the pilot plant. All materials, used for the experiment, vessel, beaker and tubes were made of plastic. A 1.25 l and a 2.35 l plastic beaker were used as flow-through „cells“, samples were taken directly out of the drainage, see grey insert at upper right in Figure 4.45. For each experiment 10 l of synth. concentrate with an initial pH of 5 was produced. Composition and concentration of the various utilised solutions are listed in Table 4.9,  $\text{SiO}_2$  concentration depends on the experiment. Constant flow of the concentrates was adjusted to 0.5 l/min. Flow and amount of caustic soda, added to the concentrates, varied from 2.5 to 15 mmol/min, respectively from 5 to 30 mmol/l. Concentrate and caustic soda was added simultaneously at the same position near the bottom of the cell. Samples were taken as a function of time, every 2 min., equivalent to a volume throughput of 1 l concentrate. After sampling the solution was filtered through 0.45  $\mu\text{m}$  Sartorius syringe filters and directly diluted by 1:25 for ICP-OES and 1:100 for IC measurements.



Figure 4.45: Experimental setup of the flow-through cell experiments

Table 4.9: Composition of the applied synthetic concentrates. The combination and concentration of the single electrolytes depends on the experimental setup and the question of interest

	Composition of the applied synthetic concentrates in mol/kg				
	MgCl <sub>2</sub>	NaCl	CaCl <sub>2</sub>	Na <sub>2</sub> SO <sub>4</sub>	Si-stocksol'n
comp. 1	0.120	-	-	-	variable
comp. 2	0.120	1.350	-	-	variable
comp. 3	0.120	1.350	0.046	-	variable
comp. 4	-	1.350	0.046	0.063	variable
comp. 5	0.120	1.290	0.120	0.063	variable
comp. ED/RO	Concentration of electrolytes are based on main electrolytes of RO/EDR concentrates, Table 2.1 on page 14, including K <sup>+</sup> , Sr <sup>2+</sup> and NO <sub>3</sub> <sup>-</sup>				variable

### Results of the flow-through experiments: Influence of electrolytes and salt concentration

*Experimental parameters: concentrate: 0.5 l/min, NaOH: 10 mmol/min, cell volume: 1.25 l, initial SiO<sub>2</sub> concentration: ~116 mg/l. These parameters reflect the standards for all experiments, only one parameter varied in further experiments, as noted.*

In Figure 4.46 results of flow-through cell experiments as a function of the composition and the salt concentration of these synth. concentrates are opposed. As far as the utilised concentrates contain the same amount of Mg<sup>2+</sup>, removal of SiO<sub>2</sub> remains nearly constant at 74 to 78%. Also in magnesium-free solutions, such as concentrates made of composition 4, a significant decrease of nearly 50% of the amount of SiO<sub>2</sub> was formed. The removal of SiO<sub>2</sub> remains lower by 8 to 10% in synth. RO concentrate than in synth. EDR concentrate.

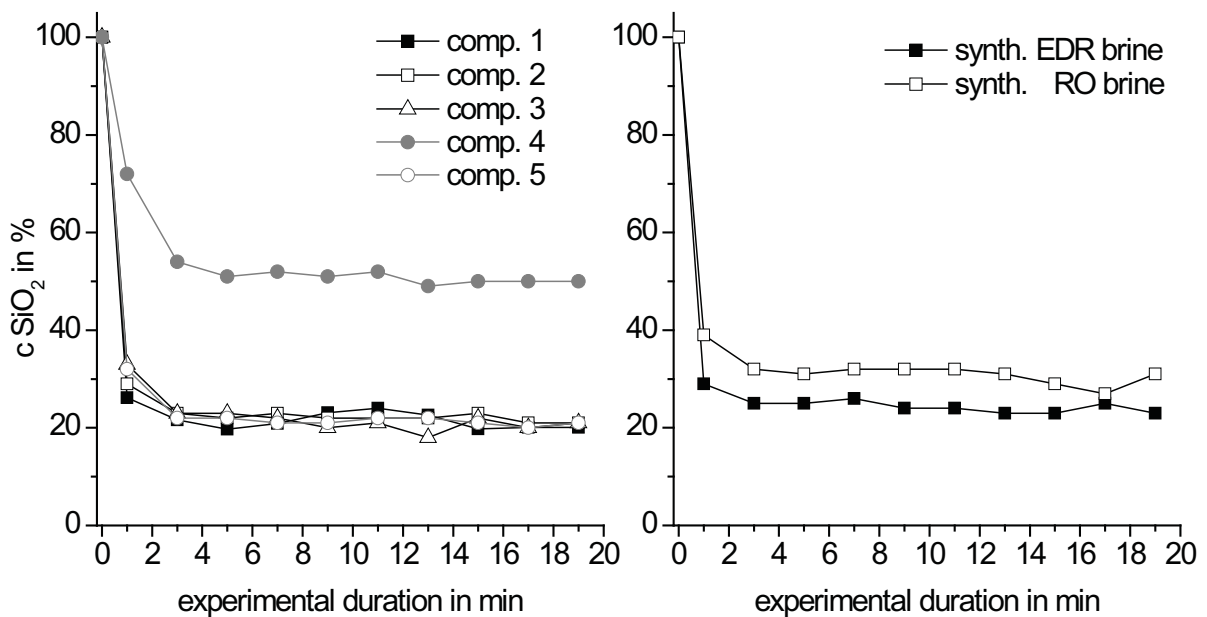


Figure 4.46: SiO<sub>2</sub> removal in flow-through cell experiments from synth. concentrates with composition 1 to 5 and synth. RO and EDR brines (Table 4.8)

### Results of the flow-through experiments: Influence of initial concentration of $\text{SiO}_2$

Parameter varied: initial  $\text{SiO}_2$  concentration from 6 to 98 mg/l

The initial concentration of  $\text{SiO}_2$  significantly affects the decrease of silicic acid at constant addition of caustic soda in synth. EDR concentrate (Figure 4.47). The higher the initial amount of  $\text{SiO}_2$ , the higher the entire amount of removed  $\text{SiO}_2$ . Even at very low initial concentration of silicic acid no complete removal of  $\text{SiO}_2$  was observed.

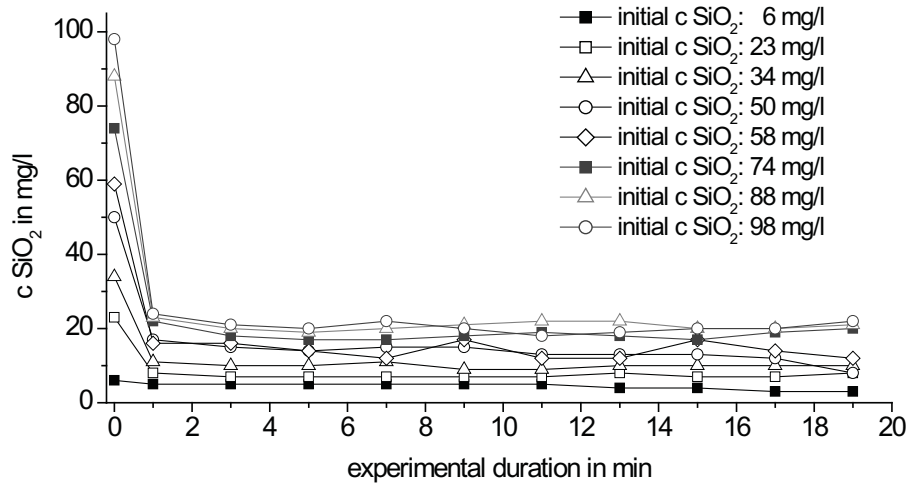


Figure 4.47:  $\text{SiO}_2$  removal from synth. EDR concentrates as a function of the initial concentration of  $\text{SiO}_2$

### Results of the flow-through experiments: Influence of concentrate retention time as a function of the cell volume

Parameter varied: cell volume at 1.25 and 2.35 l

At a concentrate flow of 0.5 l/min the average residence time is 2.5 min (150 sec) for 1 l concentrate in the 1.25 l cell and 4.7 min (282 sec) for the 2.35 l cell. Removal of silicic acid is slightly higher in the 2.35 l cell than in the 1.25 l cell (Figure 4.48).

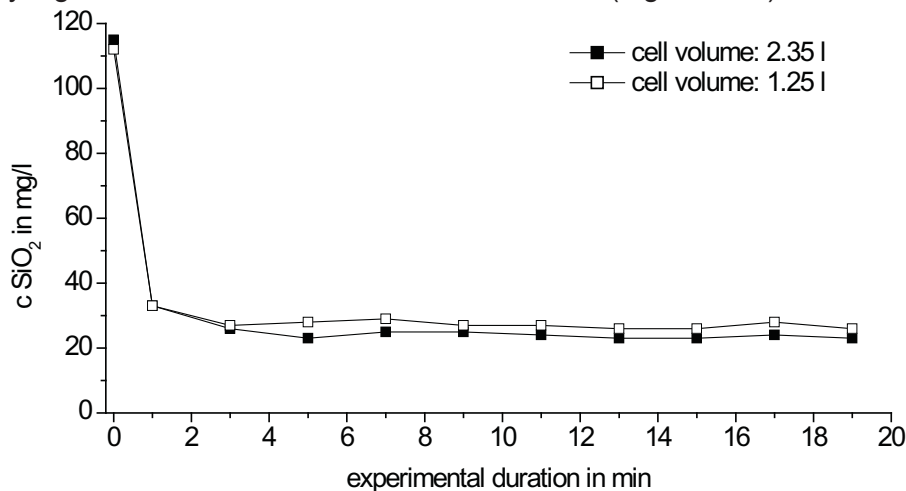


Figure 4.48:  $\text{SiO}_2$  removal from synth. EDR concentrates as a function of the cell volume

### Results of the flow-through experiments: Influence of the dosage of caustic soda

Parameter varied: NaOH at 10 mmol/min (5 ml of 2 molar and 10 ml of 1 molar NaOH)

Different dosage of the caustic soda at a constant concentration of 10 mmol/min, corresponding to 20 mmol/l, affects SiO<sub>2</sub> removal from synth. EDR concentrates only slightly (Figure 4.49). The impact of addition of a larger volume of NaOH in combination with lower concentration, 1 molar and 10ml instead of 2 molar and 5 ml, seems to be slightly more effective.

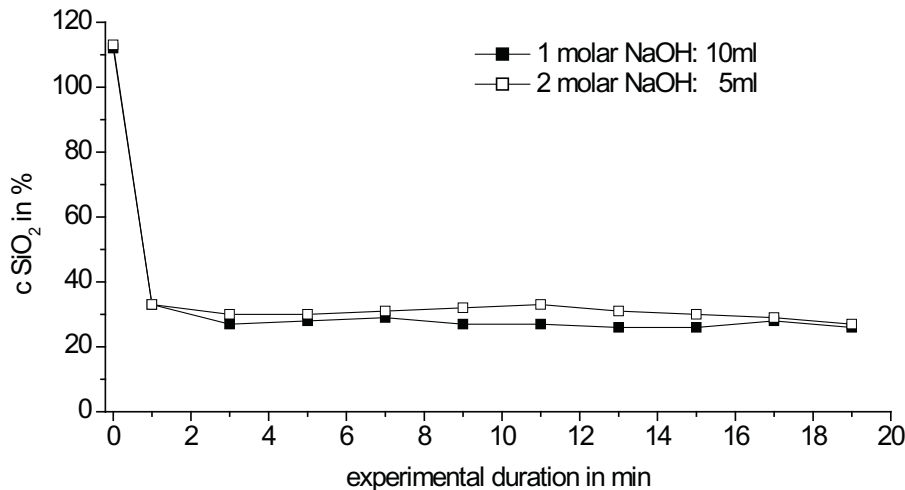


Figure 4.49: SiO<sub>2</sub> removal from synth. EDR concentrates as a function of the additive volume at same addition of 10 mmol/min NaOH

Parameter varied: NaOH from 2.5 to 15 mmol/min, initial SiO<sub>2</sub> concentration: ~100 and 40 mg/l.

With increasing amounts of caustic soda, added to synth. EDR concentrates with initial SiO<sub>2</sub> concentration of 100 mg/l and 40 mg/l respectively, a increasing removal of SiO<sub>2</sub> was observed (Figure 4.50 a and b). The higher the initial concentration of silicic acid, the higher the entire removal of silicic acid.

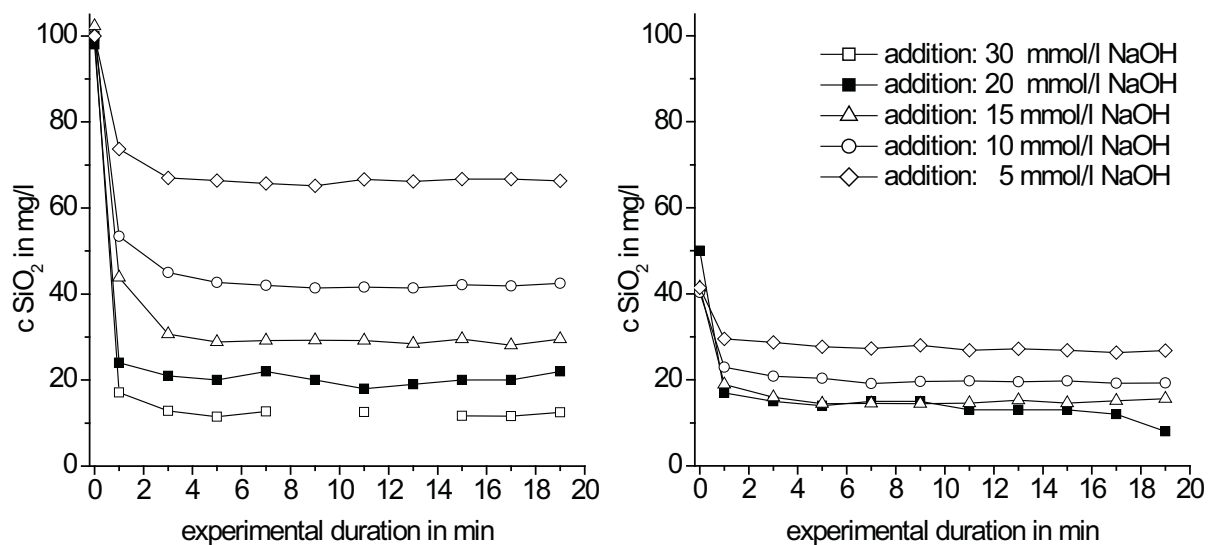


Figure 4.50: SiO<sub>2</sub> removal from synth. EDR concentrates as a function of the added amount of caustic soda (a) and as a function of the initial SiO<sub>2</sub> concentration (b)

### 4.3.3 Discussion

The experimental results of Chapter 4.2 rule out that silica scaling is caused by membrane pore blockage of large oligomers or by the formation of amorphous silica. Nevertheless, the experiments have shown that very small amounts of in situ precipitated hydroxides are required to adsorb appreciable amounts of silicic acid. Deposits of brucite may be removed by cleaning the membrane surfaces with weak acids. In contrast, compounds made of small hydroxide particles with adsorbed silicic acid on the surfaces, similar to a thin coating, are more difficult to dissolve.

The experiments of Chapter 4.3 were focused on investigations concerning a controlled removal of silicic acid from aqueous salt solutions, similar to the EDR brine of the pilot plant. Therefore, two different methods were investigated:

- First, the adsorption of silicic acid on mineral surfaces, produced by technical processes. For this purpose, materials were tested in batch experiments regarding their applicability for replaceable cartridges. Original EDR brine as well as synth. EDR concentrates were utilised for experiments.
- Second, the adsorption of silicic acid on surfaces of in situ precipitated brucite. Surfaces of freshly precipitated hydroxide exhibit, in most cases, very large areas in comparison to particles, produced by industrial processes. Especially titration experiments of Chapter 4.2.3 have revealed the high velocity of interactions between freshly precipitated hydroxides and silicic acid at pH values  $>8$  with beginning dissociation of silicic acid. Therefore, flow-through cell experiments were conducted to investigate whether a controlled and continuous removal of silicic acid is feasible by addition of caustic soda.

Increasing amounts of  $\text{SiO}_2$  in EDR brine, mixed with various amounts of seasand are related to the marginal dissolution of the silicate (Figure 4.43). An affinity of silicic acid for accretion on mineral surfaces was neither observed for seasand nor for tobermorite. In particular, tobermorite was significantly dissolved in the brine even at comparatively low amounts. Additionally, in contrast to mixtures of EDR brine and seasand, the pH increases to 6.8. This can be related to the dissolution process of small amounts of calcite,  $\text{CaCO}_3$ , and to the dissolution of the calcium silicate hydrate. As mentioned several times in the discussion of Chapter 4.2, silicic acid in solutions exist mainly as uncharged monomers and oligomers before dissociation starts at a pH of 7 to 8. Such an increase of the pH was observed for mixtures of brucite and EDR brine (Table 4.8). With increasing amounts of brucite an increasing pH up to a value of 9 was detected, combined with increasing removal of  $\text{SiO}_2$  from solution. The same but more distinctive observation was made for mixtures of hydrotalcite and EDR brine. Experiments, conducted in synth. EDR brine with variable initial concentration of  $\text{SiO}_2$ , affirm this result.

Materials like brucite and hydrotalcite, produced by industrial processes, show a significant adsorption capacity for silicic acid. Unfortunately, the required amount of brucite (10 g, respectively 5 g per 100 ml EDR brine) for nearly complete removal of silicic acid is too high for an effective use in replaceable cartridges at the industrial scale (Figure 4.44).

Whereas an increasing pH in the EDR unit of the pilot plant promotes precipitation of sparingly soluble salts as a worst-case scenario, the concerted addition of caustic soda as pretreatment to the mix of EDR/RO concentrate (Figure 2.1) provides the opportunity for a controlled removal of silicic acid by adsorption on in situ precipitated brucite.

Metal hydroxides, in particular, exhibit surfaces with a high affinity for the interaction with silicic acid in aqueous solutions. In this function they are applied for controlled silica removal in industrial processes (Iler, 1979, p. 79, Sheikholeslami, 2002, Nalco, 2009, p. 5.12). Even though adsorption of silicic acid on surfaces of aluminium (Iler, 1979, p. 80) or iron hydroxides (Nalco, 2009, p. 5.12) is very effective, due to handling and compatibility of magnesium in the treatment of drinking water, precipitation of brucite is one of the most common methods, used for silica removing. For this purpose, lime softening by utilisation of calcium-magnesium oxides, produced by calcination of dolomite, is the most popular method. Also the successful applicability of caustic soda as pretreatment of feed water of RO units are described by Al-Rehaili et al. (2003) and Sheikholeslami and Bright (2002).

Flow-through cell experiments (Chapter 4.3.2) investigated the applicability of the use of caustic soda for brucite precipitation and silicic acid adsorption. Due to the complex composition of the RO and EDR brine, flow-through cell experiments were focused on specific questions concerning the influence of

- composition and concentration of aqueous salt solutions
- initial amount of  $\text{SiO}_2$
- retention time of concentrate/additive mixture in the flow-through cell
- dosage of caustic soda with respect to flow and concentration

Before discussing the experimental results some remarks concerning two parameters of the synth. concentrates should be noted.

First, compositions of synth. concentrates, especially of synth. EDR concentrates, were limited to the main electrolytes  $\text{Na}^+$ ,  $\text{Mg}^{2+}$ ,  $\text{Ca}^{2+}$ ,  $\text{K}^+$ ,  $\text{Sr}^{2+}$ ,  $\text{Cl}^-$ ,  $\text{SO}_4^{2-}$  and  $\text{NO}_3^-$  for flow-through cell experiments. Although the large impact of minor ions like  $\text{Zn}^+$ ,  $\text{Ni}^{2+}$  and  $\text{Cu}^{2+}$  on silicic acid removal was discovered in EDR brine titration experiments of Chapter 4.2.3.2, their utilisation is ruled out because these electrolytes are not constituents of the raw water. Their presence in the brine was a matter of undesired corrosion of metal parts of the pilot plant in contact with chemically aggressive process concentrates. The second parameter concerns the initial pH

values of flow-through cell experiments. The initial pH for all synth. concentrates was adjusted to 5 instead of 2. As mentioned before, based on experiments in Chapter 4.2 silica scaling at pH values below 5 can be avoided. Thereafter, acidification of the RO concentrate to pH 2 before feeding it into the EDR unit seems to be unnecessary. Experimental results of flow-through cell experiments are discussed in the following paragraphs:

Increasing salt concentration of solutions, made of compositions 1 to 3 and 5 of Table 4.8, did not affect the adsorption process as long as the initial concentration of  $Mg^{2+}$  remained constant (Figure 4.46 a and b). Experiments revealed that removal of  $SiO_2$  mainly depends on the initial  $Mg^{2+}$  concentration in synth. concentrates. Although the amount of magnesium in synth. RO concentrates was 6 times lower than in synth. EDR concentrates (0.02 instead of 0.12 mol/kg), the removal of silicic acid decrease only by about 7%. Therefrom, it may be concluded that enough magnesium is present in solutions to ensure the continuous removal of silicic acid. Interestingly, silica removal of nearly 50% was observed in magnesium-free solutions (composition 4, Table 4.8). This solution contains solely sodium, calcium, chloride and sulphate as main electrolyte species. Here, gypsum was formed as a consequence of the addition of caustic soda and an adsorption of silicic acid on gypsum surfaces can be assumed. In the presence of both electrolytes,  $Ca^{2+}$  and  $Mg^{2+}$  in solutions, no additional adsorption behavior was observed. In contrast, the removal was similar to that of  $SiO_2$  in pure  $MgCl_2$ -solutions. The affinity of silicic acid for brucite surfaces seems to be much stronger than for gypsum and furthermore, adsorption on hydroxide surfaces seems to be the dominant reaction. Within this work it was not possible to find out whether this lesser affinity can be related to a smaller surface area of gypsum crystals or a lack of positively charged surface groups.

With constant amount of  $Mg^{2+}$  in solution the initial concentration of silicic acid affects significantly the removed fraction of  $SiO_2$ . With increasing initial concentration of  $SiO_2$ , the amount of removed  $SiO_2$  increases (Figure 4.47 and Figure 4.51). This result may be explained based on one assumption of the titration experiments where a correlation between increasing initial amounts of silicic acid and increasing amount of charged silicic acid as a consequence of dissociation was inferred, p. 92. As a result, the higher the amount of charged monomers and polymers of silicic acid in solution, the more can be adsorbed on hydroxide surfaces.

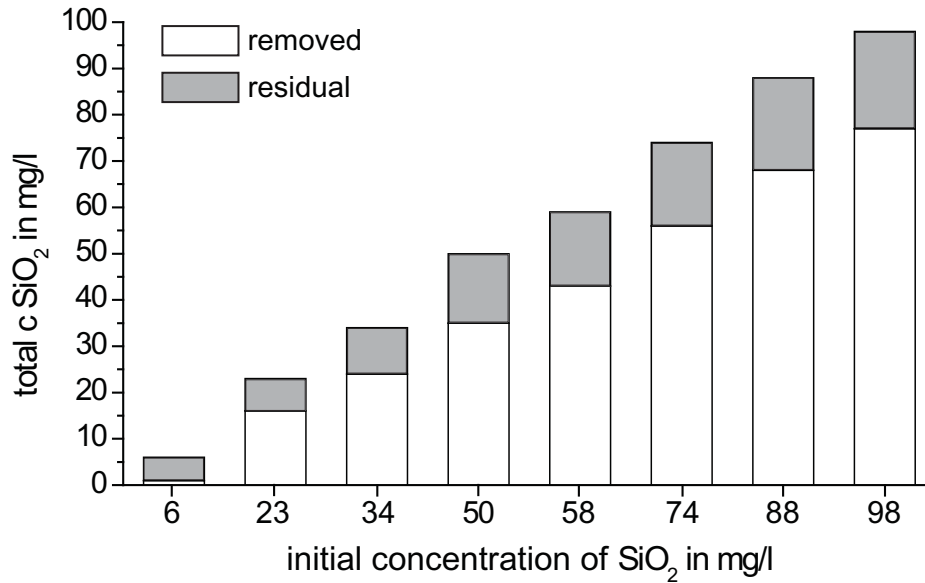


Figure 4.51: Removed and residual concentration of SiO<sub>2</sub> of flow-through experiments, conducted as a function of the initial concentration of silicic acid, see Figure 4.47, p. 108.

Also, the aforementioned reasons explain the increasing removal of SiO<sub>2</sub>, whereas for the residual fraction of SiO<sub>2</sub> in solution a comprehensive explanation is still lacking. Therefore, the following points should be considered:

- 1) Retention time of the concentrate/additive mixture in the flow-through cell has a very limited influence on the total removal of silicic acid (Figure 4.48).
- 2) Based on results of titration experiments with original EDR brine and synth. EDR brine, the amount of caustic soda required for a complete removal of 115 mg/l SiO<sub>2</sub> in flow-through cell experiments was calculated to approximately 15 mmol/l. Here, utilised concentration of caustic soda with a concentration of 20 mmol/l was applied in excess.
- 3) From batch experiments (Chapter 4.2.3.3, p. 85) it was concluded that with decreasing initial concentration of silicic acid a decreasing amount of caustic soda is required for a complete removal of silicic acid.
- 4) Both solutions were added at the same position near the bottom of the cell.

Even by excessive addition of caustic soda no complete removal of SiO<sub>2</sub> was achieved, not even at comparatively low concentrations of silicic acid in the synth. concentrates which seems to contradict earlier experiments. Two possible explanations will be discussed in the following paragraphs.

Due to the insignificant influence of the retention time on silicic acid removal it is concluded that the main part of the adsorption process takes place directly during mixing of concentrate and additive at the feeding position. If true, time for (a) precipitation of brucite, (b) dissociation of

silicic acid and (c) adsorption of silicic acid on positively charged surface groups of the hydroxide is very short. As mentioned before, all three processes **a** to **c** take place simultaneously. Due to the residual concentration of  $\text{SiO}_2$  in solutions it is obvious that one or more processes did not run to completion. In particular, the required complete dissociation of silicic acid for a successful adsorption process was not reached. In addition, the concentrate/additive mixture was stirred to ensure thorough mixing of additive and concentrate to avoid brucite plugging at the end piece of the additive tube. It is possible that, due to the stirrer velocity, parts of the feeded concentrate were swirled too fast in the direction of the overfall at the top of the cell. As a consequence, fractions of the concentrate were not able to interact with the additive within the provided time.

Investigations concerning the additive dosage affirm these considerations. Additive flow has no or only insignificant influence of silicic acid removal (Figure 4.49). In contrast, the increasing additive concentration leads to an increase of the removed amount of  $\text{SiO}_2$  from solutions (Figure 4.50 a and b and Table 4.10).

Table 4.10: Comparison between removed and residual amounts of  $\text{SiO}_2$  as well as removal of  $\text{SiO}_2$  per mmol caustic soda

admixed NaOH in mmol/l	initial c $\text{SiO}_2$ : 100mg/l			initial c $\text{SiO}_2$ : 40mg/l		
	removed $\text{SiO}_2$ in mg/l	residual $\text{SiO}_2$ in mg/l	removal of $\text{SiO}_2$ in mg/mmol	removed $\text{SiO}_2$ in mg/l	residual $\text{SiO}_2$ in mg/l	removal of $\text{SiO}_2$ in mg/mmol
30	88	12	3	-	-	-
20	80	20	4	37 <sup>a</sup>	13 <sup>a</sup>	1.8 <sup>a</sup>
15	71	29	5	25	15	1.7
10	58	42	6	20	20	2.0
5	34	66	7	13	27	2.5

a. initial c  $\text{SiO}_2$ : 50mg/l

A correlation is observed between added amount of caustic soda and removed fraction of  $\text{SiO}_2$ . With increasing application of caustic soda the effective removal of silicic acid per mmol NaOH decreases significantly, Table 4.9. The influence of this tendency is stronger at higher initial concentration of  $\text{SiO}_2$  in solution. Herefrom it is concluded, that the added amounts of caustic soda were not used as effectively as in batch experiments. Furthermore, the position of the additive dosage in the volume affects the removal of silicic acid. This statement is based on the following considerations: (a) formation of hydroxide seeds and (b) dissociation of silicic acid are promoted optimally which, (c) in combination, leads to a successful adsorption. Regarding the application of caustic soda as an additive for silica removal by in situ precipitation of brucite or other metal hydroxides at the industrial scale, this observation has consequences on the design of reaction vessels and optimal feeding position of additive and concentrate.

## 5 Geochemical modelling of brine evaporation

Original EDR brine and synth. EDR concentrates were evaporated at various relative humidities. Evaporation rate, pH, density, electrolyte concentration and precipitates were investigated as a function of the loss of water. The experimental results were compared with the calculations with the GWB.

### 5.1 Parameterisation of a database: evaporation of EDR brine as a function of the relative humidity

#### Experimental setup

Original EDR brine and synth. EDR concentrates (Chapter 2.1.2) were utilised for the evaporation experiments. Synth. EDR concentrates and original brine were filtered through a 0.2  $\mu\text{m}$  membrane filter after production and directly before starting the experiments. Immediately after filtration, solutions were filled to equal volumes into two plastic vessels and stirred continuously during evaporation by a magnetic stirrer. The distance between ventilator and liquid surface was kept within a range of 2 - 4 cm. As soon as the distance of 4 cm to the ventilator was reached, solutions were transferred into plastic vessels of lower height but equal diameter to reset the distance to the ventilator to 2 cm (Figure 5.1).



Figure 5.1: Experimental setup of the evaporation experiments in the climate chamber.

One of the solutions was filtered regularly to remove the precipitates for further investigations. The other solution was evaporated without filtration (Figure 5.2). During the day the pH was measured in both solutions. At the same time liquid samples were taken from both solutions for measurement of the electrolyte concentration. For this purpose the liquid samples were filtered with a 0.45  $\mu\text{m}$  syringe membrane filter and diluted immediately after filtration. The dilution fac-

tor depends on the concentration of the electrolytes during evaporation and on the formation of minerals.

Evaporation experiments with synth. EDR brine were conducted at 25°C at 35%, 50% and 75% relative humidity (rH) in a climate chamber. Original EDR concentrate was evaporated at 25°C and 50% rH.

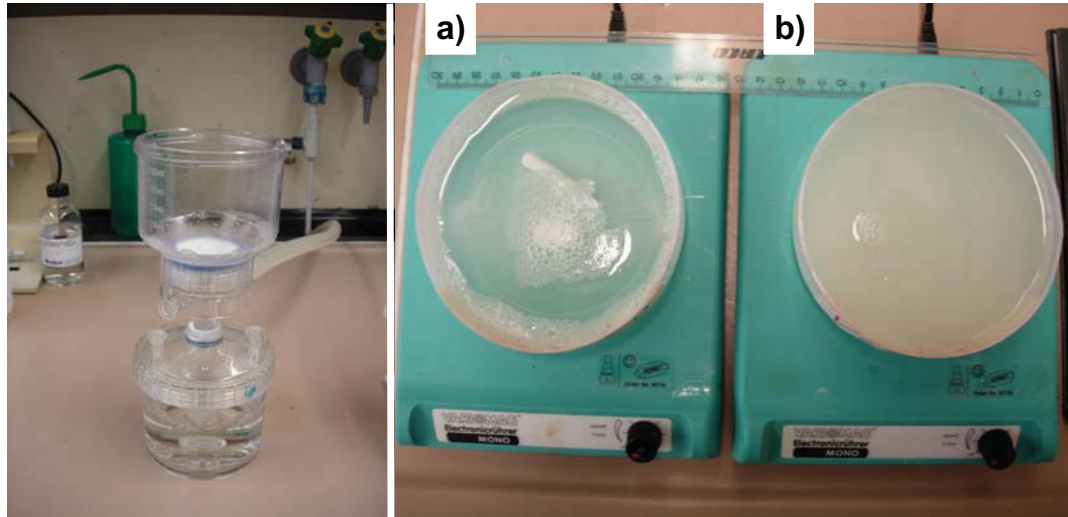


Figure 5.2: Membrane filtration station (left side) for salt filtration. Filtered (left) and unfiltered (right) original EDR brine after 93,75 h of evaporation (right side).

### Results of the evaporation experiments: density

In Table 5.1 experimental and calculated values of the density of NaCl solutions of different concentrations are noted. Experimental and calculated values of solution densities are in good accordance up to high molality.

Table 5.1: Comparison of calculated and experimental densities of different NaCl solutions

NaCl mol/kg	density exp.	density calc.
1.5	1.05	1.05
3	1.10	1.09
5	1.16	1.14

The densities of the concentrates were calculated with the respective electrolyte concentrations at every sampling step (Figure 5.3). Density increases continuously with increasing evaporation, independent of the relative humidity. After exceeding 75% of evaporation the density increases only slightly with further evaporation.

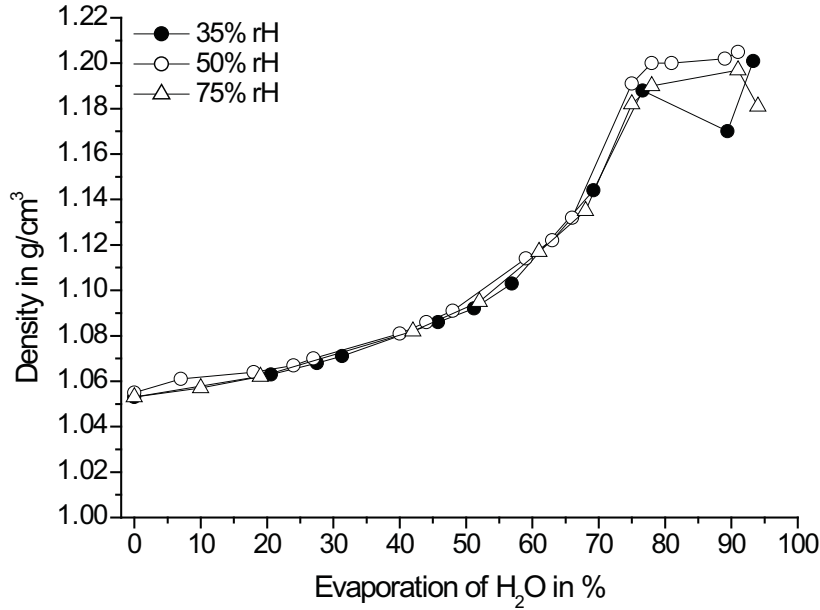


Figure 5.3: Change of density by evaporation of 1095 grams of synth. EDR concentrates as a function of the loss of water at different relative humidities.

### Results of the evaporation experiments: evaporation rate

Figure 5.4 shows the evaporation of water as a function of the duration of the experiments. With increasing relative humidity the evaporation rate of synth. EDR concentrates decreases. The time required to evaporate 95% of the solution at 75% rH was twice as much as evaporating the same fraction of solution at 50% rH. Evaporation of synth. EDR brine at 35% rH requires one third time less than evaporation at 50% rH.

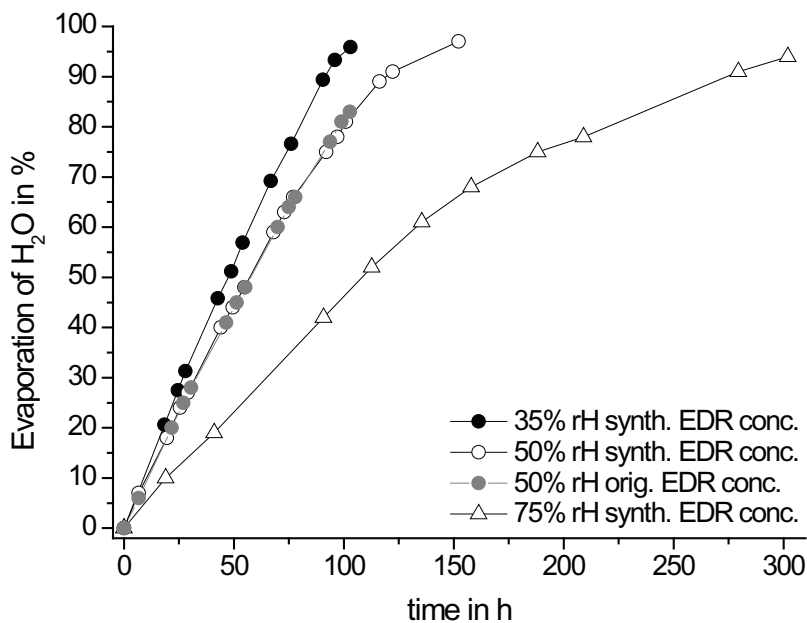


Figure 5.4: Evaporation of H<sub>2</sub>O from 1095 grams of synth. EDR concentrates at 35%, 50% and 75% relative humidity as a function of time.

### Results of the evaporation experiments: pH

Initial pH values of 4 and 2 for the synth. EDR concentrates were chosen. In Figure 5.5 the change of the pH as a function of the evaporation of water at various relative humidities is presented. Experimental values are compared with calculated pH values in dependence of the initial pH of the salt solutions. Measured and calculated pH values decrease from the start of evaporation. The lower the relative humidity, the lower will be the final pH after evaporation. At 75% rH the pH decreases continuously until about 75% water has been evaporated. Thereafter, the pH increases upon further evaporation. Calculated pH values fit well the measured values of the synth. EDR concentrate, evaporated at 50% rH (initial pH of 4). The pH values of concentrates, evaporated at 35% rH and 75% rH, are similar up to a loss of water of 75%. Calculated and measured pH values of original brine (initial pH of 2, evaporated at 50% rH) match with each other up to a loss of water of 75%. With further evaporation the calculated pH values are higher than the measured ones.

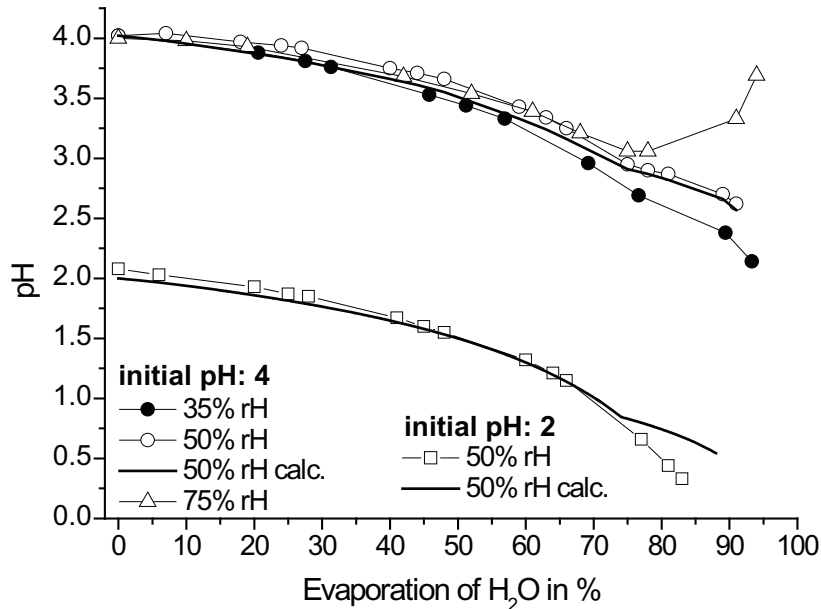


Figure 5.5: Change of the pH as a function of the loss of water by evaporation of 1095 grams of synth. EDR concentrates at different relative humidities. Experimental and calculated pH values are compared as a function of the loss of water.

### Results of the evaporation experiments: electrolyte concentration

Electrolyte concentrations of the evaporation experiment at 50% rH are presented in Figures 5.6 to 5.10. Measured values (exp.) are compared with calculated values. Here, electrolyte concentration was calculated for the case that precipitation of minerals is not allowed (without precip.) and for the case that precipitation of minerals is allowed at every step of the evaporation experiment (with precip.).

The amounts of  $\text{Na}^+$  and  $\text{Cl}^-$  increase continuously up to 75% evaporation of  $\text{H}_2\text{O}$  (Figure 5.6a). In contrast to the calculated electrolyte concentration without precipitation, the measured electrolyte concentration of  $\text{Na}^+$  decreases slightly with further evaporation. The measured values of  $\text{Cl}^-$  remain nearly constant. The measured electrolyte concentrations and electrolyte concentrations in systems where precipitation is allowed, agree well with each other for both species up to an evaporation of 75% of  $\text{H}_2\text{O}$  (Figure 5.6b). With further evaporation the calculated values in the system with precipitation are lower than the measured amounts of the electrolytes. The difference between measured and calculated values remains nearly constant.

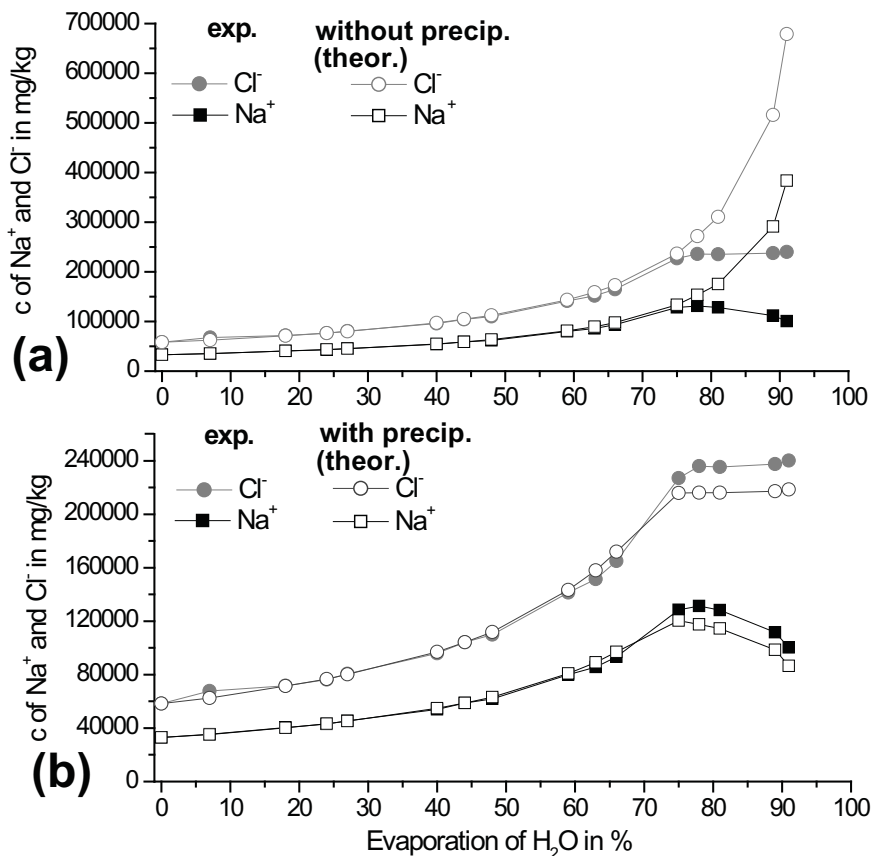


Figure 5.6: **(a)** Comparison between measured  $\text{Cl}^-$  and  $\text{Na}^+$  concentrations and calculated electrolyte concentrations without precipitation in synth. EDR brines as a function of the loss of water (initial amount of synth. EDR concentrate: 1095 gram). **(b)** Comparison of measured  $\text{Cl}^-$  and  $\text{Na}^+$  concentrations and calculated electrolyte concentrations with precipitation in synth. EDR brines as a function of the loss of water.

In Figure 5.7a the measured and the calculated electrolyte concentrations without precipitation of  $\text{Ca}^{2+}$  and  $\text{SO}_4^{2-}$  are presented. The values are in good accordance up to an evaporation of 27% of water. With increasing evaporation the measured amount of  $\text{SO}_4^{2-}$  in the brine remains nearly constant until 80% of the water have been evaporated. Upon further evaporation the amount of sulphate increases.  $\text{Ca}^{2+}$  concentration decreases after 27% of water have been evaporated.  $\text{Ca}^{2+}$  is nearly completely removed from solution above an evaporation of 90% of water.

During the early stages of evaporation, the calculated values (precipitation was allowed) of the electrolyte concentration of  $\text{SO}_4^{2-}$  are lower than the measured ones (Figure 5.7b). Values are in good accordance between 40 and 65% evaporation of water. With ongoing evaporation the measured values are slightly lower than the calculated values. Calculated values of  $\text{Ca}^{2+}$  are higher than the measured values up to an evaporation of 27%. With further evaporation, the measured and calculated values are in good accordance.

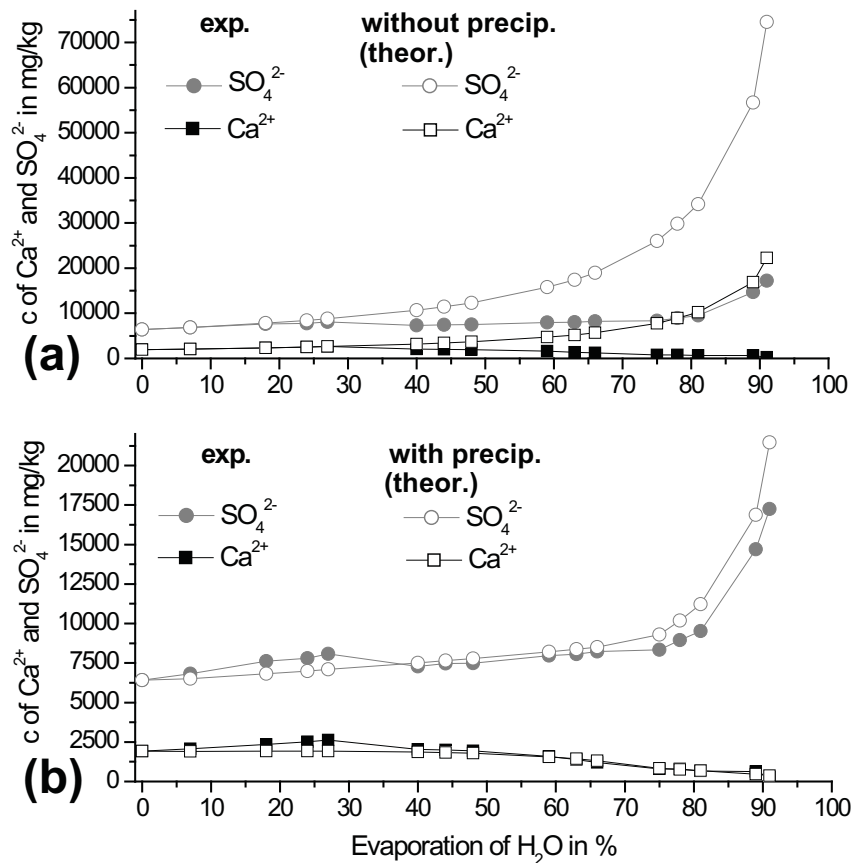


Figure 5.7: **(a)** Comparison between measured  $\text{SO}_4^{2-}$  and  $\text{Ca}^{2+}$  concentrations and calculated electrolyte concentrations without precipitation in synth. EDR brines as a function of the loss of water (initial amount of synth. EDR concentrate: 1095 gram). **(b)** Comparison between measured  $\text{Cl}^-$  and  $\text{Na}^+$  concentrations and calculated electrolyte concentrations with precipitation in synth. EDR brines as a function of the loss of water.

Measured and calculated values (with and without precipitation) of  $Mg^{2+}$  agree well (Figure 5.8). The  $Mg^{2+}$  concentration increases continuously during the evaporation of the synth. EDR concentrate.

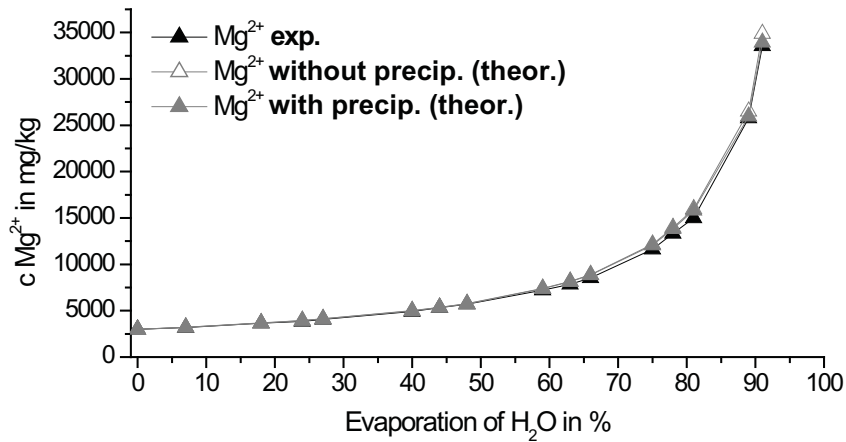


Figure 5.8: Comparison between measured  $Mg^{2+}$  concentration and calculated electrolyte concentration with and without precipitation in synth. EDR brines as a function of the loss of water (initial amount of synth. EDR concentrate: 1095 gram).

In Figure 5.9 the measured and calculated values (with and without precipitation) of  $K^+$  and  $NO_3^-$  are presented as a function of the evaporation of water. All values are in good agreement, electrolyte concentrations increase continuously.

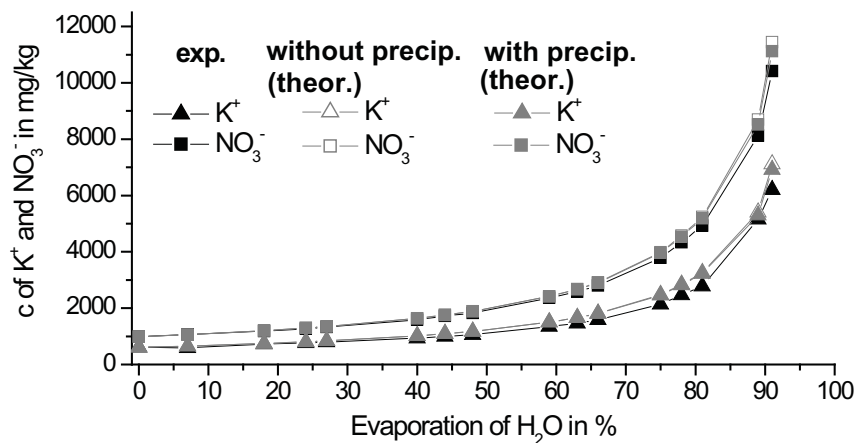


Figure 5.9: Comparison between measured  $K^+$  and  $NO_3^-$  concentrations and calculated electrolyte concentrations with and without precipitation in synth. EDR brines as a function of the loss of water (initial amount of synth. EDR concentrate: 1095 gram).

Calculated values with and without precipitation of the  $\text{Sr}^{2+}$  concentration are also in good accordance (Figure 5.10). The measured amounts of strontium remain nearly constant up to an evaporation of 65% and decrease with further evaporation.

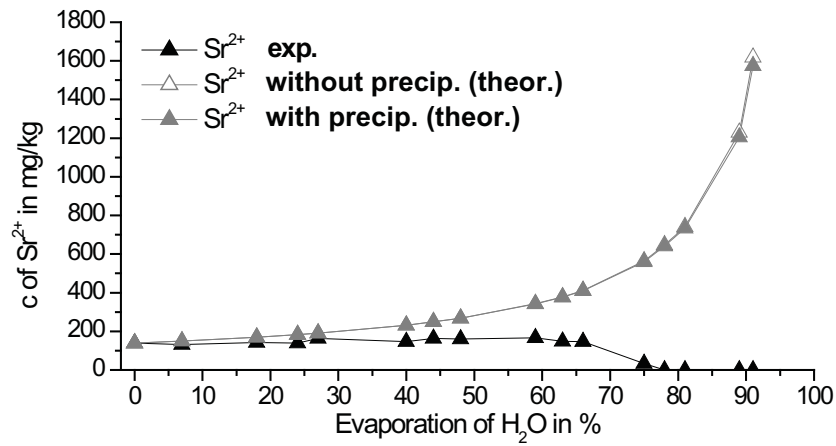


Figure 5.10: Comparison between measured  $\text{Sr}^{2+}$  concentration and calculated electrolyte concentration with and without precipitation in synth. EDR brines as a function of the loss of water (initial amount of synth. EDR concentrate: 1095 gram).

In Figure 5.11 the measured electrolyte concentrations of the filtered and the unfiltered solutions are compared.  $\text{Na}^+$ ,  $\text{Cl}^-$ ,  $\text{Ca}^{2+}$  and  $\text{SO}_4^{2-}$  concentrations show small deviations, whereas the  $\text{Mg}^{2+}$ ,  $\text{K}^+$ ,  $\text{Sr}^{2+}$  and  $\text{NO}_3^-$  concentrations agree well.

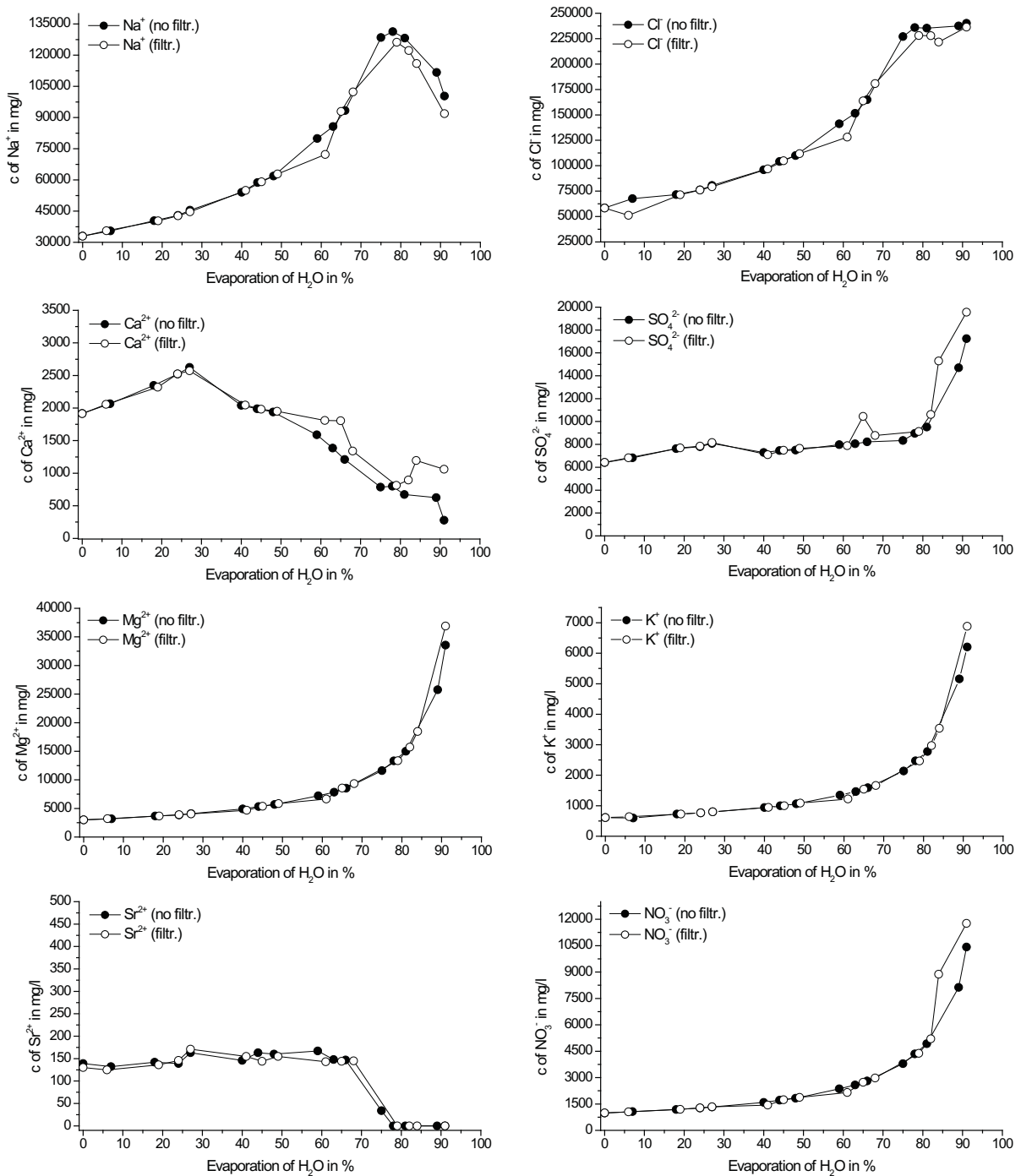


Figure 5.11: The measured concentration of  $\text{Na}^+$ ,  $\text{Cl}^-$ ,  $\text{Ca}^{2+}$ ,  $\text{SO}_4^{2-}$ ,  $\text{Mg}^{2+}$ ,  $\text{K}^+$ ,  $\text{Sr}^{2+}$  and  $\text{NO}_3^-$  of the filtered and the unfiltered synth. EDR concentrates are shown as a function of the loss of water (initial amount of synth. EDR concentrate: 1095 gram).

### Results of the evaporation experiments: characterisation of the precipitates

Results of the analysis of the precipitates, formed during evaporation of the synth. EDR concentrate (initial pH of 4) at 50% rH, are presented exemplarily for all evaporation experiments. Time of sampling is shown as a function of the evaporation of H<sub>2</sub>O (Figure 5.12).

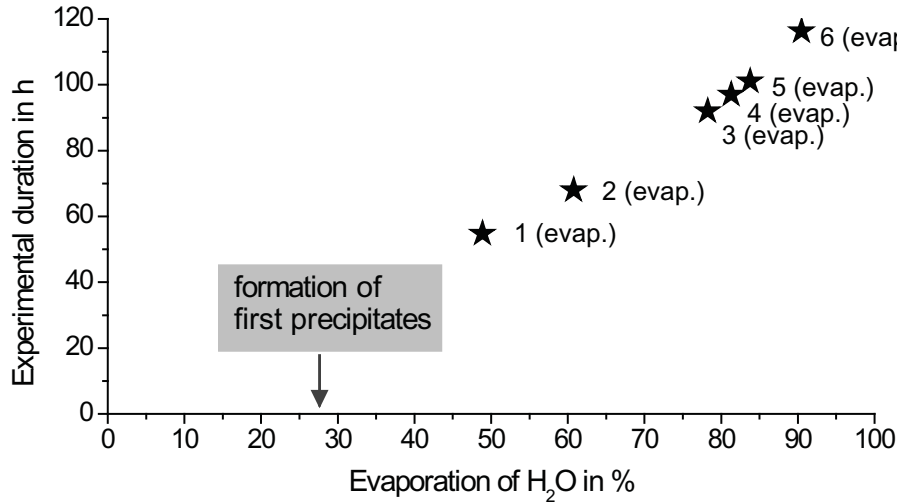


Figure 5.12: Time of sampling of precipitates, formed during the evaporation of 1095 grams of synth. EDR concentrate (initial pH of 4) at 50% rH

X-ray diffraction patterns of precipitates **1 (evap.)** to **6 (evap.)** are shown in Figure 5.13. Samples **1 (evap.)** and **2 (evap.)** are mainly made of gypsum. Halite is present as a minor constituent. In contrast, in samples **3 (evap.)** to **6 (evap.)** halite is the dominant compound of the precipitates and gypsum is present as a minor constituent.

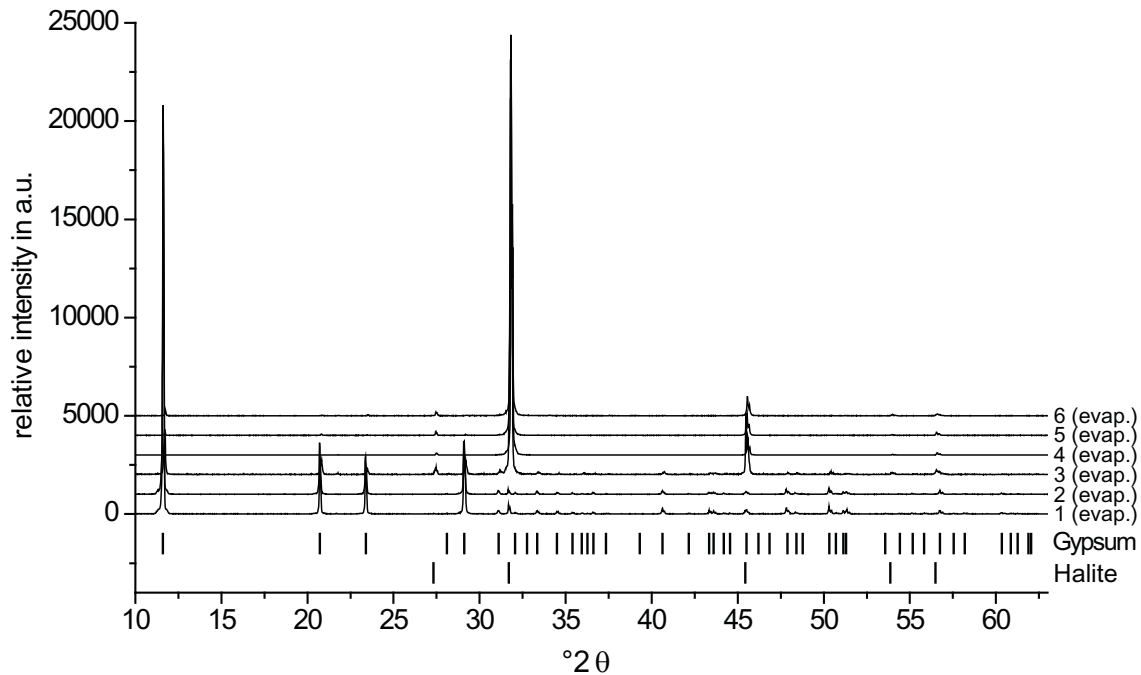


Figure 5.13: X-ray diffractograms of the precipitates **1 (evap.)** to **6 (evap.)**. Samples were taken at different evaporation steps. Patterns were normalised to the main peak of gypsum at 11.6° 2 theta for a better comparison of the mineral fractions in the samples.

### Results of the evaporation experiments: changes in pH as a function of the application of KCl or $\text{KHCO}_3$ respectively during brine production

For production of the regular synth. EDR concentrates, KCl was added to adjust the potassium concentration in the brine (see Chapter 2.1.2). Changes in pH as a function of the initial pH during evaporation of the synth. EDR concentrates were investigated (Figure 5.14). In solutions with an initial pH of 5, the pH decreases slightly to 4.8. After exceeding an evaporation of 650 grams water, the pH starts to increase up to 5.4. In solutions with an initial pH of 4, the pH decreases continuously during evaporation.

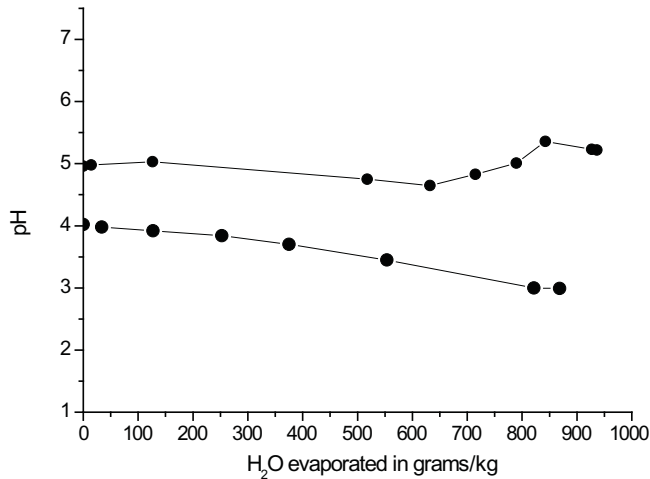


Figure 5.14: Changes of the pH of synth. EDR concentrates with initial pH values of 4 and 5 are plotted as a function of the evaporated amount of water.

Synth. EDR concentrate with  $\text{HCO}_3^-$  in solution was produced by utilization of  $\text{KHCO}_3$ . The change of the pH in these solutions was investigated as a function of the evaporated amount of water (Figure 5.15). The pH decreases during evaporation in solutions with an initial pH of 4.1 or lower. Whereas in solutions with an initial pH > 4.1 the pH increases significantly.

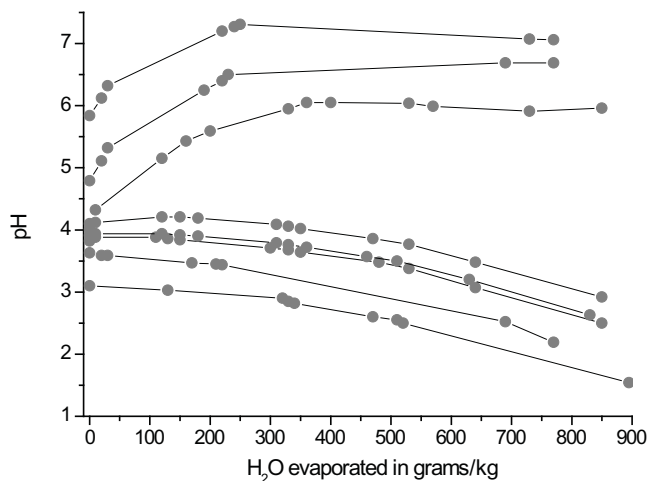


Figure 5.15: Change of the pH of synth. EDR concentrates with various initial pH values are plotted as a function of the evaporated amount of water.

## 5.2 Geochemical modelling: prediction of mineral precipitation

### Results of the geochemical modelling: mineral saturation and changes of the pH

For the geochemical calculation of the evaporation experiments two different basic systems were defined: the first one contains dissolved  $\text{CO}_2(\text{g})$  and the second one does not. The amount of minerals, formed during evaporation, and changes of the pH value were calculated for synth. EDR concentrates with initial pH values of 4 and 2.

In Figure 5.16 the calculated amounts of minerals formed during the evaporation of a synth. EDR concentrate of an initial pH of 4 are shown. The presence of  $\text{CO}_2(\text{g})$  in solution has no influence on the precipitation of minerals from the EDR brine. Saturation of gypsum ( $\text{CaSO}_4 \times 2\text{H}_2\text{O}$ ) is exceeded after evaporation of 50 g of water. It becomes the main precipitate in solution up to a loss of 750 g of water. With continuing evaporation halite ( $\text{NaCl}$ ) becomes the dominating mineral in the system. At the same time anhydrite ( $\text{CaSO}_4$ ) is calculated to be the stable calcium sulphate mineral in solution. With evaporation of the last 9 grams of water, polyhalite ( $\text{K}_2\text{MgCa}_2(\text{SO}_4)_4 \times 2\text{H}_2\text{O}$ ), carnallite ( $\text{KMgCl}_3 \times 6\text{H}_2\text{O}$ ), kieserite ( $\text{MgSO}_4 \times \text{H}_2\text{O}$ ) and bischofite ( $\text{MgCl}_2 \times 6\text{H}_2\text{O}$ ) are formed. Amorphous silica ( $\text{SiO}_2(\text{am})$ ) is present as a minor precipitate during the whole evaporation.

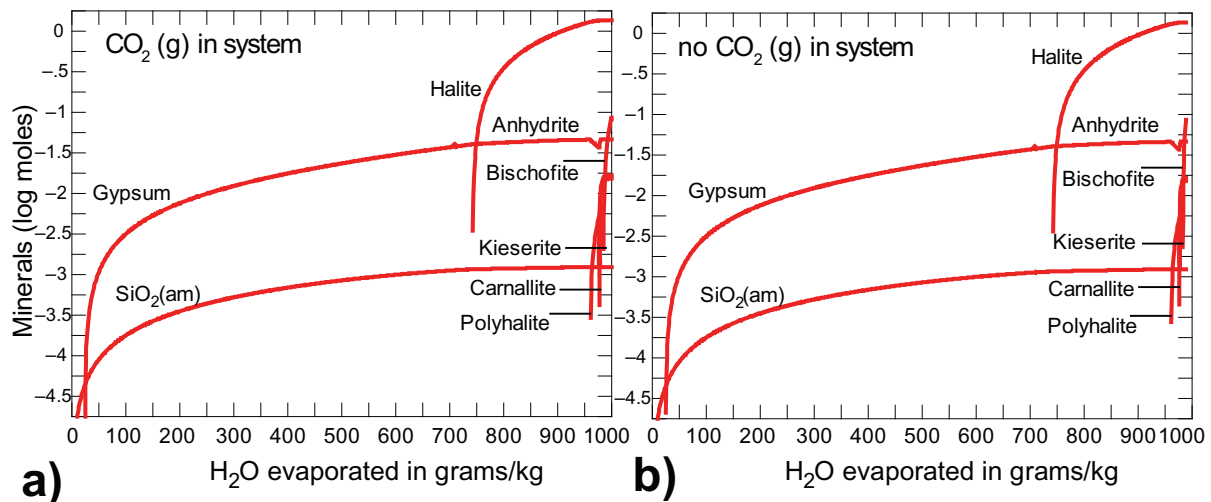


Figure 5.16: Calculated amounts of minerals as a function of the evaporation of water, formed during the evaporation of a synth. EDR concentrate with an initial pH of 4. **a)** in equilibrium with  $\text{CO}_2(\text{g})$ , **b)** no  $\text{CO}_2(\text{g})$  in system

Even at a low initial pH of 2, the formation of specific minerals and their amounts does not change significantly (Figure 5.17).

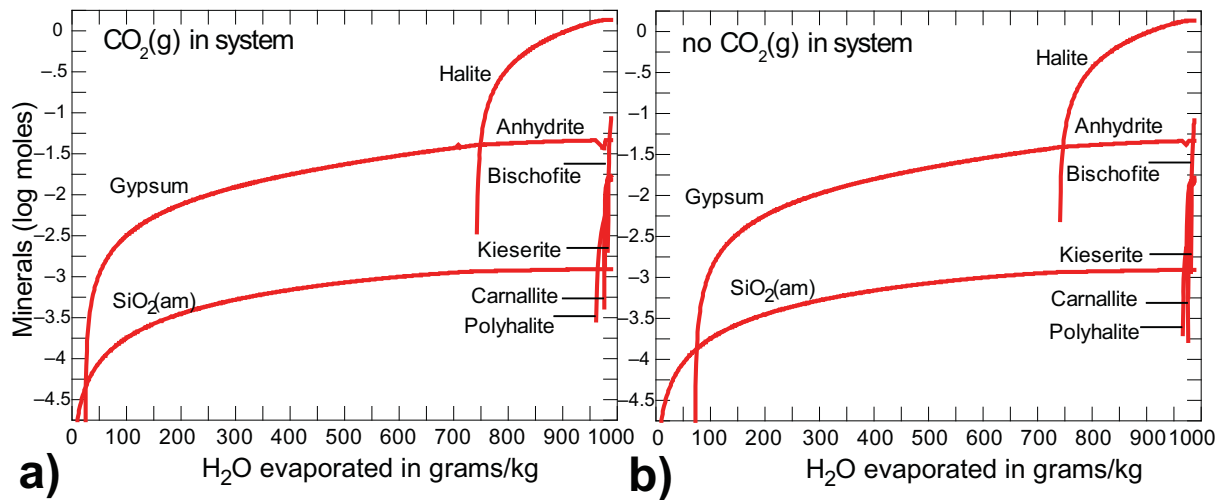


Figure 5.17: Calculated amount of minerals as a function of the evaporation of water, formed during the evaporation of a synth. EDR concentrate with an initial pH of 2. **a)** in equilibrium with CO<sub>2</sub>(g), **b)** no CO<sub>2</sub>(g) in system

The pH depends significantly on the presence (respectively absence) of CO<sub>2</sub>(g). In equilibrium with CO<sub>2</sub>(g) the pH is calculated to rise from the initial pH values of 2 and 4 to 6.52 in the synth. EDR concentrates. With evaporation of water the pH rises slightly to 7. Loss of water in excess of 900 g leads to a decrease of the pH to 5.3 (Figure 5.18). In contrast, if the basic system of the synth. EDR concentrates was set to contain no CO<sub>2</sub>(g), a slight decrease of the pH is calculated directly with beginning evaporation. After exceeding a loss of water of 900 g, the pH decreases to 0.

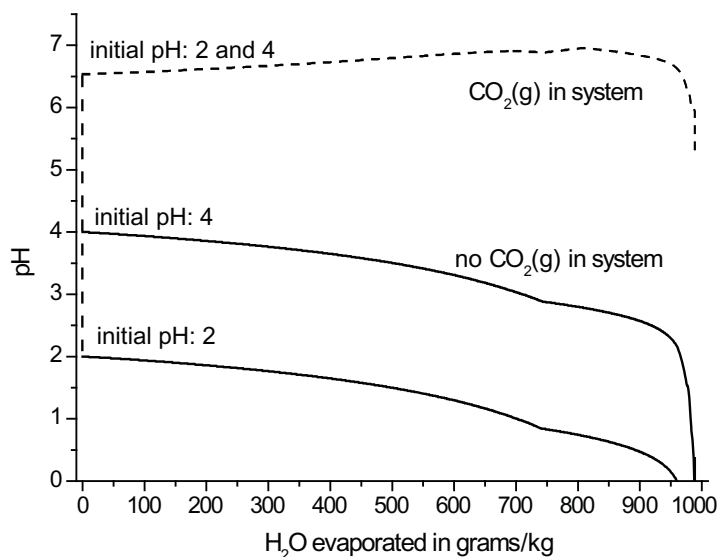


Figure 5.18: Calculated pH values of synth. EDR concentrates as a function of the evaporated amount of water and in dependence of the equilibrium with CO<sub>2</sub>(g). For CO<sub>2</sub>(g) in the system both curves are superimposed.

### 5.3 Discussion

At the start of the project, evaporation experiments at the WAIV unit were conducted with single salt solutions only (Gilron et al., 2003). To evaluate the results of the geochemical calculation of EDR brine evaporation, a database for several parameters had to be established. Therefore, evaporation experiments with synth. EDR concentrate and original EDR brine were carried out. Investigation of evaporation rate, density, pH, electrolyte concentration and mineral formation as a function of the loss of water during evaporation was of particular interest. In this framework the pH during evaporation was investigated either as a function of the initial pH and as a function of the presence of  $\text{HCO}_3^-$  in solution. In the following paragraphs some specific results of the evaporation experiments are discussed in detail.

#### **Influence of the relative humidity**

Experiments revealed some notable facts about the influence of the relative humidity and salt concentration concerning the evaporation rate. As expected, the evaporation rate decreases with increasing relative humidity. At 35 and 50% rH synth. EDR concentrates were evaporated rapidly up to 90% loss of water within only 30 h difference (see Figure 5.4). To reach the same evaporation level at a rH of 75%, 190 h were required. To understand the low evaporation rate at relative high humidity, the vapour pressure of salt solutions has to be taken into account. Above the surface of a saturated NaCl solution, a rH of 75% is adjusted due to the vapour pressure of the salt solution (Greenspan, 1977). The lower the relative humidity of the environment in comparison to the relative humidity on the liquid surface, the easier was the removal of water molecules. During the evaporation of synth. EDR concentrates halite precipitates. From this time on, relative humidity above the brines surface and relative humidity of the environment are nearly equal. As a consequence, the evaporation rate slows down significantly. At the same time the pH of this brine starts to increase in contrast to the pH of salt solutions evaporated at 35 and 50% rH. for which the pH decreases continuously during evaporation (see Figure 5.5). In contrast to these two salt solutions the only difference during evaporation was the duration. The residual concentrate remained in contact with the environmental atmosphere over a comparatively long time. The increase of the pH may be the first sign of establishing an equilibrium between atmosphere and solution.

#### **Equilibrium with $\text{CO}_2(\text{g})$ or not? That's the question...**

The chemistry of artificial salt concentrates like the original EDR brine or the synth. EDR concentrates is not directly comparable with brines, formed by natural processes. During the pre-treatment for the desalination process (acidification of the RO brine to a pH of 2) and the following desalination, the geochemical system of the brine is largely disturbed. Within the short time periods between the different process steps a readjustment to a chemical equilibrium is

impossible. Moreover, desalination by membrane processes acts as a closed system. An exchange of carbon dioxide between brine and atmosphere is completely blocked. Due to acidification and treatment in the EDR unit the hydrogen carbonate concentration in solution decreased to a minimum. The system was “reopened” to the atmosphere during evaporation in the WAIV unit.

Evaporation of the original brine with an initial pH of 2 revealed that the pH starts to decrease with beginning evaporation. Geochemical modelling of this process shows the same results as long as the solution is not allowed to adjust an equilibrium with carbon dioxide in the atmosphere (Figure 5.18). If the program was set to establish this equilibrium, the calculated pH rises directly to a value of 6.52, independent of the initial pH of the solution.

To initiate an exchange between the carbonate species in solution and  $\text{CO}_2(\text{g})$  in the atmosphere,  $\text{KHCO}_3$  instead of  $\text{KCl}$ , was added during the concentrate production. Thereafter, the amount of carbonate species in solution rises significantly. By evaporation of several synth. EDR concentrates with different initial pH values, a notable observation was made. Dissolved carbonate in solution has a great impact on the pH during evaporation. In solutions with an initial pH below 4.1 the pH decreases continuously with evaporation. In solution with a pH above 4.1 the pH rises during evaporation (Figure 5.19a). An explanation of this observation can be found by a closer look on the dissociation of carbonic acid in water and salt solutions. In the Hägg-diagram of Figure 5.19 the species concentrations  $\text{H}_2\text{CO}_3$ ,  $\text{HCO}_3^-$  and  $\text{CO}_3^{2-}$  are compared with the concentrations of  $\text{H}_3\text{O}^+$  and  $\text{OH}^-$  for seawater.

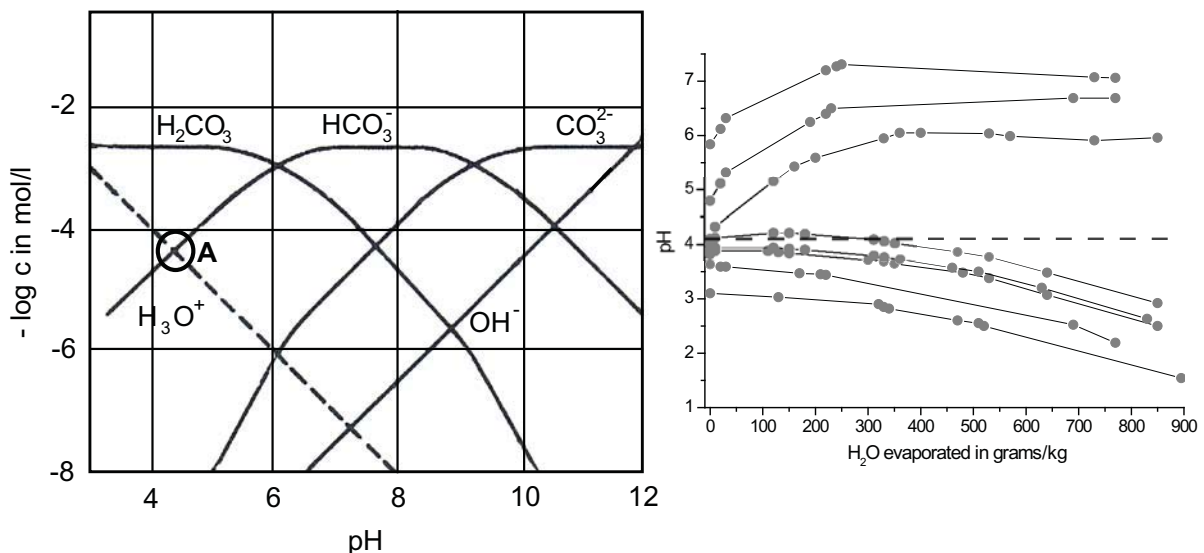


Figure 5.19: Hägg-diagram of seawater, after Stumm and Morgan, (1996). Species distribution of  $\text{H}_2\text{CO}_3$ ,  $\text{HCO}_3^-$ ,  $\text{CO}_3^{2-}$ ,  $\text{H}_3\text{O}^+$  and  $\text{OH}^-$  are plotted as a function of the pH.

In this diagram, the fractions of hydrogen carbonate ( $\text{HCO}_3^-$ ) and hydronium ( $\text{H}_3\text{O}^+$ ) are of special interest. With  $\text{HCO}_3^- > \text{H}_3\text{O}^+$  the solutions has the capacity to neutralise acid in solution **(5 - 1)**.



If the concentration of  $\text{H}_3\text{O}^+ > \text{HCO}_3^-$  the solution loses this ability. In seawater the fraction of  $\text{H}_3\text{O}^+$  is equal to the fraction of  $\text{HCO}_3^-$  at a pH of 4.5, see point **A** in Figure 5.19 (Stumm and Morgan, 1996, p. 159). Additionally it is known that the solubility of dissolved carbon dioxide decreases with increasing salt concentration (Harvie et al., 1984). As a consequence, fractions of the aqueous dissolved  $\text{CO}_2(\text{g})$  start to degas **(5 - 2)** (Bethke, 1996, p. 264).



With progressing evaporation the electrolyte concentration increases and the solubility of carbon dioxide decreases continuously. Simultaneously, the pH decreases in solutions with an initial pH of 4.1 and lower. Due to the fact that, for higher initial pH values, the pH rises with evaporation it can be concluded that the ability for neutralising acid in solution is fixed in the EDR concentrates to a pH of 4.1, instead of a pH of 4.5 in seawater. This change can be explained by the shift of the  $\text{pK}_1$  and  $\text{pK}_2$  values of carbonic acid to lower values with increasing NaCl concentration in solution. The minimum for  $\text{pK}_1$  values lies at 1.25 mol/kg NaCl. With further increase of the salt concentration  $\text{pK}_1$  and  $\text{pK}_2$  values start to increase (Harned and Bonner, 1945, He and Morse, 1993, Thurmond and Millero, 1982 and Millero et al., 2007) (Figure 5.20).

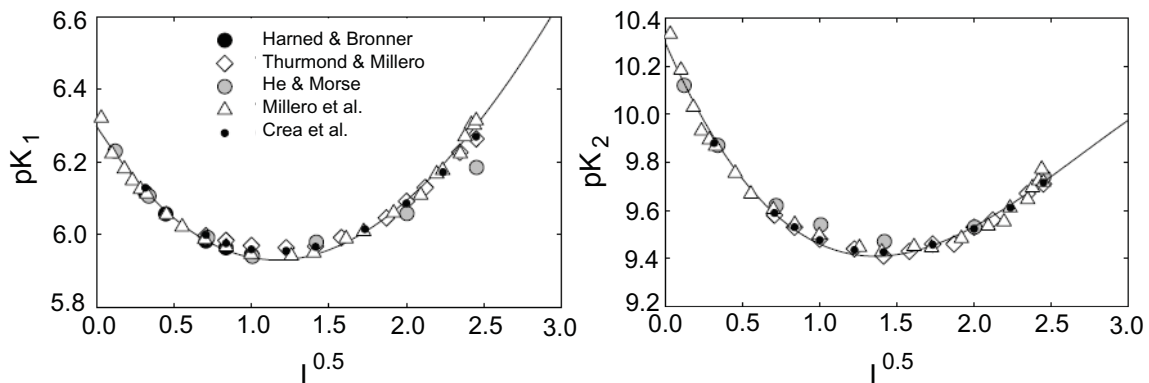


Figure 5.20:  $\text{pK}$  values of carbonic acid in NaCl solutions as a function of the ionic strength at 25°C, after Millero et al. (2007).

With decreasing  $\text{pK}_1$  the species distribution of carbonic acid in solution shifts to lower pH values. As a consequence, the ability for neutralizing acid also decreases.

The primary question whether a chemical equilibrium in the brine can be adjusted during evaporation must be negated. With each fraction of water loss from solution the brine needs to re-adjust the chemical equilibrium of dissolved species, of the minerals in the system and of the

gas exchange between solution and atmosphere. Results of the theoretical calculations, where the equilibrium can be calculated for every single step revealed a large discrepancy between the calculated and the measured pH values in carbonate-containing solutions. In contrast, changes of the pH in carbon dioxide-free solutions are comparable with theoretical calculations. Nevertheless, the original EDR brine reaches pH values below 1 during evaporation which is an unacceptable result. If a pH of 2 is maintained during the desalination process in the EDR unit, a pretreatment of the brine before evaporation in the WAIV unit is required to avoid the formation of a highly aggressive solution. In this respect two scenarios may be considered: addition of a base or the addition of a hydrogen carbonate phase like  $\text{NaHCO}_3$ . The advantage (adding a hydrogen carbonate) lies in the pH adjustment before and during the evaporation. Even though the solution will not reach an equilibrium with the atmosphere, hydrogen carbonate in solution will prevent the pH to decrease strongly.

### **Reliable prediction of the formation of minerals**

While the formation of inorganic solids in the membrane modules has to be avoided, this precipitation is going to occur in the WAIV unit. Here the question is not whether minerals precipitate during the concentration process, it is a question of when and which minerals will be formed.

Notably, the presence of carbonate species in solution has no influence on the mineral species, formed during evaporation of the EDR concentrate. Here, results of XRD measurements and theoretical calculations are in good accordance. Only the prediction of anhydrite in precipitates, formed at an evaporation >700 grams of water is not consistent with reality: water-free calcium sulphate was not detected in XRD measurements. The calculated formation of anhydrite is related to the dehydration of gypsum in the precipitates (Bethke, 1996, p. 272 and Hardie, 1968). This is a slow process, not to happen in the WAIV unit if precipitates are removed regularly from solution.

The amount of  $\text{Sr}^{2+}$  decreases during evaporation without the formation of a Sr-mineral like Celestite ( $\text{SrSO}_4$ ), confirmed by XRD measurements.  $\text{Sr}^{2+}$  is known to substitute  $\text{Ca}^{2+}$  in gypsum (Ichikuni and Musha, 1978 and Kushnir, 1980). Thereafter,  $\text{Sr}^{2+}$  is coprecipitated with gypsum.

A second small discrepancy between calculated and measured results of the evaporation experiments concerns the progression of  $\text{Na}^+$ ,  $\text{Cl}^-$ ,  $\text{Ca}^{2+}$  and  $\text{SO}_4^{2-}$  in solution. For both ion pairs,  $\text{Ca}^{2+} - \text{SO}_4^{2-}$  and  $\text{Na}^+ - \text{Cl}^-$ , the detected electrolyte concentrations show a further increase when calculated concentrations remain constant or decrease due to the first formation of gypsum, resp. halite (Figure 5.6b and Figure 5.7b). Not till the measured ion concentrations of these electrolytes decrease, a white turbidity of the solution was observed and minerals were

detected by XRD. This leads to the conclusion, that a nucleation time is required for the formation of both minerals even if the solution is saturated with the respective ion species. As a consequence, the formation of minerals in solution is retarded. If this process shall be accelerated, both minerals can be added to the solution as seeds.

## 6 Final conclusions and outlook

This thesis was written within the framework of a German - Israeli (BMBF - MOST) cooperation project based on the key activities of the German cooperation partners. The aim of this project was the desalination of brackish water in arid inland areas to near zero liquid discharge (NZLD). Different tools for desalination and evaporation were utilised. Brackish water was desalinated by reverse osmosis (RO) and electro dialysis reversal (EDR), volume reduction of EDR concentrate was reached by evaporation of EDR brine in the Wind Aided Intensified Evaporation unit (WAIV). This special combination of methods raises several questions:

- Is it possible to calculate the mineral saturation state of this artificial brine at every step of the water treatment in the pilot plant?
- Will minerals precipitate during desalination in the brine stream and what kind of material will be formed?
- What are the conditions for precipitation?
- Is there a way to avoid precipitation in the membrane units?
- What kind of minerals will be formed at which stage of the evaporation?

To answer these questions, the mineral saturation state was calculated with the *Geochemist's Workbench* and various laboratory experiments were conducted.

The **first objective** of this thesis was to develop tool for reliable prediction of the mineral saturation state at any point of the desalination and evaporation process: The modelling program *The Geochemist's Workbench 6.0* was successfully extended with Pitzer parameters from the literature for the interaction of  $\text{H}_4\text{SiO}_4$ ,  $\text{H}_3\text{SiO}_4^-$ ,  $\text{H}_2\text{SiO}_4^{2-}$  and  $\text{NO}_3^-$  in the concentration range of the process brines. The mineral saturation state of the feed water of RO, EDR and WAIV was successfully calculated. The only restriction of the software concerned the calculation of the solubility of amorphous silica. Experiments revealed that brines, oversaturated with respect to amorphous silica, keep their metastable state over a long period of time (days to weeks). Due to the fact that the exact kinetic conditions of this process in the EDR brine are still not known, the respective information, required for the calculations, were not available and further investigations are required. The interaction parameters of silicic acid work well in the concentration range of the process brines but, applied to more concentrated solutions, they perform poorly. They need to be refined for solutions of higher ionic strength than the process concentrates. Nevertheless, geochemical calculations provide important information on the saturation state of minerals as a function of pH and salt concentration in the process concentrates (RO, EDR and WAIV concentrate). This information was applied to investigate the formation conditions of scales on the EDR membrane surfaces.

The **second objective** concerned the characterisation of precipitates in the membrane units and investigation of formation conditions of inorganic deposits in the EDR unit. Measures of scaling prevention in the EDR unit were examined:

Desalination in the RO unit of the pilot plant proceeded undisturbed due to the utilisation of antiscalants. Within the EDR unit scaling occurred on membrane surfaces and on the spacer. Deposits were characterised and formation conditions of the inorganic solids were determined. Furthermore, various parameters regarding a controlled removal of silicic acid were evaluated. Characterisation of the deposits, adhering to exchanger membrane surfaces and spacer of the EDR unit revealed brucite and gypsum as the main compounds. The higher the amount of magnesium in the deposits, the higher was the fraction of detected silicon. Formation of gypsum and brucite at a pH of 2, similar to the pH of the feed water of the EDR unit, can be excluded by solubility experiments and geochemical calculation of the saturation state of these minerals as a function of the pH in the feed water and in the EDR concentrate. The presence of these minerals is an indicator that pH increases from 2 to values above 9.5 within this unit. This observation raised the question which kind of process is responsible for this large increase (of the pH) in the EDR membrane stack.

The main reason for the pH shift to higher values was assumed to be concentration polarisation of electrolytes on exchanger membrane surfaces. Within the membrane stack of the EDR unit, different incident scenarios can cause concentration polarisation: First, membrane channels can be mechanically blocked by large oligomers of an electrolyte species and/or by precipitation of sparingly soluble compounds. Here, silica scaling was in focus of this work. Second, procedural reasons like a decrease of feed water flow velocity or a retardation in alternating the electrical poles of the EDR unit promotes concentration polarisation.

The first scenario can be excluded due to the investigation of formation conditions of the deposits in the EDR unit. Based on solubility and seeding experiments, silica scaling, effected by precipitation of amorphous silica or large silicic acid oligomers, can be excluded at  $\text{pH} < 5$ . The pH of the feed water of the EDR unit is 2. Formation of amorphous silica requires a process of nucleation which means oligomerisation and polymerisation followed by polycondensation of silicic acid in solution. Up to pH 4 the main fraction of the silicic acid remains as uncharged monomer which show no signs of oligomerisation during the experiment.

Seeding experiments revealed some notable facts concerning the geochemistry of silicic acid as a function of the pH in the artificial EDR brine. Original and synth. EDR brines, oversaturated with respect to amorphous silica, keep their metastable state over days and weeks without precipitation of amorphous silica, even in the presence of seeds. According to geochemical calculation of the solubility of amorphous silica in different fluids, silicic acid concentration in the

original EDR brine is 2.3 times higher than the calculated solubility and 3.6 times higher in the synth. EDR concentrates. Equilibrium adjustment between solid and electrolyte species in solution is mainly influenced by the pH. Seeding experiments revealed that formation of large silicic acid oligomers occurs rapidly at pH values  $\geq 5$  which is related to the increasing impact of  $\text{OH}^-$  with increasing pH.  $\text{OH}^-$  acts as a catalyst for dissolution of amorphous silica and polymerisation of silicic acid at pH  $< 7$ . At pH values  $\leq 4$  neither formation of large oligomers nor an impact of seeds ( $\text{SiO}_{2(\text{am})}$ ) on the metastable state was obtained. Furthermore, the dissolution rate of amorphous silica is much higher than the polymerisation or accretion rate of silicic acid at pH values  $\leq 6$  in the synth. EDR concentrates. This behaviour leads to the disequilibrium between solid and liquid. The high salt concentration in solution causes the “salting out” (see p. 80) effect of amorphous silica: The solubility of  $\text{SiO}_{2(\text{am})}$  decreases with increasing salt concentration. Here, the impact of divalent cations is much larger than the impact of monovalent cations.

Titration experiments simulate an increase of the pH up to high values. At pH values  $< 7$ ,  $\text{OH}^-$  acts as a catalyst, whereas at pH values  $> 7$ ,  $\text{OH}^-$  ions are consumed by dissociation of the uncharged monomer ( $\text{H}_4\text{SiO}_4$ ) to the charged monomer ( $\text{H}_3\text{SiO}_4^-$ ). Increasing consumption of caustic soda with increasing concentration of  $\text{SiO}_2$  in solution is related to this dissociation reaction. Even if brucite is precipitated from solution, this buffer reaction was maintained. Additionally, only a constant, small amount of  $\text{Mg}^{2+}$  is extracted until silicic acid has been removed completely from solution. Therefrom it can be concluded that dissociation of silicic acid is the primary reaction before significant amounts of metal hydroxides are precipitated from the EDR brine.

For a complete removal of silicic acid from EDR brine, the required total amount of caustic soda depends mainly on the initial pH and on the initial concentration of  $\text{SiO}_2$  in solution. It is made of the quantity of  $\text{OH}^-$  ions needed to raise the pH above a value of 8, the required amount of  $\text{OH}^-$  ions for the complete dissociation reaction and a very small amount of  $\text{OH}^-$  ions for metal hydroxide precipitation.

Due to the fact that pK values of silicic acid shift to lower pH with increasing salt concentration, charged monomers ( $\text{H}_3\text{SiO}_4^-$  and  $\text{H}_2\text{SiO}_4^{2-}$ ) are available for the adsorption reaction at slightly lower pH values. The composition of the measured metals in solution ( $\text{Cu}^{2+}$ ,  $\text{Zn}^{2+}$ ,  $\text{Ni}^{2+}$  and  $\text{Mn}^{2+}$ ) indicates corrosion in the metal equipment of the pilot plant. Precipitated hydroxides from original EDR brine are mostly composed of mixed metal hydroxides.

The transfer of these results to an applicable method of complete removal of silicic acid by in situ precipitation of metal-hydroxide was evaluated by considering brucite only. Results of the flow-through cell experiments provided useful information on a controlled removal of silicic acid

from process concentrates of the pilot plant: On one hand, these experiments confirmed the calculations regarding the required amount of caustic soda for  $\text{SiO}_2$  removal. On the other hand they pointed out the significance of the influence of reaction vessel design and feeding place of brine and additive (caustic soda) on the efficiency of the adsorption process. In this context, a closer examination of different dosage positions for brine and additive is required for optimising the silicic acid removal.

Utilisation of technical inorganic compounds in exchanger columns can not be recommended. The required quantity of inorganic compounds for a complete removal of  $\text{SiO}_2$  is disproportional to the process conditions.

The **third objective** of this work was the parameterisation of a dataset concerning the evaporation of EDR brine in the WAIV unit. Compilation of this dataset provides the opportunity to evaluate the calculated results regarding their reliability and applicability of geochemical modelling to artificial systems like desalination and evaporation processes.

Results of the evaporation experiments were used as reference parameters to evaluate the geochemical calculations regarding their reliability. In this context, evaporation rate, density, pH, electrolyte concentration and formation of minerals as a function of the loss of water were in focus of the experiments and the calculations.

The relative humidity (rH) influences the evaporation rate significantly. The more the rH of the environmental atmosphere approaches the rH above the liquid's surface, the more the evaporation rate decreases. Additionally, the evaporation rate decreases with increasing salt concentration. While the formation of inorganic solids in the membrane modules has to be avoided, this precipitation is expected to happen in WAIV unit. Here it is not the question whether minerals precipitate during the concentration process, it is a question of when and which minerals will be formed. Gypsum and Halite form the main portion of precipitated minerals up to an evaporation of 95% water from EDR brine.

Changes of the pH during evaporation depend mainly on the presence of carbonic acid in solution and on the adjustment of an equilibrium between  $\text{CO}_2(\text{g})$  in the liquid and in the atmosphere. If equilibrium is adjusted, pH increases to a value of 6.5 independent of the initial pH of the solution. If  $\text{CO}_2(\text{g})$  in solution is not in equilibrium with the environment, the initial pH controls further changes of the pH. In this case, the EDR brine loses the capacity to neutralise acid in solution when the pH decreases below a value of 4.1. Thereafter, in solutions with an initial pH above 4.1 the pH increases with ongoing evaporation and decreases in solutions with an initial pH below 4.1. If no  $\text{CO}_2(\text{g})$  is present in solution, the pH decreases with ongoing evaporation, independent of the initial pH.

Geochemical modelling of the evaporation of EDR brine matches the results of the experiments

regarding the electrolyte concentration and the formation of minerals. For this kind of calculation one has to keep in mind that formation of anhydrite by dehydration of gypsum is a slow reaction and will not occur in the evaporation process of the WAIV unit if precipitates are removed regularly from the brine. The saturation state of gypsum and halite in the brine was calculated correctly but the induction period for nuclei growth was not considered. In the real system the electrolyte concentration of the ion pairs  $\text{Ca}^{2+} - \text{SO}_4^{2-}$  and  $\text{Na}^+ - \text{Cl}^-$  still increases after exceeding the solubility product and decreases rapidly after formation of the first precipitates. In this case, addition of gypsum and halite seeds can be useful to control the time of formation of the respective mineral.

When calculating the pH as a function of the loss of water, one has to consider that the presence of carbon dioxide influences the pH significantly. Brines, produced during desalination, are artificial solutions and therefore not comparable with natural brines. The amount of carbon dioxide in salt concentrates depends on the process which is used for water treatment and has to be considered by setting-up the basic system of calculations for the chemistry of the brine.



---

## References

- Al-Jayyousi O. (2001) Capacity building for desalination in Jordan: necessary conditions for sustainable water management. *Desalination* **141**, 169-179.
- Al-Rehaili A. M. (2003) Comparative chemical clarification for silica removal from RO groundwater feed. *Desalination* **159**, 21-31.
- Allam A. R., Saaf E.-J., and Dawoud M. A. (2002) Desalination of brackish groundwater in Egypt. *Desalination* **152**, 19-26.
- Bethke C. M. (1996) *Geochemical Reaction Modeling*. Oxford University Press, Inc, New York.
- Block J. and O.B. Waters J. (1968) The  $\text{CaSO}_4\text{-Na}_2\text{SO}_4\text{-NaCl-H}_2\text{O}$  System at 25° to 100° C. *Journal of Chemical and Engineering Data* **13**, 336-344.
- Clesceri L. S., Greenberg A. E., and Trussel R. R. (1998) *Standard Methods for the Examination of Water and Wastewater*. American Public Health Association, American Water Association, Water Environment Federation.
- Davies C. W. (1962) *Ion Association*. Butterworths, London.
- Dreizin Y., Tenne A., and Hoffmann D. (2008) Integrating large scale seawater desalination plants within Israel's water supply system. *Desalination* **220**, 132-149.
- Einav R. and Lokiec F. (2003) Environmental aspects of a desalination plant in Ashkelon. *Desalination* **156**, 79-85.
- Feldmann I. (1956) Use and Abuse of pH measurement. *Ninth Annual Summer Symposium - Analytical Problems in Biological Systems* **28**(12), 1859 - 1866.
- Felmy A. R., Cho H., Rustad J. R., and Mason M. J. (2001) An aqueous thermodynamic model for polymerized silica species to high ionic strength. *Journal of Solution Chemistry* **30**(6), 509 - 525.
- Galster H. (1991) *pH Measurement*. VCH, Weinheim.
- Gilron J., Folkman Y., Savliev R., Waisman M., and Kedem O. (2003) WAIV - wind aided intensified evaporation for reduction of desalination brine volume. *Desalination* **158**, 205-214.
- Gleick P. H. (1996) Water Resources. In *The Encyclopedia of Climate and Weather* (ed. S. H. Schneider), pp. 817-823. Oxford Univ. Press, New York.
- Gleick P. H. (2006) *The World's Water 2006 - 2007*. Island Press, Washington.
- Glueckstern P. and Priel M. (1996) Optimized brackish water desalination plants with minimum impact on the environment. *Desalination* **108**, 19-26.
- Greenly L. F., Lawler D. F., Freeman B. D., Marrot B., and Moulin P. (2009) Reverse Osmosis desalination: Water sources, technology, and today's challenges. *Water Research* **43**, 2317-2348.

- Greenspan L. (1977) Humidity fixed points of binary saturated aqueous solutions. *Journal of Research of the Bureau of Standards* **81A**(1), 89 - 96.
- Hardie L. A. (1968) The origin of the Recent non-marine evaporite deposit of Saline Valley, Inyo County, California. *Geochimica et Cosmochimica Acta* **32**, 1279 - 1301.
- Harned H. S. and Bonner F. T. (1945) The First Ionization of Carbonic Acid in Aqueous Solutions of sodium Chloride. *Journal of the American Chemical Society* **67**, 1026 - 1031.
- Harvie C. E., Møller N., and Weare J. H. (1984) The prediction of mineral solubilities in natural waters: The Na-K-Mg-Ca-H-Cl-SO<sub>4</sub>-OH-HCO<sub>3</sub>-CO<sub>3</sub>-CO<sub>2</sub>-H<sub>2</sub>O system to high ionic strengths at 25°C. *Geochimica et Cosmochimica Acta* **48**, 723-751.
- He S. and Morse J. W. (1993) The carbonic acid system and calcite solubility in aqueous solutions from 0 to 90°C. *Geochimica et Cosmochimica Acta* **57**, 3533 - 3554.
- Helgeson H. C. (1969) Thermodynamics of Hydrothermal Systems at Elevated Temperatures and Pressures. *American Journal of Science* **267**, 729 - 804.
- Hollemann A. F. and Wiberg N. (1995) *Lehrbuch der Anorganischen Chemie*. de Gruyter, Berlin.
- Ichikuni M. and Musha S. (1978) Partition of strontium between gypsum and solution. *Chemical Geology* **21**, 359 - 363.
- Icopini G. A., Brantley S. L., and Heaney P. J. (2005) Kinetics of silica oligomerisation and nanocolloid formation as a function of pH and ionic strength at 25°C. *Geochimica et Cosmochimica Acta* **69**, 293-303.
- Iler R. K. (1979) *The Chemistry of Silica*. Wiley, New York.
- Ingri N. (1959) Equilibrium Studies of Polyanions IV. Silicate Ions in NaCl Medium. *Acta Chemica Scandinavica* **13**, 758 - 775.
- Kim Y. M., Kim S. J., Kim Y. S., Lee S., and Kim I. S. (2009) Overview of systems engineering approaches for a large-scale seawater desalination plant with a reverse osmosis network. *Desalination* **238**, 312-332.
- Krauskopf K. B. and Bird D. K. (1995) *Introduction to Geochemistry*. McGraw-Hill, New York.
- Kushnir J. (1980) The coprecipitation of strontium, magnesium, sodium, potassium and chloride ions with gypsum. An experimental study. *Geochimica et Cosmochimica Acta* **44**, 1471 - 1482.
- Lagerström G. (1959) Equilibrium Studies of Polyanions III. Silicate Ions in NaClO<sub>4</sub> Medium. *Acta Chemica Scandinavica* **13**, 722 - 736.
- Liang Z.-H., Zhu Y.-J., and Hu X.-L. (2004) β-Nickel Hydroxide Nanosheets and their Thermal Decomposition to Nickel Oxide Nanosheets. *Journal of Physical Chemistry* **108**, 3488 - 3491.
- Luckas M. and Krissmann J. (2001) *Thermodynamik der Elektrolytlösungen*. Springer-Verlag, Berlin.

- Marshall W. L. and Slusher R. (1966) Thermodynamics of Calcium Sulfate Dihydrate in Aqueous Sodium Chloride Solutions, 0-110°. *The Journal of Physical Chemistry* **70**(12), 4015-4027.
- Marshall W. L. (1980) Amorphous silica solubilities - I. Behaviour in aqueous sodium nitrate solutions; 25 - 300°C, 0-6 molal. *Geochimica et Cosmochimica Acta* **44**, 907-913.
- Marshall W. L. and Warakowski J. M. (1980) Amorphous silica solubilities - II. Effect of aqueous salt solutions at 25°C. *Geochimica et Cosmochimica Acta* **44**, 915 - 924.
- Mazo R. M. and Mou C. Y. (1991) Introduction to the Statistical Mechanics of Solutions. In *Activity Coefficients in Electrolyte Solutions* (ed. P. D. Kenneth S. Pitzer), pp. 29-74. CRS Press.
- Merkel B. J. and Planer-Friedrich B. (2005) *Groundwater Geochemistry. A Practical Guide to Modeling of Natural and Contaminated Aquatic Systems*. Springer-Verlag, Berlin.
- Mickley M. C. (2001) Membrane Concentrate Disposal: Practices and Regulation. U.S. Department of the Interior, Bureau of Reclamation, Mickley & Associates.
- F. Millero F. H., T. Graham, D. Pierrot. (2007) The dissociation of carbonic acid in NaCl solutions as a function of concentration and temperature. *Geochimica et Cosmochimica Acta* **71**, 46 - 55.
- Mortimer C. E. and Müller U. (2007) *Chemie. Das Basiswissen der Chemie*. Thieme, Stuttgart.
- Nalco (2009) *The Nalco Water Handbook*. McGraw Hill, New York.
- Pitzer K. S. (1973) Thermodynamics of Electrolytes. I. Theoretical Basis and General Equations. *The Journal of Physical Chemistry* **77**(2), 268 - 277.
- Pitzer K. S. and Mayorga G. (1973) Thermodynamics of Electrolytes. II. Activity and Osmotic Coefficients for Strong Electrolytes with One or Both Ions Univalent. *The Journal of Physical Chemistry* **19**, 2300 - 2308.
- Pitzer K. S. and Mayorga G. (1974) Thermodynamics of Electrolytes. III. Activity and Osmotic Coefficients for 2-2 Electrolytes. *Journal of Solution Chemistry* **3**(7), 539 - 546.
- Pitzer K. S. and Kim J. J. (1974) Thermodynamics of Electrolytes. IV. Activity and Osmotic Coefficients for Mixed Electrolytes. *Journal of the American Chemical Society* **96**(18), 5701 - 5707.
- Pitzer K. S. (1975) Thermodynamics of Electrolytes. V. Effects of Higher-Order Electrostatic Terms. *Journal of Solution Chemistry* **4**(3), 249 - 265.
- Pitzer K. S. (1991) Ion Interaction Approach: Theory and Data Correlation. In *Activity Coefficients in Electrolyte Solutions* (ed. P. D. Kenneth S. Pitzer), pp. 75-154. CRS Press, Boca Raton.
- Pokrovsky O. S. and Schott J. (2004) Experimental study of brucite dissolution and precipitation in aqueous solutions: Surface speciation in chemical affinity control. *Geochimica et Cosmochimica Acta* **68**(1), 31-45.

- Oren Y., Korngold E., Datrophe N., Messalem R., Volkman Y., Aronov L., Weisman M., Bouriakov N., Glueckstern P., and Gilron J. (2010) Pilot studies on high recovery BWRO-EDR for near zero liquid discharge approach. *Desalination* **261**, 321 - 330.
- Reardon E. J. (1990) An ion interaction model for the determination of chemical equilibria in cement/water systems. *Cement and Concrete Research* **20**, 175 - 192.
- Riedel E. (2002) *Anorganische Chemie*. de Gruyter, Berlin.
- Robinson R. A. and Stokes R. H. (1968) *Electrolyte Solutions*. Butterworths, London.
- Smykatz-Kloss W. (1967) Über die Möglichkeit der halbquantitativen Mineralbestimmung mit der DTA ohne Flächenintegration. *Contributions to Mineralogy and Petrology* **16**, 274 - 178.
- Smykatz-Kloss W. (1974) *Differential Thermal Analysis; Application and Results in Mineralogy*. Springer, Berlin.
- Sheikholeslami R. and Bright J. (2002) Silica and metals removal by pretreatment to prevent fouling of reverse osmosis membranes. *Desalination* **143**, 255-267.
- Sjöberg S. (1996) Silica in aqueous environments. *Journal of Non-Crystalline Solids* **196**, 51-57.
- Srivastava O. K. and Secco E. A. (1967) Studies on metal hydroxy compounds. I. Thermal analysis of zinc derivatives  $\epsilon$ -Zn(OH)<sub>2</sub>, Zn<sub>5</sub>(OH)<sub>8</sub>Cl<sub>2</sub>·H<sub>2</sub>O,  $\beta$ -ZnOHCl, and ZnOHF. *Canadian Journal of Chemistry* **45**, 579 - 583.
- Stumm W. and Morgan J. J. (1996) *Aquatic Chemistry*, pp. 1022. Wiley, New York.
- Thurmond V. and Millero F. J. (1982) Ionization of Carbonic Acid in Sodium Chloride Solutions at 25°C. *Journal of Solution Chemistry* **11**(7), 447 - 456.
- Webb T. L. (1970) Oxides and Hydroxides of Monovalent and Divalent Metals. In *Differential Thermal Analysis*, Vol. 1 (ed. R. C. Mackenzie), pp. 238 - 270. Academic Press, London.
- Weber C. F. and Beahm E. C. (1996) *Chemical Modeling of Waste Sludges*. Oak Ridge National Laboratory.
- Young M. E., Macumber P. G., Watts M. D., and Al-Toqy N. (2004) Electromagnetic detection of deep freshwater lenses in a hyper-arid limestone terrain. *Journal of Applied Geophysics* **57**, 43-61., 1968

## Appendix A

### Basic principles of Reverse Osmosis (RO), Electrodialysis Reversal (EDR) and Wind Aided Intensified Evaporation (WAIV).

#### A.1 Basic principle of Reverse Osmosis (RO)

Reverse Osmosis (RO) utilises an effect which is well-known from nature. If a salt solution and pure water are separated by a water-permeable membrane, water molecules diffuse from the pure water to the salt solution caused by striving for equilibrium of the two different chemical systems. Within a U-Tube the process leads to different solution levels and represents a pressure difference which is referred to the osmotic pressure (Figure A.1a). The loss of water molecules leads to a decrease of the water volume on the pure water side (light blue). In contrast the volume of the salt solution increases by dilution (dark blue). Forcing water molecules to diffuse out of the salt solution (dark blue) into the pure water (light blue), a higher pressure than the osmotic one is required (Figure A.1b). This method is called Reverse Osmosis. The required pressure for salt water desalination is directly correlated with the salinity of a solution and to the amount of permeate which should be produced (Greenley et al., 2009).

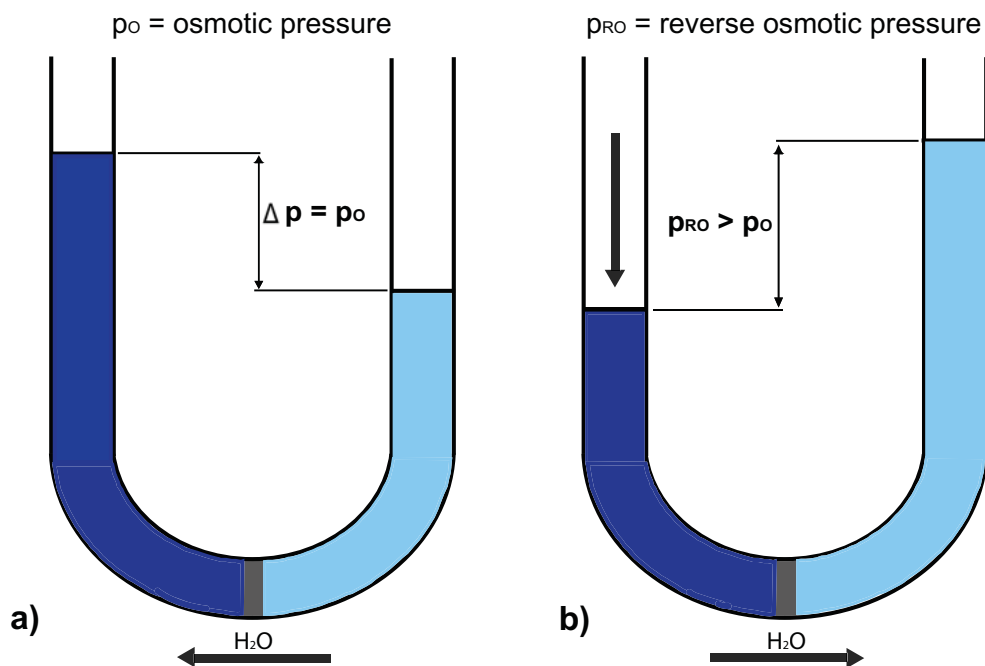


Figure A.1: Basic principle of osmosis (a) and reverse osmosis (b)

In technical aspects it is divided into low- and high-pressure RO. Low pressure osmosis (<30 bar) is used in water desalination for brackish water, the high pressure osmosis (up to 80 bar) for seawater desalination. Here, the recovery rate can reach 45% for high pressure osmosis units. Water recovery of brackish water depends on the salt content and varies between 75 and 90% (Greenley et al., 2009).

## A.2 Basic principle of Electrodialysis Reversal (EDR)

Membranes in an EDR unit are arranged in a stack module. These membranes are selective for the transfer of positively respectively negatively charged ions. Cation exchange membranes and anion exchange membranes are stacked in an alternating fashion. For water desalination, feed water is fed into these channels except the one which is adjacent to the electrodes. Perpendicular to the membrane surface an electric potential is generated. Figure A.2 shows the operation mode of an EDR unit. Due to the electrical potential, anions start to diffuse to the anode and cations to the cathode. Electrolytes can pass their corresponding exchange membranes but are withheld by the opposed membrane. This leads to a nearly saltfree permeate flow in one channel and to a concentration of electrolytes in the other channel. EDR units in technical processes compose tens of channels.

To obviate membrane scaling caused by the high amount of electrolytes in the concentrate channels, the polarity is reversed regularly. This inverts permeate to concentrate channels and concentrate to permeate channels for a short time.

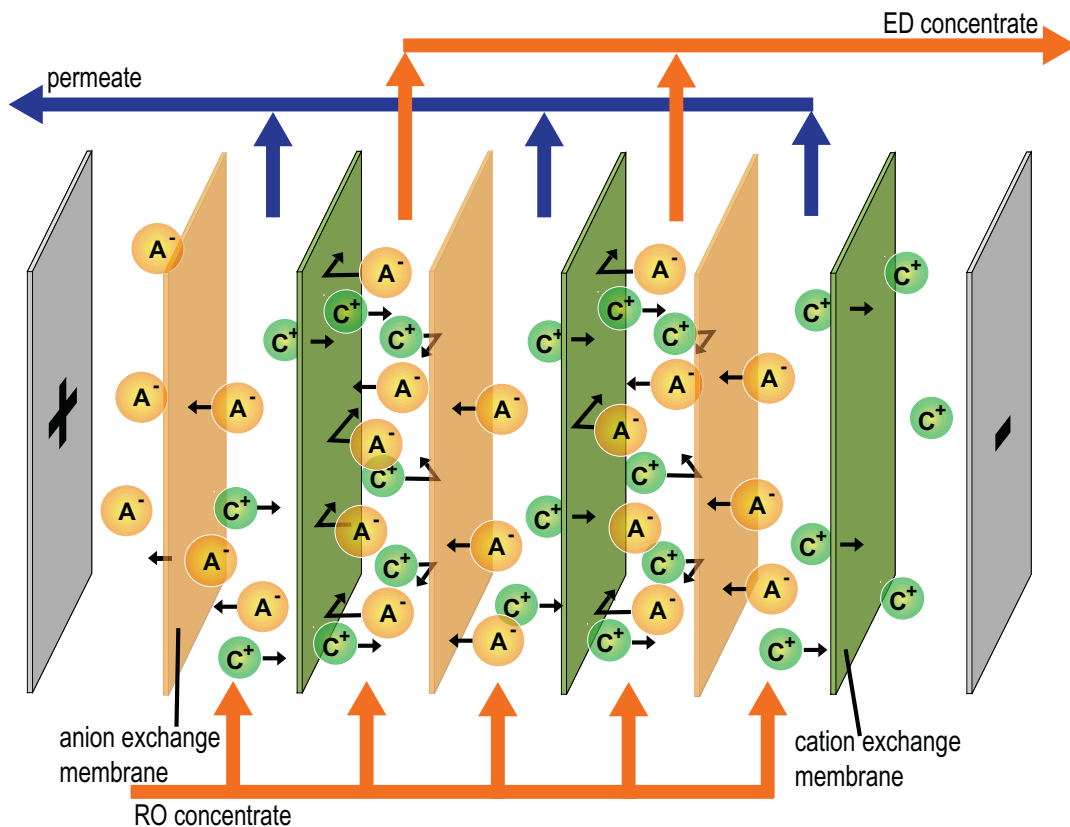


Figure A.2: Basic principle of Electrodialysis

### A.3 Basic principle of the Wind Aided Intensified Evaporation Unit (WAIV)

The evaporation rate of brines in open pans decreases with increasing salt concentration. To accelerate evaporation it is necessary to reduce the volume-to-surface ratio by enlarging the average evaporation surface.

The basic principle of the WAIV unit is based on two natural energy sources which are usually available in arid and semi-arid areas with low relative humidities. These are wind and solar power. Wind energy increases with increasing distance to the ground, so the unit setup is placed at a few meters height. To accelerate the evaporation rate, a woven geotextile with high surface area is placed above the EDR concentrate storage tank and wetted continuously with the brine. Evaporation of water and precipitation of salts takes place during the downflow of the concentrate, Gilron et al., 2003.

## Appendix B

### Pitzer-equations and specific interaction parameters

#### B.1 Calculation of activity coefficients based on the Pitzer-equations

The excess free energy of a salt solution is calculated by a series expansion in form of virial equations **(B - 1)**.

$$\frac{G^{\text{ex}}}{n_w RT_K} = f^{\text{dh}}(I) + \sum_i \sum_j \lambda_{ij}(I) m_i m_j + \sum_i \sum_j \sum_k \mu_{ijk} m_i m_j m_k \quad (\text{B - 1})$$

The parameter  $G^{\text{ex}}$  represents the excess free energy,  $R$  the gas constant,  $T$  the temperature in Kelvin and  $n_w$  the number of kilograms of water. The concentration  $m$  of ion species is noted in molal units.

The first virial coefficient  $f^{\text{dh}}$  includes the term of the Debye-Hückel equation. The second virial coefficient  $\lambda_{ij}$  describes the interaction between two ionic species  $i$  and  $j$  and the third coefficient  $\mu_{ijk}$  represents the interaction of three ionic species  $i$ ,  $j$  and  $k$  among each other. In contrast to the first two virial coefficients the third coefficient is independent of the ionic strength.

For the calculation of activity coefficients, the equation of the excess free energy, **(B - 2)**, is differentiated respectively to concentration. For the calculation of the osmotic coefficient it is differentiated respectively to pressure.

The expressions of activity coefficients for cations  $\gamma_M$ , anions  $\gamma_X$  and neutral species  $\gamma_N$  are described in equations **(B - 2)** to **(B - 4)**.

$$\begin{aligned} \ln \gamma_M = & z_M^2 F + \sum_{a=1}^{N_a} m_a (2B_{Ma} + ZC_{Ma}) + \sum_{c=1}^{N_c} m_c \left( 2\Phi_{Mc} + \sum_{a=1}^{N_a} m_a \Psi_{Mca} \right) \\ & + \sum_{a=1}^{N_a-1} \sum_{a'=a+1}^{N_a} m_a m_{a'} \Psi_{aa'M} + |z_M| \sum_{c=1}^{N_c} \sum_{a=1}^{N_a} m_c m_a C_{ca} + \sum_{n=1}^{N_n} m_n 2\lambda_{nM} \end{aligned} \quad (\text{B - 2})$$

$$\begin{aligned} \ln \gamma_X = & z_X^2 F + \sum_{c=1}^{N_c} m_c (2B_{cX} + ZC_{cX}) + \sum_{a=1}^{N_a} m_a \left( 2\Phi_{Xa} + \sum_{c=1}^{N_c} m_c \Psi_{Xac} \right) \\ & + \sum_{c=1}^{N_c-1} \sum_{c'=c+1}^{N_c} m_c m_{c'} \Psi_{cc'X} + |z_X| \sum_{c=1}^{N_c} \sum_{a=1}^{N_a} m_c m_a C_{ca} + \sum_{n=1}^{N_n} m_n (2\lambda_{nM}) \end{aligned} \quad (\text{B - 3})$$

$$\ln \gamma_N = \sum_{c=1}^{N_c} m_c (2\lambda_{mc}) + \sum_{a=1}^{N_a} m_a (2\lambda_{ma}) \quad (\text{B - 4})$$

Subscripts M, c and c' indicate cations, X, a and a' anions and N neutral electrolytes. The variable m stands for the molal concentration of electrolytes and z for the ion charge.  $N_c$  and  $N_a$ , specifies the total number of cations and anions, respectively, in solution. Z represents the total charge of the electrolytes in solution **(B - 5)**:

$$Z = \sum_i m_i |z_i| \quad (\text{B - 5})$$

Short-range forces between cation - anion pairs are expressed by the second virial coefficient  $B_{MX}$  **(B - 6)**, where the semi-empirical parameters  $\beta^{(0)}$ ,  $\beta^{(1)}$  and  $\beta^{(2)}$  are specific for every ion pair. The value of  $\alpha_{MX}$  for the interaction of two single-charged ions, noted as 1-1 electrolytes, is  $2.0 \text{ kg}^{1/2} \cdot \text{mol}^{1/2}$  as well as for 2-1, 3-1 and 4-1 electrolytes. For 2-2 electrolytes the value is  $1.4 \text{ kg}^{1/2} \cdot \text{mol}^{1/2}$  due to an electrostatic ion-pairing effect.

$$B_{MX} = \beta_{MX}^{(0)} + \beta_{MX}^{(1)} g(\alpha_{MX} \sqrt{I}) + \beta_{MX}^{(2)} g(12 \sqrt{I}) \quad (\text{B - 6})$$

$$B'_{MX} = \beta_{MX}^{(1)} g'(\alpha_{MX} \sqrt{I})/I + \beta_{MX}^{(2)} g'(12 \sqrt{I})/I \quad (\text{B - 7})$$

$$B_{MX}^{\phi} = B_{MX} + I B'_{MX} \quad (\text{B - 8})$$

The values of g and g' are calculated by the expression **(A - 9)** and **(A - 10)** where x is equal to  $\alpha_{MX} \sqrt{I}$ .

$$g(x) = \frac{2[1 - (1+x)e^{-x}]}{x^2} \quad (\text{B - 9})$$

$$g'(x) = \frac{2[1 - (1+x + x^2/2)e^{-x}]}{x^2} \quad (\text{B - 10})$$

Short-range forces between electrolytes of the same charge are very small, because of their mutual repulsion. Nevertheless for concentrated solutions they still must be taken into account. Including the semi-empirical parameter  $\theta_{ij}$  into equation **(B - 11)** allows us to calculate the term  $\Phi_{ij}$ .

$$\Phi_{ij} = \theta_{ij} + {}^E\theta_{ij}(I) \quad (\text{B - 11})$$

$$\Phi'_{ij} = {}^E\theta'_{ij}(I) \quad (\text{B - 12})$$

$$\Phi_{ij}^{\phi} = \Phi_{ij} + I \Phi'_{ij} \quad (\text{B - 13})$$

The interaction of ion triplets are considered in the Pitzer equation within the third virial coefficient  $C_{MX}$ ,  $\Psi_{cc'X}$  and  $\Psi_{aa'M}$ . Therefore, the semi-empirical parameter  $C_{MX}^f$ ,  $\Psi_{cc'X}$  and  $\Psi_{aa'M}$  must be known.

$C_{MX}$  is calculated by the expression **(B - 14)**.

$$C_{MX} = \frac{C_{MX}^{\phi}}{2\sqrt{|z_M z_X|}} \quad (\text{B - 14})$$

The factor F, equation **(B - 15)**, includes the extended Debye-Hückel term.

$$F = -A^{\phi} \left( \frac{\sqrt{I}}{1 + 1.2\sqrt{I}} + \frac{2}{1.2} \ln(1 + 1.2\sqrt{I}) \right) + \sum_{c=1}^{N_c} \sum_{a=1}^{N_a} m_c m_a B'_{ca} \quad (\text{B - 15})$$

$$+ \sum_{c=1}^{N_c-1} \sum_{c'=c+1}^{N_c} m_c m_{c'} \Phi'_{cc'} + \sum_{a=1}^{N_a-1} \sum_{a'=a+1}^{N_a} m_a m_{a'} \Phi'_{aa'}$$

Here,  $A^f$  is  $2.303 A/3$ . In this term A represents the Debye-Hückel parameter and the parameter I the ionic strength of the solution **(3 - 10)**.  $B'_{ca}$ , respectively  $B'_{MX}$ , is given by equation **(B - 7)**.

As mentioned before, not only the interaction of dissolved electrolytes takes place, also interactions of dissolved electrolytes with water molecules must be taken into account which influences the activity of water,  $a_w$ . These interactions are considered by the osmotic coefficient which is included in equation **(B - 16)**. The activity of water  $a_w$  is calculated by dividing the molecular weight of water W by 1000g of water, multiplied by the expression of the osmotic coefficient.

$$\ln a_w = -\frac{W}{1000} \left( \sum_i m_i \right) \phi \quad (\text{B - 16})$$

For the calculation of the osmotic coefficient **(A - 17)** the expression of  $B_{ca}^{\phi}$  and  $\Phi_{ij}^{\phi}$  are noted in equation **(B - 6)** and **(B - 11)**.

$$\sum_i m_i (\phi - 1) = 2 \frac{-A^{\phi} I^{3/2}}{1 + 1.2\sqrt{I}} + \sum_{c=1}^{N_c} \sum_{a=1}^{N_a} m_c m_a (B_{ca}^{\phi} + Z C_{ca}) \quad (\text{B - 17})$$

$$+ \sum_{c=1}^{N_c-1} \sum_{c'=c+1}^{N_c} m_c m_{c'} \left( \Phi_{cc'}^{\phi} + \sum_{a=1}^{N_a} m_a \Psi_{cc'a} \right)$$

$$+ \sum_{a=1}^{N_a-1} \sum_{a'=a+1}^{N_a} m_a m_{a'} \left( \Phi_{aa'}^{\phi} + \sum_{c=1}^{N_c} m_c \Psi_{aa'c} \right)$$

$$+ \sum_{n=1}^{N_n} \sum_{a=1}^{N_a} m_n m_a \lambda_{na} + \sum_{n=1}^{N_n} \sum_{c=1}^{N_c} m_n m_c \lambda_{nc}$$

If the semi-empirical parameters  $\beta^{(0)}$ ,  $\beta^{(1)}$ ,  $\beta^{(2)}$ ,  $C^{\phi}$ ,  $\theta$ ,  $\lambda$  and  $\Psi$  for the interaction of the electrolytes in aqueous solutions of high salinity are known the activity coefficients of single ion species can be calculated by the Pitzer-equations. Moreover, the osmotic coefficient and the activity of water can be estimated.

## B.2 Pitzer parameters for silicic acid and nitrate

Database *thermo\_phrqpitz* of the modelling program *The Geochemist's Workbench 6.0* had to be extended for the interaction parameters of silicic acid and nitrate. These parameters were required for the calculation of the mineral saturation of the brines investigated in this work. Pitzer parameters for both electrolytes were taken from literature.

Table B.1: Pitzer parameter  $\beta^{(0)}$ ,  $\beta^{(1)}$ ,  $\beta^{(2)}$ ,  $c\phi$ , for anion - cation interaction parameter

		$\beta^{(0)}$	$\beta^{(1)}$	$\beta^{(2)}$	$c\phi$	Reference
<b>H<sub>2</sub>SiO<sub>4</sub><sup>--</sup></b>	<b>Ca<sup>++</sup></b>	0.2000	3.1973	-54.2400	0	a
	<b>H<sup>+</sup></b>	0.0217	0	0	0.0411	a
	<b>K<sup>+</sup></b>	0.0499	0.7793	0	0	a
	<b>Mg<sup>++</sup></b>	0.2210	3.3430	-37.2300	0.0250	a
	<b>MgOH<sup>+</sup></b>	0	0	0	0	a
	<b>Na<sup>+</sup></b>	0.0196	1.1130	0	0.0050	a
<b>H<sub>3</sub>SiO<sub>4</sub><sup>-</sup></b>	<b>Ca<sup>++</sup></b>	0.2145	2.5300	0	0	a
	<b>H<sup>+</sup></b>	0.2106	0.5320	0	0	a
	<b>K<sup>+</sup></b>	-0.0003	0.1735	0	0	a
	<b>Mg<sup>++</sup></b>	0.4746	1.7290	0	0	a
	<b>MgOH<sup>+</sup></b>	0	0	0	0	a
	<b>Na<sup>+</sup></b>	0.0454	0.3890	0	0	a
<b>NO<sub>3</sub><sup>-</sup></b>	<b>Ba<sup>++</sup></b>	-0.0323	0.8025	0	0	b
	<b>Ca<sup>++</sup></b>	0.1291	0.7944	0.4288	0	b
	<b>H<sup>+</sup></b>	0.1119	0.3206	0	0	b
	<b>K<sup>+</sup></b>	-0.0816	0.0494	0	0	b
	<b>Mg<sup>++</sup></b>	0.3000	1.1926	0.3045	0	b
	<b>Mn<sup>++</sup></b>	0.3370	1.5424	0	0	b
	<b>Na<sup>+</sup></b>	0.0068	0.1783	0	0	b
	<b>Sr<sup>++</sup></b>	0.1346	1.3800	0	0	b

Ref. a: Reardon, 1990

Ref. b: Weber and Beahm, 1996

Table B.2: Pitzer parameter  $\theta$  of the anion - anion interaction

		$\theta$	Reference
<b>H<sub>2</sub>SiO<sub>4</sub><sup>--</sup></b>	<b>H<sub>3</sub>SiO<sub>4</sub><sup>-</sup></b>	0	a
	<b>Cl<sup>-</sup></b>	0.0160	b
<b>NO<sub>3</sub><sup>-</sup></b>	<b>OH<sup>-</sup></b>	-0.0547	b

Ref. a: Reardon, 1990

Ref. b: Weber and Beahm, 1996

Table B.3: Pitzer parameter  $\lambda$  of the cation - neutral and the anion - neutral interaction

		$\lambda$	Reference
<b>H4SiO4</b>	<b>Ca++</b>	0.0183	a
	<b>H+</b>	0.0510	a
	<b>K+</b>	0.0510	a
	<b>Mg++</b>	0.1830	a
	<b>MgOH+</b>	0	a
	<b>Na+</b>	0.1000	a
	<b>Cl-</b>	-0.0050	a
	<b>CO3--</b>	0	a
	<b>HCO3-</b>	0	a
	<b>H2SiO4--</b>	0	a
	<b>H3SiO4-</b>	0	a
	<b>OH-</b>	0	a
<b>SO4--</b>	-0.0970	a	

Ref. a: Reardon, 1990

Table B.4: Pitzer parameter  $\Psi_{cc'a}$  of the cation - cation - anion interactions

$\Psi_{c c' a}$						
cation	cation'	H2SiO4--	H3SiO4-	Reference	NO3-	Reference
<b>Ca++</b>	<b>H+</b>	0	0	a	-0.0044	b
	<b>K+</b>	0	0	a	-0.0126	b
	<b>Mg++</b>	0.0240	0	a		
	<b>MgOH+</b>	0	0	a		
	<b>Na+</b>	-0.0550	0	a	-0.0174	b
<b>K+</b>	<b>H+</b>	0.1970	-0.0265	a	-0.0103	b
	<b>Mg++</b>	-0.0840	0	a		
	<b>MgOH+</b>	0	0	a		
	<b>Na+</b>	-0.0100	0	a	-0.0060	b
<b>Mg++</b>	<b>H+</b>	0	-0.1780	a		
	<b>MgOH+</b>	0	0	a		
	<b>Na+</b>	-0.0150	0	a		
<b>MgOH+</b>	<b>H+</b>	0	0	a		
<b>Na+</b>	<b>H+</b>	0	-0.0129	a	-0.0027	b
	<b>MgOH+</b>	0	0	a		

Ref. a: Reardon, 1990

Ref. b: Weber and Beahm, 1996

Table B.5: Pitzer parameter  $\Psi_{caa'}$  of the cation - anion - anion interaction

cation	anion	$\Psi_{caa'}$		Reference	NO3-	Reference
		H2SiO4--	H3SiO4-			
Ca++	Cl-	-0.0180		a	-0.0170	b
	CO3--	0	0	a		
	H2SiO4--		0	a		
	HCO3-	0	0	a		
	OH-	0	0	a	0.0577	b
	SO4--	0	0	a		
H+	Cl-	0	0.0130	a		
	CO3--	0	0	a		
	H2SiO4--		0	a		
	HCO3-	0	0	a		
	OH-	0	0	a		
	SO4--	0	0	a		
K+	Cl-	0	0	a	-0.0031	b
	CO3--	0	0	a		
	H2SiO4--		-0.0677	a		
	HCO3-	0	0	a		
	OH-	-0.0500	0	a	-0.0032	b
	SO4--	0	-0.0677	a		
Mg++	Cl-	-0.0040	0	a	0	b
	CO3--	0	0	a		
	H2SiO4--		-0.0425	a		
	HCO3-	-0.1610	0	a		
	OH-	0	0	a		
	SO4--	0	-0.0425	a		
MgOH+	Cl-	0	0	a		
	CO3--	0	0	a		
	H2SiO4--		0	a		
	HCO3-	0	0	a		
	OH-	0	0	a		
	SO4--	0	0	a		
Na+	Cl-	0.0014	-0.0060	a	-0.0060	b
	CO3--	-0.0050	0	a		
	H2SiO4--		-0.0094	a		
	HCO3-	-0.0050	0	a		
	OH-	-0.0090	0	a	-0.0002	b
	SO4--	0	-0.0094	a		

Ref. a: Reardon, 1990

Ref. b: Weber and Beahm, 1996